

**PHYSIOLOGICALLY BASED PHARMACOKINETIC
MODELLING AS A TOOL FOR DOSE OPTIMISATION IN
SPECIAL POPULATION GROUPS**

KHAIRULANWAR BIN BURHANUDDIN

Doctor of Philosophy

ASTON UNIVERSITY

August 2024

© Khairulanwar Bin Burhanuddin, 2024

Khairulanwar Bin Burhanuddin asserts their moral right to be identified as the author
of this thesis.

This copy of the thesis has been supplied on condition that anyone who consults it is
understood to recognise that its copyright belongs to its author and that no quotation
from the thesis and no information derived from it may be published without
appropriate permission or acknowledgement.

ABSTRACT

Aston University

Physiologically Based Pharmacokinetic Modelling as a Tool for Dose Optimisation in Special Population Groups

Khairulanwar Bin Burhanuddin

Doctor of Philosophy

2024

This thesis explores the application of physiologically based pharmacokinetic (PBPK) modelling, an approach that predicts drug disposition by integrating physiological and drug parameters. The objective is to elucidate the impact of physiological alterations within special populations on drug pharmacokinetics, aiming to identify optimal dosing that accounts for exposure differences.

The initial section focuses on fluvoxamine dose optimisation in pregnant women, considering their CYP2D6 phenotypes. The study revealed that fluvoxamine maternal concentrations significantly decreased during gestation, while the foetal concentrations increased substantially in poor metabolisers (PM) but remained constant in ultra-rapid (UM) and extensive metabolisers (EM). The recommended dose for UM and EM reached 300 mg daily at gestational weeks 15 and 35, respectively. Conversely, a consistent 100 mg daily for PM is sufficient to maintain the therapeutic concentration throughout the gestation.

The succeeding part discusses the imatinib dosing strategy in obese adults with cancer. Results showed significant differences in maximum concentration (C_{max}) and area-under-the-curve (AUC) between obese and lean adults but not in trough concentrations (C_{min}). The therapeutic drug monitoring (TDM) approach using the PBPK model demonstrated that the same TDM-guided dosing adjustment could be applied to lean, overweight, and obese adults to restore C_{min} to the target concentration level.

The last segment centres on the paediatric obesity population using amlodipine as a case study. Findings showed significant differences in predicted C_{max} and AUC were observed across ages 2 to 18 years with a fixed dose regimen, while weight-based dosing showed no difference in C_{max} from ages 2 to 9 years. Thus, a 1.25 – 1.5-fold dose increase is needed to attain the same C_{max} as in non-obese children when using a fixed dose.

In summary, PBPK modelling effectively assessed the influence of physiological changes in special populations on drug pharmacokinetics and ascertained the optimal dose from a pharmacokinetic perspective.

Keywords: PBPK; pharmacokinetics; pregnancy; foetal; fluvoxamine; cancer obesity; imatinib; TDM; paediatric obesity; amlodipine

ACKNOWLEDGEMENT

In the name of the Almighty God, the Most Gracious and Most Merciful, I express my heartfelt praise and deepest gratitude to the Divine Creator, the source of all knowledge, wisdom, and inspiration.

To my esteemed supervisor, Dr. Raj K. S. Badhan, I extend my profound appreciation for your invaluable guidance and unwavering support throughout these years. Undoubtedly, you are an outstanding supervisor and teacher. I am grateful for all the knowledge and inspiration I have gained under your mentorship.

To my associate supervisor, Professor Afzal Mohammed, thank you for your advice and facilitation throughout my journey in completing this thesis.

To my beloved wife, Nelfiroma Binti Sudirman, I am deeply grateful for your unconditional love, prayers, and unwavering support. Your presence is a divine gift, and I am thankful for the strength and encouragement that have sustained me throughout this academic journey. To my daughters and son, Salsabila, Kameeleya, and Umar Elfian, thank you for always brightening my day and constantly inspiring me in each step of this journey.

To both of my parents, I genuinely appreciate all the encouragement to complete the PhD journey, and I truly believe your prayers are one of the main reasons for achieving this milestone.

To my colleagues and friends in room MB432, Aston University main buildings, I treasure all the intellectual discourse and thoughtful discussion we engaged in while working hard to achieve our shared mission of advancing the pharmaceutical field.

Thank you to the Ministry of Health Malaysia for the scholarship and opportunity for my educational journey at Aston University, Birmingham, United Kingdom.

TABLE OF CONTENTS

ABSTRACT	2
ACKNOWLEDGEMENT	3
TABLE OF CONTENTS.....	4
LIST OF PUBLICATIONS.....	9
LIST OF ABBREVIATIONS	10
LIST OF FIGURES	17
LIST OF SUPPLEMENTARY FIGURES	20
LIST OF TABLES	22
LIST OF SUPPLEMENTARY TABLES	23
CHAPTER 1 - INTRODUCTION	24
1.1 Background	25
1.1.1 Modelling and simulation in assisting the dose optimisation process in special populations.	26
1.2 Pharmacokinetic modelling.....	30
1.3 'Two-stage' approach, non-compartmental and compartmental modelling	30
1.4 Population pharmacokinetic (PopPK) modelling	34
1.5 Physiologically based pharmacokinetic (PBPK) modelling.....	36
1.5.1 Fundamentals and concept.....	38
1.5.1.1 Assumptions	39
1.5.1.2 System data.....	40
1.5.1.3 Compound data	41
1.5.2 Model development strategy	42
1.5.3 Software	43
1.6 Applications in pharmaceutical product development and regulatory acceptance	44
1.7 Physiologically based pharmacokinetic (PBPK) in special populations	48
1.7.1 Pregnant women.....	48
1.7.2 Adults with obesity and cancer.....	52
1.7.3 Paediatric populations.....	55
1.7.3.1 Paediatric obesity	57
1.8 Aims and objectives.....	59

CHAPTER 2 - OPTIMISING FLUVOXAMINE MATERNAL/FOETAL EXPOSURE DURING GESTATION: A PHARMACOKINETIC VIRTUAL CLINICAL TRIALS STUDY	60
2.1 Introduction	61
2.2 Methodology.....	63
2.2.1 Step 1: Development and verification of fluvoxamine model in a healthy population	64
2.2.2 Step 2: Validation of fluvoxamine PBPK model in pregnancy	67
2.2.3 Step 3: Validation of fluvoxamine foetoplacental PBPK model	68
2.2.4 Step 4: Influence of CYP2D6 phenotype and dose adjustment during gestation ..	68
2.2.5 Predictive performance	69
2.2.6 Data and statistical analysis.....	69
2.3 Results	70
2.3.1 Step 1: Development and validation of fluvoxamine model in a healthy population	70
2.3.2 Step 2: Verification of fluvoxamine model in pregnancy and the impact of pregnancy on fluvoxamine level.....	81
2.3.3 Step 3: Validation of fluvoxamine foetoplacental PBPK model	83
2.3.4 Step 4: Impact of CYP2D6 phenotype and dose adjustment during gestation....	83
2.4 Discussion.....	101
2.4.1 Step 1: Validation of fluvoxamine model in healthy subjects.....	101
2.4.1.1 PBPK model parameters	101
2.4.1.2 Validation in healthy subjects and CYP2D6 phenotype populations	102
2.4.2 Step 2: Verification of fluvoxamine pregnancy model and the impact of pregnancy on fluvoxamine concentration	103
2.4.2.1 Verification of fluvoxamine pregnancy model	103
2.4.2.2 The impact of pregnancy on fluvoxamine concentration.....	103
2.4.3 Step 3: Validation of fluvoxamine foetoplacental PBPK model	104
2.4.4 Step 4: Impact of CYP2D6 phenotype and dose adjustment during gestation...	105
2.4.4.1 Impact of CYP2D6 phenotype in the pregnant population	105
2.4.4.2 Maternal plasma concentration changes throughout pregnancy	105
2.4.4.3 Umbilical cord concentration changes throughout pregnancy	106
2.4.4.4 Fluvoxamine dosing during pregnancy.....	107
2.5 Conclusion	109
2.6 Supplementary materials	110

CHAPTER 3 - THE APPLICATION OF PHYSIOLOGICALLY BASED PHARMACOKINETIC (PBPK) MODELLING TO DOSE OPTIMISING OF IMATINIB PHARMACOKINETICS IN OBESE CANCER POPULATIONS	117
3.1 Introduction	118
3.2 Methodology	120
3.2.1 Step 1: Verification of the imatinib model in healthy, cancer and Caucasian populations	121
3.2.2 Step 2: Validation of lean, overweight and obese cancer population with imatinib compound model	123
3.2.3 Step 3: Comparison of physiological parameters and imatinib pharmacokinetics parameters between lean, overweight, and obese cancer populations	124
3.2.4 Step 4: Imatinib therapeutic drug monitoring (TDM) in lean, overweight and obese cancer populations.....	125
3.2.5 Prediction performance	126
3.2.6 Data and statistical analysis	126
3.3 Results	127
3.3.1 Step 1: Imatinib model validation in healthy, cancer and caucasian populations	127
3.3.2 Step 2: Validation of lean, overweight, and obese cancer population with imatinib compound model	132
3.3.3 Step 3: Comparison of physiological parameters and imatinib pharmacokinetics parameters between lean, overweight and obese cancer populations	134
3.3.3.1 Comparison of physiological parameters between lean, overweight and obese cancer populations.....	134
3.3.3.2 Comparison of imatinib pharmacokinetic parameters between lean, overweight and obese adult cancer populations	137
3.3.4 Virtual therapeutic drug monitoring (TDM) of imatinib in lean, overweight and obese cancer populations	140
3.4 Discussion.....	144
3.4.1 Step 1: Imatinib model validation in healthy, cancer and Caucasian populations	144
3.4.2 Step 2: Validation of lean, overweight and obese cancer population model with imatinib compound model	145
3.4.3 Step 3: Comparison of physiological parameters and imatinib pharmacokinetics parameters between lean, overweight, and obese cancer populations	146
3.4.3.1 Analysis of physiological parameters across lean, overweight, and obese cancer populations	146

3.4.3.2	Assessment of imatinib pharmacokinetic parameters between lean, overweight and obese adult cancer populations	148
3.4.4	Step 4: Virtual therapeutic drug monitoring (TDM) of imatinib in the lean, overweight, and obese cancer population	150
3.4.5	Sensitivity analysis for α 1-acid glycoprotein (AGP) and CYP3A4 hepatic abundances	153
3.5	Conclusion	155
CHAPTER 4 – THE IMPACT OF PAEDIATRIC OBESITY ON DRUG PHARMACOKINETICS: A VIRTUAL CLINICAL TRIALS CASE STUDY WITH AMLODIPINE		
156		
4.1	Introduction	157
4.2	Methodology	160
4.2.1	Step 1: Development of the paediatric obesity population	161
4.2.1.1	Age, weight and height relationship	161
4.2.1.2	Haematocrit-Age relationship	161
4.2.1.3	Protein binding-to-age relationship	161
4.2.1.4	Glomerular filtration rate (GFR)-to-age relationship	162
4.2.2	Step 2: Validation of a paediatric obesity population with metformin and ceftazidime compound files	162
4.2.2.1	Step 2.1: Validation with metformin	162
4.2.2.2	Step 2.2: Validation with ceftazidime	165
4.2.3	Step 3: Verification with amlodipine	166
4.2.4	Step 4: Influence of obesity on amlodipine pharmacokinetic parameters and dose adjustment in the paediatric obesity population	169
4.2.5	Prediction performance	170
4.2.6	Data and statistical analysis	170
4.3	Results	171
4.3.1	Step 1: Development of the paediatric obesity population	171
4.3.2	Step 2: Validation of the paediatric obesity population	171
4.3.2.1	Step 2.1: Validation with metformin	171
4.3.2.2	Step 2.2: Validation with ceftazidime	174
4.3.3	Step 3: Verification of the amlodipine model	175
4.3.4	Step 4: Impact of paediatric obesity on amlodipine pharmacokinetics	181
4.3.4.1	Comparison of non-obese and obese paediatrics	181
4.3.4.2	Dose adjustments in paediatric obesity	183
4.4	Discussion	185

4.4.1 Step 1: Development of the paediatric obesity population	185
4.4.2 Step 2: Validation of paediatric population with metformin and ceftazidime	186
4.4.3 Step 3: Validation of the amlodipine model.....	187
4.4.4 Step 4: Impact of obesity on amlodipine pharmacokinetics and dose optimisation in obese children population	188
4.4.4.1 Influence of obesity on amlodipine pharmacokinetics.....	188
4.4.4.2 Dose adjustment in paediatric obesity.....	189
4.5 Conclusion	192
4.6 Supplementary materials	193
4.6.1 Results for Step 1: Development of the paediatric obesity population	193
4.6.1.1 Age, weight and height relationship	193
4.6.1.2 Haematocrit-to-age relationship	198
4.6.1.3 Serum albumin-to-age relationship	200
4.6.1.4 Alpha-1-acid glycoprotein (AGP)-to-age relationship.....	202
4.6.1.5 Glomerular filtration rate (GFR)-to-age relationship	204
4.6.2 Supplementary figures	206
CHAPTER 5 – CONCLUSION AND FUTURE WORK.....	213
5.1 Conclusion	214
5.2 Future work	217
REFERENCES	218

LIST OF PUBLICATIONS

Peer-reviewed published articles:

1. **Burhanuddin, K.** and Badhan, R. Optimising Fluvoxamine Maternal/Foetal Exposure during Gestation: A Pharmacokinetic Virtual Clinical Trials Study. *Metabolites*, 2022. 12(12): 1281. <https://doi.org/10.3390/metabo12121281>
2. **Burhanuddin, K.**, Mohammed, A.R. and Badhan, R. The impact of paediatric obesity on drug pharmacokinetics: a virtual clinical trials case study with amlodipine. *Pharmaceutics*, 2024. 16(4): 489. <https://doi.org/10.3390/pharmaceutics16040489>

Conference Proceedings:

1. **Khairulanwar Burhanuddin** and Raj K. S. Badhan, 2022. Dose optimisation of an antidepressant drug during pregnancy: A pharmacokinetic virtual clinical trial study for fluvoxamine. The 4th Interdisciplinary Postgraduate Research Conference, Aston University, Birmingham, United Kingdom. (Oral presentation)
2. **Khairulanwar Burhanuddin** and Raj K. S. Badhan, 2023. Development of a paediatric obesity population group: Exploration of the need for dose adjustment with amlodipine. The Pharmacokinetics PKUK 2023 Meeting, Lancaster, United Kingdom. (Poster presentation)

LIST OF ABBREVIATIONS

ADAM	Advance dissolution, absorption, and metabolism
AGP	α 1-acid glycoprotein
AIOM	<i>Associazione Italiana Oncologia Medica</i>
AMD	<i>Associazione Medici Diabetologi</i>
ASCO	American Society of Clinical Oncology
AUC	Area-under-the-curve
AUC _{0-24ss}	Area-under-the-curve for 24 hours at steady-state
AUC _{0-infss}	Area-under-the-curve to infinity at steady-state
AUC _{0-t}	Area-under-the-curve to the last time point
AUC _{0-tss}	Area-under-the-curve to time at steady-state
AUC _{inf}	Area-under-the-curve to infinity
AUC _t	Area-under-the-curve for the total hour at steady-state
AUMC	Area-under-the-first moment curve (AUMC)
B/P	Blood-to-plasma ratio
BA	Bioavailability
BE	Bioequivalence
BMI	Body mass index
BNFc	British national formulary for children
BSA	Body surface area
C	Drug concentration
Caco-2	Human epithelial colorectal adenocarcinoma cells
CAH	Congenital adrenal hyperplasia
CCB	Calcium channel blockers

CCyR	Complete cytogenic response
CDC	Centre for Disease Control and Prevention
C_{pl}^f	Foetal-placental concentration
CL	Clearance
CL/F	oral clearance
CL _H	Hepatic clearance
CL _{int}	In vitro intrinsic clearance
CL _{int,T}	In vitro transporter-mediated intrinsic clearance
CL_{pl}^t	Tissue-placenta permeability clearance
CL _{int,app}	Apparent in vitro intrinsic clearance
CL _{int,scaled}	Hepatic intrinsic clearance
CL _{PD}	Passive diffusion clearance
CL _{PDF}	Placenta-foetal permeability clearance
CL _{PDM}	Maternal-placenta permeability clearance
C_{pl}^m	Maternal-placental concentration
C _{max}	Maximum concentration
C _{max,ss}	Maximum concentration at steady-state
C _{min}	Trough concentration
CML	Chronic myeloid leukaemia
CPIC	Clinical Pharmacogenetics Implementation Consortium
CV	Coefficient variation
CYP	Cytochrome P450
DPWG	Dutch Pharmacogenetics Working Group
eGFR	Estimated glomerular filtration rate

ELN	European LeukemiaNet
EM	Extensive metaboliser
EMA	European Medicines Agency
fa	fraction of dose absorbed
fu	Unbound fraction
f_{uGut}	Unbound fraction of drug in enterocytes
f_{uinc}	Fraction of unbound drug in vitro microsomal incubation
f_{umic}	Fraction of unbound drug in the in vitro microsomal incubation
G. I.	Gastrointestinal
GFR	Glomerular filtration rate
GIST	Gastrointestinal stromal tumour
GSTs	Glutathione S-transferases
GW	Gestational week
h	hour
HAS	Human serum albumin
HBD	Hydrogen-bonded donors
HIMel CL_{int}	Human intestinal microsomes in vitro intrinsic clearance
HLM CL_{int}	Human liver microsomes invitro intrinsic clearance
HV	Healthy volunteer
IATDMCT	International Association of Therapeutic Drug Monitoring and Clinical Toxicology
IBW	Ideal body weight
ICH	International Council for Harmonisation of Technical Requirements for Pharmaceuticals for Human Use
IV	Intravenous
IVIVE	In vitro-in vivo extrapolation

J_{\max}	In vitro maximum rate of transporter-mediated efflux or uptake
J_{OCT2}	In vitro OCT2 flux per unit of electrochemical gradient
k_a	Absorption rate constant
K_i	Concentration of inhibitor that supports half-maximal inhibition
k_{inact}	Inactivation rate of the enzyme
K_m	Michaelis-Menten constant
K_p	unbound tissue partition coefficients
K_p scalar	Tissue partition coefficient
L	Litre
LBW	Lean body weight
Log P	Octanol-to-water partition coefficient
mg	Milligram
μg	Microgram
MDCK-II	Madin-Darby canine kidney cells
MHRA	Medicines and Healthcare Products Regulatory Authority, United Kingdom
MIDD	Model-informed drug development
mL	Millilitre
MMR	Major molecular response
MRT	Mean residence time
MTT	Mean transit time
NEurCaucasian	North European Caucasian
ng	Nanogram
NHANES	National Health and Nutrition Examination Survey
nmol	Nanomole

ns	Not significant
OAT	Organic anion transporter
OCD	Obsessive compulsive disorder
OCT	Organic cation transporter
OD	Once daily
OOBR	Overall objective benefit rate
PAH	Pulmonary arterial hypertension
P_{app}	Apparent permeability
PBPK	Physiologically based pharmacokinetic
P_{eff}	Human jejunum effective permeability
P-gp	P-glycoprotein
PILs	Patient information leaflets
pKa	Ionisation coefficient
PLLR	Pregnancy and lactation labelling final rule
PLs	Package leaflets
PM	Poor metaboliser
PMDA	Pharmaceuticals and Medical Devices Agency, Japan
PNAS	Post-natal adaptation syndrome
PopPK	Population pharmacokinetic
PPHN	Persistent pulmonary hypertension
PSA	Polar surface area
PS_T	Permeability rate-limited
PTN	Paediatric Trial Network
PTSD	Post-traumatic stress disorder

Q_{pl}^f	Foetal blood flow rate
Q_G	Plasma flow rate to gastrointestinal
Q_K	Plasma flow rate to kidney
Q_L	Plasma flow rate to liver
Q_M	Plasma flow rate to muscle
Q_{pl}^m	Maternal blood flow rate
QSAR	Quantitative structure-activity relationship
Q_T	Blood flow rate
r	Drug-transport rate
RAF	Relativity activity factor
RAF/REF	Relative activity factor or relative expression factor
r_s	Spearman's rank correlation coefficient
SD	Standard deviations
SIE	<i>Società Italiana Endocrinologia</i>
SIF	<i>Società Italiana Farmacologia</i>
SmPC	Summary of product characteristics
SSRI	Selective serotonin reuptake inhibitors
SULTs	Sulfotransferases
T	Nominal residence time in bile subcompartment
$t_{1/2}$	Elimination half-life
TBW	Total body weight
TDM	Therapeutic drug monitoring
TKIs	Tyrosine kinase inhibitors
T_{max}	Time to maximum concentration

TTP	Time to progression
TW	Therapeutic window
UGTs	UDP-glucuronosyltransferases
UK	United Kingdom
UM	Ultra-rapid metaboliser
USFDA	United States Food and Drug Administration
USPI	United States prescribing information
V_d	Volume of distribution
V_{pl}^f	Foetal-placental volume
V_{pl}^m	Maternal-placental volume
V_{max}	Maximum rate of metabolism
VPC	Visual predictive check
V_{ss}	Volume of distribution at steady-state
V_T	Compartment volume
WHO	World Health Organisation

LIST OF FIGURES

Figure 1.1 A wide range of quantitative models categorised under model-informed drug development (MIDD) applied in the drug development stages.....	27
Figure 1.2 Application of modelling and simulation throughout the drug development cycle.	29
Figure 1.3 Plasma concentration-time and first-moment versus time curve.....	31
Figure 1.4 Illustration of common compartmental models for intravenous bolus administration with the correlated plasma-concentration profile.	33
Figure 1.5 Illustration of one-compartment model of concentration-time profile following intravenous bolus administration showing observed and predicted value.....	35
Figure 1.6 Illustration of body compartments for the methotrexate distribution by Bischoff et al. (1971).....	37
Figure 1.7 Schematic diagram of typical PBPK models.....	38
Figure 1.8 Illustration of perfusion vs. permeability rate-limited tissue models.....	39
Figure 1.9 General steps to develop a PBPK model	42
Figure 1.10 The predictive performance on PBPK applications for regulatory submissions.	46
Figure 1.11 Illustration of the pregnancy PBPK models in (A) Gastroplus®, (B) Simcyp®, and (C) Open Systems Pharmacology	51
Figure 1.12 Recommended workflow when applying MIDD in paediatric drug development.	56
Figure 2.1 A four-step workflow for fluvoxamine gestational model development	63
Figure 2.2 Comparison between simulated trial and observed data.	75
Figure 2.3 Simulated single-dose studies in model development.	76
Figure 2.4 Single-dose studies simulated in the model validation stage.	77
Figure 2.5 Multiple-dose studies simulated in model development and validation.	78
Figure 2.6 Simulated single-dose studies in model validation for CYP2D6 phenotype.	79
Figure 2.7 Predicted maximum concentration and steady-state concentration for single-dose and multiple-dose studies.....	80
Figure 2.8 Predicted steady-state C_{min} fluvoxamine maternal concentration.....	81
Figure 2.9 Simulated fluvoxamine foetal (umbilical cord) concentrations.....	83
Figure 2.10 Simulated fluvoxamine maternal concentrations in CYP2D6 phenotype population.	84
Figure 2.11 Simulated fluvoxamine umbilical cord concentrations in CYP2D6 phenotype population.	89
Figure 2.12 Predicted clearance, area-under-the-curve, and cord concentration based on the recommended doses.....	100
Figure 3.1 Four-step workflow model for Imatinib model verification, TDM and exploration	120

Figure 3.2 Imatinib dose adjustment guided by TDM process	125
Figure 3.3 Comparison of model-predicted vs. observed concentration data of imatinib in healthy adults (A), adult cancer (B – G) and European adults (H-I).	130
Figure 3.4 Comparison of imatinib simulated profiles with observed plasma profiles at steady-state in cancer populations	131
Figure 3.5 Predicted and observed imatinib trough concentrations (C_{min}) in cancer populations were stratified according to the body mass index (BMI) classification..	133
Figure 3.6 Radar graph comparing the mean of lean, overweight and obese adult cancer physiological parameters.....	135
Figure 3.7 Comparison between normal, overweight and obese adult cancer physiological parameters.....	136
Figure 3.8 Comparison of predicted imatinib pharmacokinetic parameters at steady-state between lean, overweight and obese cancer populations.....	139
Figure 3.9 Comparison of predicted imatinib pharmacokinetic parameters at steady-state between lean, overweight and obese cancer populations.....	141
Figure 3.10 TDM-guided dose adjustment according to the target trough concentrations..	152
Figure 3.11 Impact of the CYP3A4 hepatic enzyme abundances and α 1-acid glycoprotein (AGP) changes on the maximum concentration (C_{max}) (A), trough concentration (C_{min}) (B), and area-under-the-curve (AUC) (C).	154
Figure 4.1 A 4-stage workflow was implemented to develop, verify, and explore the amlodipine dose in the paediatric population [156]. AGP, α 1-acid glycoprotein; GFR, glomerular filtration rate.....	160
Figure 4.2 Simulated metformin plasma concentration in healthy adults (A-B), obese adults (C), paediatric (D), and paediatric obesity (E-F).	173
Figure 4.3 Simulated steady-state plasma concentration of ceftazidime for the paediatric population. Solid lines represent the predicted mean concentration-time profile, with dotted lines representing the 5 th and 95 th percentile ranges. Solid circles represent the mean of the observed clinical data from Maharaj et al. (2021) [383].....	174
Figure 4.4 Simulated plasma concentration of amlodipine single-dose in healthy adults. ..	177
Figure 4.5 Simulated plasma concentration of amlodipine multiple-dose in healthy adults.	178
Figure 4.6 Simulated steady-state trough concentration (C_{min}) of amlodipine multiple-dose in the paediatric population.	179
Figure 4.7 Simulated plasma concentration of amlodipine in paediatric with and without obesity.....	180
Figure 4.8 Simulated steady-state amlodipine plasma concentration profiles in healthy and obese children for age groups of 2 to 6 years old, 6.01 to 12 years old and 12.01 to 18 years old.	181

Figure 4.9 Predicted AUC (A) and C_{max} (B) at steady-stated for healthy and obese paediatric for four doses and three different age groups..... 182

Figure 4.10 Predicted C_{max} in obese and non-obese paediatric with weight-based dose (A) and fixed-dose approaches for dose adjustment. 184

LIST OF SUPPLEMENTARY FIGURES

Figure S 2-1 Foetoplacental compartment permeability-limited model	110
Figure S 2-2 Percentage of Ultrarapid Metaboliser (UM) population with trough concentration below 60 ng/mL.....	111
Figure S 2-3 Percentage of UM population with peak concentration above 230 ng/mL	112
Figure S 2-4 Percentage of Extensive Metaboliser (EM) population with trough concentration below 60 ng/mL.....	113
Figure S 2-5 Percentage of EM population with peak concentration above 230 ng/mL	114
Figure S 2-6 Percentage of Poor Metaboliser (PM) population with trough concentration below 60 ng/mL.....	115
Figure S 2-7 Percentage of PM population with peak concentration above 230 ng/mL	116
Figure S 4-1 Simulated BMI-for-age curves for paediatric obesity from 2 to 18 years old for males (A) and females (B).....	194
Figure S 4-2 Simulated Height-for-age curve for paediatric obesity from 2 to 18 years old for males (A) and females (B).....	195
Figure S 4-3 Simulated Weight-for-height curves for paediatric obesity from 2 to 18 years old for males (A) and females (B).....	196
Figure S 4-4 Simulated Weight-for-height curves for paediatric obesity from 2 to 5 years old for males (A) and females (B).....	197
Figure S 4-5 Simulated Haematocrit-to-age relationship for paediatric obesity from 2 to 8 years old (Grey circle).	199
Figure S 4-6 Predicted Serum albumin-to-age relationship for paediatric obesity from 2 to 18 years old (Grey circle).	201
Figure S 4-7 Predicted AGP-to-age relationship for paediatric obesity from 2 to 18 years old (Grey circle).	203
Figure S 4-8 Absolute GFR (mL/min)-to-age relationship for paediatric obesity from 8 to 9 years old (A) and BSA-adjusted GFR (mL/min/1.73m ²)-to-age correlation for paediatric obesity from 4 to 18 years old (B).	205
Figure S 4-9 Comparison of predicted clearance (A) and volume of distribution (B) at steady-state for healthy and obese paediatric doses.	206
Figure S 4-10 Predicted maximum concentrations (C _{max}) versus daily doses for age group 2 to 6 years old.	207
Figure S 4-11 Predicted C _{max} versus daily doses for age group 6.01 to 12 years old.....	208
Figure S 4-12 Predicted C _{max} versus daily doses for age group 12.01 to 18 years old.....	209
Figure S 4-13 Summary of pharmacokinetic parameters at steady-state in healthy paediatric from 2 to 18 years old.	210

Figure S 4-14 Summary of pharmacokinetic parameters at steady-state in paediatric obesity from 2 to 18 years old administered with weight-based dose.	211
Figure S 4-15 Summary of pharmacokinetic parameters at steady-state in paediatric obesity from 2 to 18 years old administered with fixed dose.	212

LIST OF TABLES

Table 1.1 The application of PBPK modelling throughout drug development stages.....	44
Table 1.2 Physiological changes during pregnancy and potential impact on drug pharmacokinetics ^a	49
Table 1.3 Summary of physiological changes in obese and cancer adults.....	53
Table 1.4 Summary of physiological changes in obese adults and children.....	58
Table 2.1 Fluvoxamine compound parameters with a full PBPK model	64
Table 2.2 Published data used in fluvoxamine model development and validation.	65
Table 2.3 Pharmacokinetics of single- and multiple-dose studies (predicted and observed)	71
Table 2.4 Predicted fluvoxamine plasma concentration across the maternity period	82
Table 2.5 Summary of predicted fluvoxamine plasma concentrations during gestation.....	85
Table 2.6 Summary of simulated fluvoxamine umbilical cord concentrations during gestation	90
Table 2.7 Percentage of subjects with trough and peak outside the therapeutic window	94
Table 2.8 Summary of recommended daily dose, predicted clearance, AUC, and umbilical cord concentrations based on the recommended doses.....	97
Table 3.1 Imatinib compound parameter values validated and used for simulation.....	122
Table 3.2 Observed and predicted pharmacokinetic parameters of imatinib for healthy subjects.....	127
Table 3.3 Observed and predicted pharmacokinetic parameters of imatinib for cancer subjects.....	128
Table 3.4 Comparison of simulated imatinib pharmacokinetic parameters at steady-state between lean, overweight, and obese cancer population	138
Table 3.5 Predicted imatinib trough plasma concentrations at different doses in cancer subjects following the application of therapeutic drug monitoring (TDM)	142
Table 4.1 Metformin compound parameters used for validation studies	162
Table 4.2 Datasets of Metformin and Ceftazidime used for validation of the paediatric obesity population.	164
Table 4.3 Ceftazidime compound parameters used for validation and simulation	165
Table 4.4 Amlodipine compound parameters used in validation and simulation.....	166
Table 4.5 Validation datasets used for verification of the amlodipine model.....	168
Table 4.6 Observed versus predicted pharmacokinetic parameters for metformin.....	172
Table 4.7 Observed and predicted amlodipine pharmacokinetic parameters in adult.....	175

LIST OF SUPPLEMENTARY TABLES

Table S 4-1 Summarised results from literature search for haematocrit values in paediatric obesity	198
Table S 4-2 Summarised results from the literature search for serum albumin values in paediatric obesity	200
Table S 4-3 Summarised results from the literature search for AGP values in paediatric obesity	202
Table S 4-4 Summarised results from the literature search for GFR values in paediatric obesity	204

CHAPTER 1 - Introduction

1.1 Background

In the context of clinical practice, a successful treatment lies in achieving an optimal treatment outcome, and selecting an appropriate dose of medication is one of the critical inputs of the whole treatment management [1]. An effective dose is a delicate balance between maximising the therapeutic effect while minimising the risk of adverse effects. The process of deciding appropriate and effective drug doses for special populations, such as pregnant women, adult and paediatric obesity, and oncology patients is a complex and critical task and remains a challenge for prescribers [2, 3]. The intricate interplay between physiological alterations and pharmacokinetic changes in special populations is the challenging part of identifying an effective and safe dose.

In terms of official dosing guidance for special populations, the primary public documents on the expected drug effects issued by regulatory authorities to guide prescribers, health professionals and end-users are the summary of product characteristics (SmPC) or United States Prescribing Information (USPI) and package leaflets (PLs) or patient information leaflets (PILs). The details in SmPC or USPI delineate the information on how to use the specific medication safely and effectively, including information for pregnant women, paediatrics, renal impairment, liver impairment and potentially other special populations [4]. As for the PLs or PILs, they come together with the medicines containing information derived from the SmPC and written in a straightforward and easy-to-understand language for the end-users [5].

Although the information on the effect of drugs on special populations is made available in the SmPC and PILs, the information is still limited to specific populations such as pregnant women, paediatrics, and several others. Furthermore, the data shared is not always on the need for dose adjustment in special populations but more on the previous exposure and possible impact on the population as well as potential adverse risks associated to the foetus based on clinical data generated from non-clinical, clinical studies and nowadays modelling and simulations [4, 6].

Although the information on optimal doses for specific medicines in special populations is not always available from the SmPC or USPI, clinical practice guidelines for specific medical conditions or classes of medication potentially address the information gap. Clinical practice guidelines are developed based on systematic reviews and assessments of evidence available in medical research realms by a group of experts and specialists within the particular domain [7, 8]. Thus, guidelines may include recommendations for the treatment management of specific diseases in special populations based on the countries and regional-specific practices, such as the use of psychotropic drugs during pregnancy and lactation [9], treatment

strategy for obese adult patients with cancer [10], management of paediatric obesity [11-13], and other conditions and populations. Nevertheless, there are areas and gaps that need to be addressed by research communities to improve the overall effectiveness and inclusivity of treatment practices.

There are a few reasons for the lack of recommendations and data to guide treatment management in various special populations, such as the strict set of criteria for patient recruitment in clinical trials and the patient subpopulation groups are typically categorised as high-risk and vulnerable and challenging to recruit in a standard clinical trial setting [3, 14]. Scientific advancement methods such as modelling and simulation techniques have been applied to bridge and support the optimisation of dosing regimens in special populations [15-17].

Furthermore, regulatory authorities' acceptance of modelling and simulation data to support dosing recommendations during registration and clinical trial applications has increased over the years [18]. The increase was illustrated by Zhang et al. (2020) [19] and Grimstein et al. (2019) [20], where the percentage of new drug approvals with physiologically based pharmacokinetic (PBPK) data supporting the drug registration as one of the modelling and simulation approaches increased up to 45% in 2019 compared to the previous year.

1.1.1 Modelling and simulation in assisting the dose optimisation process in special populations.

Several terms are used to indicate the modelling and simulation in the drug development stage and clinical practice, such as model-based drug development, in silico analysis, model-informed drug development (MIDD), model-integrated evidence, and others. Among all, MIDD is the most recent and commonly used term, particularly by the United States Food and Drug Administration (USFDA), to illustrate the myriad of quantitative modelling and simulation used and implemented during various drug discovery and development stages (Figure 1.1) [21].

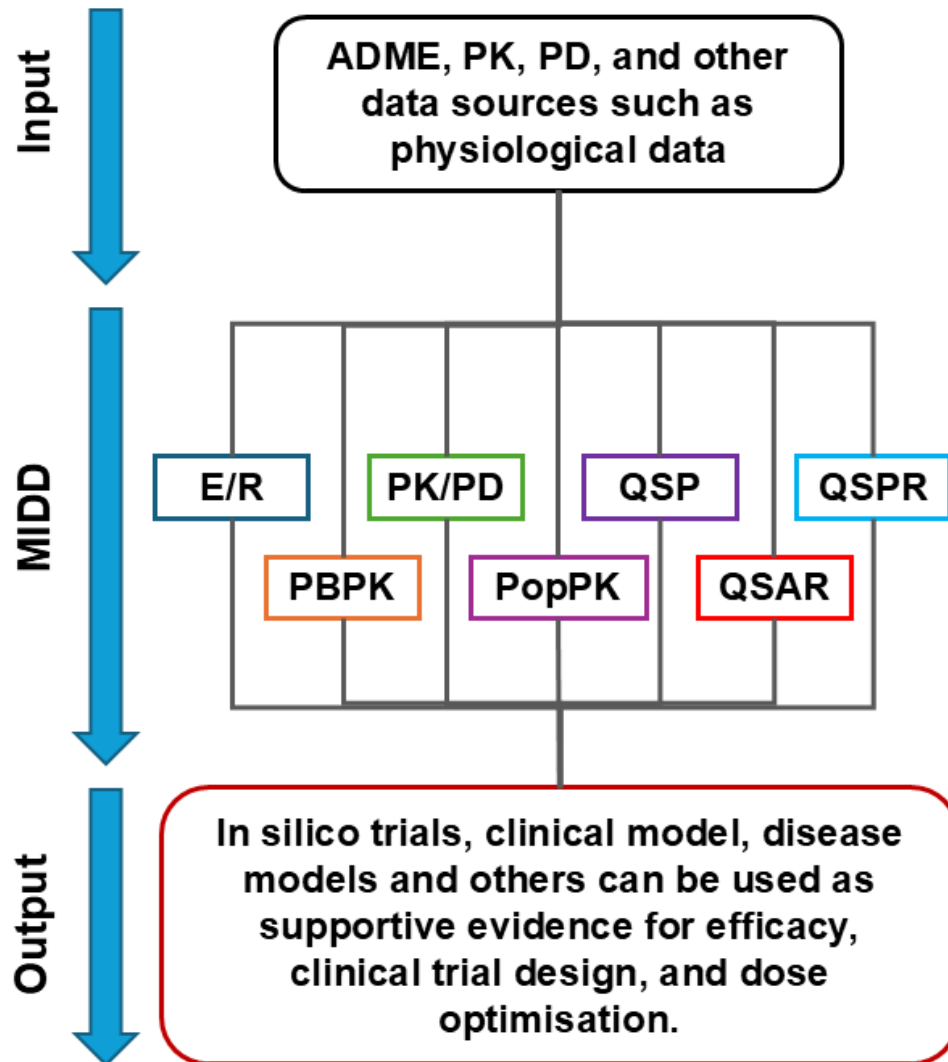


Figure 1.1 A wide range of quantitative models categorised under model-informed drug development (MIDD) applied in the drug development stages.

Adapted from Liu et al. (2021) [21]. PK, pharmacokinetic; PD, pharmacodynamic; ADME, absorption, distribution, metabolism, excretion; E/R: exposure-response; PBPK: physiologically-based pharmacokinetic modelling; PK/PD, pharmacokinetic/pharmacodynamic; PopPK, population pharmacokinetic; QSP, quantitative system pharmacology; QSAR, quantitative structure-activity relationship; QSPR, quantitative structure-property relationship

The USFDA has recognised MIDD in the Prescription Drug User Fee Act for fiscal years 2018 to 2022 (known as PDUFA VI) and generally defined the term as the development and application of exposure-based, biological, and statistical models derived from the data generated during pre-clinical and clinical stages to make an informed decision during the drug development processes [22]. The application of MIDD throughout the drug development stages is diverse, starting from the early stage in the laboratory, such as target identification, followed by various types of modelling in the pre-clinical phase, like an extrapolation of the animal dose to human dose, and in the clinical stage, modelling is used in many ways including evaluating the drug effect in special populations and predicting optimum dose, and with the developed model, the impact of any changes occurred after approval can be assessed (Figure 1.2) [23].

In the scope of this thesis, the emphasis of modelling and simulation is placed on PBPK modelling within the domain of pharmacokinetic modelling, which will be the focus of the subsequent sections. The evolving nature of pharmacokinetic modelling concepts and applications warrants further exploration and research to improve confidence in accepting the modelling results and expand the usage in various areas, particularly clinical practices.

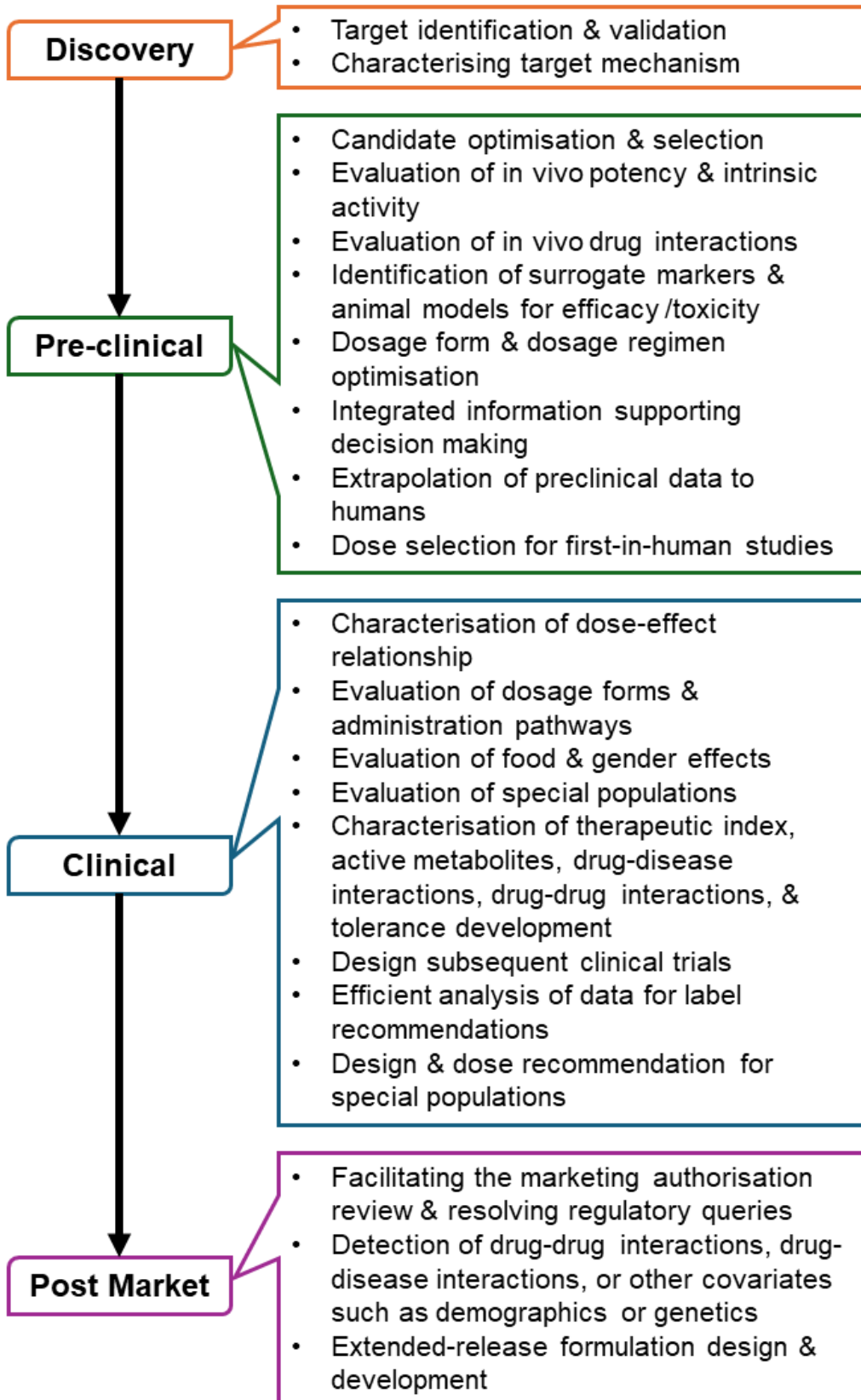


Figure 1.2 Application of modelling and simulation throughout the drug development cycle.

Adapted from Kim et al (2018) [23].

1.2 Pharmacokinetic modelling

Pharmacokinetics is defined as the drug time course study of the absorption, distribution, metabolism, and excretion with the primary goal of maximising efficacy while reducing the toxic effect of a drug in a patient. There are several techniques to study the pharmacokinetics of a drug, with each approach having its specific requirement. One of them is pharmacokinetic modelling, which uses a mathematical method to predict how a drug moves and is handled by the body.

The classic pharmacokinetic modelling, also known as the 'two-stage' approach, involves conducting studies with small numbers of subjects meeting specific criteria to limit the variability, and each subject requires extensive sampling [24]. Depending on the questions, the concentration-time profile will then be analysed by either compartmental or non-compartmental modelling [25].

Besides the classical method, there is the area of population pharmacokinetic (PopPK) modelling, also known as 'mixed-effects' modelling, which is often utilised with sparse drug concentration data, and analysis will be made at the population setting rather than individual by considering the interindividual, intraindividual, and residual variability [26]. Both techniques are considered '*top-down*' or empirical approaches, where the observed data is needed to develop the mathematical model. In contrast, '*bottom-up*' or mechanistic approaches such as PBPK modelling, which is the centre of this thesis, can generally predict the pharmacokinetic profiles without using clinical data [27].

1.3 'Two-stage' approach, non-compartmental and compartmental modelling

The 'two-stage' approach is a classic or traditional method to analyse and study the pharmacokinetics of a drug, and it is still widely used in the drug development stage. Generally, intensive sampling will be collected from each subject in the classic study, and usually, the subjects recruited are homogenous with stringent inclusion and exclusion criteria [28]. The collected samples will then be analysed either using a naïve average data approach or naïve pooled data analysis in addressing the overall data from several subjects [29]. This 'two-stage' approach is still very much used in the current drug development process, particularly in the early phase trial, such as phase 1, when the information on the drug action in humans is minimal and even widely used in the bioequivalence study [30-32].

Once the comprehensive plasma concentration data have been collected, the investigator must decide which modelling approach to apply for analysis in order to quantitatively describe the drug disposition under study. One option is the non-compartmental model, also known as

the model-independent method. The non-compartmental approach requires fewer assumptions to fit the drug's pharmacokinetic profile; among others, the drug displays linear pharmacokinetics, and the elimination phase is log-linear [33]. The aim is to estimate the essential pharmacokinetic parameters using statistical moment analysis, such as the estimation of the mean residence time (MRT), mean transit time (MTT), and area under the first moment curve (AUMC). The MRT is defined as the average time a drug spends in a body, which can be calculated from the AUMC and area under the curve (AUC) as specified in equation (1.1) [34]. Both AUMC and AUC can be obtained using the trapezoidal method from the first-moment (plasma concentration x time) versus time curve and plasma concentration-time curve, respectively (Figure 1.3).

$$\text{MRT} = \frac{\text{AUMC}}{\text{AUC}} \quad (1.1)$$

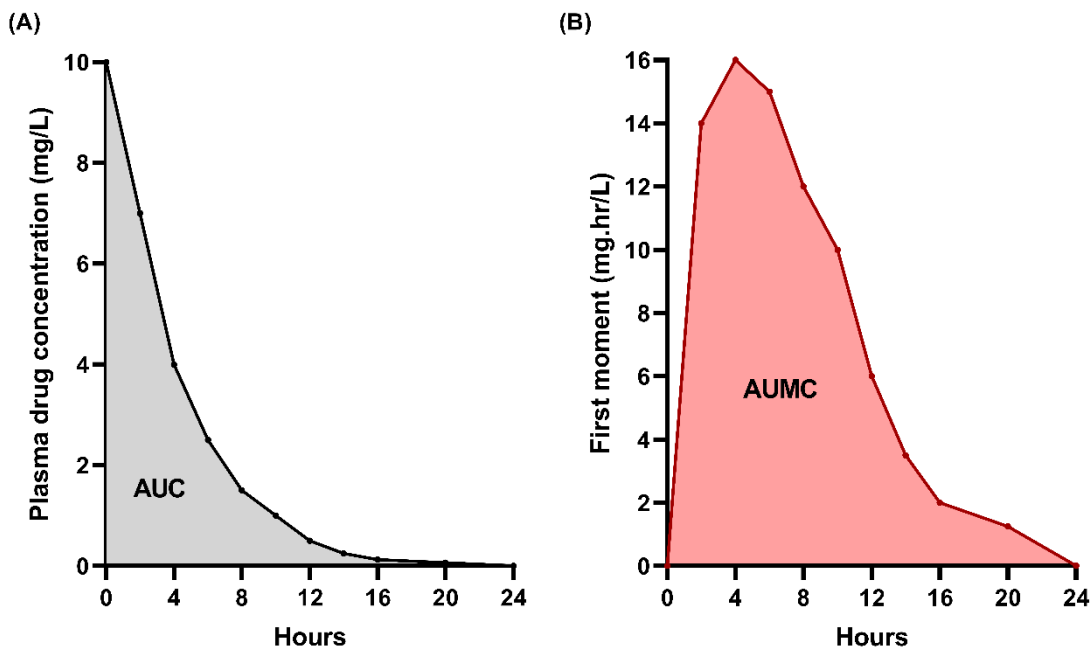


Figure 1.3 Plasma concentration-time and first-moment versus time curve.

Adapted from Rowland et al. (1995) [35]. The plasma concentration-time curve is in black (A), and the plasma concentration x time-time curve is in red (B). The trapezoidal method for black and red graphs will obtain AUC and AUMC, respectively.

For any drug administered through the extravascular route, the MRT in equation (1.1) is replaced with MTT to address the average drug transit time from absorption to elimination [36]. All the other essential pharmacokinetics parameters can then be calculated from the MRT and AUC, which include the elimination half-life ($t_{1/2}$), clearance (CL), and volume of distribution at steady-state (V_{ss}).

In contrast, compartmental modelling uses the concept of drug absorption, distribution, metabolism, and elimination translated into logical-mathematical terms to create simple models of complex physiological processes. Generally, a body is represented by a compartment or several manageable compartments to express the drug disposition and estimate the pharmacokinetic parameters such as volume of distribution (V_d), $t_{1/2}$, elimination rates, and others [34]. A compartment is regarded as a group of tissues with similar drug distribution rates with assumptions of homogenous drug concentration [36].

The assumptions made for each compartment do not precisely represent any specific organs and tissues like in the mechanistic pharmacokinetics model. The main compartment usually means central, where rapid absorption occurs, with the additional compartments added when distribution and metabolism happen at a slower rate, while the elimination can either be from the main compartment only or at another compartment [37]. The numbers of compartments are typically determined by the shape of the plasma concentration-time profile facilitated with the known characteristics of the physicochemical properties of the drug under investigation (Figure 1.4). The application of compartmental modelling can be upscaled from individual to population by considering interindividual variability, which will be discussed further in a different section.

Both the non-compartmental and compartmental approach have their advantages and disadvantages. The availability of necessary data and resources is the deciding factor on which modelling approach to use. For example, the information on sampling timing is not critical in the non-compartmental approach. Furthermore, the non-compartmental approach is straightforward and quick, with less experienced modellers able to perform the analysis compared to the compartmental modelling [34, 36].

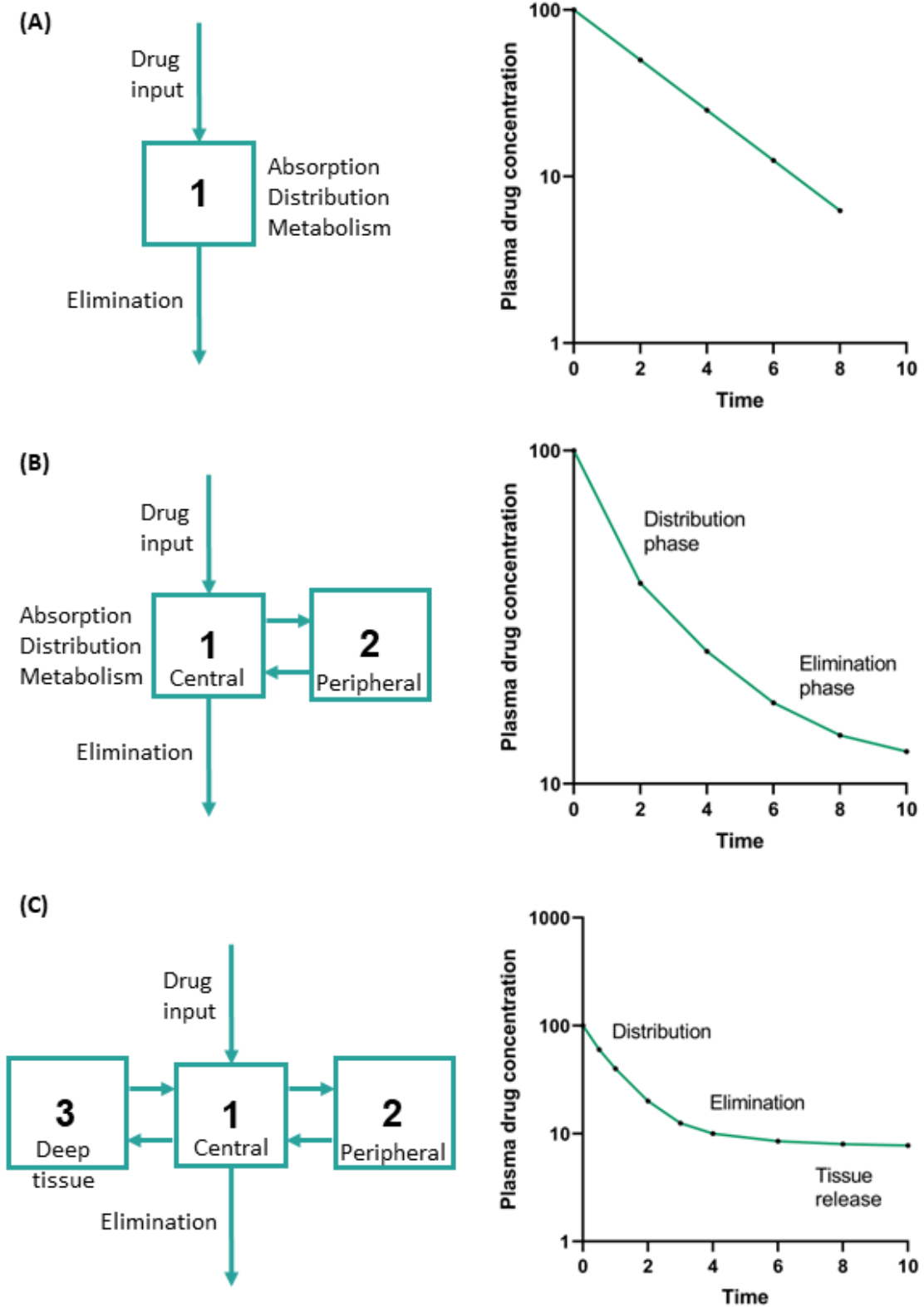


Figure 1.4 Illustration of common compartmental models for intravenous bolus administration with the correlated plasma-concentration profile.

(A) One-compartment model; (B) Two-compartment model; (C) Three-compartment model. All three diagrams showed the three basic compartmental models used to fit the plasma-concentration profile for a single intravenous bolus drug.

1.4 Population pharmacokinetic (PopPK) modelling

Population pharmacokinetics (PopPK) modelling is an empirical or '*top-down*' approach, where plasma concentration data is required for the model development, similar to the classical model. However, the concentration required is less intensive than the non-compartmental and compartmental modelling. Therefore, the data can be sparse and collected from a large number of subjects, with only a few samples needed from each subject, which is commonly applied in the late-phase clinical trial design [28]. In addition, the PopPK can determine and measure the inter-subject, inter-occasion, and intra-subject variabilities that may cause the pharmacokinetics variabilities, and it is commonly performed in patients who have taken different doses at various time periods or other routes of administration instead of healthy subjects [25]. The target is that the optimal dosing strategy for patients can be determined by considering the variabilities. Thus, improving the drug development processes and, ultimately, patient care.

The PopPK analysis studies the population level instead of the individual level. The term PopPK also refers to 'mixed-effect' modelling, which is the mixture of fixed and random effects. For example, parameters such as CL and V_d are fixed effects, and factors that impact those parameters are covariates, such as age, weight, creatinine clearance, comorbidities, comedications, and a few others, while random effects are inter-subject, intra-subject, and inter-occasion variabilities [24]. The random effects represent the distribution of some model elements. The three essential components of the distribution assumptions are (1) the shape of the distribution, (2) the central tendency (mean, median, mode), and (3) the variation of individual distribution value around the central tendency (variance), where the first two assumptions are tested during model development, and the third assumption achieved when the estimation of population variance as a random variable was made [38].

Understanding the concept of individual and population models is essential to ensure the appropriate model is used during the model development. In the individual model, the difference between observed data and the model-predicted data for an individual is minimised, where the error is denoted by ' ϵ ' (Figure 1.5). In contrast, the population model is more elaborate and accounts for variability at the population level, where the variation between individual and population value is denoted ' η ' (Figure 1.5).

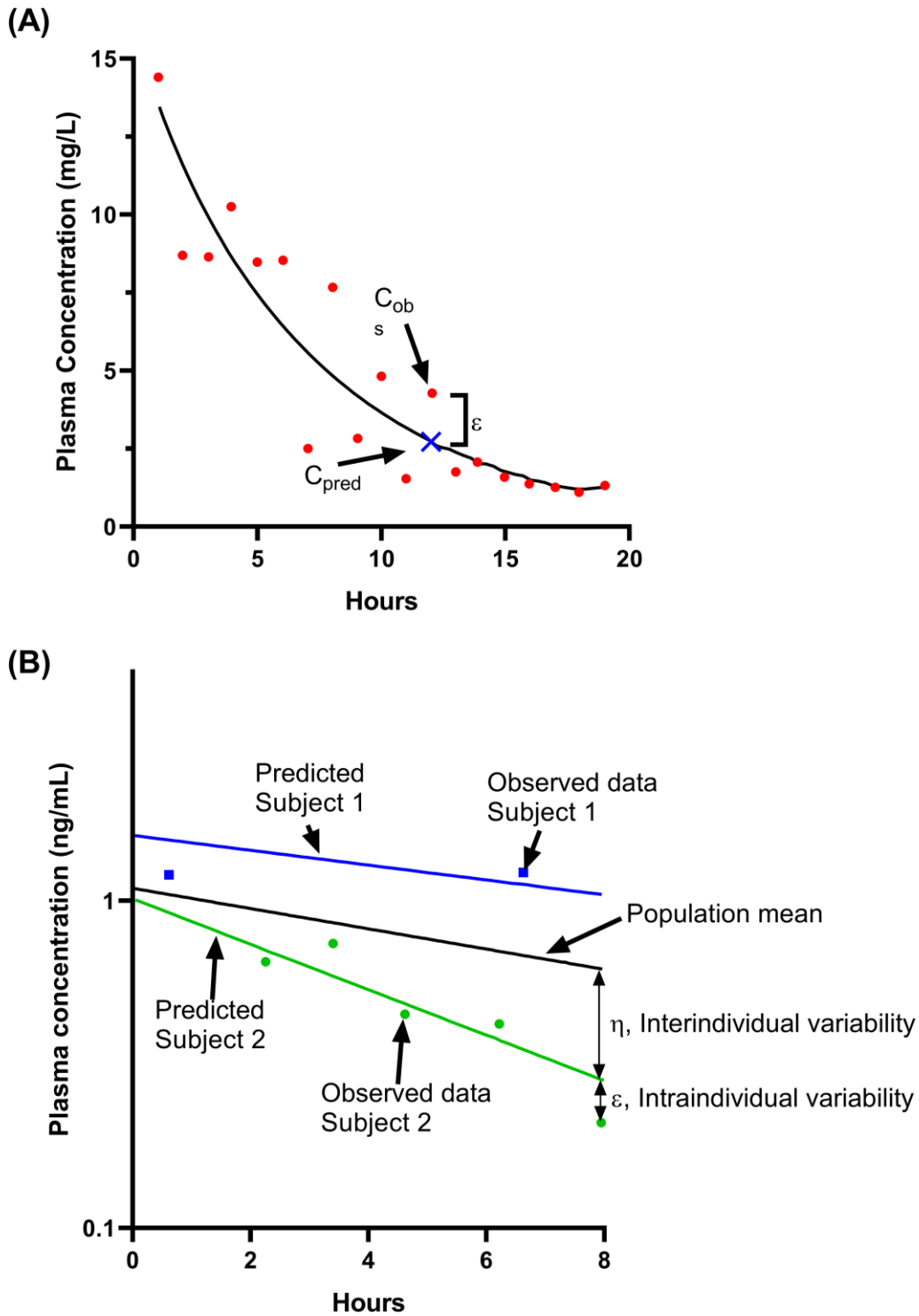


Figure 1.5 Illustration of one-compartment model of concentration-time profile following intravenous bolus administration showing observed and predicted value.

(A) Predicted individual one-compartment model data fit the observed individual data; (B) One-compartment model fit with one population plot, two predicted individual plots and observed data from 2 subjects. Solid circles in (A) represent observed individual data, solid circles in (B) represent observed data of subject 2, and solid squares in (B) represent observed data of subject 1. C_{obs} represent the measured concentrations, and C_{pred} designate predicted concentrations. Adapted from Huang et al. (2021) [37].

There are several methods to perform the PopPK modelling, which include (1) naïve pooled data analysis, (2) naïve average data analysis, (3) two-stage approach, and (4) nonlinear mixed-effects modelling. The naïve pooled and average data require an intense sampling from individual subjects to estimate the population mean, and the inter-subject variability is ignored in the covariance estimation [29]. As for the two-stage approach, there are standard, iterative, and Bayesian methods where typically rich individual data is needed [29]. Among all, nonlinear mixed-effect modelling is commonly used in handling sparse sampling.

Since this thesis focuses on the special populations where concentration samples are typically limited, the PBPK modelling tool was utilised.

1.5 Physiologically based pharmacokinetic (PBPK) modelling

In contrast to PopPK, PBPK modelling is a '*bottom-up*' approach and uses the same mathematical framework as compartmental modelling, namely a series of differential equations to represent a substantial number of compartments. The distinction is that each compartment in PBPK represents different organs and tissues, which are parameterised with the knowledge of physiological variables, and the mechanistic framework can quantitatively describe the absorption, distribution, metabolism, and excretion. The PBPK was introduced in 1937 by Teorell, with one of the earliest applications described by Bischoff et al. (1971) [39] for the pharmacokinetics of methotrexate in mice, rat, and human (Figure 1.6) [27]. PBPK modelling started to grab the attention of pharmaceutical industries when the computational advancement could solve the mathematical complexity to deal with a massive number of parameters as inputs, which is evident from the increasing trend of publications and regulatory acceptance over the past few decades [40].

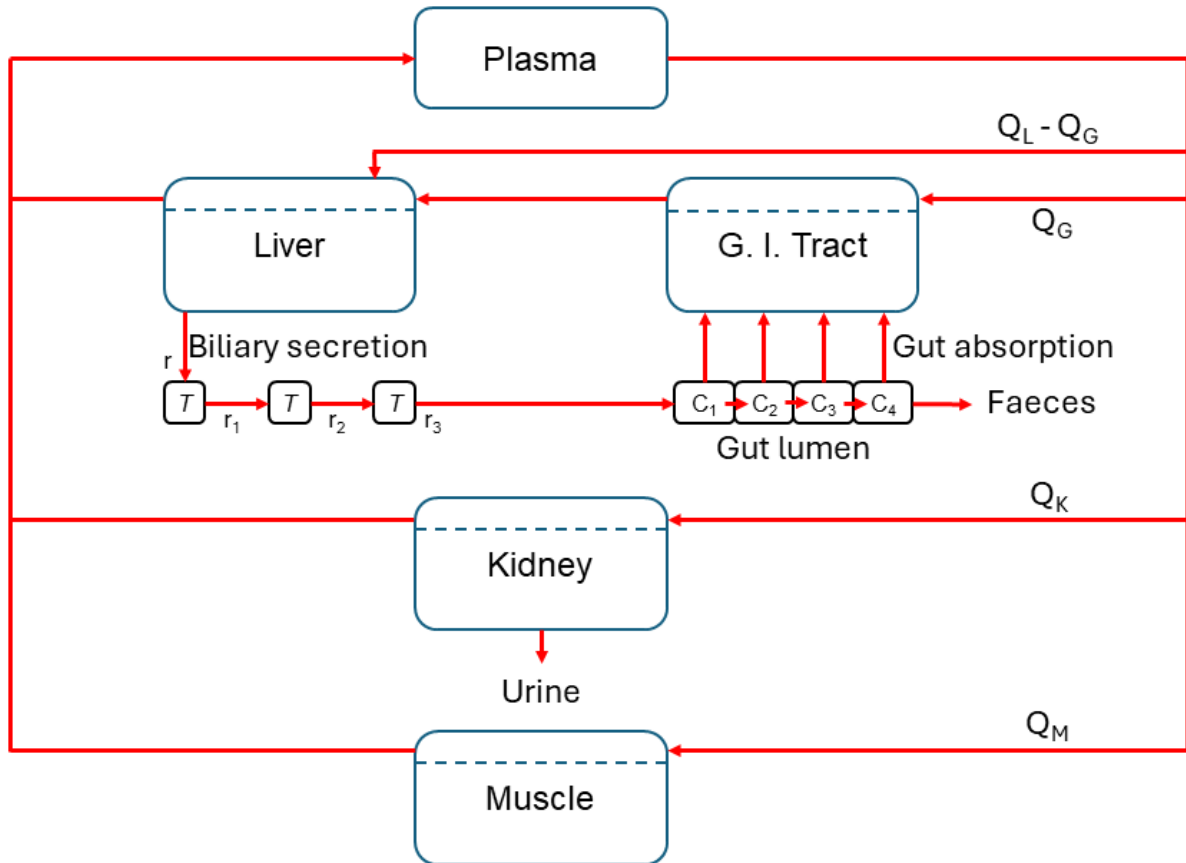


Figure 1.6 Illustration of body compartments for the methotrexate distribution by Bischoff et al. (1971).

Adapted from Bischoff et al. (1971) [39]. G.I., gastrointestinal; Q_L , plasma flow rate to liver; Q_G , plasma flow rate to gastrointestinal; Q_K , plasma flow rate to kidney; Q_M , plasma flow rate to muscle; T , nominal residence time in bile subcompartment; r , drug-transport rate in bile; C , drug concentration.

1.5.1 Fundamentals and concept

Physiologically based pharmacokinetic (PBPK) models are built of many compartments that represent different tissues and organs in the body, such as lung, heart, adipose tissue, brain, gut, liver, kidney, muscle, and others connected by the arterial and venous blood. Furthermore, models can also be specific for certain physiological barrier tissues such as the gut, muscle, and liver (Figure 1.7).

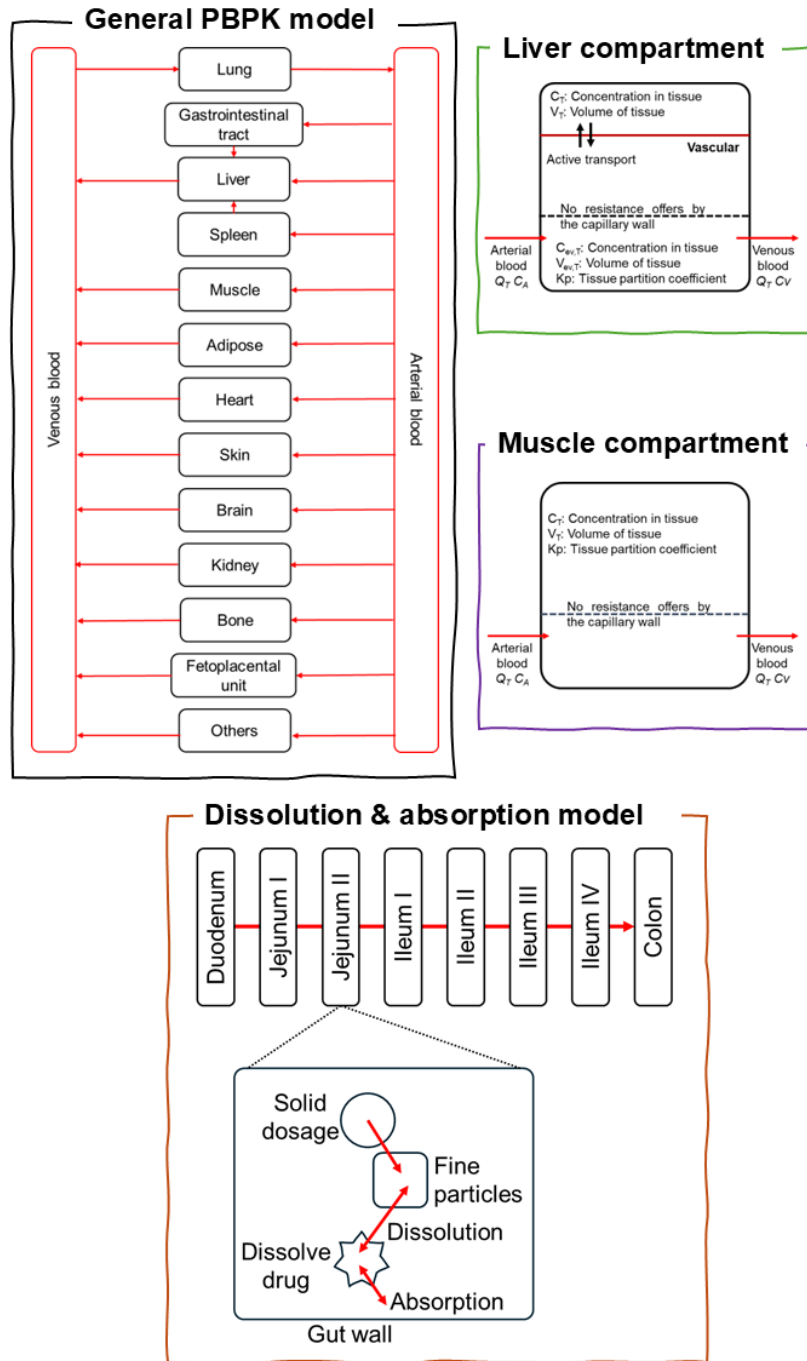


Figure 1.7 Schematic diagram of typical PBPK models.

Adapted from Peters (2021) [41].

The physiological information used for each compartment is grouped under 'system data' defined by the tissue volume or weight and tissue blood flow rate specific to the species of interest. In addition, the data on organ perfusion rate, glomerular filtration rate, transporter, and enzyme abundance are also integrated into the equation and grouped under 'system data' [42]. In order to express the pharmacokinetics of a drug, 'compound data' on the absorption (lipophilicity, solubility, polar surface area (PSA), and hydrogen-bonded donors (HBD)), distribution (octanol to water partition coefficient ($\log P$), ionisation coefficient (pKa), blood to plasma ratio (B/P), and unbound tissue partition coefficients (K_p)), metabolism and elimination (intrinsic clearance) are required to be integrated and to enable the plasma-concentration profiles while considering the variability with the simulated population of interest [27].

1.5.1.1 Assumptions

The tissues and organs' compartments are connected by the circulating blood system, arterial and venous. Thus, each compartment amounts to a volume (V_T) in which the information can be obtained from published literature [42-45]. The blood flow into and out of the compartments is represented by the blood flow rate (Q_T). Drug partitioning into and within the tissue compartments is defined by the K_p , the fraction unbound of drug in plasma (f_{u_p}), and the permeability-surface area metric (PS_T) [27]. Each tissue compartment is assumed to be well-stirred, and the distribution of the drug into the tissue can either be perfusion rate-limited or permeability rate-limited, depending on the compound's physicochemical properties (Figure 1.8).

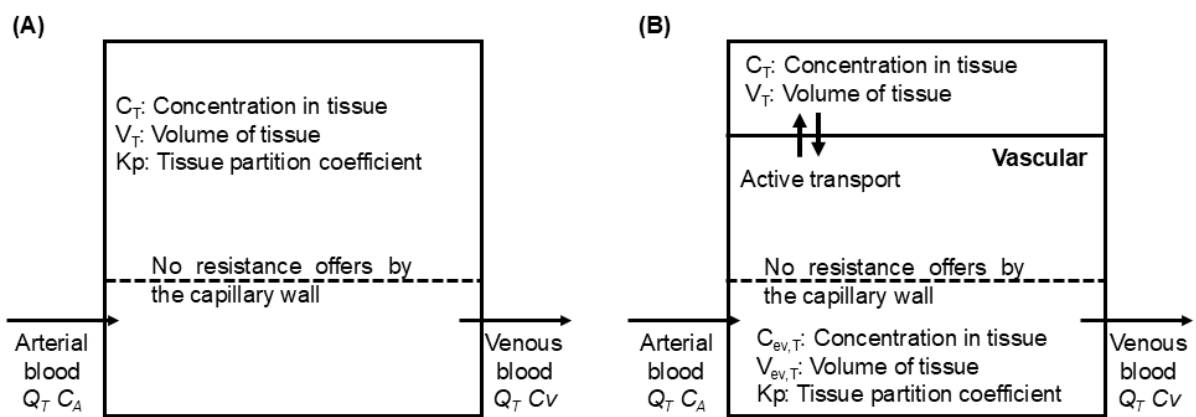


Figure 1.8 Illustration of perfusion vs. permeability rate-limited tissue models

(A) Perfusion rate-limited; (B) Permeability rate-limited. C_A , concentration in arterial blood; C_T , concentration in tissue; C_V , concentration in venous blood; $C_{ev,T}$, concentration in extravascular; $V_{ev,T}$, volume in extravascular.

Perfusion rate-limited processes are those where the blood flow to the tissue is the limiting process, while the permeability rate-limited divides the tissue into extracellular and intracellular spaces separated by a diffusional barrier, which the permeability across this barrier is the limiting process instead of blood flow [27]. Whereas, the perfusion rate-limited model assumes that the total drug concentration in blood and tissue is equilibrium at steady-state, with equal K_p and f_{up} . The time taken to reach the steady-state depends on the V_T , Q_T , and K_p . In contrast, the permeability rate-limited model assumes that at equilibrium, the f_{up} is equal, but the time to reach equilibrium is highly dependent on the compound permeability through the diffusion barrier rather than blood flow [46].

In general, most of the PBPK models assume the tissue compartment is well-stirred and perfusion rate-limited [46]. The use of a perfusion rate-limited assumption is justified for small and lipophilic drugs distributed into organs, and commonly, highly perfused tissue will reach the steady-state faster. On the other hand, the hydrophilic and large molecules, including biologic products, are limited by permeability.

1.5.1.2 System data

The PBPK models for common species such as rat, dog, and human have been published and are incorporated into commercially available PBPK software [42, 46, 47]. In addition, the models can be adapted to simulate pharmacokinetics profiles for special populations such as pregnant women, paediatric, specific ethnicity, and particular disease states such as renal impairment and hepatic impairment [48-51].

The nature of mechanistic models allows the inclusion of physiological and biochemical variability in the system parameters so that pharmacokinetic estimation can be made for the population instead of an individual. Variability is expected in the 'system data' due to inter-individual variability, impacting the pharmacokinetics parameter predictions. Therefore, the variability is incorporated into the models with a defined limit of 30% coefficient variation (CV) [41]. The virtual population can then be generated based on data and formulae considering the demographic, anatomical, and physiological variables using a Monte-Carlo approach that allows for randomness, thus mimicking the variability in the observed data in clinical studies [52]. This *prior* approach provides an opportunity to make a prediction before conducting clinical studies as opposed to the PopPK or statistical approach, which requires clinical data to address the variability.

1.5.1.3 Compound data

The key to prediction success is well-defined compound-specific data on absorption, distribution, metabolism, and elimination.

For absorption, the critical measurement is the permeation of the compound through cell membranes, which is measured as human effective permeability (P_{eff}). The value can be predicted from *in silico* models or *in vitro* studies using either the human epithelial colorectal adenocarcinoma cells (Caco-2) or Madin-Darby canine kidney cells (MDCK-II) [53]. The measurement obtained from the *in vitro* study resulting in apparent permeability (P_{app}) is then needed to scale up to the *in vivo* value using the linear regression that correlates the P_{app} and P_{eff} applied by Sun et al. (2002) [54]. As for the *in-silico* method, quantitative structure-activity relationship (QSAR) parameters such as the number of HBD and PSA are required for the estimation of P_{eff} . The formulae have been used to estimate passive absorption in the human intestine for various drugs [55]. In addition, input on compound solubility and lipophilicity is crucial for a reliable PBPK simulation, as shown by several publications [56, 57].

The key compound parameter for distribution is the K_p value, which characterises the drug's movement into different tissues in the body. The K_p value is a ratio of the total compound concentration in tissue to the total compound concentration in plasma at a steady-state. Commonly, the value is obtained from pre-clinical studies; however, the mechanistic method has been used in recent years due to its cost-effectiveness [58]. The mechanistic approach developed by Poulin and Theil [59], Rodgers and Rowland [60], and Schmitt [61] used the physicochemical properties, *in vitro* data on compound binding characteristics and tissue composition (lipids, proteins, and water) to lipids and proteins such as molecular weight (MW), pKa, f_{up} , and log P to estimate the value. The prediction performance of mechanistic equations showed good accuracy compared to several other methods [62]. However, the mechanistic equation may not be suitable for modelling specific target tissue due to the oversimplification of tissue kinetics.

Hepatic clearance is the parameter of interest for metabolism and excretion. The human hepatic clearance (CL_H) can be predicted from the *in vitro* test using physiological scaling factors based on the type of liver cells used during the *in vitro* assays, either microsomes or hepatocytes [63]. There are advantages and disadvantages of using each cell, such as the isolation of microsomal cells is more straightforward and cost-effective, but the predictability is better with hepatocytes because it contains both phase I and II enzymes [64]. The apparent *in vitro* intrinsic clearance ($CL_{\text{int,app}}$) is then extrapolated to the human hepatic intrinsic clearance ($CL_{\text{int,scaled}}$). The CL_H can then be predicted from the $CL_{\text{int,scaled}}$ value using a well-

stirred liver model or several other models. This approach has been widely used and extensively validated [64, 65].

Regarding renal and biliary excretion, there are various approaches to predict the intrinsic organ clearance for renal and biliary, with some of the methods still evolving and reviewed [27, 46]. However, the most common approach is an allometric-based from one species to another species, described by Mahmood (2012) [66] for biliary excreted drugs and Paine et al. (2011) [67] for renally excreted drugs. Besides, the in vitro-in vivo scaling approach has also been employed for the biliary excreted drug [68].

1.5.2 Model development strategy

A proper strategy is crucial to successfully incorporating all the information on the population system data and compound data for the development of a PBPK model. Typically, there are at least five steps used in the PBPK model development: (1) Specify the general model structure, (2) specify the tissue and organs model, (3) set down the model equation, (4) define the model parameter, and (5) simulation and parameter estimation (Figure 1.9).

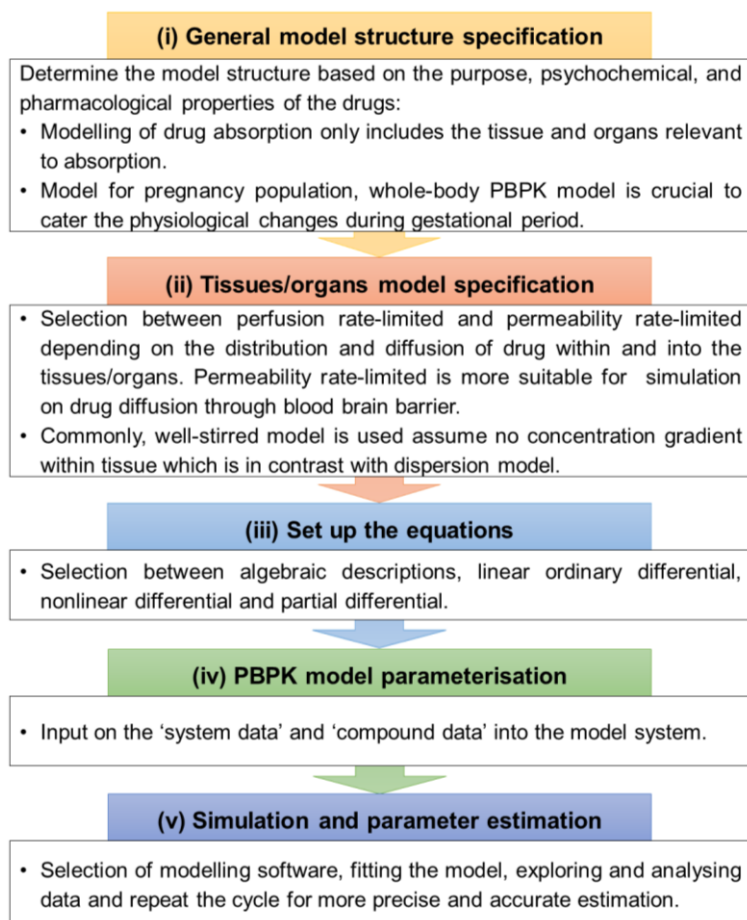


Figure 1.9 General steps to develop a PBPK model

1.5.3 Software

The software used to perform PBPK modelling can generally be divided into specialised software for PBPK modelling and general mathematical programming software. The specialised software is commercially available, such as Simcyp[®] Population-Based Simulator (Simcyp, UK) (<https://www.certara.com/software/simcyp-pbpbk/>), Open Systems Pharmacology consisting of PK-Sim[®] and MoBi[®] (Bayer Technology Services, Germany) (<https://www.open-systems-pharmacology.org/>), and GastroPlus[®] (SimulationPlus, US) (<https://www.simulations-plus.com/software/gastroplus/>). The specialised software is suitable for inexperienced modellers since the software is less flexible for the model development process. In addition, the add-on function of virtual population simulation allowed for the estimation of pharmacokinetics in a special population such as paediatric and pregnancy. The software can also simulate complex pharmacokinetics with multiple metabolites and drug interactions [69, 70]. Nonetheless, the software is still relatively complicated, where a substantial understanding of fundamental pharmacokinetics and clinical pharmacology is required to recognise the various models offered in the software and further determine the appropriate model to be used.

On the other hand, mathematical programming software packages such as MATLAB[®] (<http://www.mathworks.com/products/matlab/>), R software (<https://www.r-project.org/>), and several others provide a programming language platform to model the code, equations, and graphical output to develop the PBPK models. Advanced programming and modelling skills with experience in PBPK modelling are required to successfully develop the PBPK model using this software due to the vast flexibility for creating the model from scratch [69]. For example, the PBPK model built using MATLAB[®] software can be seen in a publication by Lin et al. (2017) [71], which assesses the performance of the PBPK models in the toxicology area and Reali et al. (2023) [72], who developed a minimal PBPK model for the development of an anti-tuberculosis drug to be used in the pre-clinical drug development stage. As for R software, a publication by Rostami et al. (2022) [73] developed a PBPK model using the software assessing nicotine exposure in humans after consumption of nicotine-containing products through various routes, including buccal cavity, upper respiratory tract and lower respiratory tract.

From the software usage perspective, based on the trend over the last two decades, more than 70% of the publications on PBPK modelling were developed using commercial-off-the-shelf software such as Simcyp[®], Gastroplus[®] and PK-Sim[®] [74-76].

1.6 Applications in pharmaceutical product development and regulatory acceptance

Physiologically based pharmacokinetic (PBPK) models have been used throughout the drug development cycle, starting from the early stages of lead compound development when data on the compound is still limited to the late stages when the compound data is plenty. The application of PBPK modelling can start as early as candidate selection, during the transition phase of pre-clinical to clinical, such as determining the safe and optimum first-in-human dose, and at the clinical stages like potential drug-drug interaction assessment, facilitating in clinical trial design, alternative for the need of bioequivalence study and dose recommendation for the special population such as paediatric and pregnant women (Table 1.1) [50, 51, 77-82].

Table 1.1 The application of PBPK modelling throughout drug development stages

Model target	Example
Lead optimisation	<u>Characterisation of a novel, selective dopamine D3 receptor agonist as a potential compound to treat drug addiction in humans:</u> The compound structure gave an early signal that the compound possibly has poor bioavailability. However, the predicted human pharmacokinetics profiles extrapolated from the animal PBPK model utilising in vitro and pre-clinical data proclaim the compound as a promising candidate for human testing [83].
Translation from animal dose to human dose	<u>Prediction of first-in-human dose from pre-clinical data:</u> The plasma concentration profiles for the first-in-human trial of a new non-steroidal progesterone receptor were predicted for a range of doses using the PBPK model combined with the clearance estimation from the intrinsic clearance of in vitro assay from human liver microsomes and dog [84].
Optimisation of clinical trial design	<u>Inclusion of renally impaired patient in a pivotal clinical trial:</u> Estimation of an appropriate orteronel dose for renally impaired patients allows the inclusion of renally impaired patients in the pivotal study. Thus, optimised the trial design and excluded the need for an additional human trial [85].
Drug-drug interaction	<u>Drug-drug interaction modelling of polatuzumab vedotin:</u> Clinical data from brentuximab vedotin, the analogous of polatuzumab vedotin, was used to predict the polatuzumab vedotin drug-drug interaction and support the drug label [86].
Specific population	
Pregnant women	<u>Venlafaxine dosing recommendation in pregnant women:</u> The predicted trough plasma concentration significantly decreased in pregnant women with extensive (EM) and ultrarapid metaboliser (UM) CYP 2D6 phenotypes. Thus, a dosing regimen was simulated for pregnant women with both phenotypes using the PBPK model [87].
Paediatric	<u>Facilitate the development of new hydrocortisone formulations for congenital adrenal hyperplasia (CAH) in adolescents:</u> The PBPK model for hydrocortisone in children with CAH dose prediction in adolescents has assisted in the approval of hydrocortisone modified-release hard capsules by the European Regulatory Authority [88].

Various guidelines issued by regulatory authorities since 2012 on PBPK modelling and the increasing trend in the number of submissions with the PBPK model as supporting documents to USFDA and European Medicines Agency (EMA) since 2008 showed the regulatory confidence in the modelling data to support the regulatory decision [20, 89]. Physiologically based pharmacokinetics (PBPK) modelling data submitted to support regulatory decisions are categorised according to the high, medium, or low impact and assessed according to the therapeutic context and availability of supportive data [90]. High impact submission indicates that the modelling data has a better chance of being accepted for labelling and regulatory decisions, while the medium impact submission is reviewed on a case-to-case basis with a likelihood for regulatory acceptance, whereas low impact submission has a lower chance of regulatory acceptance due to limited experience and substantial knowledge gaps [90]. The main high impact PBPK models are the drug-drug interaction and, in a particular situation, the paediatric population where the modelling data alone will support the drug label, whereas the medium impact stands between the mixture of modelling and clinical data or modelling data to support the clinical trial applications [89-91]. The area of acceptability correlated to the impact level is further summarised in Figure 1.10.

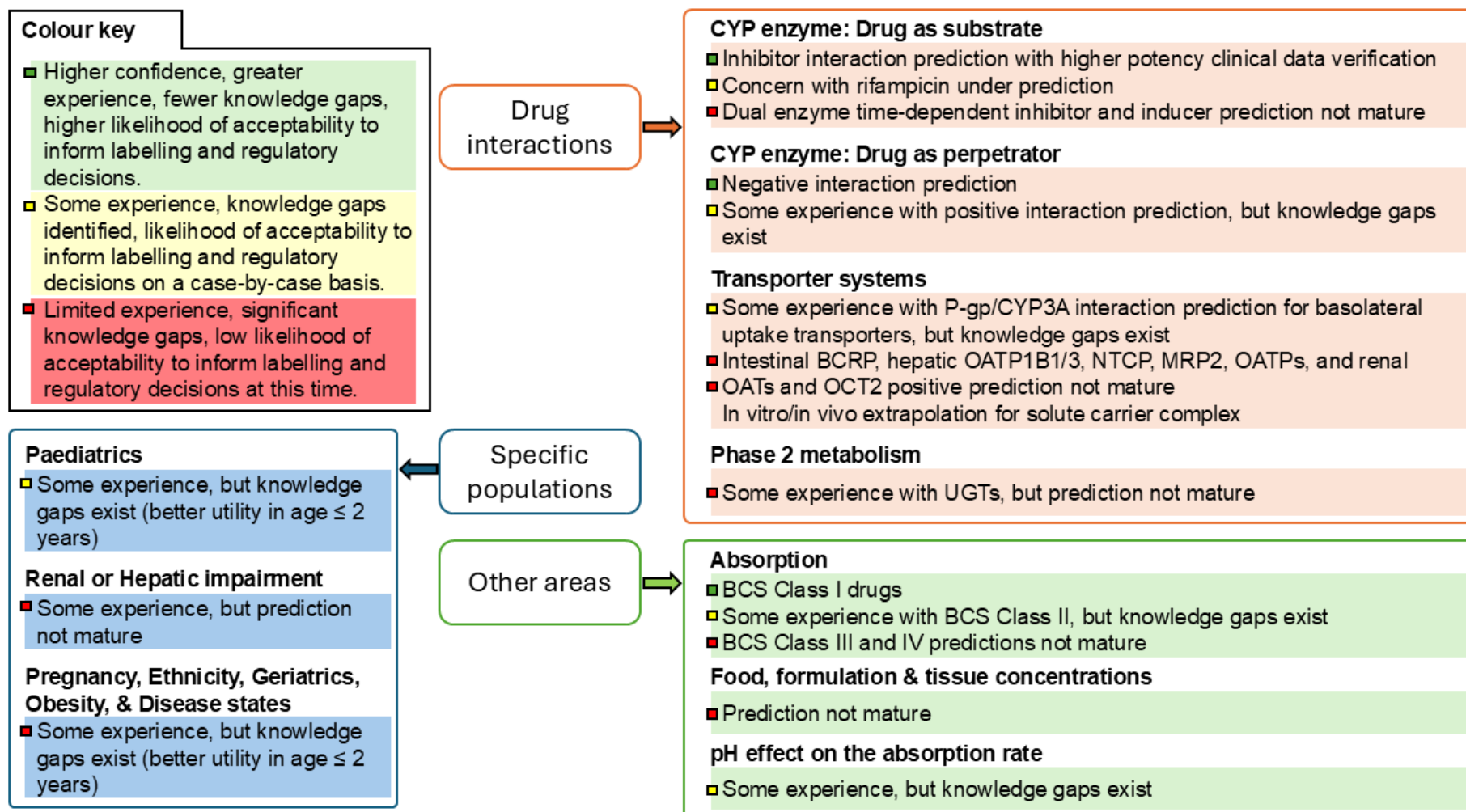


Figure 1.10 The predictive performance on PBPK applications for regulatory submissions.

Adapted from Certara (2019) [92]

The efforts from regulatory agencies to encourage industries to utilise the PBPK modelling and further improve the usage of PBPK modelling to support regulatory decisions can be seen in several initiatives. For example, the USFDA has awarded a grant for research in complex generics, where one of the focus areas is to implement the PBPK modelling to support generic product registration [93]. The outcome can be seen in the approval of generic diclofenac sodium topical gel (1%) with PBPK modelling data, replacing the need for a comparative clinical endpoint study [94]. On the other hand, a grant was awarded to the Medicines and Healthcare Products Regulatory Agency (MHRA), United Kingdom, to work on the PBPK modelling for the pregnant population, which resulted in at least two publications and a workshop on pregnancy PBPK modelling [95-97].

Moving to the other side of the world, the Pharmaceuticals and Medical Devices Agency (PMDA), a Japanese regulatory agency, has received 17 product submissions in the year 2014 to 2016 that were supported with PBPK modelling data, with 48% of it in the drug-drug interaction area [98]. Furthermore, in 2021, PMDA issued a guideline for the analysis reports involving PBPK models, which further showed that PBPK modelling is accepted across the globe as one of the tools in advancing the drug development process [99]. On top of that, a presentation during a workshop on MIDD organised by PMDA in March 2021 described several initiatives taken by PMDA in modernising the reviews on modelling and simulation, such as the development of the project team within PMDA and the analysis of the accumulated electronic study data submission to improve regulatory decision across various therapeutic areas and products [100].

In terms of harmonisation of regulatory standards for the MIDD among various regulatory authorities across all continents, the works have been going on under the International Council for Harmonisation of Technical Requirements for Pharmaceuticals for Human Use (ICH) with the issuance of various guidelines that are related to a particular area of MIDD such as dose-response studies, ethnic factors, clinical trials in paediatrics, drug interaction studies and several others [101]. Currently, the ICH is working on MIDD general principles guidelines to harmonise the regulatory standards of MIDD practice and reports for regulatory submission and further optimise the utilisation of MIDD approaches in drug development and the regulatory decision-making process [102].

1.7 Physiologically based pharmacokinetic (PBPK) in special populations

The flexibility of PBPK models on the population 'system data' can be exploited to simulate populations that undergo a significant ontogeny change in a specific period, such as paediatric, pregnant women and cancer patients. The input on physiological and biochemical changes during a particular duration of months or years, integrated with 'compound data,' enables simulation to be made to see the impact of those changes on the pharmacokinetics of medicines.

1.7.1 Pregnant women

The anatomical, physiological, and biochemical changes that occur during the gestational period are complex and have been reported to impact drug pharmacokinetics. Generally, the changes throughout pregnancy are viewed according to trimesters, where 1st trimester is from 0 to 12 gestational weeks, 2nd trimester is from 13 to 27 gestational weeks, and 3rd trimester is from 28 gestational weeks to full-term (38 to 40 gestational weeks). This classification is based on the foetal growth as well as the physiological and physical changes of the pregnant women. As for PBPK modelling, the changes are captured across the gestational period based on various published literature [43, 103].

The physiological changes with the potential impact on the drug pharmacokinetics are described in Table 1.2. Besides, changes in body weight, body surface area (BSA), eating habits, comorbidities, and others during pregnancy may also impact drug administration, metabolism, distribution, and excretion. The combination of all factors may lead to the need for dosing adjustment for certain drugs to maintain the drug efficacy throughout the gestational period [104]. A review article reported that the compounds which are extensively metabolised by hepatic enzymes and with the liver as the primary elimination route might require dose adjustment in order to maintain the same exposure and effect throughout the duration of pregnancy [51].

Table 1.2 Physiological changes during pregnancy and potential impact on drug pharmacokinetics^a.

Physiological changes in pregnancy	Impact on pharmacokinetics
Absorption	
<ul style="list-style-type: none"> • Increased gastric pH • Decreased intestinal motility • Altered metabolic enzyme • Increased transporter expression (P-gp) 	<ul style="list-style-type: none"> • Increased absorption of basic drugs • Reduced drug absorption • Changes the bioavailability • Reduce bioavailability
Distribution	
<ul style="list-style-type: none"> • Increased maternal body fat • Increased body water, plasma, and blood volume • Changes in protein binding • Decreased plasma protein concentration (albumin, α-acid glycoprotein) 	<ul style="list-style-type: none"> • Increased or decreased in the volume of distribution depending on the type of drug, either lipophilic or hydrophilic • The changes in the unbound fraction of drugs may impact the intrinsic clearance
Metabolism	
<ul style="list-style-type: none"> • Increased enzyme activity (CYP3A4, CYP2D6, CYP2C9, UGT1A4, UGT1A9) • Decreased enzyme activity (CYP1A2, CYP2C19) • Increase hepatic blood flow 	<ul style="list-style-type: none"> • Decreased the concentration of metabolism substrate • Increased the concentration of metabolism substrate • Increased hepatic clearance
Excretion	
<ul style="list-style-type: none"> • Increased renal blood flow • Increased glomerular filtration rate (GFR) • Increased transporter expression (OCT2, OAT1, P-gp) 	<ul style="list-style-type: none"> • Increased clearance for renally excreted drugs

^a Compilation from several published references [43, 105-107].

P-gp, P-glycoprotein; CYP, cytochrome P450; OCT, organic cation transporter; OAT, organic anion transporter

The physiological changes that occur during pregnancy, including the body weight and hepatic metabolism enzymes, have been incorporated in the PBPK commercial software with an addition of a foetoplacental unit on the basic structure [43, 105]. The pregnancy PBPK model structure for the three leading PBPK software is illustrated in Figure 1.11. The Open Systems Pharmacology software includes the foetoplacental compartment and separates the unit into the placental, amniotic fluid, and foetus [108]. As for the Simcyp[®], the unit consists of the placenta, foetus, umbilical cord, membrane, and amniotic fluid, with the uterus and mammary glands integrated into the maternal muscle compartment [105]. For Gastroplus[®], the unit includes the foetus, uterus, placenta, and amniotic fluid [109].

Reviews by Abduljalil et al. (2020) [51] showed that the simulation of the drug's pharmacokinetics during the gestational period using pregnancy PBPK modelling had been developed for at least 46 drugs. In addition, several recent publications on pharmacokinetic predictions during pregnancy using the PBPK modelling approach on several other compounds, such as metronidazole and venlafaxine, further added the number of compounds, thus improving the confidence in using the pregnant women population model to predict drug exposure during the gestational period and enhance the trust to rely on PBPK model prediction [87, 110].

The pregnancy PBPK modelling is considered low-impact in terms of the likelihood of supporting the regulatory decision due to a significant information gap needed for the model qualifications [90, 97]. For model qualifications, input on the 'system data' needs to be verified with simulation on another compound with similar distribution and elimination behaviour as the drug of interest [97]. Thus, drugs with complex distribution and elimination processes involving various enzymes and transporters may need a considerable amount of data for model qualification. Nevertheless, ongoing efforts to improve the accuracy and precision of pregnancy simulation will boost regulatory confidence with the aim of providing a high-impact regulatory decision.

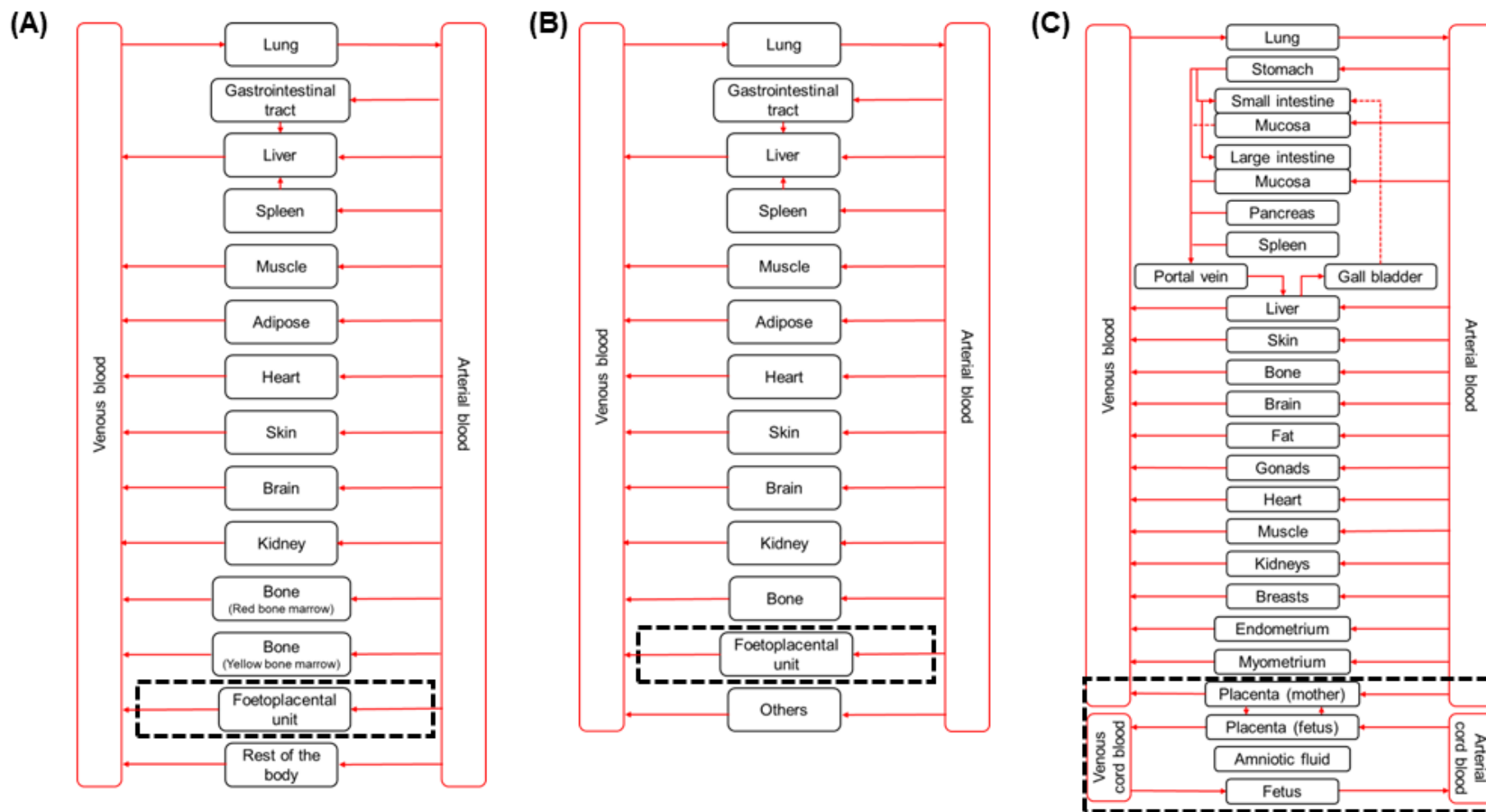


Figure 1.11 Illustration of the pregnancy PBPK models in (A) Gastroplus®, (B) Simcyp®, and (C) Open Systems Pharmacology

Dashed lines indicate the foetoplacental compartment. Adapted from Chaphekar et al. (2020) [111]

1.7.2 Adults with obesity and cancer

Recognised as a global health crisis, obesity presents a staggering prevalence of more than 2.6 billion in 2020 and is projected to soar beyond 4 billion by 2035 worldwide [112]. Obesity has been linked to major chronic diseases, such as diabetes, hypertension, cardiovascular disease, mental illness, and several others [113, 114]. Furthermore, literature has reported that obesity increases the risk of cancers, one of the leading causes of death in 2019, with approximately 10 million deaths occurring worldwide in 2020 [115, 116].

The physiological alterations that occur in obese and cancer patients are intricate and known to change the drug pharmacokinetics. Various guidelines and systematic reviews were published to address the dose adjustment that needs to be made for each population, with obese patients on the dosing guidance on antimicrobial agents [117] and several other medications [118] and cancer patients with dosing adjustment for voriconazole [119], opioids for pain treatment [120], and several other medications [121, 122]. The interplay with both obesity and cancer further complicates the physiological changes that are inherently complex in each population. The pharmacological alterations in obese and cancer populations that influence drug pharmacokinetics include tissue composition, plasma proteins, renal functions, and metabolism enzymes [123-125]. The physiological alternations that manifest in obese and cancer populations are summarised in Table 1.3.

Considering the complex physiological changes in adults with obesity and cancer population and the impact on drug absorption, distribution, metabolism, and excretion, dealing with the dosing adjustment requires a critical consideration. Furthermore, most antineoplastic agents are administered according to body size, such as weight and BSA, the primary physiological changes in obesity [126, 127]. The body-size-based dosing schedules have led to various practices in deciding the chemotherapy dose in obese patients, including using ideal body weight (IBW), adjusted IBW, or capping the BSA at 2.0 m² to ensure an optimum dose is administered and avoid toxicity [128, 129].

Several dosing guidelines for antineoplastic agents in cancer patients with obesity have been published, for example, Appropriate Chemotherapy Dosing for Obese Adult Patients With Cancer: American Society of Clinical Oncology (ASCO) Clinical Practice Guideline in 2012 [126] and the update in 2021 [10], Antineoplastic dosing in overweight and obese cancer patients: an *Associazione Italiana Oncologia Medica (AIOM)/ Associazione Medici Diabetologi (AMD)/ Società Italiana Endocrinologia (SIE)/ Società Italiana Farmacologia (SIF)* multidisciplinary consensus position paper in 2021 [127], and several other guidelines for specific condition, such as patient undergoing haematopoietic cell transplantation [130, 131].

Table 1.3 Summary of physiological changes in obese and cancer adults

	Obese	Cancer
Anatomy and physiology		
Weight	Increase	No change
Organs		
Blood flow	Increase	No change
Weight	Increase	No change
Plasma protein bindings		
Albumin	No change	Decrease
α 1-acid glycoprotein (AGP)	Increase	Increase
Blood component		
Haematocrit	No change	Decrease
Hepatic metabolism enzyme		
Phase 1 metabolism	Increase or decrease depending on enzymes.	Increase or decrease depending on enzymes.
CYP3A4	Decrease	Decrease
CYP2E1	Increase	Inconclusive
CYP1A2	Inconclusive	Decrease
CYP2C19	Inconclusive	Decrease
Phase 2 metabolism	Lack of information	Lack of information
Renal clearance		
Glomerular filtration rate (GFR)	Increase	Abnormal renal function is higher in cancer patients.

Information in the table was available from Ghobadi et al. (2011) [124], Launay-Vacher et al. (2007) [132], Janus et al. (2010) [133], Cheeti et al. (2013) [125], and Schwenger et al. (2018) [134]. Phase 1 metabolism involves reduction, oxidation, or hydrolysis reactions and is catalysed by cytochrome P450 (CYP) enzymes. Phase 2 metabolism involves conjugation reactions and is catalysed by several enzymes such as UDP-glucuronosyltransferases (UGTs), sulfotransferases (SULTs), or glutathione S-transferases (GSTs).

From the absorption, distribution, metabolism, and excretion perspective, the impact depends on both the drug characteristics and physiological alterations.

With respect to absorption, the change in gastric emptying and gut perfusion might influence the absorption of drugs that are administered orally, such as tyrosine kinase inhibitors (TKIs), while the change in the mass of adipose tissue and the blood flow to subcutaneous tissue may impact the absorption of antineoplastics that are administered subcutaneously [135].

In terms of distribution, the change in body fat composition, blood flow and plasma protein binding components from the physiological side of the obese cancer population, together with the lipophilicity and binding status of the compounds, are the main determinants influencing drug distributions [136-138]. For example, imatinib, one of the TKIs, is highly bound to AGP, which is reported to increase in both obese and cancer patients and, thus, expected to lower the total amount of free drug in plasma [138, 139].

The metabolism primarily takes place in the liver and is subjected to phase I and phase II metabolism. Information on various CYP enzyme activities that regulate phase I metabolism in adults with cancer and obese populations is still limited, with only CYP3A4 being reported to decrease in both cancer and obese populations [124, 134]. As for phase II metabolism, the information is limited (Table 1.3). In addition, an increase in blood flow to the liver and an increase in liver size may influence drug metabolism.

With respect to elimination through urine, compounds such as carboplatin, cisplatin and others, in which dosing adjustment is needed in renal-impaired patients, may also be affected in obese cancer patients [133, 140]. An increase in GFR has been reported in obese patients, while data for the cancer population is still lacking [141, 142]. Nevertheless, a higher percentage of renal insufficiency has been reported in the cancer populations, which will affect the drugs that are renally excreted [132, 133].

The flexibility to input population system data in PBPK modelling is able to address the dose adjustment that might be needed in adults with obesity and cancer population. To date, the utilisation of PBPK modelling to assess the necessity for dose adjustment of any drug in adults with obese and cancer populations is yet to be explored. Therefore, chapter 3 of this thesis focuses on the application of PBPK in imatinib dose optimisation in the adult obese cancer population.

1.7.3 Paediatric populations

According to ICH, paediatric populations are classified into five different age classes;

- preterm newborn infants,
- term newborn infants (birth to 27 days),
- infants and toddlers (28 days to 23 months),
- children: two to 11 years old,
- adolescents: 12 to 16-18 years old (depending on region).

To a certain extent, the classification is arbitrary, and the growth and developmental issues across different group classes may significantly overlap [143]. In addition, the physiological, cognitive, organ maturation, and psychosocial changes across the age classes are non-linear, particularly from newborns to children [144].

The 'system data' for paediatrics based on different age classes have been compiled by Edginton et al. (2006) [144], which include the body weight, height, portal blood flow, organ blood flow, cardiac output, total blood volume, total body water, extracellular water, total lipid, and total protein. The information is classified according to age and simulated using five compounds with different physicochemical properties, which results in acceptable predicted performance. Furthermore, the information has been incorporated into the main commercially available software such as Gastroplus[®], Simcyp[®], and PK-sim[®] [144-147].

The USFDA has broadly classified the MIDD application in paediatrics into three categories: (1) dose selection and optimisation, (2) informing clinical trial design, and (3) leveraging knowledge for bridging the gap [148]. As for PBPK, paediatric population simulation is the 2nd highest area (15%) after drug-drug interaction submitted to support regulatory decisions based on submissions between 2008 and 2018 [20]. The primary use of paediatric PBPK modelling in supporting regulatory decisions is to recommend the initial dose for clinical trials involving new chemical entities, and the utilisation is expanding with recent evidence revealing that a dosing recommendation was made, replacing the need for a clinical endpoint study [20, 148, 149].

In addition, the USFDA has suggested the 'integrate-simulate-optimise' workflow to apply the MIDD in the paediatric population, and this workflow has been accepted to facilitate regulatory decisions (Figure 1.12) [148]. The paediatric PBPK modelling is considered high- to medium-impact for regulatory submission depending on the purpose of the modelling, where the application to determine the clinical trial dose and design stays at a medium-impact level, while any recommendation made for a label which replaces the need for human trial is a high-impact application with better simulation made for paediatric age two years old and above [50, 90].

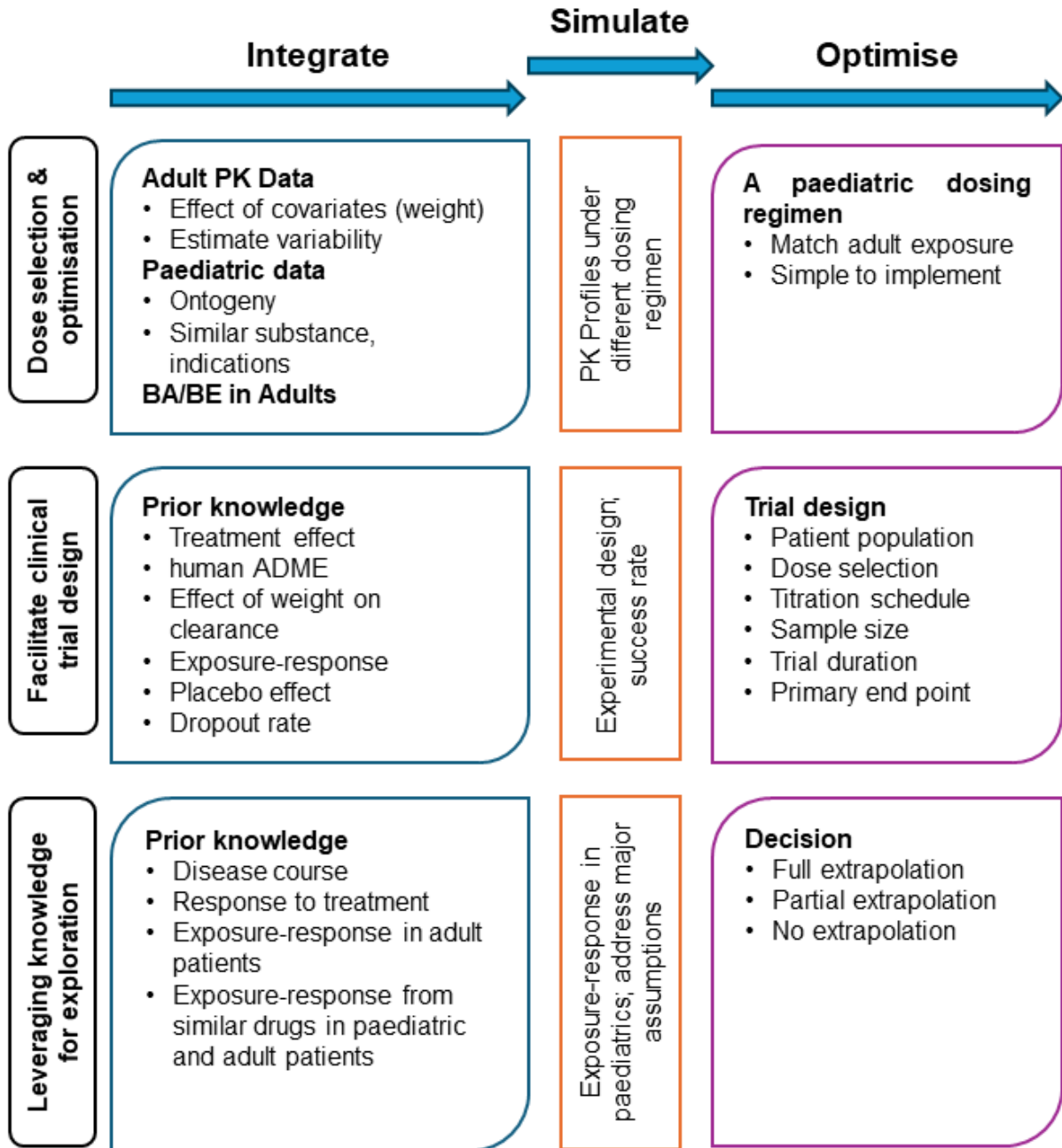


Figure 1.12 Recommended workflow when applying MIDD in paediatric drug development.

Adapted from Bi et al. (2019) [148]. BA, bioavailability; BE, bioequivalence; PK, pharmacokinetic.

The nature of mechanistic pharmacokinetic modelling with the broad scope for application in the paediatric population warrants further exploration to improve the confidence in estimation, thus increasing the number of drugs licensed for paediatric use. In addition, the model can be expanded to predict drug exposure in paediatric with obesity population, one of the special populations under exploration in this project.

1.7.3.1 Paediatric obesity

The increasing trend of obesity among children and adolescents worldwide over the past decade has led to various consequences, such as elevated susceptibility to develop non-communicable diseases [150, 151]. Physical alteration in obesity is known to affect the drug pharmacokinetics, and the complexity intensifies in paediatrics due to the interplay between age-related ontogeny and obesity-related factors. The classification of childhood obesity is based on the BMI-to-age chart as defined by the WHO and the Centre for Disease Control and Prevention (CDC), respectively. The WHO defined childhood obesity as BMI above the +3 standard deviation (SD) for ages 0 to 5 and +2 SD for ages 5 to 18, while the CDC define it as above the 95th percentile of the BMI-to-age curve [152, 153].

The foundation of BMI calculation is weight and height, the primary physical alterations that occur in paediatric obesity. These correlate with an increase in total body fat and lean body mass, which influence drug distribution. These changes and the drug's lipophilicity and hydrophilicity influence the volume of distribution (V_d) [154]. In addition, the increase in weight and size also relates to an increase in plasma and tissue volume, which correlates to a rise in cardiac output, thus potentially positively influencing the V_d [155]. Moreover, the plasma protein binding components, such as serum albumin and α 1-acid glycoprotein (AGP), also impact the drug V_d . Nevertheless, the literature suggests no difference in plasma protein binding components between obese and non-obese children [156, 157]. The same has been reported for the composition of haematocrit in plasma, which was unaffected by obesity [156].

As for drug clearance through the liver, the data on hepatic metabolism enzymes and transporter activities in paediatric obesity is still limited [158]. Nevertheless, the liver size and blood flow to the liver were reported to be larger and higher in paediatric obesity, influencing the hepatic clearance in obese children [156, 159]. For renal clearance, the main parameter of interest is the glomerular filtration rate (GFR), which has been reported to increase by 12 – 29% in children with obesity [156, 160]. In addition to the rise in GFR, an increase in kidney size will influence drug clearance, especially for drugs that are significantly eliminated through the renal route [158]. The physiological changes due to obesity that occur in both adults and children relevant to drug pharmacokinetics are summarised in Table 1.4.

Table 1.4 Summary of physiological changes in obese adults and children

	Adults	Paediatrics
Organs		
Blood flow	Increase	Increase
Weight	Increase	Increase
Plasma protein bindings		
Albumin	No change	No change
α 1-acid glycoprotein (AGP)	Increase	No change
Hepatic metabolism enzyme		
Phase 1 metabolism	Increase or decrease depending on enzymes.	Information is limited.
Phase 2 metabolism	Information is limited.	Information is limited.
Renal clearance		
Glomerular filtration rate (GFR)	Increase	Increase

Information in the table was available from Gerhart et al. (2022) [156], Ghobadi et al. (2011) [124], Chagnac et al. (2000) [141], and Iyanagi et al. (2007) [161]. Phase 1 metabolism involves reduction, oxidation, or hydrolysis reactions and is catalysed by cytochrome P450 enzymes. Phase 2 metabolism involves conjugation reactions and is catalysed by several enzymes such as UDP-glucuronosyltransferases (UGTs), sulfotransferases (SULTs), or glutathione S-transferases (GSTs).

Contemporary dosing strategies employed in paediatric obesity populations have highlighted that over 60% of medications given to obese children resulted in plasma concentrations that fall outside the therapeutic range and exhibit clinically significant changes in drug pharmacokinetics [162]. Furthermore, there are various dosing strategies for paediatric obesity, with the standard approach applied in clinical practice based on body weight, such as total body weight (TBW) and ideal body weight (IBW), or based on body size, such as BSA [163]. More complex dosing strategies for paediatric obesity, which require special skills, have also been presented in the literature, such as allometric scaling, clearance-based scaling, and PBPK modelling [164].

Focusing on the PBPK modelling, the advantage of considering the changes of physiological parameters in obese children coupled with compound data has been applied in verifying the current dosing approach for paediatric obesity and proposing a new dosing regimen [156]. To date, the PBPK modelling has been implemented for paediatric obesity on metformin, midazolam, clindamycin, trimethoprim, sulfamethoxazole, fentanyl, methadone and midazolam compounds [156, 165-167].

1.8 Aims and objectives

This thesis aims to demonstrate the application of PBPK modelling in illustrating the influence of physiological changes in special populations on drug pharmacokinetics profiles and identifying the optimal dose to compensate for the exposure differences.

The general aim was fulfilled by employing the PBPK modelling techniques in three special populations:

- i. *Chapter 2: Pregnant women population treated with fluvoxamine:*
 - To evaluate the impact of pregnancy on maternal and foetal fluvoxamine plasma concentrations.
 - To elucidate the influence of CYP2D6 polymorphism on maternal and foetal concentrations.
 - To identify the optimum dosing regimen for pregnant women throughout gestation, considering the CYP2D6 phenotype status.

- ii. *Chapter 3: Obesity and its impact on imatinib pharmacokinetics in the cancer population:*
 - To delineate differences in physiological parameters between lean, overweight, and obese cancer populations.
 - To assess the influence of obesity on the imatinib concentrations in the adult cancer population.
 - To evaluate the effectiveness of TDM-guided dose adjustment to restore the imatinib trough concentrations into the target concentration level in lean, overweight, and obese cancer populations.

- iii. *Chapter 4: Paediatric obesity population with a case study of amlodipine:*
 - To develop and validate the paediatric obesity population model.
 - To address the influence of obesity on amlodipine pharmacokinetics in paediatrics.
 - To identify the dosage modification required for amlodipine in obese paediatric to attain the same exposure as non-obese paediatric.

CHAPTER 2 - Optimising fluvoxamine maternal/foetal exposure during gestation: A pharmacokinetic virtual clinical trials study

Disclaimer

This chapter has been published as follows:

Burhanuddin, K. and Badhan, R. Optimising Fluvoxamine Maternal/Foetal Exposure during Gestation: A Pharmacokinetic Virtual Clinical Trials Study. *Metabolites*, 2022. 12(12):1281.

DOI: 10.3390/metabo12121281

2.1 Introduction

The rates of pregnant women diagnosed with depression have been reported as high as 25%, with a higher prevalence in the second and third trimesters [168-170]. Proper treatment is vital because poor management may lead to a myriad of complications for the mother and the foetus, such as malnutrition due to poor diet, preterm deliveries, foetal growth retardation, and miscarriages [171]. Thus, ensuring the optimisation of doses through gestation is essential; accordingly, plasma concentration levels are used as a guide in this respect [172]. In terms of the treatment selection, the use of selective serotonin reuptake inhibitors (SSRI) such as fluoxetine, fluvoxamine, paroxetine, sertraline, citalopram, and escitalopram has increased over the years from 1.5% in 1996 to between 3 – 6% in the last decade [173, 174].

Fluvoxamine is used for the treatment of several conditions, such as major depression, obsessive-compulsive disorder (OCD), and social anxiety disorder. In addition, fluvoxamine has also been used in an off-labelled manner for various indications, such as post-traumatic stress disorder (PTSD), panic disorder, binge-eating disorder, and others [175-178]. Before the Pregnancy and Lactation Labelling Final Rule (PLLR) was implemented by the United States Food and Drug Administration (USFDA) in 2015, fluvoxamine was in category C of pregnancy risk based on the adverse effects noted in the foetus in a non-clinical study on pregnant rats, but no adequate information in humans was presented in order to draw conclusions from the findings [6, 179]. This has been updated to highlight that no clear associated risk of significant congenital disability or miscarriage was linked with fluvoxamine usage based on several human observational studies [180].

In the context of the post-natal period, SSRIs have been reported to lead to Post Natal Adaptation Syndrome (PNAS), in which case they cross the placenta, and this traversal may result in increased concentrations in the developing foetus, thus impacting foetal respiratory, cardiovascular, and neurological development [181-183]. Unfortunately, information on fluvoxamine's efficacy and plasma concentrations in the pregnant population is lacking, particularly with respect to a large-scale and well-controlled trial, which may be due to the ethical and safety concerns surrounding recruiting pregnant women as subjects. However, despite this lack of information, a study by Westin et al. (2017) [184] highlighted that fluvoxamine plasma concentrations significantly drop in the third trimester, possibly leading to ineffective treatment. However, further research is needed due to the small amount of data. In addition, the impact of pregnancy on fluvoxamine plasma concentration levels suggests the need to explore the dosing regimens in the pregnant population.

Cytochrome P450 2D6 (CYP2D6) is a highly polymorphic drug-metabolism enzyme and is the primary hepatic enzyme responsible for fluvoxamine metabolism, with fluvoxamine acid being

the major metabolite that is inactive and excreted through urine [185]. In this respect, a physiologically based pharmacokinetic (PBPK) simulation showed that dose increments are required for paroxetine, an antidepressant metabolised primarily by the same hepatic enzyme, in order to maintain the plasma concentration within the therapeutic window during gestation [186]. This result relates to an analysis of therapeutic drug-monitoring (TDM) services by Westin et al. (2017) [184], which showed that the fluvoxamine dose needs to be doubled to maintain the same plasma concentration as the prenatal period based on a linear mixed model analysis. However, the model was developed without considering the physiological changes that occurred throughout pregnancy and different CYP2D6 phenotypes.

The advancement of PBPK modelling with respect to simulating virtual clinical trials has provided a platform for addressing the scarcity of pharmacokinetic data, particularly in special populations such as pregnant women [51, 186-191]. The physiological changes that occur during pregnancy are complex and include changes in cardiac output, plasma volume, body fat, protein binding, hepatic enzyme processes, and the glomerular filtration rate, which can impact drug distribution and excretion and may necessitate dosing adjustment to maintain a drug's effectiveness [104, 192-195]. The application of PBPK and virtual clinical trials in guiding the dose selection for the pregnant population has been applied for at least 46 compounds, of which 33 compounds showed that dose adjustment might be needed, particularly for the drugs that were metabolised extensively by hepatic enzymes [51].

Due to a paucity of fluvoxamine-related pharmacokinetic data on the pregnant populations, this study, for the first time, applied the concept of PBPK and virtual clinical trials in assessing the influence of pregnancy on both maternal and foetal fluvoxamine plasma concentrations. Furthermore, a dosing regimen has been identified for pregnant women considering the CYP2D6 phenotype status to maintain the plasma concentration within the therapeutic window during the perinatal period. This study aimed to utilise the concept of mechanistic, pharmacokinetic modelling and virtual clinical trials to: (1) evaluate the impact of gestational changes on fluvoxamine maternal and foetal concentration levels; (2) elucidate the influence of CYP2D6 polymorphism on maternal and foetal concentrations; and (3) determine the optimal dosing adjustment strategy considering the CYP2D6 phenotype status throughout gestation.

2.2 Methodology

This study used the PBPK modelling tool, Simcyp® Version 20 (Simcyp Ltd., Certara, Sheffield, UK), to develop and conduct virtual clinical trials on both healthy and pregnant subjects.

The Simcyp Simulator implements a minimal or full-body PBPK model. The former is a “lumped” four-compartment model and considers systemic, portal vein, and liver concentrations with the addition of a “single adjusting compartment” representing a lump of all tissues except for the liver and portal vein. The full PBPK model is a generic, whole-body, 14-compartment model with the ability to incorporate additional compartments, such as a foetal-placental unit during pregnancy.

A four-step workflow was implemented to develop, validate, and simulate studies involving fluvoxamine (Figure 2.1).

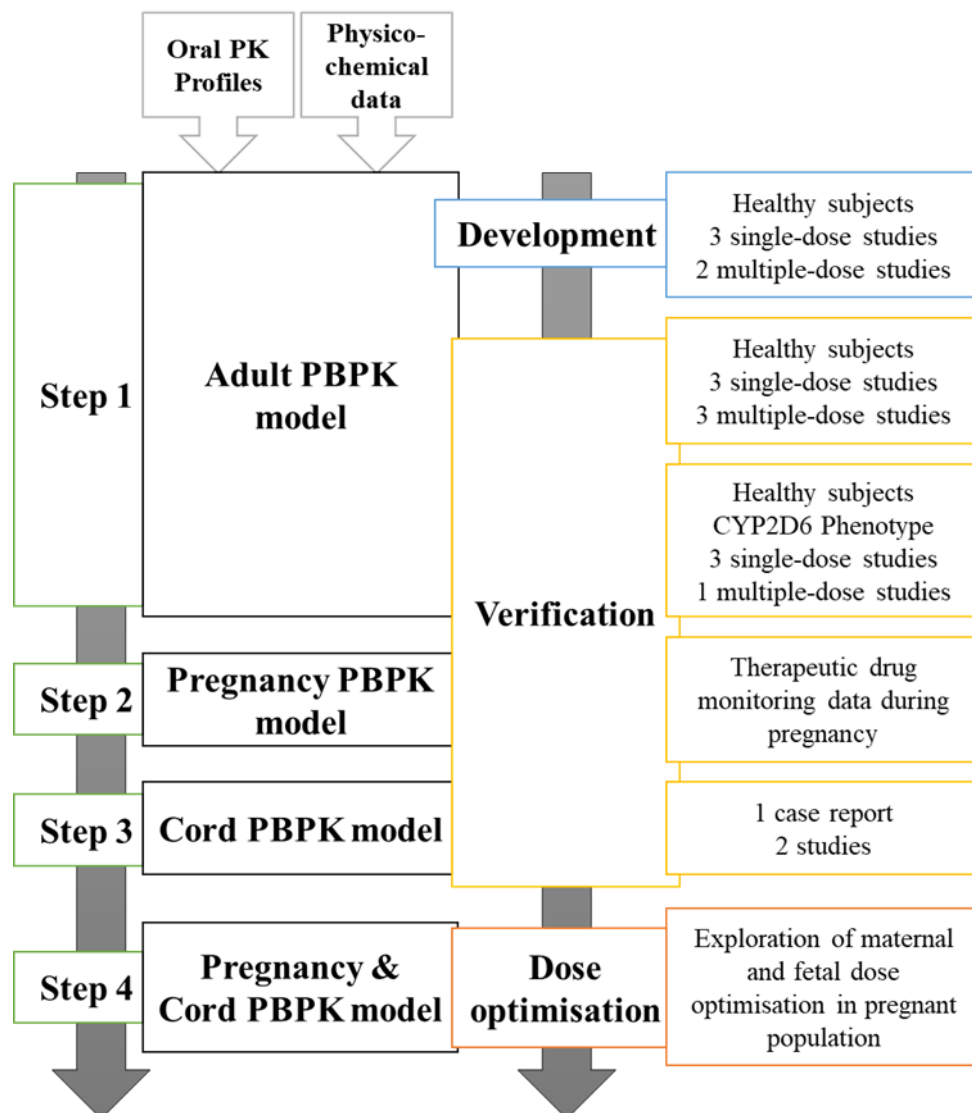


Figure 2.1 A four-step workflow for fluvoxamine gestational model development

2.2.1 Step 1: Development and verification of fluvoxamine model in a healthy population

The “healthy volunteer” (HV) population group available in Simcyp® was used for simulation as a baseline population for non-pregnant females.

The fluvoxamine compound file developed by Simcyp®, which is available in the simulator, was employed with modifications made to a few parameters. First, the distribution model was changed from a minimal-PBPK model to a full-body PBPK distribution model with an estimation of tissue partition coefficients (K_p) to calculate the V_{ss} using the Rodgers and Rowland approach [60, 196]. The calculated V_{ss} was in line with several published studies [197, 198]. The changes made to the distribution model are necessary to ensure that the tissue physiological temporal changes were considered throughout gestation when implementing the data on the pregnant population. Further, adaptations were made to the absorption rate constant (k_a), fraction of dose absorbed (f_a) and blood-to-plasma ratio (B/P) [199, 200], with final compound parameters detailed in Table 2.1.

Table 2.1 Fluvoxamine compound parameters with a full PBPK model

Parameters	Fluvoxamine	Notes
Compound type	Monoprotic Base	
Molecular weight (g/mol)	318.3	
Log P	3	
pKa 1	8.7	
f_u	0.14	
B/P	0.826	Predicted in Simcyp® based on Log P, plasma pH, haematocrit, and f_u [199, 200]
V_{ss} (L/kg)	35.48	Full PBPK model with K_p scalar of 13
K_p	13	Estimated using Simcyp® parameter estimation function
k_a (h^{-1})	0.15	Optimised through sensitivity analysis guided by data from USFDA (2021) [180]
f_a	0.8	Optimised through sensitivity analysis guided by data from USFDA (2021) [180]
Lag time (h)	0	
Absorption Model	First Order	
Distribution Model	Full PBPK	
CL_{PDM} & CL_{PDF}	0.253	Predicted from HBD and PSA information using Winiwarter et al. (1998) [55] method

Log P, partition coefficient; B/P, blood-to-plasma ratio; f_u , unbound fraction; V_{ss} , steady-state volume of distribution; K_p , tissue partition coefficient; k_a , absorption rate constant; f_a , extend of absorption; CL_{PDM} , maternal-placenta permeability clearance; CL_{PDF} , placenta-foetal permeability clearance; HBD, hydrogen bond donor; PSA, polar surface area.

Plasma concentration data from three single-dose and three multiple-dose studies were applied to establish the fluvoxamine model and confirm modifications to the fluvoxamine compound. Thereafter, validation was conducted with three single-dose and three multiple-dose studies. In addition, the model was further validated using CYP2D6 extensive metaboliser (EM) and poor metaboliser (PM) populations with plasma concentration data published from three single-dose and one multiple-dose study. All studies used to develop and validate the amended fluvoxamine model are detailed in Table 2.2.

Virtual clinical trials were run in Simcyp® with a 10 x 10 study design. The subjects' age, male-to-female ratio, and dosage regimen were correlated with the study design used in the development and verification.

Table 2.2 Published data used in fluvoxamine model development and validation.

Study	Study Design	Number of Subjects	Age (Years)	Dosing regimen
Studies used for Model Development				
De Vries et al. (1993) [201]	Crossover with 7 days washout between each dose	12 healthy males	22 – 41	25 mg/ 50 mg/ 100 mg single-dose under fasted condition
Van Harten et al. (1991) [202]	Crossover with 7 days washout between each period	8 healthy males and 4 healthy females	18 – 30	50 mg single-dose under fed and fasted condition
Bahrami et al. (2007) [203]	Crossover bioequivalence study with 3 weeks washout period	24 healthy males	27.2 ± 3.1	100 mg single-dose
De Vries et al. (1992) [204]	Multiple-dose	3 healthy males and 3 healthy females	25 – 31	50 mg on day 1, followed by 50 mg twice daily from day 4 to day 31
Fleishaker et al. (1994) [205]	Multiple-dose	10 healthy males and 10 healthy females	20 – 44	50 mg daily for 3 days, followed by 100 mg daily for 7 days
Studies used for Model Validation				
Orlando et al. (2010) [206]	Single-dose	10 healthy males	35 ± 7	50 mg single-dose under fasted condition
Debree et al. (1983) [207]	Single-dose	9 healthy males and 1 healthy female	20 – 25	100 mg single-dose under fasted condition
USFDA (2008) [208]	Single-dose Study code: S1141107	15 healthy males and 13 healthy females	20.3 – 44.7	100 mg single-dose under fasted condition

Spigset et al. (1998) [209]	Multiple-dose	10 healthy males	28.9 ± 5.2	12.5 mg twice daily for 1st week, followed by 25 mg twice daily for 2nd week, followed by 50 mg twice daily for 3rd week, followed by 100 mg twice daily for 4th week
USFDA (2008) [208]	Multiple-dose Study code: 1098001	12 healthy males with EM CYP2D6	19 – 43	100 mg daily for 10 days under fasting condition
USFDA (2008) [208]	Multiple-dose Study code: 1098002	12 healthy males with EM CYP2D6	21 – 44	100 mg daily for 10 days under fasting condition

Studies used for validation with CYP2D6 EM and PM population

Carrillo et al. (1996) [210]	Single-dose	EM: 3 healthy males & 2 healthy females, PM: 2 healthy males & 1 healthy female	EM: 26 – 40 PM: 31 – 49	50 mg single-dose under fasting condition
Spigset et al. (1997) [211]	Single-dose	EM: 7 healthy males & 3 healthy females, PM: 5 healthy males	EM: 28.7 ± 8.1 PM: 24.0 ± 1.6	50 mg single-dose under fasting condition
Hartter et al. (2000) [212]	Single-dose	EM: 4 healthy males, PM: 1 healthy male	34 – 55	50 mg single-dose
Christensen et al. (2002) [213]	Single-dose & Multiple-dose	EM: 7 healthy subjects, PM: 5 healthy subjects	22 – 45	Period 1: EM-50 mg single-dose PM-25 mg single-dose Period 2: EM-25 mg twice daily for 7 days PM-25 mg daily for 7 days Period 3: EM-10 mg twice daily for 7 days PM-10 mg daily for 7 days

Age represented by range or mean ± standard deviation (SD)

2.2.2 Step 2: Validation of fluvoxamine PBPK model in pregnancy

After developing and verifying the fluvoxamine model in the HV population, the pregnant population model developed by Simcyp® was used for simulation. The pregnant population incorporated in the Simcyp® simulator includes the essential physiological changes that occur throughout the gestational period. The pregnant population established in Simcyp® incorporates the physiological changes in tissue composition/blood volume, renal/liver function, and temporal changes in enzyme activities throughout the maternal period, particularly with respect to CYP2D6, which plays an essential role in fluvoxamine metabolism [51, 105, 214].

Specifically, a gestational age-dependant function is incorporated into Simcyp Pregnancy to reflect the increase in CYP2D6 enzyme abundance throughout gestation and is based on a study by Ryu et al. (2016) [215], with the function (2.1) expressed as:

$$\text{CYP2D6 (fold change in activity)} = 1 \times (1 + 0.0163 \times \text{GW} + 0.0009 \times \text{GW}^2) \quad (2.1)$$

where GW represents gestational week. This function is then propagated within the model to alter baseline CYP2D6 expression (9.4 pmol/mg protein) [216].

In order to validate the fluvoxamine model in the pregnant population, fluvoxamine pharmacokinetics throughout the entire gestational period were simulated using 10 trials x 10 patient design. A 100 mg daily oral dose was utilised, and pharmacokinetic data samples were collected in the last 24 hours of every 5th GW. As for baseline, a similar study design was simulated with a healthy female population dosed with 100 mg of fluvoxamine daily. Then, the simulated steady-state trough plasma concentrations were verified with observed data from TDM services in Norway published by Westin et al. (2017) [184]. The data were collated from three pregnant women taking 100 mg of fluvoxamine per day, consisting of three serum drug concentrations at baseline and five serum drug concentrations during pregnancy. The data presented individually allowed for extraction and comparison with the fluvoxamine model simulated in the pregnant population.

After verifying the fluvoxamine administration during pregnancy virtual trial simulation, the fluvoxamine plasma concentration trend was explored. The therapeutic range for fluvoxamine recommended by Consensus Guidelines for Therapeutic Drug Monitoring in Neuropsychopharmacology: Update 2017 [172], was applied as a guide to review the effective level of fluvoxamine plasma concentration during pregnancy as an antidepressant from the TDM perspective. The recommended range is between 60 ng/mL – 230 ng/mL [172].

2.2.3 Step 3: Validation of fluvoxamine foetoplacental PBPK model

In order to predict foetal exposure, the foetoplacental model within the Simcyp Pregnancy model was utilised. This model incorporates an “additional” set of compartments that account for the foetal blood and the foetal lumped body, with the description of transplacental clearance. Simcyp® uses a permeability-limited model for the foetoplacental compartment in Simcyp®. The model described the compound flux between the maternal, placental, and foetal clearance values with respect to the maternal-placental Cotyledon clearance values (CL_{PDM} and CL_{PDF}) (Figure S 2-1).

Given the paucity of data on fluvoxamine’s transplacental permeability, an in vitro–in vivo extrapolation (IVIVE) method reported by Winiwarter et al. (1998) [55] was used, which utilises hydrogen bond donors (HBD), polar surface area (PSA), and correction for placental villous surface area to yield both CL_{PDM} and CL_{PDF} (Table 2.1). The placental villous surface area was derived from a meta-analysis of reported values and calculated using Equation (2.2) as follows:

$$\begin{aligned} \text{Placental villous surface area (m}^2\text{)} = \\ (0.135 \times \text{GW}) - (0.023 \times \text{GW}^2) + (0.0015 \times \text{GW}^3) - (0.00002 \times \text{GW}^4) \end{aligned} \quad (2.2)$$

The umbilical cord concentration in the full-term pregnant population was simulated with a design consisting of 10 trials × 10 subjects. Then, the predicted umbilical cord concentrations were validated with three observed umbilical cord concentrations from three different studies [217-219].

2.2.4 Step 4: Influence of CYP2D6 phenotype and dose adjustment during gestation

Considering that CYP2D6 is the main CYP enzyme involved in fluvoxamine metabolism, the fluvoxamine PBPK model was validated based on the ultra-rapid metaboliser (UM), EM, and PM CYP2D6 status in healthy subjects. In addition, the various CYP2D6 metabolisers in the pregnant population in Simcyp® have been validated by Almurjan et al. (2020) [186] for the paroxetine compound. Thus, the fluvoxamine plasma concentration profiles in UM, EM, and PM CYP2D6 populations were predicted to assess the impact of CYP2D6 phenotype on plasma concentrations throughout gestation. Simulation with a 10 × 10 trial design was predicted throughout the entire gestational period, with pharmacokinetic data samples collected during the last 24 hours of every 5th GW from a population of entirely UM, EM, or PM CYP2D6 phenotypes.

The predictions covered a range of fluvoxamine doses from 50 mg daily to a maximum of 300 mg daily, with increments of 25 mg daily and doses above 150 mg daily administered in two divided doses.

The influence of the CYP2D6 phenotype on pregnant women and its transference to the foetus were assessed at the starting dose of 50 mg daily, as well as the minimum and maximum maintenance doses of 100 mg and 300 mg daily, respectively. Regarding dose adjustment, the percentage of (maternal) subjects with a peak concentration above 230 ng/mL and trough concentration below 60 ng/mL were assessed for every 5th GW and each phenotype for every dose starting from 50 mg daily up to the maximum dose of 300 mg daily.

2.2.5 Predictive performance

All the pharmacokinetics predictions made in the simulations that fell within two-fold (0.5 – 2-fold) of published data were considered 'optimal' predictive performance unless otherwise stated [144, 147, 220]. In addition, the simulations were verified visually using the visual predictive checking (VPC) strategy [221]. This strategy was used to view all the simulated concentration-time profiles in steps 1, 2 and 3 with the observed/published data. The simulations were considered acceptable when the published profile overlapped and fell within the 5th and 95th percentile of the predicted mean concentration-time profile.

2.2.6 Data and statistical analysis

The data used for development and validation were extracted using WebPlotDigitizer version 4.5 (<https://apps.automeris.io/wpd/>). In step 1, statistical analysis was conducted using a nonparametric, unpaired Student's t-test to compare the observed and predicted data. In steps 2 and 4, the nonparametric one-way ANOVA with a Dunnett's multiple comparisons post hoc test was used to compare the 5-weekly-simulated plasma concentration with the baseline (0) for maternal prediction and GW 20 for umbilical cord simulation. For the comparison between UM, EM, and PM CYP2D6 phenotypes for every 5-weekly-simulated plasma concentration in maternal and umbilical cord concentration, nonparametric one-way ANOVA with Tukey's multiple comparisons post hoc test was utilised. The significance test was performed with $p < 0.05$ for steps 1, 2, and 4. Statistical analysis was run using GraphPad Prism Version 8 for Windows (GraphPad Software, La Jolla, CA, USA).

2.3 Results

2.3.1 Step 1: Development and validation of fluvoxamine model in a healthy population

The fluvoxamine model was adapted and validated using clinical studies, which included both single- and multiple-dose studies with various dosing regimens (Table 2.2). The predicted pharmacokinetic parameters, including maximum concentration (C_{max}), time to maximum concentration (T_{max}), area-under-the-curve to the last time point (AUC_{0-t}), and area-under-the-curve to infinity (AUC_{inf}), were within 0.5 to 2-fold of the reported clinical data (Table 2.3). Moreover, the observed profiles agree with the simulated profile for single and multiple-dose studies based on the VPC, wherein the published profiles are within the 5th and 95th percentiles of the predicted plasma concentration profile, thereby confirming the successful development and validation of the fluvoxamine model in the healthy population.

The simulated plasma concentration for all single-dose studies used during model development and validation were presented in Figure 2.2, Figure 2.3, and Figure 2.4. For the comparison of the pharmacokinetic parameters in the single-dose studies, the AUC_{inf} was not within the limit, particularly with the study by Orlando et al. (2010) [206] and USFDA (2008) [208]. A similar pattern was observed for AUC_{inf} data when the single-dose 50 mg and 100 mg trials conducted by De Vries et al. (1993) [201] were compared with the spread of individual data from the simulated profiles during the model development, as shown in Figure 2.2. However, the results showed no statistical significance difference ($p > 0.05$) for all three doses of C_{max} and the AUC_{inf} of the single-dose 25 mg.

Regarding the multiple-dose study, only the C_{max} and AUC_{inf} for the study by Spigset et al. (1998) [209] were not within the two-fold range, and this was when fluvoxamine was administered at the lowest dose at week 1 (12.5 mg twice daily for seven days). The simulated plasma concentration profiles and the published concentration data used during the development and verification of the multiple-dose studies are shown in Figure 2.5.

The validation of the predicted values overlaid with the observed plasma concentrations for the graphs of the CYP2D6 EM and PM populations are presented in Figure 2.6 and Figure 2.7. Regarding the comparison of the pharmacokinetics parameters, a few parameters that were not within the two-fold range were only seen in the single-dose 50 mg study by Spigset et al. (1997) [211] concerning the AUC_{inf} in both the EM and PM and the AUC_{0-t} for the PM, as well as the C_{max} for PM CYP2D6 for the single-dose 50 mg study by Carrilo et al. (1996) [210].

Table 2.3 Pharmacokinetics of single- and multiple-dose studies (predicted and observed)

References	Dosing	PK Parameters	Observed	Predicted	Predicted/ Observed
Model Development					
			Geometric Mean (Range)		
De Vries et al. (1993) [201]	Single dose 25 mg	C _{max} (ng/mL)	8.80 (4.70 - 13.00)	7.77 (3.19 - 20.49)	0.88
		AUC _{inf} (ng/mL.h)	209.00 (117.00 - 425.00)	230.67 (97.76 - 571.74)	1.10
		T _{max} (h) ¹	5.00 (1.00 - 8.00)	5.66 (3.40 - 13.35)	1.13
	Single dose 50 mg	C _{max} (ng/mL)	17.00 (8.40 - 28.00)	16.00 (6.39 - 40.97)	0.94
		AUC _{inf} (ng/mL.h)	448.00 (166.00 - 1115.00)	719.24 (254.16 - 3113.83)	1.61
		T _{max} (h) ¹	4.80 (2.00 - 8.00)	5.67 (3.40 - 13.40)	1.03
	Single dose 100 mg	C _{max} (ng/mL)	36.00 (21.00 - 60.00)	32.01 (12.78 - 81.95)	0.89
		AUC _{inf} (ng/mL.h)	927.00 (325.00 - 2146.00)	1693.24 (585.86 - 10825.67)	1.83
		T _{max} (h) ¹	4.50 (3.00 - 6.00)	5.68 (3.40 - 13.35)	1.04
Van Harten et al. (1991) [202]	Single dose 50 mg - Fast	C _{max} (ng/mL)	15.40 (7.50 - 27.00)	16.00 (6.39 - 40.97)	1.04
		AUC _{0-32h} (ng/mL.h)	237.00 (102.00 - 571.00)	324.19 (139.89 - 710.72)	1.37
		T _{max} (h) ¹	6.00 (3.00 - 12.00)	5.67 (3.40 - 13.35)	0.95
	Single dose 50 mg - Fed	C _{max} (ng/mL)	15.50 (10.00 - 32.00)	16.00 (6.39 - 40.97)	1.03
		AUC _{0-32h} (ng/mL.h)	223.00 (65.00 - 587.00)	324.19 (139.89 - 710.72)	1.45
		T _{max} (h) ¹	7.00 (2.00 - 12.00)	5.67 (3.40 - 13.35)	0.81
de Vries et al. (1992) [204]	Single dose 50 mg - Day 1	C _{max} (ng/mL)	30.00 (13.10)	17.82 (9.63)	0.59
		AUC _{inf} (ng/mL.h)	652.00 (319.00)	882.08 (717.30)	1.35
		T _{max} (h) ¹	6.00 (4.00 - 8.00)	5.63 (3.25 - 14.50)	0.94
	Multiple dose 50 mg twice daily from Day 4 to Day 31	C _{max} (ng/mL)	93.00 (96.16)	81.55 (60.34)	0.88
		AUC _{0-12h} (ng/mL.h)	873.00 (782.44)	920.77 (707.31)	1.05
		T _{max} (h) ¹	5.00 (1.00 - 10.00)	3.48 (2.65 - 4.20)	0.70

			Arithmetic Mean (SD)		
Fleishaker et al. (1994) [205]	Single dose 50 mg - Day 1	C_{max} (ng/mL)	21.50 (4.89)	16.77 (6.70)	0.78
		AUC_{0-24h} (ng/mL.h)	328.00 (84.60)	283.65 (107.45)	0.86
		T_{max} (h)	5.70 (1.49)	5.67 (1.45)	0.99
	Multiple dose 50 mg daily for 3 days followed by 100 mg daily for the 7 days	C_{max} (ng/mL)	99.30 (35.00)	80.32 (36.45)	0.81
		AUC_{0-24h} (ng/mL.h)	1762.00 (737.00)	1614.20 (786.04)	0.92
		T_{max} (h)	7.95 (4.91)	4.75 (0.78)	0.60
Bahrami et al. (2007) [203]	Single dose 100 mg – Test	C_{max} (ng/mL)	46.20 (29.00)	34.65 (13.94)	0.75
		AUC_{0-48h} (ng/mL.h)	866.20 (480.00)	872.88 (351.91)	1.01
		AUC_{inf} (ng/mL.h)	1308.00 (781.00)	1641.58 (902.86)	1.26
		T_{max} (h)	5.30 (2.00)	5.68 (1.45)	1.07
	Single dose 100 mg - Reference	C_{max} (ng/mL)	48.50 (28.00)	34.65 (13.94)	0.71
		AUC_{0-48h} (ng/mL.h)	802.20 (360.00)	872.88 (351.91)	1.09
		AUC_{inf} (ng/mL.h)	1224.90 (430.00)	1641.58 (902.86)	1.34
		T_{max} (h)	5.60 (2.10)	5.68 (1.45)	1.01
Model Validation					
			Arithmetic Mean (SD)		
Orlando et al. (2010) [206]	Single dose 50 mg	C_{max} (ng/mL)	15.00 (3.00)	17.32 (6.97)	1.15
		AUC_{inf} (ng/ml.h)	304.00 (84.00)	820.98 (452.53)	2.70
		T_{max} (h) ²	5.00 (4.00 - 8.00)	5.47 (3.40 - 13.40)	1.08
			Geometric Mean (SD)		
Debree et al. (1983) [207]	Single dose 100 mg	C_{max} (ng/mL)	49.30 (17.00)	32.01 (13.94)	0.65
		AUC_{0-24h} (ng/mL.h)	523.90 (122.90)	545.44 (228.11)	1.04
		AUC_{inf} (ng/mL.h)	817.00 (194.30)	958.18 (472.25)	1.17
		T_{max} (h) ¹	5.00 (2.00 - 8.00)	5.68 (3.40 - 13.40)	1.14

		Arithmetic Mean (SD)			
USFDA (2008) [208]	Single dose 100 mg	C_{max} (ng/mL)	41.88 (18.99)	34.65 (13.94)	0.83
		AUC_{inf} (ng/mL.h)	959.33 (520.71)	2071.01 (1435.11)	2.16
		T_{max} (h) ¹	6.00 (4 .00 - 16.00)	5.68 (3.40 - 13.35)	0.95
Spigset et al. (1998) [209]	Week 1 – 12.5 mg twice daily for 7 days	C_{max} (nmol/L)	25.10 (9.40)	57.96 (29.62)	2.31
		AUC_{12h} (nmol.h/L)	236.00 (95.00)	652.00 (339.68)	2.76
	Week 1 – 25 mg twice daily for 7 days	C_{max} (nmol/L)	76.30 (22.10)	107.53 (60.63)	1.41
		AUC_{12h} (nmol.h/L)	745.00 (258.00)	1457.38 (795.37)	1.96
	Week 1 – 50 mg twice daily for 7 days	C_{max} (nmol/L)	244.00 (97.90)	261.50 (141.94)	1.07
		AUC_{12h} (nmol.L.h)	2391.00 (949.00)	2960.86 (1643.50)	1.24
	Week 1 – 100 mg twice daily for 7 days	C_{max} (nmol/L)	738.00 (314.00)	439.88 (254.36)	0.60
		AUC_{12h} (nmol.h/L)	7545.00 (3239.00)	5943.80 (3317.30)	0.79
USFDA (2008) [208]	Multiple dose 100 mg daily for 10 days (Prot. C)	C_{max} (ng/mL)	107.00 (73.52)	79.41 (31.39)	0.74
		AUC_{0-24h} (ng/mL.h)	1738.55 (1392.42)	1587.74 (669.76)	0.91
	Multiple dose 100 mg daily for 10 days (Prot. D)	C_{max} (ng/mL)	129.59 (62.86)	85.97 (42.84)	0.66
		AUC_{0-24h} (ng/mL.h)	2109.30 (1085.63)	1677.97 (905.71)	0.80
Model validation for EM and PM CYP2D6 Phenotype population					
Carrillo et al. (1996) [210]	Single dose 50 mg -EM CYP2D6	C_{max} (nmol/L)	85.90 (42.50)	61.03 (28.98)	0.71
		AUC_{0-32h} (nmol/L.h) ³	1097.90 (180.35)	1220.62 (55.36)	1.11
		AUC_{inf} (nmol/L.h)	1352.00 (733.00)	2065.41 (1033.85)	1.53
		T_{max} (h)	4.4 (2.1)	5.57 (1.52)	1.27
	Single dose 50 mg -PM CYP2D6	C_{max} (nmol/L)	178.10 (27.50)	78.81 (33.53)	0.44
		AUC_{0-72h} (nmol/L.h) ³	4648.59 (237.46)	2889.62 (118.60)	0.62
		AUC_{inf} (nmol/L.h)	5290.00 (332.00)	6287.38 (2990.77)	1.19
		T_{max} (h)	4.60 (2.30)	7.01 (1.82)	1.52

Spigset et al. (1997) [211]	Single dose 50 mg -EM CYP2D6	C_{max} (nmol/L)	44.50 (12.30)	61.03 (28.98)	1.37
		AUC_{0-48h} (nmol/L.h) ³	870.00 (110.00)	1530.00 (70.00)	1.76
		AUC_{inf} (nmol/L.h)	1000.00 (410.00)	2610.00 (1280.00)	2.61
		T_{max} (h)	7.80 (2.40)	5.57 (1.52)	0.71
	Single dose 50 mg -PM CYP2D6	C_{max} (nmol/L)	50.40 (17.80)	78.81 (33.53)	1.56
		AUC_{0-48h} (nmol/L.h) ³	1090.00 (160.00)	2280.00 (90.00)	2.09
		AUC_{inf} (nmol/L.h)	1310.00 (670.00)	4950.00 (2220.00)	3.78
		T_{max} (h)	6.60 (2.10)	7.01 (1.82)	1.06
Hartter et al. (2000) [212]	Single dose 50 mg -EM CYP2D6	C_{max} (ng/mL)	13.00 (3.7)	19.43 (9.22)	1.49
		AUC_{0-28h} (μ g/L.h)	185.50 (33.60)	360.58 (163.21)	1.94
	Single dose 50 mg -PM CYP2D6 ⁴	C_{max} (ng/mL)	48.00	25.09 (10.67)	0.52
		AUC_{0-28h} (μ g/L.h)	612.00	512.06 (206.59)	0.84
Chtistensen et al. (2002) [213]	Single dose 50 mg -EM CYP2D6	C_{max} (nmol/L)	58.14 (37.90)	61.03 (28.98)	1.05
	Single dose 25 mg -PM CYP2D6	C_{max} (nmol/L)	23.20 (2.28)	39.41 (16.76)	1.70

AUC_{inf} , area-under-the-curve to infinity; AUC_{0-t} , area-under-the-curve to the last time point; AUC_t , area-under-the-curve for the total hour at steady-state; C_{max} , maximum plasma concentration; T_{max} , time to reach maximum plasma concentration; ¹Arithmetic Mean (Range); ²Median; ³the AUC_{0-t} was calculated from the published graph; ⁴only 1 subject, thus, no standard deviation was reported.

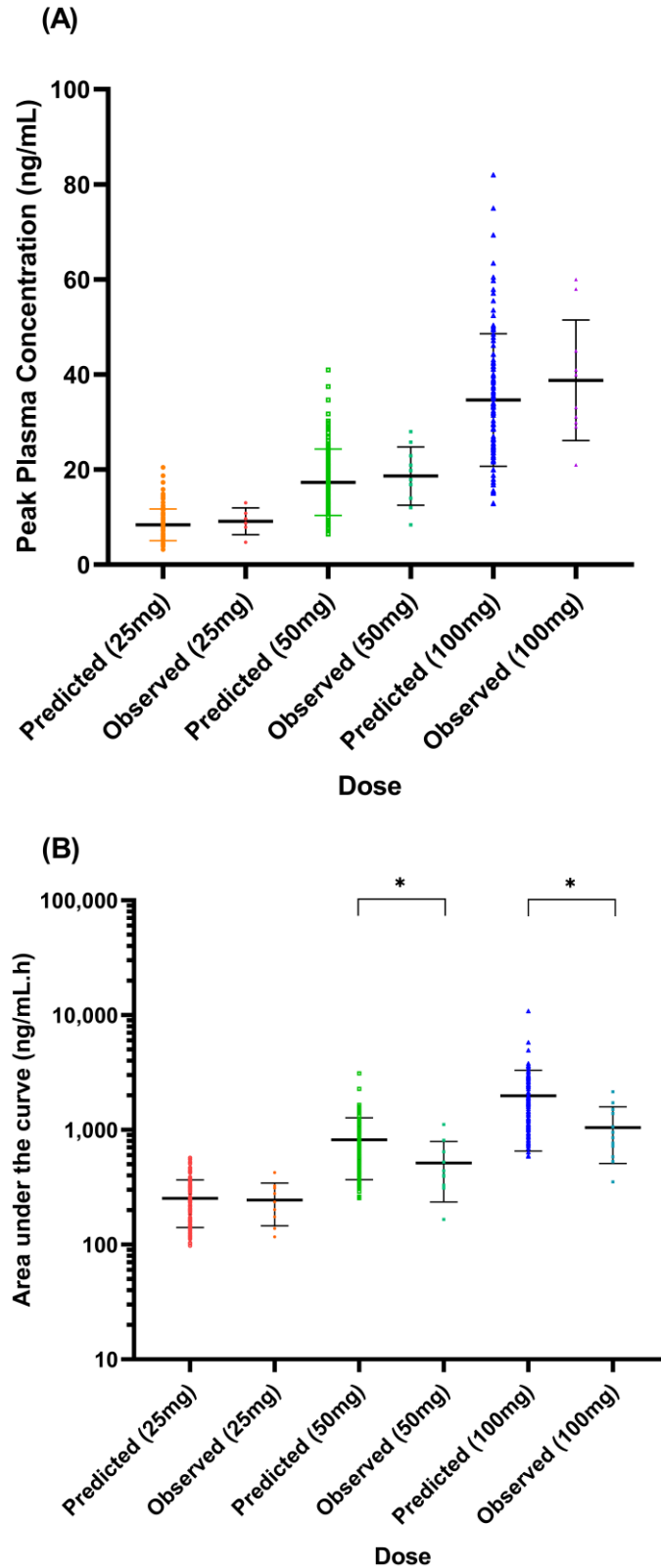


Figure 2.2 Comparison between simulated trial and observed data.

(A) C_{max} and (B) AUC_{inf} from De Vries et al. (1993) [201]. Coloured data points arranged vertically represent the predicted and observed data for each dose; horizontal lines on the coloured data points represent the mean and standard deviation (SD). * $p < 0.05$.

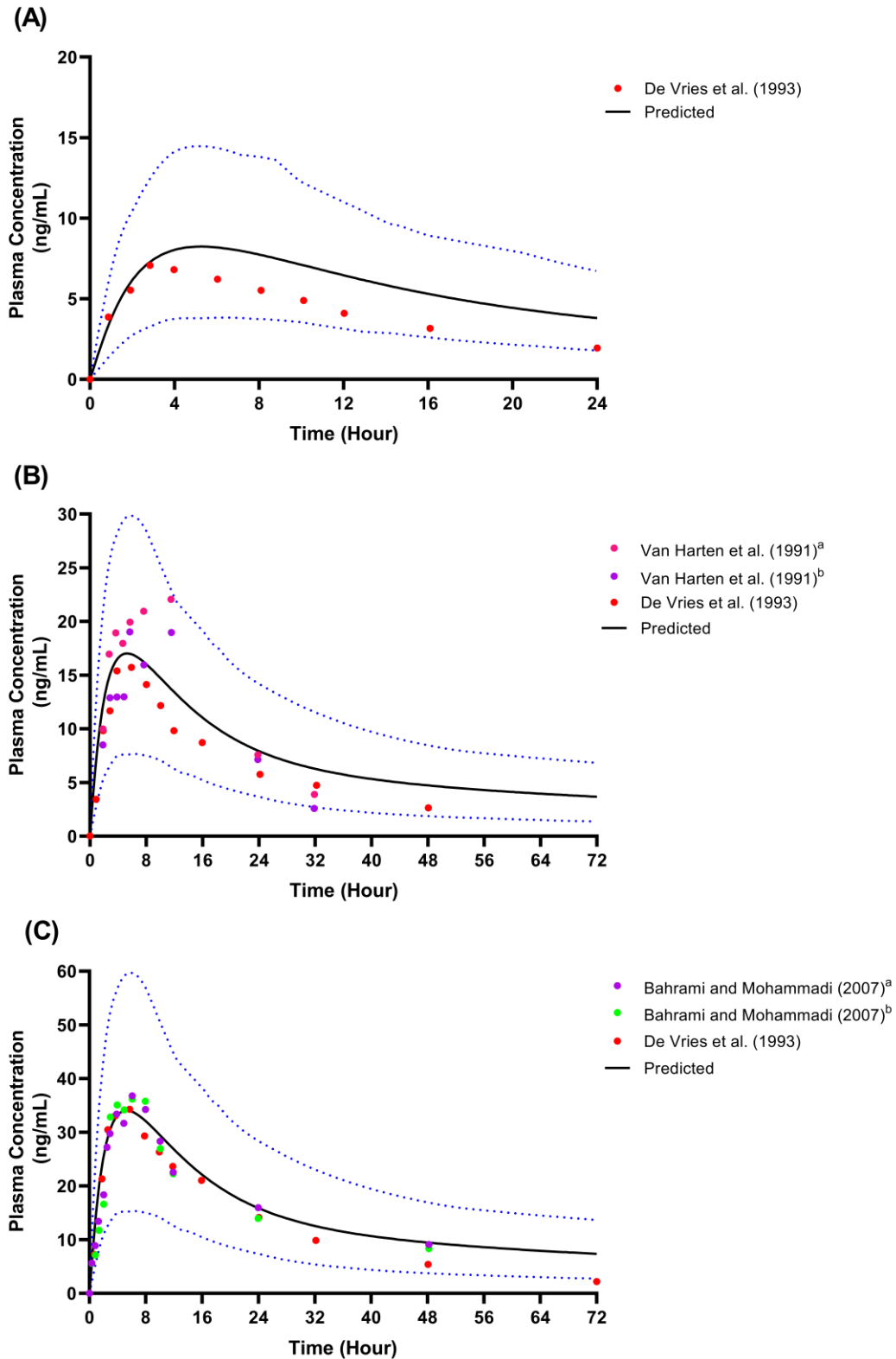


Figure 2.3 Simulated single-dose studies in model development.

(A) Single-dose 25 mg [201]; (B) Single-dose 50 mg [201, 202]; (C) Single-dose 100 mg [201, 203]. Solid lines represent the mean predicted concentration-time profile, with dotted lines representing the 5th and 95th percentile ranges. Solid circles represent observed clinical data from each study. Van Harten et al. (1991)^a represents the 50 mg fed study [202]; Van Harten et al. (1991)^b represents the 50 mg fast study [202]. Bahrami and Mohammadi (2007)^a represents the 100 mg test formulation study [203]; Bahrami and Mohammadi (2007)^b represents the 100 mg reference formulation study [203].

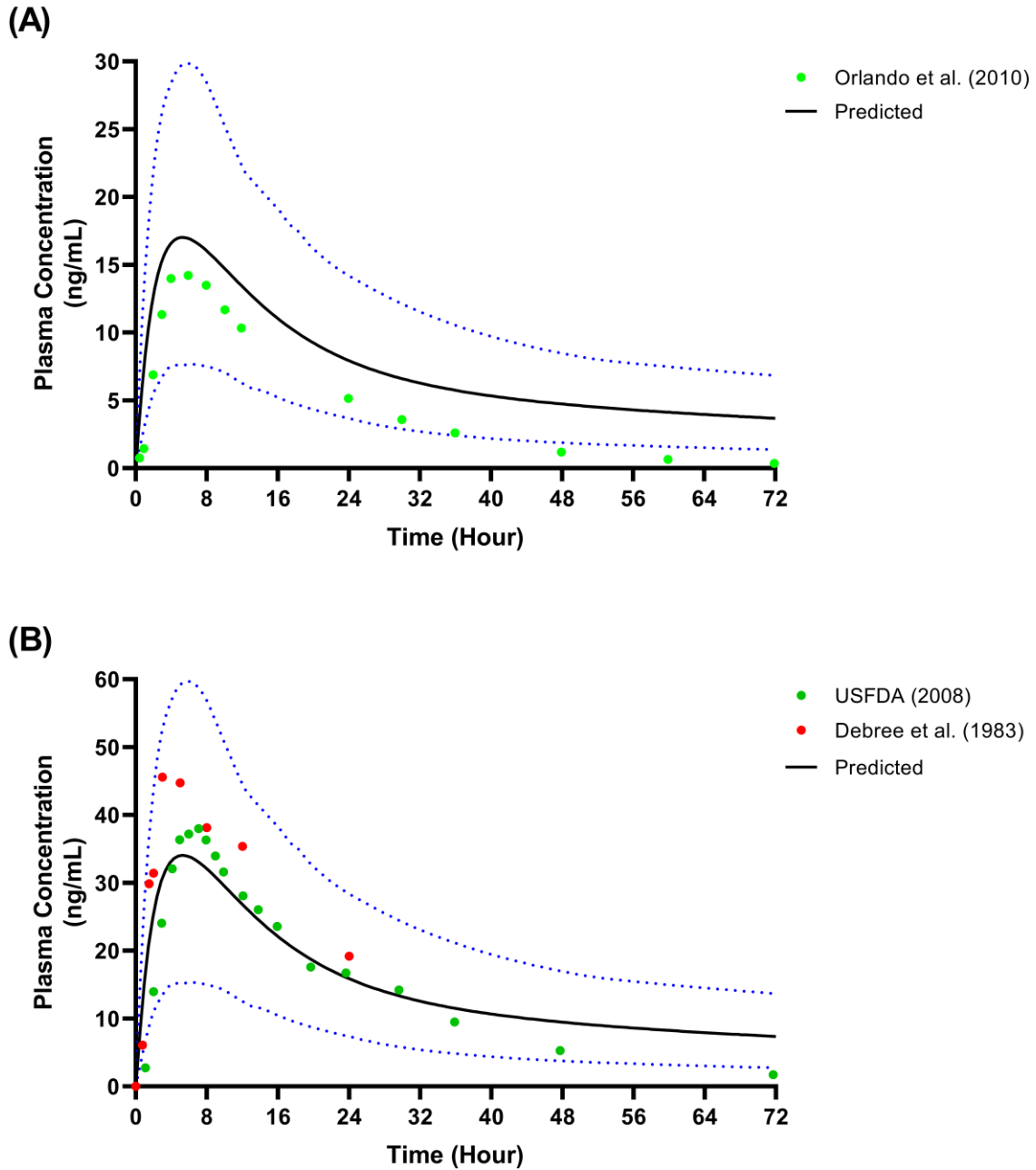


Figure 2.4 Single-dose studies simulated in the model validation stage.

(A) Single-dose 50 mg [206]; (B) Single-dose 100 mg [207, 208]. Solid lines represent the mean predicted concentration-time profile, with dotted lines representing the 5th and 95th percentile ranges. Solid circles represent observed clinical data from each study.

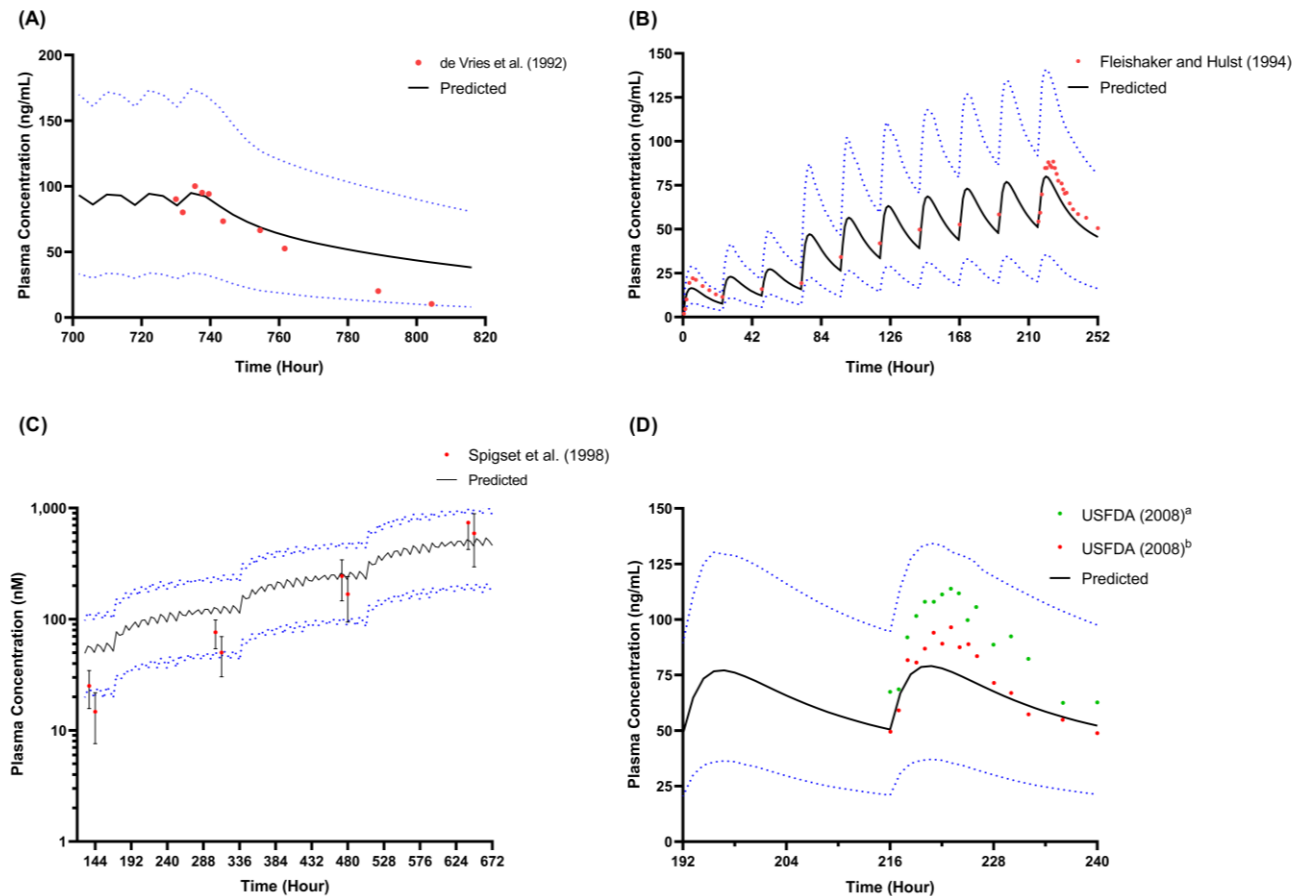


Figure 2.5 Multiple-dose studies simulated in model development and validation.

(A) Multiple-dose 50 mg twice daily from day 4 to day 31 [204]; (B) Multiple-dose 50 mg daily for 3 days followed by 100 mg daily for 7 days [205]; (C) Multiple-dose 12.5 mg twice daily for week 1, 25 mg twice daily for week 2, 50 mg twice daily for week 3, and 100 mg twice daily for week 4 [209]; (D) Multiple-dose 100 mg daily for 10 days [208]. Solid lines represent the mean predicted concentration-time profile, with dotted lines representing the 5th and 95th percentile ranges. Solid circles represent observed clinical data from each study, with error bars indicating SD. USFDA (2008)^a represents a bioavailability study with prototype D [208]; USFDA (2008)^b represents a bioavailability study with prototype C [208].

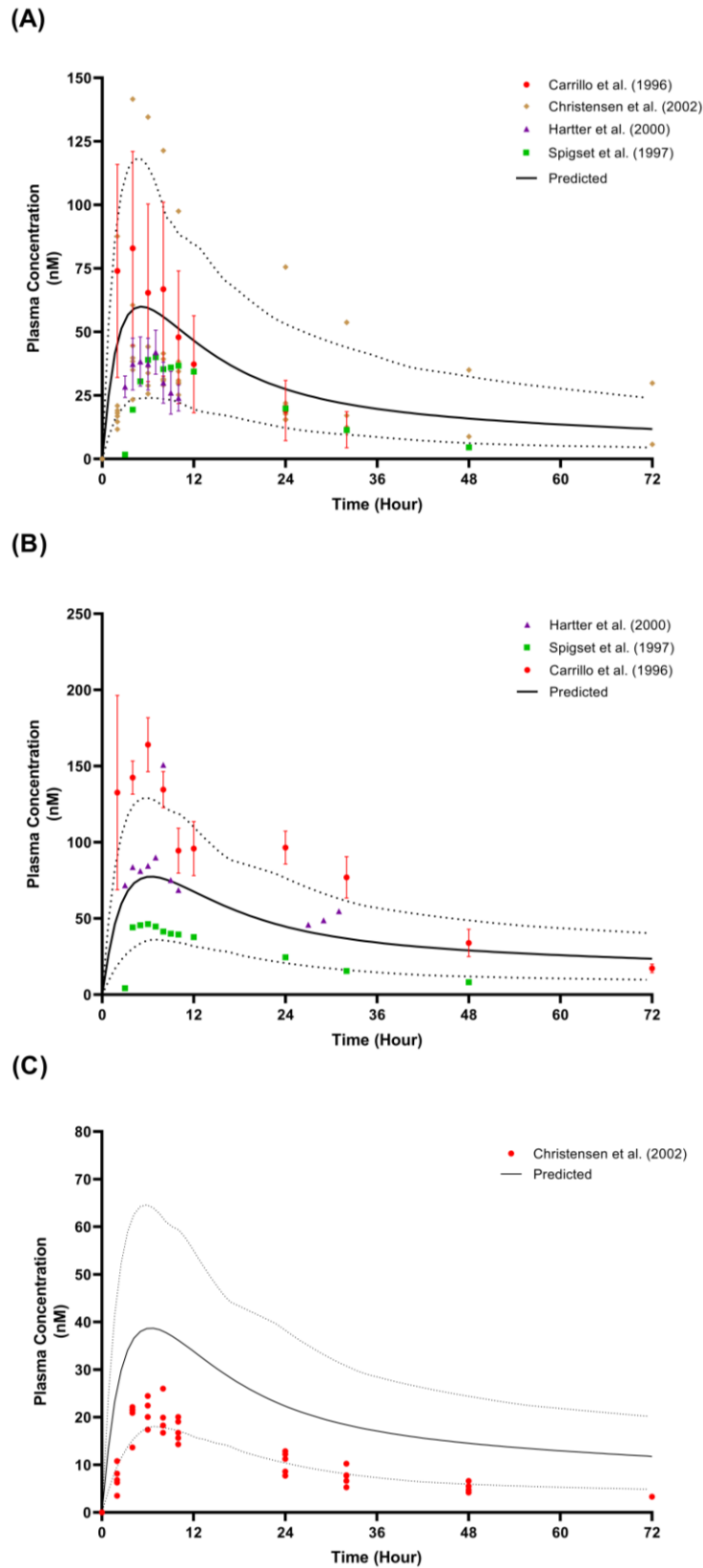


Figure 2.6 Simulated single-dose studies in model validation for CYP2D6 phenotype.

(A) Single-dose 50 mg in EM CYP2D6 population [210-213]; (B) Single-dose 50 mg in PM CYP2D6 population [210-212]; (C) single-dose 25 mg in PM CYP2D6 population [213]; solid lines represent the mean predicted concentration-time profile, with dotted lines representing the 5th and 95th percentile ranges. Solid circles represent observed clinical data from each study, with error bars indicating SD.

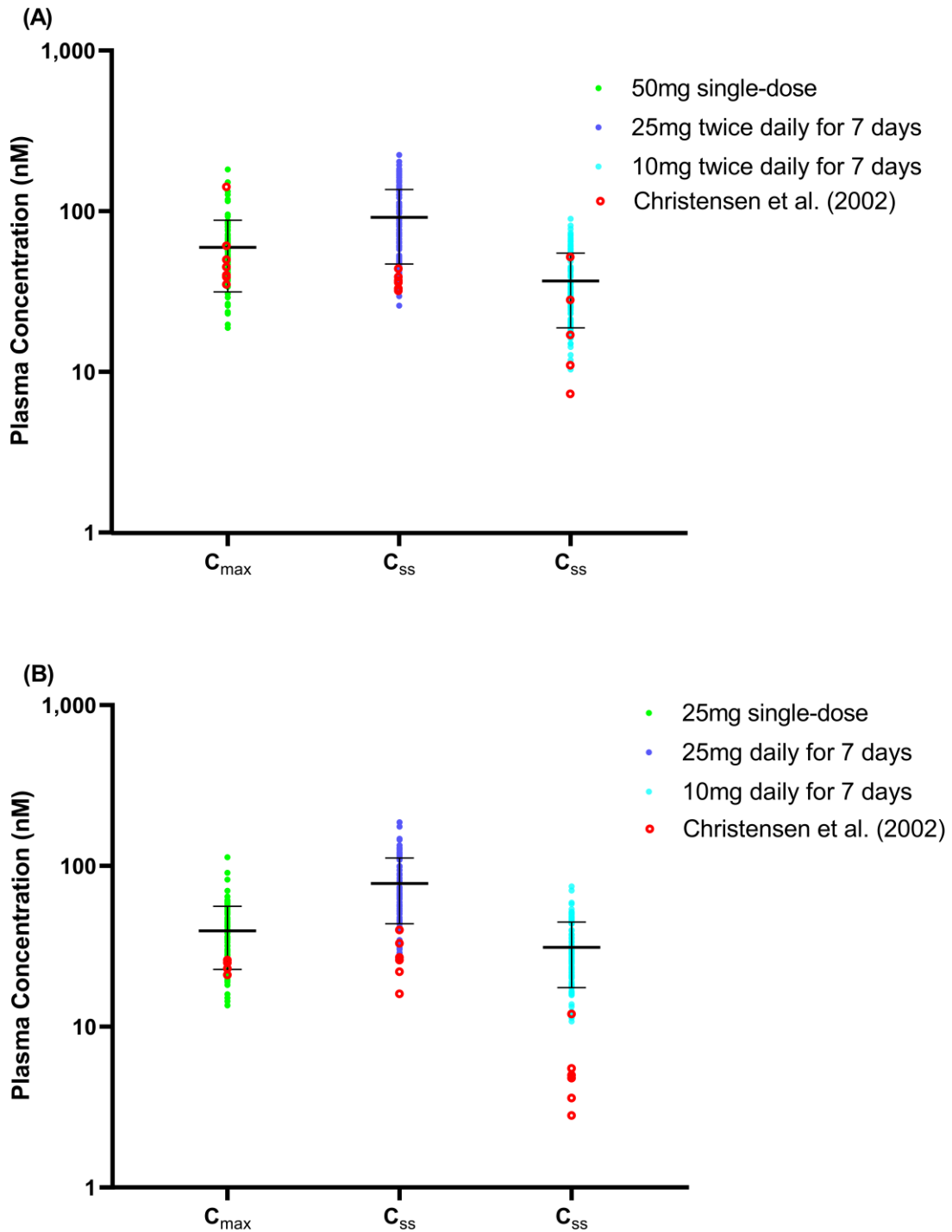


Figure 2.7 Predicted maximum concentration and steady-state concentration for single-dose and multiple-dose studies.

(A) EM CYP2D6 phenotype population; (B) PM CYP2D6 phenotype population; solid circles arranged vertically represent the predicted values for each dose. Horizontal lines on the coloured data points represent the mean and SD. Red, open circles represent the observed individual data from Christensen et al. (2002) [213]. C_{max} , maximum concentration for single-dose; C_{ss} , average trough concentration at steady-state for Day 6 and Day 7.

2.3.2 Step 2: Verification of fluvoxamine model in pregnancy and the impact of pregnancy on fluvoxamine level

In order to verify the applicability of the model throughout gestation, the predicted fluvoxamine steady-state trough plasma concentrations (C_{\min}) following a daily 100 mg dose throughout pregnancy was validated with the reported TDM trough concentrations data throughout gestation reported by Westin et al. (2017) [184] (Figure 2.8). The model predictions were within the range reported by Westin et al. (2017) [184], with mean plasma concentrations showing a reducing trend from GW 10 towards term (Table 4).

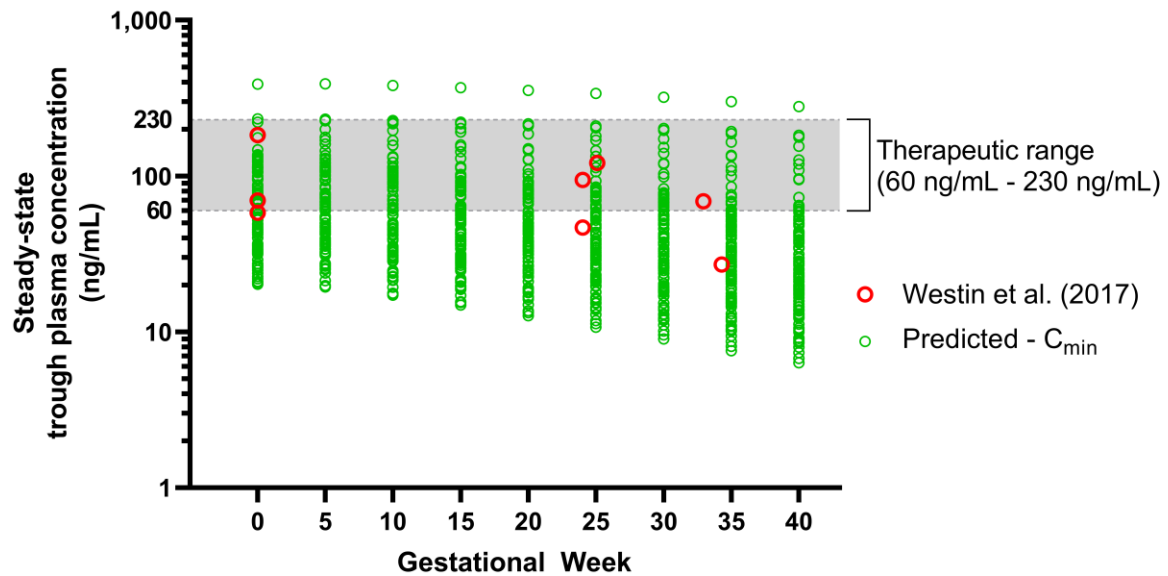


Figure 2.8 Predicted steady-state C_{\min} fluvoxamine maternal concentration.

Green, open circles represent the post-dose trough concentration sampled at 24 h post-dose and assembled every 5 GWs throughout the maternity period. Red, open circles represent reported plasma concentrations collected from 3 pregnant women from Westin et al. (2017) [184]. '0' refers to the baseline predicted in the non-pregnant female population. The grey shaded region represents the fluvoxamine therapeutic window (TW).

When compared to the baseline, C_{\min} and C_{\max} started to decrease from GW 10 by -5.13% and -5.69% , and -48.46% and -49.37% in GW 40, respectively. Furthermore, the decrease was statistically significant compared to the baseline commencing from GW 25 and 20 onwards for the C_{\min} and C_{\max} , respectively. The trend showed that the mean of C_{\min} falls below the therapeutic window at GW 25 onwards. The percentage of subjects with C_{\min} below 60 ng/mL increased at the early stage of the 3rd trimester (GW 30) and up to 85% at GW 40. A similar trend was noted for C_{\max} . As for the mean, the C_{\min} started to fall below the therapeutic concentration at GW 20 with 59.84 ± 51.76 ng/mL.

Table 2.4 Predicted fluvoxamine plasma concentration across the maternity period

	Gestational Week (GW)								
	0 (Baseline)	5	10	15	20	25	30	35	40 (Full term)
Steady-state C _{min} (ng/mL)	75.23 (52.73)	76.34 (56.97)	71.37 (55.5)	65.72 (53.73)	59.84 (51.76)	54.04 (49.62)	48.52 (47.31)	43.32 (44.8)	38.4 (42.05)
% change from baseline	0	1.48	-5.13	-12.64	-20.46	-28.17	-35.50	-42.42	-48.96
<i>p-value</i> *		0.9998	0.9966	0.6707	0.1718	0.0215	0.0016	<0.0001	<0.0001
% C _{min} < 60 ng/mL# (%)	46	48	54	58	66	68	74	80	85
Steady-state C _{max} (ng/mL)	112.5 (64.17)	113.1 (67.3)	106.1 (65.56)	97.87 (63.45)	89.09 (61.06)	80.29 (58.43)	71.85 (55.61)	64.03 (52.63)	56.96 (49.53)
% change from baseline	0	0.53	-5.69	-13.00	-20.81	-28.63	-36.13	-43.08	-49.37
<i>p-value</i> *		>0.9999	0.9739	0.3875	0.0385	0.0012	<0.0001	<0.0001	<0.0001
% C _{max} > 230 ng/mL# (%)	17	20	23	29	38	45	56	60	67

C_{min}, trough plasma concentration; C_{max}, maximum plasma concentration; **p-value*: statistical significance test between each GW with baseline; $p < 0.05$, statistically significant difference; #Efficacy threshold (60 ng/mL – 230 ng/mL) as recommended in Consensus Guidelines for Therapeutic Drug Monitoring in Neuropsychopharmacology: Update 2017 [172]; Mean (SD).

2.3.3 Step 3: Validation of fluvoxamine foetoplacental PBPK model

Since there is a higher risk of congenital disabilities for newborns of women treated with SSRIs, a fluvoxamine foetoplacental PBPK model was validated to review the trend regarding the fluvoxamine levels in the umbilical cord. The model was validated only by the VPC with the reported values by Hostetter et al. (2000) [217], Sit et al. (2011) [218], and Rampono et al. (2009) [219]. Even though the individual observed values are sparse, the values fall within the range of the predicted cord concentrations (Figure 2.9).

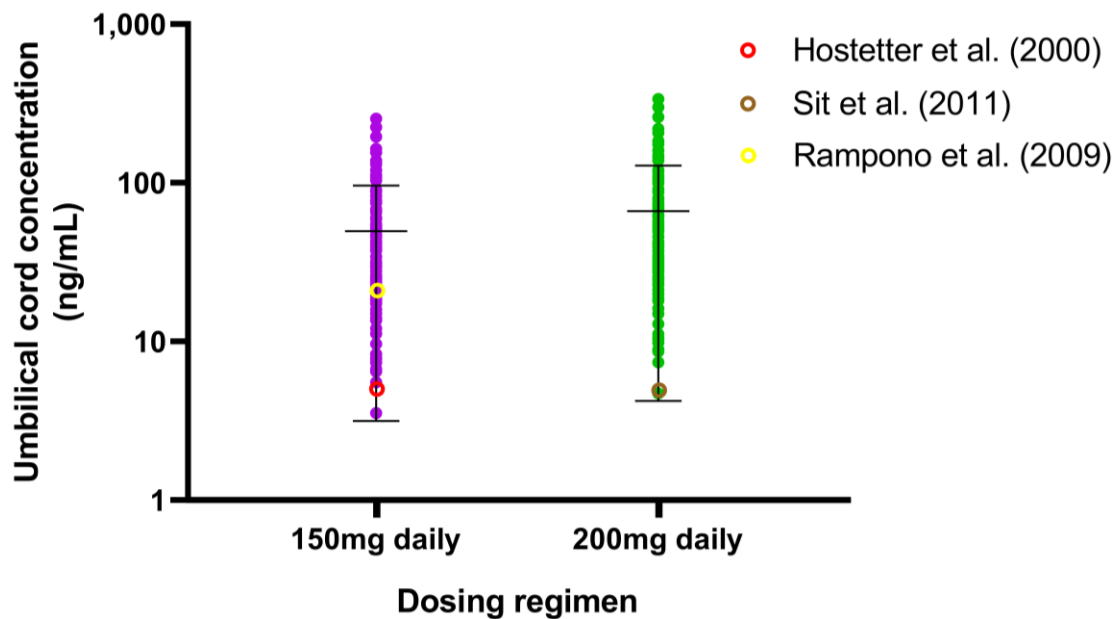


Figure 2.9 Simulated fluvoxamine foetal (umbilical cord) concentrations.

Doses were administered to steady-state with sampling on the final 30-h period of GW 40. Solid circles represent individual predicted cord concentrations. Coloured open circles represent the observed umbilical cord concentrations from Hostetter et al. (2000) [217], Sit et al. (2011) [218], and Rampono et al. (2009) [219]. Horizontal lines on the coloured data points represent the mean and SD.

2.3.4 Step 4: Impact of CYP2D6 phenotype and dose adjustment during gestation

Given the several-fold increase in the C_{max} , AUC, and $t_{1/2}$ in PM CYP2D6 compared to the EM CYP2D6 [222], the impact of the CYP2D6 phenotype on the fluvoxamine levels in the pregnant population was explored. The plasma concentration levels for both the mother (GW 0 – 40) and umbilical cord (GW 20 – 40) were compared across the UM, EM, and PM CYP2D6 phenotypes (Figure 2.10 and Figure 2.11) and the changes as compared to the baseline (0) for the mother (Table 2.5), while the percentage changes regarding the umbilical cord concentration from GW 20 are reported in Table 2.6.

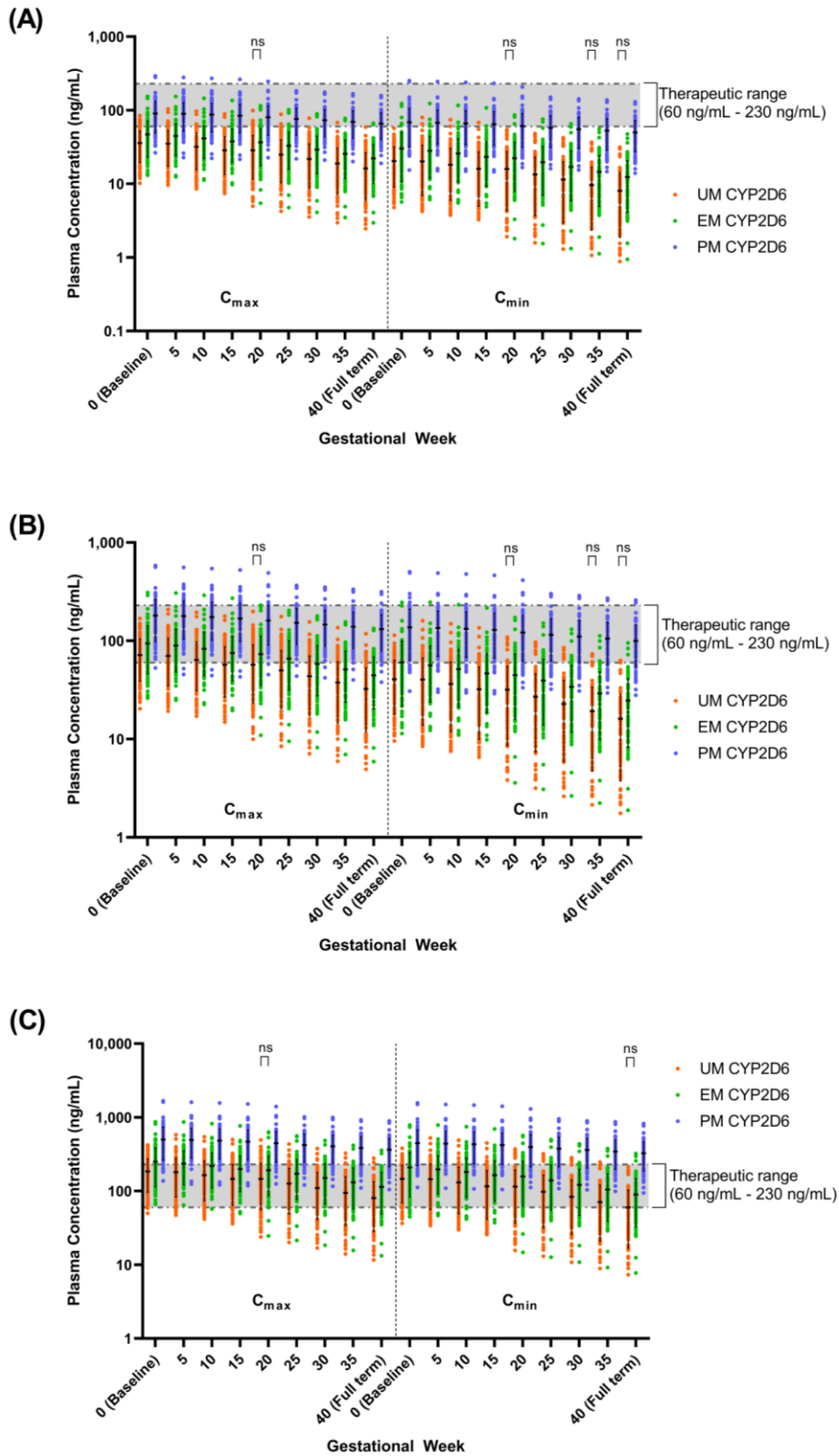


Figure 2.10 Simulated fluvoxamine maternal concentrations in CYP2D6 phenotype population.

(A) 50 mg daily; (B) 100 mg daily; (C) 300 mg daily. Coloured solid circles represent individual, predicted maternal concentrations. C_{max} , maximum concentration; C_{min} , minimum concentration. Horizontal lines on the coloured solid circles represent mean and standard deviations. The shaded region represents the fluvoxamine TW. Comparison between each CYP2D6 phenotype for every 5 GWs showed statistically significant difference except between UM and EM at GW labelled as 'ns', $p > 0.05$.

Table 2.5 Summary of predicted fluvoxamine plasma concentrations during gestation

Daily dose	Phenotype		Gestational Week (GW)								
			0 (Baseline)	5	10	15	20↓	25	30	35	40 (Full term)
50 mg	UM CYP2D6	Steady-state C _{min} (ng/mL)	20.34 (11.28)	20.19 (13.18)	18.19 (12.16)	16.04 (10.99)	15.90 (11.52)	13.43 (9.68)	11.40 (8.40)	9.61 (7.21)	8.05 (6.15)
		% change from baseline		-0.72	-10.55	-21.13	-21.82	-33.94	-43.93	-52.75	-60.40
		<i>p-value</i> *		0.9999	0.5661	0.0229	0.0171	<0.0001	<0.0001	<0.0001	<0.0001
		% C _{min} < 60 ng/mL [#]	100	98	98	99	100	100	100	100	100
		Steady-state C _{max} (ng/mL)	35.82 (16.28)	35.09 (17.59)	31.98 (16.38)	28.49 (14.99)	28.57 (16.75)	24.98 (14.64)	21.80 (13.08)	18.86 (11.57)	16.20 (10.16)
		% change from baseline		-2.04	-10.72	-20.47	-20.24	-30.27	-39.15	-47.34	-54.77
	<i>p-value</i> *		0.9995	0.3221	0.0037	0.0043	<0.0001	<0.0001	<0.0001	<0.0001	
	% C _{max} > 230 ng/mL [#]	0	0	0	0	0	0	0	0	0	
	EM CYP2D6	Steady-state C _{min} (ng/mL)	30.14 (19.33)	28.07 (16.06)	25.80 (15.07)	23.27 (13.90)	22.36 (14.29)	19.69 (12.66)	17.00 (11.05)	14.54 (9.56)	12.36 (8.20)
		% change from baseline		-6.87	-14.40	-22.80	-25.82	-34.67	-43.61	-51.75	-59.01
		<i>p-value</i> *		0.8536	0.1452	0.0033	0.0006	<0.0001	<0.0001	<0.0001	<0.0001
		% C _{min} < 60 ng/mL [#]	93	95	98	98	97	98	99	100	100
		Steady-state C _{max} (ng/mL)	46.99 (23.79)	44.73 (20.46)	41.44 (19.29)	37.65 (17.91)	36.64 (18.90)	32.91 (17.07)	29.11 (15.27)	25.53 (13.55)	22.20 (11.94)
		% change from baseline		-4.81	-11.80	-19.89	-22.02	-29.96	-38.04	-45.68	-52.76
	<i>p-value</i> *		0.9358	0.1602	0.0019	0.0004	<0.0001	<0.0001	<0.0001	<0.0001	
% C _{max} > 230 ng/mL [#]	0	0	0	0	0	0	0	0	0		
PM CYP2D6	Steady-state C _{min} (ng/mL)	68.51 (36.54)	67.54 (32.65)	66.21 (31.92)	64.58 (30.97)	60.80 (29.7)	57.69 (26.25)	55.29 (25.09)	52.68 (23.83)	49.88 (22.49)	
	% change from baseline		-1.43	-3.37	-5.75	-11.26	-15.80	-19.30	-23.10	-27.19	
	<i>p-value</i> *		0.9997	0.9944	0.9102	0.302	0.0564	0.0102	0.0011	<0.0001	
	% C _{min} < 60 ng/mL [#]	44	45	48	50	58	60	65	65	69	

	Steady-state C _{max} (ng/mL)	90.43 (40.94)	89.40 (37.15)	87.17 (36.23)	84.38 (35.04)	80.17 (34.19)	76.21 (30.35)	73.03 (29.04)	69.54 (27.62)	65.77 (26.08)
	% change from baseline		-1.14	-3.60	-6.68	-11.34	-15.72	-19.24	-23.10	-27.27
	<i>p-value</i> *		0.9997	0.9848	0.7071	0.164	0.0184	0.0018	<0.0001	<0.0001
	% C _{max} > 230 ng/mL [#]	2	1	1	1	1	0	0	0	0
100 mg UM CYP2D6	Steady-state C _{min} (ng/mL)	40.70 (22.58)	40.41 (26.40)	36.41 (24.34)	32.11 (22.01)	31.82 (23.08)	26.89 (19.39)	22.82 (16.82)	19.23 (14.45)	16.11 (12.31)
	% change from baseline		-0.72	-10.55	-21.13	-21.82	-33.94	-43.93	-52.75	-60.41
	<i>p-value</i> *		0.9999	0.5666	0.023	0.0172	<0.0001	<0.0001	<0.0001	<0.0001
	% C _{min} < 60 ng/mL [#]	78	78	84	92	90	94	94	97	99
	Steady-state C _{max} (ng/mL)	71.70 (32.59)	70.23 (35.22)	64.01 (32.80)	57.02 (30.01)	57.18 (33.54)	49.99 (29.32)	43.63 (26.19)	37.75 (23.18)	32.42 (20.34)
	% change from baseline		-2.04	-10.72	-20.46	-20.24	-30.27	-39.15	-47.34	-54.77
	<i>p-value</i> *		0.9995	0.3225	0.0038	0.0043	<0.0001	<0.0001	<0.0001	<0.0001
	% C _{max} > 230 ng/mL [#]	0	0	0	0	0	0	0	0	0
EM CYP2D6	Steady-state C _{min} (ng/mL)	60.33 (38.70)	56.19 (32.17)	51.64 (30.17)	46.57 (27.84)	44.76 (28.65)	39.42 (25.37)	34.03 (22.14)	29.11 (19.15)	24.73 (16.43)
	% change from baseline		-6.87	-14.40	-22.81	-25.82	-34.66	-43.60	-51.75	-59.01
	<i>p-value</i> *		0.8538	0.1455	0.0033	0.0006	<0.0001	<0.0001	<0.0001	<0.0001
	% C _{min} < 60 ng/mL [#]	60	62	72	78	78	83	89	96	97
	Steady-state C _{max} (ng/mL)	94.04 (47.64)	89.52 (40.96)	82.95 (38.62)	75.34 (35.85)	73.35 (37.87)	65.87 (34.20)	58.27 (30.60)	51.09 (27.15)	44.43 (23.91)
	% change from baseline		-4.81	-11.80	-19.89	-22.01	-29.96	-38.04	-45.67	-52.75
	<i>p-value</i> *		0.9359	0.1607	0.0019	0.0004	<0.0001	<0.0001	<0.0001	<0.0001
	% C _{max} > 230 ng/mL [#]	2	1	1	1	1	0	0	0	0

PM CYP2D6	Steady-state C _{min} (ng/mL)	137.03 (73.09)	135.07 (65.31)	132.41 (63.84)	129.15 (61.95)	121.60 (59.40)	115.38 (52.50)	110.58 (50.17)	105.37 (47.66)	99.77 (44.98)
	% change from baseline		-1.43	-3.37	-5.75	-11.26	-15.80	-19.30	-23.10	-27.19
	<i>p-value</i> *		0.9997	0.9944	0.9103	0.302	0.0565	0.0102	0.0011	<0.0001
	% C _{min} < 60 ng/mL [#]	7	7	7	7	11	11	13	17	19
	Steady-state C _{max} (ng/mL)	180.86 (81.88)	178.80 (74.3)	174.34 (72.45)	168.77 (70.08)	160.34 (68.38)	152.43 (60.71)	146.05 (58.08)	139.08 (55.23)	131.54 (52.17)
	% change from baseline		-1.14	-3.60	-6.69	-11.34	-15.72	-19.24	-23.10	-27.27
	<i>p-value</i> *		0.9997	0.9848	0.707	0.1641	0.0184	0.0018	<0.0001	<0.0001
% C _{max} > 230 ng/mL [#]	22	18	15	13	16	7	4	4	4	
300 mg UM CYP2D6	Steady-state C _{min} (ng/mL)	146.24 (76.37)	144.43 (87.69)	130.69 (81.21)	115.76 (73.81)	114.73 (77.53)	97.84 (65.77)	83.65 (57.51)	70.98 (49.80)	59.88 (42.77)
	% change from baseline		-1.24	-10.63	-20.84	-21.55	-33.09	-42.80	-51.46	-59.06
	<i>p-value</i> *		0.9997	0.4863	0.0144	0.0103	<0.0001	<0.0001	<0.0001	<0.0001
	% C _{min} < 60 ng/mL [#]	9	13	15	21	28	32	38	51	65
	Steady-state C _{max} (ng/mL)	184.13 (87.29)	180.98 (97.07)	164.56 (90.20)	146.38 (82.30)	146.20 (89.44)	126.68 (77.14)	109.74 (68.24)	94.32 (59.82)	80.52 (52.01)
	% change from baseline		-1.72	-10.63	-20.50	-20.60	-31.20	-40.40	-48.78	-56.27
	<i>p-value</i> *		0.9996	0.378	0.0062	0.0058	<0.0001	<0.0001	<0.0001	<0.0001
% C _{max} > 230 ng/mL [#]	28	31	22	13	15	10	6	6	2	
EM CYP2D6	Steady-state C _{min} (ng/mL)	209.09 (124.25)	196.46 (103.95)	181.21 (97.8)	164.03 (90.56)	157.89 (95.00)	139.86 (84.78)	121.61 (74.65)	104.83 (65.14)	89.70 (56.41)
	% change from baseline		-6.04	-13.33	-21.55	-24.48	-33.11	-41.84	-49.86	-57.10
	<i>p-value</i> *		0.8938	0.1619	0.0034	0.0006	<0.0001	<0.0001	<0.0001	<0.0001
	% C _{min} < 60 ng/mL [#]	5	3	4	5	11	13	20	25	38

	Steady-state C_{\max} (ng/mL)	249.43 (134.54)	236.20 (114.15)	218.50 (107.52)	198.28 (99.70)	192.26 (105.20)	171.75 (94.46)	150.93 (83.85)	131.50 (73.82)	113.68 (64.51)
	% change from baseline		-5.30	-12.40	-20.51	-22.92	-31.14	-39.49	-47.28	-54.42
	<i>p-value</i> *		0.917	0.1583	0.0023	0.0005	<0.0001	<0.0001	<0.0001	<0.0001
	% C_{\max} > 230 ng/mL [#]	50	47	37	27	25	21	16	9	3
PM CYP2D6	Steady-state C_{\min} (ng/mL)	446.83 (223.35)	441.25 (200.60)	432.13 (196.01)	420.84 (190.08)	396.98 (182.97)	377.01 (161.66)	361.44 (154.58)	344.51 (146.93)	326.3 (138.77)
	% change from baseline		-1.25	-3.29	-5.82	-11.16	-15.63	-19.11	-22.90	-26.97
	<i>p-value</i> *		0.9997	0.9936	0.8757	0.2526	0.0398	0.006	0.0005	<0.0001
	% C_{\min} < 60 ng/mL [#]	0	0	0	0	0	0	0	0	0
	Steady-state C_{\max} (ng/mL)	500.13 (236.64)	494.14 (213.61)	482.70 (208.5)	468.46 (201.93)	443.69 (195.69)	421.55 (173.34)	403.91 (165.78)	384.70 (157.60)	363.99 (148.84)
	% change from baseline		-1.20	-3.49	-6.33	-11.28	-15.71	-19.24	-23.08	-27.22
	<i>p-value</i> *		0.9997	0.9902	0.7867	0.1985	0.0257	0.0031	0.0002	<0.0001
	% C_{\max} > 230 ng/mL [#]	94	93	93	93	90	89	87	86	81

C_{\min} , trough plasma concentration; C_{\max} , maximum plasma concentration; **p-value*: statistical significance test between each GW with baseline; $p < 0.05$, statistically significant difference; [#]Efficacy threshold (60 ng/mL – 230 ng/mL) as recommended in Consensus Guidelines for Therapeutic Drug Monitoring in Neuropsychopharmacology: Update 2017 [172]; Mean (SD); ↓, initiation of foetoplacental PBPK model.

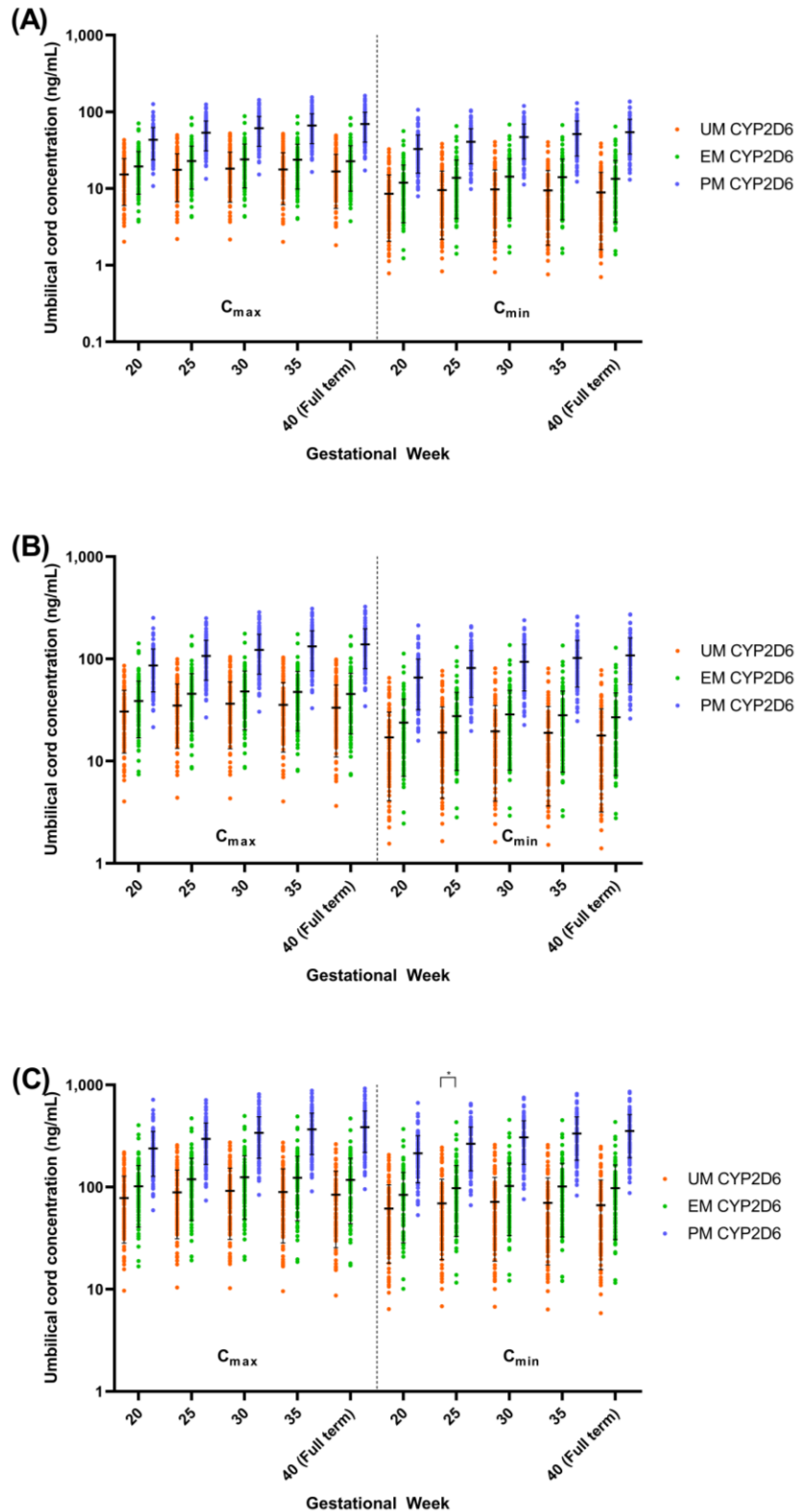


Figure 2.11 Simulated fluvoxamine umbilical cord concentrations in CYP2D6 phenotype population.

(A) 50 mg daily; (B) 100 mg daily; (C) 300 mg daily. Coloured solid circles represent individual, predicted umbilical cord concentrations. C_{max} , maximum concentration; C_{min} , minimum concentration. Horizontal lines on the coloured solid circles represent mean and standard deviations. Comparing each CYP2D6 phenotype for every 5 GWs starting from GW 20 showed a statistically significant difference when compared with PM and a non-statistically significant difference between UM and EM at GW 25 for 300 mg daily labelled as ^{*}, $p < 0.05$.

Table 2.6 Summary of simulated fluvoxamine umbilical cord concentrations during gestation

Daily dose	Phenotype		Gestational Week (GW)				
			20	25	30	35	40 (Full term)
50 mg	UM CYP2D6	Steady-state	8.60	9.61	9.84	9.54	8.98
		C_{\min} (ng/mL)	(6.46)	(7.34)	(7.70)	(7.63)	(7.31)
		% change from GW-20		11.69	14.40	10.96	4.43
		<i>p-value</i> *		0.7359	0.5769	0.7761	0.9888
		Steady-state	15.36	17.65	18.35	17.88	16.8
		C_{\max} (ng/mL)	(9.22)	(10.80)	(11.55)	(11.56)	(11.13)
	EM CYP2D6	% change from GW-20		14.91	19.48	16.42	9.39
		<i>p-value</i> *		0.3882	0.1715	0.3036	0.7637
		Steady-state	11.90	13.76	14.28	14.02	13.34
		C_{\min} (ng/mL)	(8.25)	(9.60)	(10.08)	(9.99)	(9.58)
		% change from GW-20		15.71	20.08	17.88	12.13
		<i>p-value</i> *		0.4456	0.2287	0.3151	0.6341
PM CYP2D6	Steady-state	19.37	22.79	24	23.71	22.58	
	C_{\max} (ng/mL)	(10.81)	(12.78)	(13.63)	(13.64)	(13.16)	
	% change from GW-20		17.67	23.92	22.42	16.58	
	<i>p-value</i> *		0.1931	0.041	0.0594	0.2244	
	Steady-state	33.00	40.91	47.10	51.39	54.31	
	C_{\min} (ng/mL)	(16.85)	(19.52)	(22.46)	(24.44)	(25.74)	
100 mg	UM CYP2D6	% change from GW-20		23.95	42.72	55.71	64.58
		<i>p-value</i> *		0.0424	<0.0001	<0.0001	<0.0001
		Steady-state	43.22	53.59	61.42	66.47	69.54
		C_{\max} (ng/mL)	(19.21)	(22.26)	(25.56)	(27.65)	(28.91)
		% change from GW-20		23.98	42.11	53.78	60.88
		<i>p-value</i> *		0.0139	<0.0001	<0.0001	<0.0001
	EM CYP2D6	Steady-state	17.22	19.23	19.69	19.10	17.98
		C_{\min} (ng/mL)	(12.94)	(14.69)	(15.43)	(15.28)	(14.63)
		% change from GW-20		11.68	14.39	10.95	4.41
		<i>p-value</i> *		0.7365	0.5781	0.777	0.9889
		Steady-state	30.75	35.33	36.73	35.8	33.63
		C_{\max} (ng/mL)	(18.46)	(21.62)	(23.13)	(23.15)	(22.29)
EM CYP2D6	% change from GW-20		14.90	19.47	16.42	9.38	
	<i>p-value</i> *		0.3889	0.1721	0.3042	0.7647	
	Steady-state	23.81	27.55	28.59	28.07	26.70	
	C_{\min} (ng/mL)	(16.54)	(19.23)	(20.2)	(20.02)	(19.20)	
	% change from GW-20		15.71	20.07	17.86	12.11	
	<i>p-value</i> *		0.4463	0.2297	0.3164	0.6357	

		Steady-state	38.77	45.63	48.05	47.47	45.20
		C _{max} (ng/mL)	(21.65)	(25.60)	(27.31)	(27.33)	(26.36)
		% change from GW-20		17.67	23.92	22.42	16.58
		<i>p-value</i> *		0.1935	0.0412	0.0598	0.2253
	PM	Steady-state	66.00	81.81	94.20	102.77	108.63
	CYP2D6	C _{min} (ng/mL)	(33.70)	(39.04)	(44.93)	(48.89)	(51.48)
		% change from GW-20		23.95	42.72	55.71	64.58
		<i>p-value</i> *		0.0425	<0.0001	<0.0001	<0.0001
		Steady-state	86.44	107.18	122.84	132.93	139.06
		C _{max} (ng/mL)	(38.42)	(44.52)	(51.12)	(55.31)	(57.81)
		% change from GW-20		23.98	42.11	53.78	60.87
		<i>p-value</i> *		0.0139	<0.0001	<0.0001	<0.0001
300 mg	UM	Steady-state	62.05	69.96	72.27	70.72	67.06
	CYP2D6	C _{min} (ng/mL)	(43.4)	(49.76)	(52.72)	(52.68)	(50.82)
		% change from GW-20		12.75	16.48	13.98	8.08
		<i>p-value</i> *		0.6345	0.4114	0.5583	0.892
		Steady-state	78.68	89.65	92.71	90.21	84.94
		C _{max} (ng/mL)	(49.54)	(57.41)	(61.00)	(60.84)	(58.56)
		% change from GW-20		13.95	17.84	14.66	7.96
		<i>p-value</i> *		0.4771	0.2612	0.4329	0.8636
	EM	Steady-state	83.97	97.78	102.33	101.33	97.10
	CYP2D6	C _{min} (ng/mL)	(54.74)	(64.14)	(67.94)	(67.89)	(65.53)
		% change from GW-20		16.45	21.87	20.67	15.63
		<i>p-value</i> *		0.3650	0.1401	0.1708	0.3843
		Steady-state	101.77	119.11	124.76	123.01	117.28
		C _{max} (ng/mL)	(60.36)	(70.95)	(75.21)	(75.01)	(72.28)
		% change from GW-20		17.04	22.59	20.87	15.24
		<i>p-value</i> *		0.2577	0.0774	0.112	0.3306
	PM	Steady-state	215.23	267.09	307.70	335.79	354.74
	CYP2D6	C _{min} (ng/mL)	(103.83)	(120.31)	(138.54)	(150.74)	(158.57)
		% change from GW-20		24.09	42.96	56.01	64.82
		<i>p-value</i> *		0.0274	<0.0001	<0.0001	<0.0001
		Steady-state	239.62	296.94	340.49	369.09	387.32
		C _{max} (ng/mL)	(110.43)	(127.87)	(146.82)	(159.08)	(166.69)
		% change from GW-20		23.92	42.10	54.03	61.64
		<i>p-value</i> *		0.0194	<0.0001	<0.0001	<0.0001

C_{min}, trough umbilical cord concentration; C_{max}, maximum umbilical cord concentration; **p-value*: statistical significance test between each GW with GW-20; *p* < 0.05, statistically significant difference; Mean (SD).

A statistically significant difference between the UM and EM with respect to the PM CYP2D6 phenotype population for each 5th GW were noted across all three doses (Figure 2.10). A similar pattern was seen between the UM and EM CYP2D6 populations with few exceptions, particularly in GW 20 regarding the C_{max} and C_{min} when the foetoplacental PBPK model was initiated (Figure 2.10). However, the significant difference is minimal as compared to the PM. As for the cord concentration, the difference was significant with the PM but not between the UM and EM CYP2D6 populations across all five GWs (Figure 2.11). Since statistically significant differences were seen between the UM and EM CYP2D6 populations, the dosing regimens for each of the CYP2D6 phenotype populations were explored.

Looking at the concentration trend (Table 2.5), the same pattern was identified for both the UM and EM populations, with the concentration significantly decreasing across all three doses starting from GW 15 in both the peak and trough. Whereas for the PM population, the concentration began to drop significantly from GW 25 for the peak and GW 30 for the trough, except at the 300 mg daily dose, where the decrease started to be statistically significant at GW 25. These patterns concur with the concentration trend in the general pregnant population reported in Step 2.

Moreover, for the 50 mg daily dose at GW 40, both the trough and peak levels demonstrated 60.40% and 54.77% decreases for the UM population and 59.01% and 52.76% decreases for the EM population when compared to the baseline. Whereas for the PM population, 27.19% and 27.27% falls were noted for the trough and peak, respectively. This pattern is comparable across the 100 mg and 300 mg daily doses (Table 2.5).

Regarding the foetal cord level, both the trough and peak concentrations increased at full term compared to GW 20, and this transpired at all three-dose levels and CYP2D6 phenotype populations (Table 2.6). The PM CYP2D6 population demonstrated a significant increase across all GWs at the 50 mg daily dose (trough, 23.95% at GW 25 vs. 64.58% at full term; peak, 23.98% at GW 25 vs 60.88% at full term), 100 mg daily dose (trough, 23.95% at GW 25 vs. 64.58% at full term; peak, 23.98% at GW 25 vs. 60.87% at full term), and 300 mg daily dose (trough, 24.09% at GW 25 vs 64.82% at full term; peak, 23.92% at GW 25 vs. 61.64% at full term). Unlike the PM population, UM and EM have the same trend, in which the cord level increases until GW 30 and decreases back until the full term, with a significant difference only seen between GW 30 and GW 20 for the peak of the EM CYP2D6 population in the 50 mg daily and 100 mg daily doses (Table 2.6).

The percentage of subjects where the trough level falls below 60 ng/mL is more than 50% for both the UM and EM populations at doses of 50 mg daily and 100 mg daily. In contrast, with respect to the 300 mg daily dose for the UM population, this trend started from GW 35 when

the C_{\min} fell below 60 ng/mL for more than 50% of the subjects and did not reach 40% of the subjects for the EM population. As for the PM population, the percentage of subjects for whom the peak level rose above 230 ng/mL is more than 90% for the 300 mg daily dose; for 50 mg daily dose, more than 40% of the subjects, the peak level falls below 60 ng/mL (Table 2.5).

Since the percentage of subjects where the peak and trough levels fall outside the therapeutic windows varies between the different phenotypes of the CYP2D6 populations, the threshold of 20% outside of the therapeutic windows was used to determine the suitable dose for the pregnant population according to their phenotype (Figure S 2-2, Figure S 2-3, Figure S 2-4, Figure S 2-5, Figure S 2-6, and Figure S 2-7) [186, 188, 189].

For the UM CYP2D6 population, a fluvoxamine dose of 250 mg or 275 mg daily in the first trimester, followed by a maximum dose of 300 mg daily until the full term, is suggested to be optimum, as it corresponds to a point at which the maternal concentrations are within the therapeutic windows for most of the subjects (Table 2.7). Nevertheless, for the maximum dose of 300 mg daily, the percentage of subjects with a C_{\min} below 60 ng/mL is between 21% in GW 15 to 65% in the full term, but none of the peak concentrations are above 230 ng/mL (Table 2.7, Figure S 2-2, and Figure S 2-3).

For EM, a fluvoxamine dose of 175 mg daily is suitable up to GW 10, a 200 mg daily dose is ideal up to GW 15, and a 225 mg daily dose is advisable between GW 5 to 20, which covers the first trimester and the early second trimester. A 250 mg daily dose can be used for GW 10 to 25, while a 275 mg daily dose is effective between GW 15 to 30, covering the second trimester. As for GW 30 to full term, a maximum dose of 300 mg daily is considered the most effective, since it had the most subjects where the C_{\min} and C_{\max} fell within the therapeutic range (Table 2.7, Table 2.8, Figure S 2-4, and Figure S 2-5).

Table 2.7 Percentage of subjects with trough and peak outside the therapeutic window

Phenotype	Dose		Gestational Week								
			0	5	10	15	20	25	30	35	40
UM CYP2D6	50 mg	$C_{min} < 60$ ng/mL	100	98	98	99	100	100	100	100	100
		$C_{max} > 230$ ng/mL	0	0	0	0	0	0	0	0	0
	75 mg	$C_{min} < 60$ ng/mL	94	94	96	97	93	97	98	100	100
		$C_{max} > 230$ ng/mL	0	0	0	0	0	0	0	0	0
	100 mg	$C_{min} < 60$ ng/mL	78	78	84	92	90	94	94	97	99
		$C_{max} > 230$ ng/mL	0	0	0	0	0	0	0	0	0
	125 mg	$C_{min} < 60$ ng/mL	67	67	72	79	81	89	94	94	95
		$C_{max} > 230$ ng/mL	0	2	1	0	1	0	0	0	0
	150 mg	$C_{min} < 60$ ng/mL	55	61	66	70	72	82	89	94	94
		$C_{max} > 230$ ng/mL	1	2	2	2	1	1	1	0	0
	175 mg	$C_{min} < 60$ ng/mL	40	46	50	58	55	67	74	80	88
		$C_{max} > 230$ ng/mL	1	2	2	2	2	1	0	0	0
	200 mg	$C_{min} < 60$ ng/mL	29	32	37	49	40	53	67	74	80
		$C_{max} > 230$ ng/mL	7	5	3	2	5	2	1	0	0
	225 mg	$C_{min} < 60$ ng/mL	27	27	32	43	37	49	58	68	77
		$C_{max} > 230$ ng/mL	8	8	6	3	7	4	2	1	0
	250 mg	$C_{min} < 60$ ng/mL	15	16	25	32	33	38	51	64	72
		$C_{max} > 230$ ng/mL	15	14	8	7	9	6	2	2	1
	275 mg	$C_{min} < 60$ ng/mL	11	15	20	28	30	37	43	55	68
		$C_{max} > 230$ ng/mL	24	22	14	8	11	6	6	2	1
	300 mg	$C_{min} < 60$ ng/mL	9	13	15	21	28	32	38	51	65
		$C_{max} > 230$ ng/mL	28	31	22	13	15	10	6	6	2

EM CYP2D6	50 mg	$C_{min} < 60$ ng/mL	93	95	98	98	97	98	99	100	100
		$C_{max} > 230$ ng/mL	0	0	0	0	0	0	0	0	0
	75 mg	$C_{min} < 60$ ng/mL	80	86	90	92	91	96	97	97	98
		$C_{max} > 230$ ng/mL	1	0	0	0	0	0	0	0	0
	100 mg	$C_{min} < 60$ ng/mL	60	62	72	78	78	83	89	96	97
		$C_{max} > 230$ ng/mL	2	1	1	1	1	0	0	0	0
	125 mg	$C_{min} < 60$ ng/mL	40	46	53	61	61	74	80	84	93
		$C_{max} > 230$ ng/mL	4	3	3	2	3	2	0	0	0
	150 mg	$C_{min} < 60$ ng/mL	32	34	41	48	50	58	73	79	83
		$C_{max} > 230$ ng/mL	8	4	4	3	3	3	3	1	0
	175 mg	$C_{min} < 60$ ng/mL	19	13	19	24	35	41	46	55	74
		$C_{max} > 230$ ng/mL	9	6	5	4	3	3	3	2	0
	200 mg	$C_{min} < 60$ ng/mL	12	7	10	16	22	34	42	46	55
		$C_{max} > 230$ ng/mL	16	12	8	6	5	3	3	3	2
	225 mg	$C_{min} < 60$ ng/mL	10	5	7	10	20	24	36	42	48
		$C_{max} > 230$ ng/mL	22	15	12	9	10	5	3	3	3
	250 mg	$C_{min} < 60$ ng/mL	7	5	5	7	15	20	25	39	43
		$C_{max} > 230$ ng/mL	34	24	17	14	17	13	5	3	3
	275 mg	$C_{min} < 60$ ng/mL	6	4	5	5	12	16	22	36	42
		$C_{max} > 230$ ng/mL	45	34	26	17	21	15	11	3	3
300 mg	$C_{min} < 60$ ng/mL	5	3	4	5	11	13	20	25	38	
	$C_{max} > 230$ ng/mL	50	47	37	27	25	21	16	9	3	

PM CYP2D6	50 mg	$C_{min} < 60$ ng/mL	44	45	48	50	58	60	65	65	69
		$C_{max} > 230$ ng/mL	2	1	1	1	1	0	0	0	0
75 mg	$C_{min} < 60$ ng/mL		18	19	20	21	23	26	30	33	37
		$C_{max} > 230$ ng/mL	4	4	4	4	3	3	3	3	2
100 mg	$C_{min} < 60$ ng/mL		7	7	7	7	11	11	13	17	19
		$C_{max} > 230$ ng/mL	22	18	15	13	16	7	4	4	4
125 mg	$C_{min} < 60$ ng/mL		2	2	2	3	4	5	6	8	9
		$C_{max} > 230$ ng/mL	45	47	44	43	29	24	21	19	16
150 mg	$C_{min} < 60$ ng/mL		1	2	2	2	2	2	2	3	4
		$C_{max} > 230$ ng/mL	64	65	59	57	46	45	44	36	28
175 mg	$C_{min} < 60$ ng/mL		0	0	0	0	0	0	0	1	1
		$C_{max} > 230$ ng/mL	65	68	68	65	56	47	45	41	37
200 mg	$C_{min} < 60$ ng/mL		0	0	0	0	0	0	0	0	0
		$C_{max} > 230$ ng/mL	76	73	72	72	67	65	60	57	47
225 mg	$C_{min} < 60$ ng/mL		0	0	0	0	0	0	0	0	0
		$C_{max} > 230$ ng/mL	81	78	77	76	73	69	69	66	61
250 mg	$C_{min} < 60$ ng/mL		0	0	0	0	0	0	0	0	0
		$C_{max} > 230$ ng/mL	85	87	86	82	81	79	76	72	69
275 mg	$C_{min} < 60$ ng/mL		0	0	0	0	0	0	0	0	0
		$C_{max} > 230$ ng/mL	91	93	91	89	86	86	82	79	74
300 mg	$C_{min} < 60$ ng/mL		0	0	0	0	0	0	0	0	0
		$C_{max} > 230$ ng/mL	94	93	93	93	90	89	87	86	81

The red column indicated that the percentage of subjects with trough and peak outside the therapeutic window (60 ng/mL – 230 ng/mL) is more than 20%

Table 2.8 Summary of recommended daily dose, predicted clearance, AUC, and umbilical cord concentrations based on the recommended doses

Phenotype		Gestational Week (GW)									
		0 (Baseline)	5	10	15	20↓	25	30	35	40 (Full term)	
UM CYP2D6	Recommended daily dose (mg)	250	250	275	300	300	300	300	300	300	
	CL (L/h)	95.69 (51.51)	101.60 (59.00)	104.50 (62.05)	128.70 (77.43)	144.40 (113.00)	166.70 (131.00)	196.90 (157.80)	234.20 (190.80)	279.90 (231.30)	
	AUC (ng/mL.h)	1691.00 (836.10)	1665.00 (944.40)	1640.00 (958.40)	1611.00 (959.20)	1603.00 (1025.00)	1380.00 (877.50)	1189.00 (772.30)	1017.00 (673.40)	863.70 (582.30)	
	Cord conc.	C_{min} (ng/mL)					61.49 (43.49)	69.33 (49.85)	71.62 (52.80)	70.08 (52.74)	66.45 (50.88)
		C_{max} (ng/mL)					77.97 (49.70)	88.84 (57.58)	91.86 (61.15)	89.38 (60.98)	84.16 (58.68)
EM CYP2D6	Recommended daily dose (mg)	175, 200	175, 200, 225	175, 200, 225, 250	200, 225, 250, 275	225, 250, 275	250, 275	275, 300	300	300	
	CL (L/h)	66.97 (41.10)	74.37 (43.17)	72.33 (39.38)	81.45 (45.32)	91.63 (72.31)	106.60 (86.12)	123.40 (101.50)	149.60 (124.70)	175.90 (148.80)	
	AUC (ng/mL.h)	1743.00 (994.60)	1751.00 (905.60)	1724.00 (922.30)	1749.00 (944.70)	1776.00 (1029.00)	1664.00 (960.70)	1595.00 (933.00)	1453.00 (855.50)	1251.00 (744.90)	
	Cord conc.	C_{min} (ng/mL)					69.28 (46.30)	84.98 (56.66)	97.57 (65.93)	101.50 (68.97)	97.40 (66.77)
		C_{max} (ng/mL)					83.83 (51.01)	103.40 (62.61)	118.80 (72.98)	123.10 (76.28)	117.50 (73.72)

PM	Recommended	75, 100	75, 100	75, 100	100,	100	100	100	100, 125	100, 125
CYP2D6	daily dose (mg)									
	CL (L/h)	31.44 (14.72)	31.77 (15.88)	32.48 (16.22)	33.39 (16.68)	35.11 (16.04)	36.57 (16.46)	38.12 (17.11)	39.97 (17.85)	42.18 (18.78)
	AUC (ng/mL.h)	3373.00 (1723.00)	3331.00 (1564.00)	3257.00 (1527.00)	3618.00 (1598.00)	3422.00 (1545.00)	3251.00 (1367.00)	3116.00 (1308.00)	3340.00 (1452.00)	3162.00 (1372.00)
	Cord conc.									
	C_{\min} (ng/mL)					65.60 (33.83)	81.33 (39.24)	93.67 (45.16)	115.00 (56.94)	121.50 (59.97)
	C_{\max} (ng/mL)					86.10 (38.67)	106.80 (44.91)	122.40 (51.55)	149.00 (65.13)	155.90 (68.07)

Mean (SD); C_{\min} , trough concentration; C_{\max} , maximum concentration; CL, clearance; AUC, Area-under-the-curve; ↓, initiation of foetoplacental PBPK model; Cord conc., cord concentration.

With regard to PM, this approach revealed that a dose of 75 mg daily is suitable for GW 10, while a 100 mg daily dose is effective throughout pregnancy. It is also possible to increase the dose to 125 mg daily at GW 35 until labour, as the percentage of subjects for which the trough and peak fall within the therapeutic window is 8% and 9% for the trough and 19% and 16% for the peak for GW 35 and 40, respectively (Table 2.7, Figure S 2-6, and Figure S 2-7).

A gradual increase in the clearance from GW 5 to GW 30 was observed for both the UM and EM CYP2D6 populations, while the clearance is constant throughout pregnancy for the PM population (Figure 2.12 and Table 2.8). Likewise, the AUC remained steady throughout pregnancy for the PM population, while the AUC slightly decreased starting from GW 25 to full term for the UM and EM populations (Figure 2.12 and Table 2.8). This trend is expected since the suggested doses are higher as the pregnancy is near the full term for both UM and EM, but for PM, the recommended dose is maintained throughout the gestational period.

Based on the recommended dose, the range of the expected fluvoxamine concentration that crosses the placenta is between 5.84 ng/mL to 496.10 ng/mL across the gestational period and the CYP2D6 phenotype (Figure 2.12). A similar trend was seen in both the UM and EM populations, wherein the foetal concentration increased until GW 30 and then became stagnant until labour. Whereas the cord concentrations steadily increase for the PM population until full term (Table 2.8).

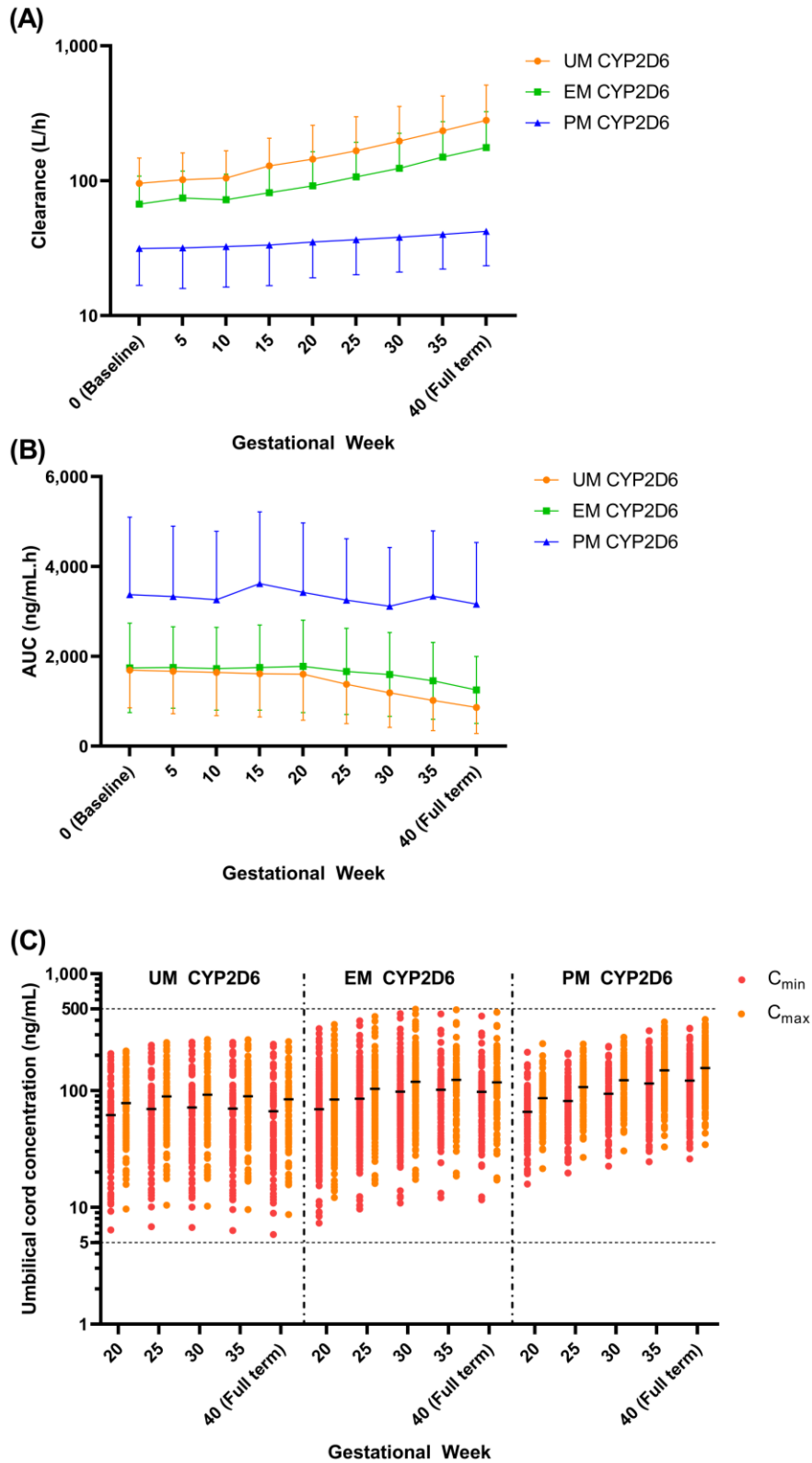


Figure 2.12 Predicted clearance, area-under-the-curve, and cord concentration based on the recommended doses.

(A) Clearance; (B) area-under-the-curve; (C) umbilical cord concentration. Top and bottom horizontal lines in (A, B) represent standard deviations. Coloured, closed circles in (C) are the predicted individual cord concentrations. Horizontal lines on the coloured, solid circles in (C) represent the mean. Dashed horizontal lines in (C) represent the range of simulated cord concentrations throughout gestational periods and all three CYP2D6 phenotypes (5 ng/mL to 500 ng/mL).

2.4 Discussion

Several observational studies have demonstrated that SSRIs, including fluvoxamine, are safe to use during pregnancy, even given the possible risk of persistent pulmonary hypertension (PPHN), for which the benefit of controlling major depression may outweigh the risk depending on the patient's situation [223-229]. However, the efficacy and impact of antidepressants in the pregnant population, particularly for fluvoxamine, are still lacking because no controlled trials have been conducted on the pregnant population.

Therapeutic drug monitoring (TDM) is one approach that can offer dose adjustment throughout gestation; however, this is often not considered viable or necessary for many drugs. However, the use of robust and validated mechanistic pharmacokinetic modelling allows for an assessment of any changes that occur in a drug's PK properties during the gestational period, one which considers the physiological changes during pregnancy and offers a pragmatic solution to the following question: "what is the correct dose during gestation?" [51, 103, 172, 186, 188-191]. Although the concept has been utilised for other compounds, this is the first time it has been used to develop a fluvoxamine PBPK pregnancy model to support maternal dosing and foetal exposure.

2.4.1 Step 1: Validation of fluvoxamine model in healthy subjects

2.4.1.1 PBPK model parameters

The modification from a minimal-PBPK model to a full-body PBPK distribution model was essential to ensure that physiological changes that occurred throughout the gestational period were considered for the PBPK pregnancy model [186, 188-191]. Furthermore, the estimation of K_p made for predicting V_{ss} using the Rodgers and Rowland approach [60, 196] resulted in a V_{ss} within two-fold of the published V_d [197, 198]. In addition, the k_a , f_a and B/P were amended based on published data and Simcyp[®] prediction [199, 200]. Finally, the modifications were guided by three single-dose and two multiple-dose studies, which were further validated through another three single-dose and three multiple-dose studies incorporating healthy subjects and four single-dose and one multiple-dose studies in CYP2D6 phenotype populations.

2.4.1.2 Validation in healthy subjects and CYP2D6 phenotype populations

The predicted PK parameters were within two-fold of the published PK studies, except for AUC_{inf} (Table 2.3). Furthermore, a similar pattern was seen for the individual AUC_{inf} comparison between the observed data by De Vries et al. (1993) [201] and the prediction, which showed a statistically significant difference for 50 mg and 100 mg formulation but not for 25 mg formulation, the overlaid PK profile, and other PK parameters including AUC_{0-t} . The AUC_{inf} is not commonly used for comparison among PK parameters, particularly in the regulatory setting, due to its reliability, specifically when the percentage differences between AUC_{inf} and AUC_{0-t} are more than 20%, as is the case here where the difference was not reported for observed data, and the difference for the prediction is more than 20% [31]. Furthermore, the total number of sampling points used is crucial for an accurate estimation of AUC_{inf} ; in this situation, the number of samples used for estimation was notably different between observed and predicted (3 to 15 samples vs >100 samples), possibly overestimating the value in one over another [230].

The imperfect prediction of the lowest dose (12.5 mg twice daily) compared to the observed Spigset et al. (1998) [209] study is compensated by a reliable prediction at the other three higher doses (25 mg twice daily, 50 mg twice daily and 100 mg twice daily) (Table 2.3 and Figure 2.5). This result may be due to the dose being lower than the minimum daily dose recommended for adults, which is 50 mg administered once daily [222]. The prediction for the PM CYP2D6 population is not ideal when weighed individually with each published study. However, an assessment of the plasma concentration profile showed that the simulated profile matched all three published studies because of the wide variation between the studies (Figure 2.6). A similar phenomenon can be seen for the prediction of multiple-dose study at the lowest dose (25 mg and 10 mg daily) when compared to the observed data by Christensen et al. (2002) [213], particularly for the PM population. The observed data fall in the lower range of the predicted data, which agrees with the prediction made by Britz et al. (2019) [231] for the fluvoxamine model (Figure 2.7).

Broader acceptance criteria, as discussed by Abduljalil et al. (2014) [232], may be considered, specifically for the PM population, since the comparisons were made between small subject samples from published works with 100 virtual patients for each simulated study and as the observed trials showed a wide variation of results. Nevertheless, the VPC strategy showed that the simulated PK profiles fall within the 5th and 95th percentile of all the 14 studies. Therefore, these results validate the fluvoxamine PBPK model in the healthy population.

2.4.2 Step 2: Verification of fluvoxamine pregnancy model and the impact of pregnancy on fluvoxamine concentration

2.4.2.1 Verification of fluvoxamine pregnancy model

Based on the literature review, Westin et al. (2017) [184] is the only publication (to date) containing fluvoxamine plasma concentration throughout the 40-week gestational period. Thus, these were the only data used to validate the fluvoxamine PBPK pregnancy model. Using the VPC strategy, the predicted fluvoxamine plasma concentrations followed the pattern of published data throughout the gestational period. Furthermore, the results showed that the difference compared to the baseline was significant from GW 20 and GW 25 for C_{max} and C_{min} , respectively, which is consistent with the published data reported by Westin et al. (2017) [184].

2.4.2.2 The impact of pregnancy on fluvoxamine concentration

The simulation demonstrated that out of 100 pregnancies, the C_{min} for more than 50% of the pregnant women falls below the minimum effective concentration of 60 ng/mL recommended by Hiemke et al. (2018) [172] for the treatment of major depression. The trend showed that the number significantly increased, particularly after GW 25 in both C_{min} and C_{max} , suggesting the need for fluvoxamine dose adjustment to maintain the same efficacy as prepartum.

The possible main factor influencing the fluvoxamine concentration during the gestational period is hepatic enzyme metabolism, specifically CYP2D6. This is because fluvoxamine is extensively metabolised in the liver, predominantly by CYP2D6, with minimal influence by CYP1A2 [185, 209, 222, 233]. Thus, the reduction in fluvoxamine plasma concentration concurs with increasing CYP2D6 activities throughout pregnancy by $25.6\% \pm 58.3\%$ at GW 14-18 to $47.8\% \pm 24.7\%$ at GW 36-40 compared to the postpartum period [234]. The same has been reported by Wadelius et al. (1997) [235], but the study only performed the phenotyping at GW 36 instead of at every trimester. Furthermore, the increasing trend of CYP2D6 enzyme's activities throughout pregnancy has also been incorporated in Simcyp® and validated based on pregnancy PBPK modelling for several compounds, namely, metoprolol and paroxetine, which are reflected in this study as well [103, 186].

On the other hand, the decreasing trend in the fluvoxamine plasma concentration throughout the gestational period further supports the findings of several publications that show the contribution of the CYP1A2 enzyme on fluvoxamine metabolism is not significant compared to the CYP2D6 enzyme [185, 209, 210, 236]. The explanation behind this is that the opposite trend between CYP2D6 and CYP1A2 activities throughout pregnancy is supposed to cancel out the impact on drug plasma concentration during pregnancy if the fractional metabolism of

a drug is equal between the two enzymes, which has not been seen in this study and study by Westin et al. (2017) [184] [103, 105, 234, 237].

Since fluvoxamine is a lipophilic drug, other physiological changes may contribute to the reduction of fluvoxamine levels, such as the expansion of intravascular and extravascular volume as well as the increase in body fat throughout the gestational period [105, 238]. In contrast, although fluvoxamine is a basic drug, the influence of changes in gastric pH and gastrointestinal motility on fluvoxamine absorption may be minimal compared to the hepatic metabolism, since fluvoxamine is highly absorbed from the gastrointestinal tract with approximately 50% bioavailability [222].

Renal changes may have minimal influence, since fluvoxamine is primarily eliminated through hepatic biotransformation with no known active metabolites, and a negligible amount of fluvoxamine is excreted unchanged in the urine [185]. Moreover, studies have shown that dose adjustment is needed for hepatic but not renal impairment patients [239-242].

2.4.3 Step 3: Validation of fluvoxamine foetoplacental PBPK model

The sparse data obtained in this study were expected, since another fluvoxamine foetoplacental model developed by Matsuoka et al. (2017) [243] was validated with data solely taken from Hostetter et al. (2000) [217]. The limited information on when the samples were taken after the last dose provides a challenge in simulating optimal timing to offer a fair comparison. Nevertheless, the fluvoxamine foetoplacental model was validated based on three published studies, which showed that all observed data fit within the standard deviation of the predicted concentration. In addition, the predicted concentrations are comparable to the Matsuoka et al. (2017) [243] predictions, particularly for the 150 mg daily doses. The fluvoxamine foetoplacental model was developed without including any specific active transport mechanism other than passive diffusion, similar to the Matsuoka et al. (2017) [243] model. Thus, the CYP2D6 activity in the mother is the main factor influencing the fluvoxamine level in the foetus.

2.4.4 Step 4: Impact of CYP2D6 phenotype and dose adjustment during gestation

2.4.4.1 Impact of CYP2D6 phenotype in the pregnant population

A notable difference was seen between the EM and PM CYP2D6 populations regarding the validation of the healthy subject models and intrinsic hepatic clearance from the verification stage in the general pregnant population. Similar information was described in the fluvoxamine prescribing information, wherein there was a several-fold increase in the C_{max} , AUC, and $t_{1/2}$ in PM CYP2D6 compared to the EM CYP2D6 [222]. Given the paucity of published data on fluvoxamine pharmacokinetics during pregnancy stratified according to CYP2D6 phenotypes, the validated fluvoxamine model in healthy CYP2D6 subjects was used to support the exploration made regarding the pregnant population according to the CYP2D6 phenotype status, in addition to the validation of CYP2D6 abundance in pregnancy performed by Almurjan et al. (2020) [186] for the paroxetine.

2.4.4.2 Maternal plasma concentration changes throughout pregnancy

The significant difference in both the trough and peak concentrations between the EM and PM phenotypes in healthy subjects is comparable to the pregnant population, as demonstrated in this study (Figure 2.10) [210, 211]. The difference between UM and EM is significant for most of the GWs across three doses but with reduced magnitude when compared with the PM. Due to this difference, the fluvoxamine dosage regimen for the UM population in pregnant women was explored. This information can also be used to investigate the difference between the UM and EM CYP2D6 phenotypes in healthy subjects, because the two guidance on dose selection for the CYP2D6 phenotypes published by the Clinical Pharmacogenetics Implementation Consortium (CPIC) and the Dutch Pharmacogenetics Working Group (DPWG) only provide dose recommendation for the EM and PM populations but not for UM CYP2D6 population due to limited information [244, 245].

Regarding the plasma concentration trend throughout the gestational period within each CYP2D6 phenotype, it is comparable to the general pregnant population. The distinction between each phenotype is mainly corresponded to when the difference became significant, which was earlier for both the UM and EM populations as it occurred at GW 5, whereas for PM, it happened at GW 30. The percentage changes compared to baseline also showed the same pattern, which was higher in UM and EM at more than 50%, whereas for PM, this change was only around 25%. These results were anticipated since there is no functional allele in the PM CYP2D6 population, and the physiological and alternative clearance changes occurring

throughout the gestational period constitute the primary factor that influences the concentration levels in the PM phenotype population [106, 246, 247]. As for the UM and EM populations, the trends are consistent with other drugs metabolised by the CYP2D6 enzyme, such as paroxetine, metoprolol, and codeine, because the abundance of the CYP2D6 enzyme increases throughout the gestational week up to the full term for both the UM and EM phenotypes [103, 186, 246, 248].

2.4.4.3 Umbilical cord concentration changes throughout pregnancy

No reported information (to date) is available to investigate the fluvoxamine foetal concentration based on the CYP2D6 phenotype. Thus, simulation of the foetal concentration of fluvoxamine was based on the limited data used to validate the general fluvoxamine foetoplacental model. Since the foetoplacental model only focuses on the passive diffusion transfer mechanism through the placenta, the main potentiating factor in comparison between the UM, EM, and PM CYP2D6 phenotypes constitute the CYP2D6 activities and physiological changes that occur throughout the gestational period. Generally, the factors that influence the crossing of a compound through the placenta are the physicochemical properties of the drug, physiological changes in the placenta such as blood flow, the involvement of active transport, and enzyme metabolism [249-251].

In the case of fluvoxamine, passive diffusion through lipid-soluble barriers of placental tissue membrane, cotyledons become the primary transfer pathway since fluvoxamine is a small molecule drug with base characteristics [249, 250, 252]. However, these characteristics did not differ between different CYP2D6 phenotypes. In addition, no data showed that fluvoxamine is transported by P-glycoproteins (P-gp), the major active efflux proteins for compound transport in the placenta [251]. Therefore, physiological changes and metabolism enzymes are the two main factors influencing fluvoxamine cord concentration.

The increasing trend in the fluvoxamine foetal concentrations in the PM population is solely due to the increase in placental blood flow throughout the gestational period, since there are no active alleles of CYP2D6 [247, 253]. In contrast, the cord concentration is consistent from GW 20 to full term for both the UM and EM populations, except for GW 30 for the peak of the EM population in all three doses. The consistent trend may be due to the counteractive effect between an increase of CYP2D6 metabolism enzymes in the mother and an increase in placenta blood flow towards full term [234, 253]. The small but significant changes in the EM population for GW 30 may not be clinically significant, since no evidence showed a direct correlation between foetal concentrations and the adverse reaction to the foetus [250, 254].

Nevertheless, close monitoring may be needed, particularly when a high foetal concentration is expected.

2.4.4.4 Fluvoxamine dosing during pregnancy

This study identified that a dose increment is needed for the UM and EM populations to maintain a fluvoxamine maternal concentration within the therapeutic area (60 ng/mL – 230 ng/mL). As for the PM population, a stable dose of 100 mg daily with an optional increase to 125 mg daily at GW 35 is sufficient to maintain a patient's fluvoxamine concentration at the optimum level. The dosing recommendation is in line with the increasing CYP2D6 activity throughout the gestational period, which is the primary enzyme metabolising fluvoxamine [185, 211, 236]. Moreover, the 0.75 to 2-fold difference in suggested dosage between PM and UM, as well as EM was anticipated since a dose reduction of 25 – 50% is recommended by the CPIC Guideline for CYP2D6 and CYP2C19 Genotypes and Dosing of Selective Serotonin Reuptake Inhibitors, 2015 [244] for normal subjects. The widening of the dosage gap when approaching full term aligns with the increase in CYP2D6 activity throughout the gestational period [234].

The recommended dose for the UM and EM populations reached a maximum dose at GW 15 and GW 35, respectively (Table 2.8). The recommendation for a maximum dose in the UM population as early as GW 15 signalled the need for close monitoring, particularly with respect to TDM and clinical effects, in order to ensure that fluvoxamine is still effective in treating major depression, while a switch of antidepressant may also be considered, which is in line with the recommendations by the CPIC Guideline for CYP2D6 and CYP2C19 Genotypes and Dosing of Selective Serotonin Reuptake Inhibitors, 2015 [244], DPWG Guideline for the Gene-drug Interaction between CYP2C19 and CYP2D6 and SSRIs, (2016) [245], and Consensus Guidelines for Therapeutic Drug Monitoring in Neuropsychopharmacology: Update 2017 [172]. In addition, the results align with the finding by Mulder et al. (2005) [255], in which a switch of antidepressants is more often needed in the UM than in the EM CYP2D6 population, but not a change of dosing regimen. The need for increments up to the maximum dose in the UM/EM populations reflects the finding uncovered by Berard et al. (2017) [256], wherein the proportion of pregnant women with depression symptoms is higher in the UM/EM than in the PM CYP2D6 population even when treated with antidepressants.

Even though the recommended dose is lower in the PM population, the AUC is approximately twice that of the UM and EM populations, which is in stark contrast to the clearance value, where an increasing trend was seen in the UM and EM populations (Figure 2.12). Therefore, the risk for adverse events is higher in the PM population for both the mother and foetus, since

fluvoxamine accumulates in the body longer due to low clearance [257]. Dose adjustment, switching, and the discontinuation of antidepressants are frequently seen in the PM population due to adverse events, as it is difficult for pregnant women who may have already suffered from morning sickness to endure further adverse drug reactions [255-258].

A similar pattern was seen in the foetal concentration, which was higher in the PM population than in both the UM and EM populations, although with a lower recommended dose. The results from six studies showed that the rate of major congenital malformations and other adverse pregnancy outcomes did not differ significantly compared to the control groups [224-229]. Nevertheless, the number of subjects was still considered too small for any informed conclusions regarding usage during pregnancy to be made [259, 260]. Moreover, the safety concern regarding the use of fluvoxamine as an SSRI is the potential risk of PPHN in newborns [223, 261]. Matsuoka et al. (2017) [243] have suggested dose tapering of 25 mg a week starting from GW 36 to reduce the risk of neonatal withdrawal syndrome, especially when the mother instantaneously discontinues the drug during pregnancy.

2.5 Conclusion

It is always a dilemma for a prescriber to decide between prescribing or withdrawing antidepressants during the perinatal period with respect to the health of both the mother and foetus. The prescriber's main challenge is to find a balance between the treatment benefit throughout pregnancy and the risk of drug toxicity, particularly to the embryo and foetus. The physiological changes and those related to the biotransformation of metabolic enzymes during the gestational period are crucial factors in determining future actions regarding depression treatment in pregnant women. For fluvoxamine, the primary elimination route is through the CYP2D6 metabolism enzyme, which is highly polymorphic and, thus, further complicates the dosing strategies in pregnant women. The developed models suggest that dose increments of fluvoxamine are needed among pregnant women, particularly for the UM and EM CYP2D6 populations. Although the fluvoxamine PBPK model developed in this study demonstrated a pragmatic method for determining a suitable dose in the perinatal setting, a confirmatory clinical trial is required to verify this study's recommendations.

Despite the fact that TDM is not commonly implemented with patients presenting with polymorphisms, this study highlighted the opportunity of using PBPK modelling for precision dosing, particularly in special populations such as pregnant women. The application of PBPK modelling combined with pre-emptive phenotyping may bring precision dosing closer to clinical settings, thereby improving the treatment of depression in the pregnant population.

2.6 Supplementary materials

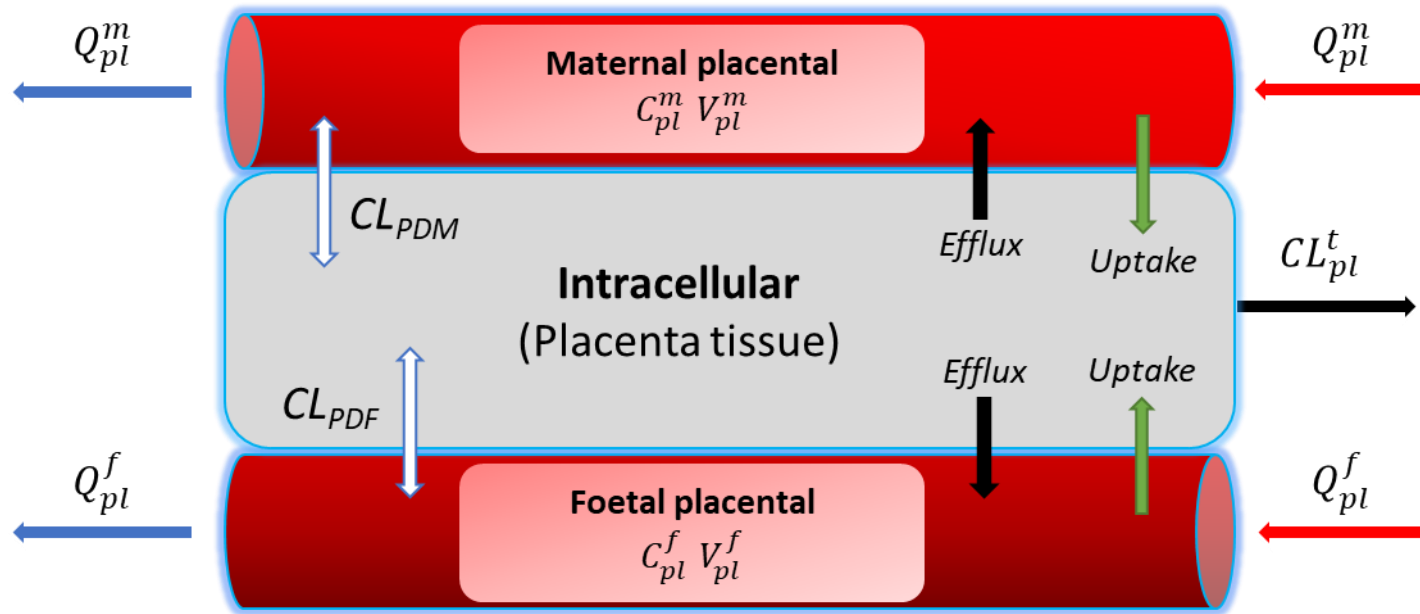


Figure S 2-1 Foetoplacental compartment permeability-limited model

CL_{PDM} , maternal–placental permeability clearance; CL_{PDF} , placental–foetal permeability clearance; CL_{pl}^t , tissue–placenta permeability clearance; Q_{pl}^m , maternal blood flow rate; Q_{pl}^f , foetal blood flow rate; C_{pl}^m , maternal–placental concentration; C_{pl}^f , foetal–placental concentration; V_{pl}^m , maternal–placental volume; V_{pl}^f , foetal–placental volume

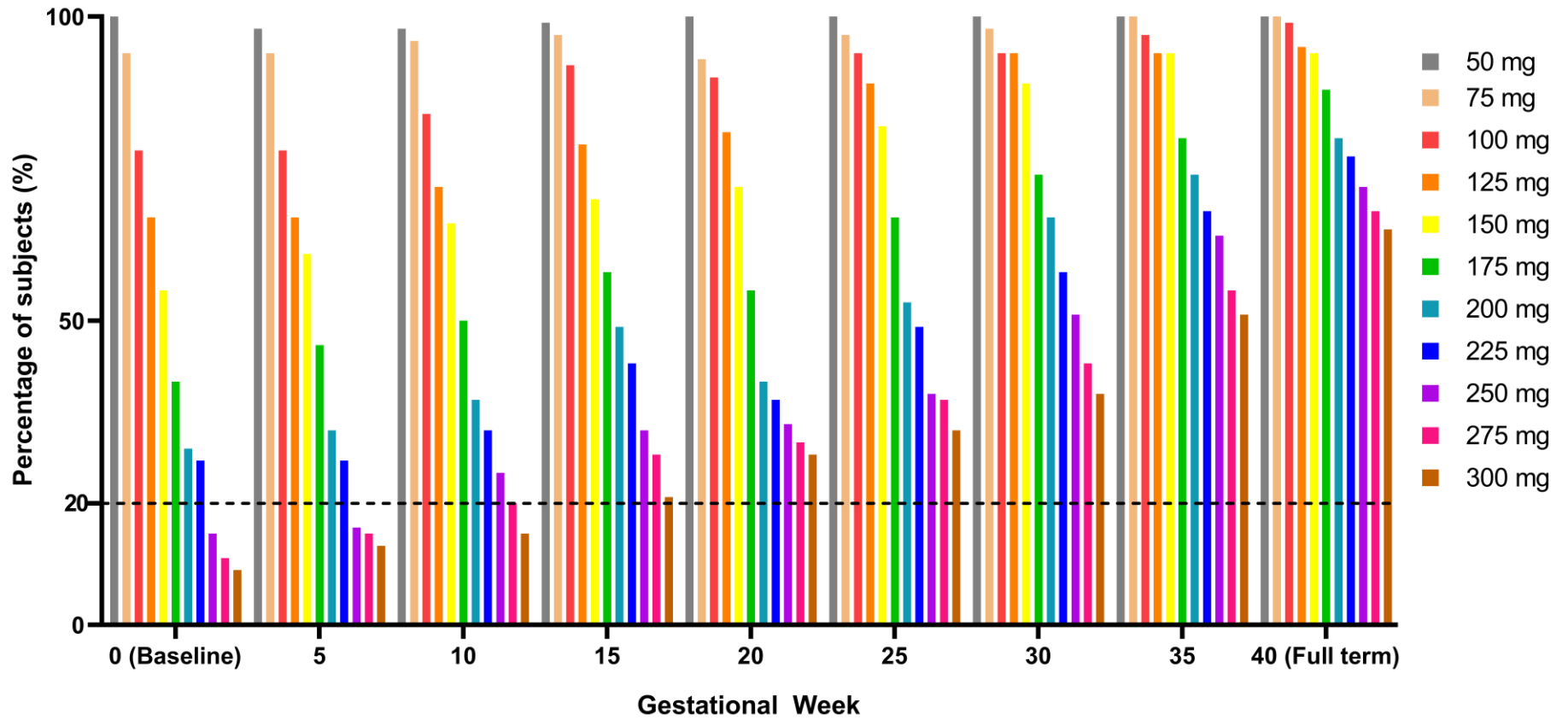


Figure S 2-2 Percentage of Ultrarapid Metaboliser (UM) population with trough concentration below 60 ng/mL

The dashed horizontal line represents the threshold of 20% of subjects.

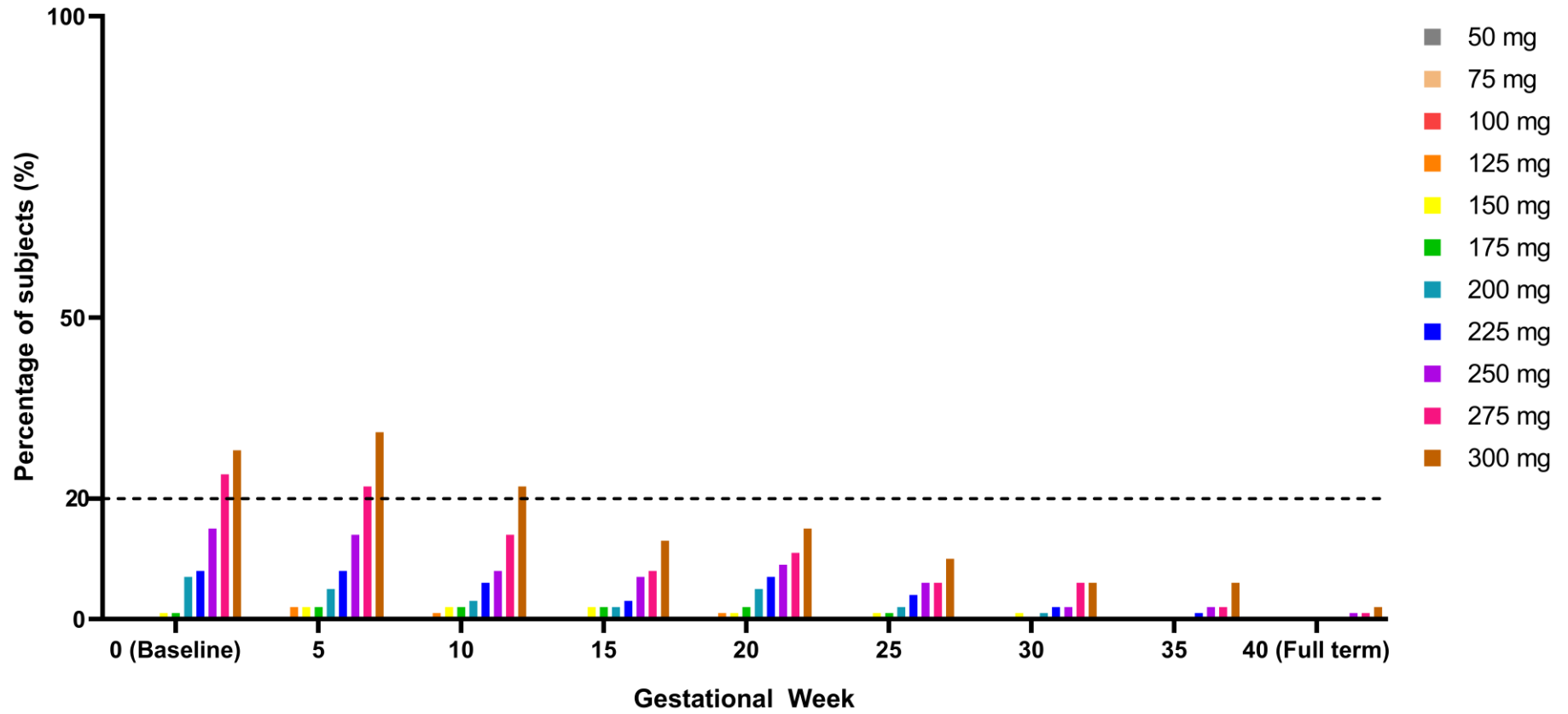


Figure S 2-3 Percentage of UM population with peak concentration above 230 ng/mL

The dashed horizontal line represents the threshold of 20% of subjects.

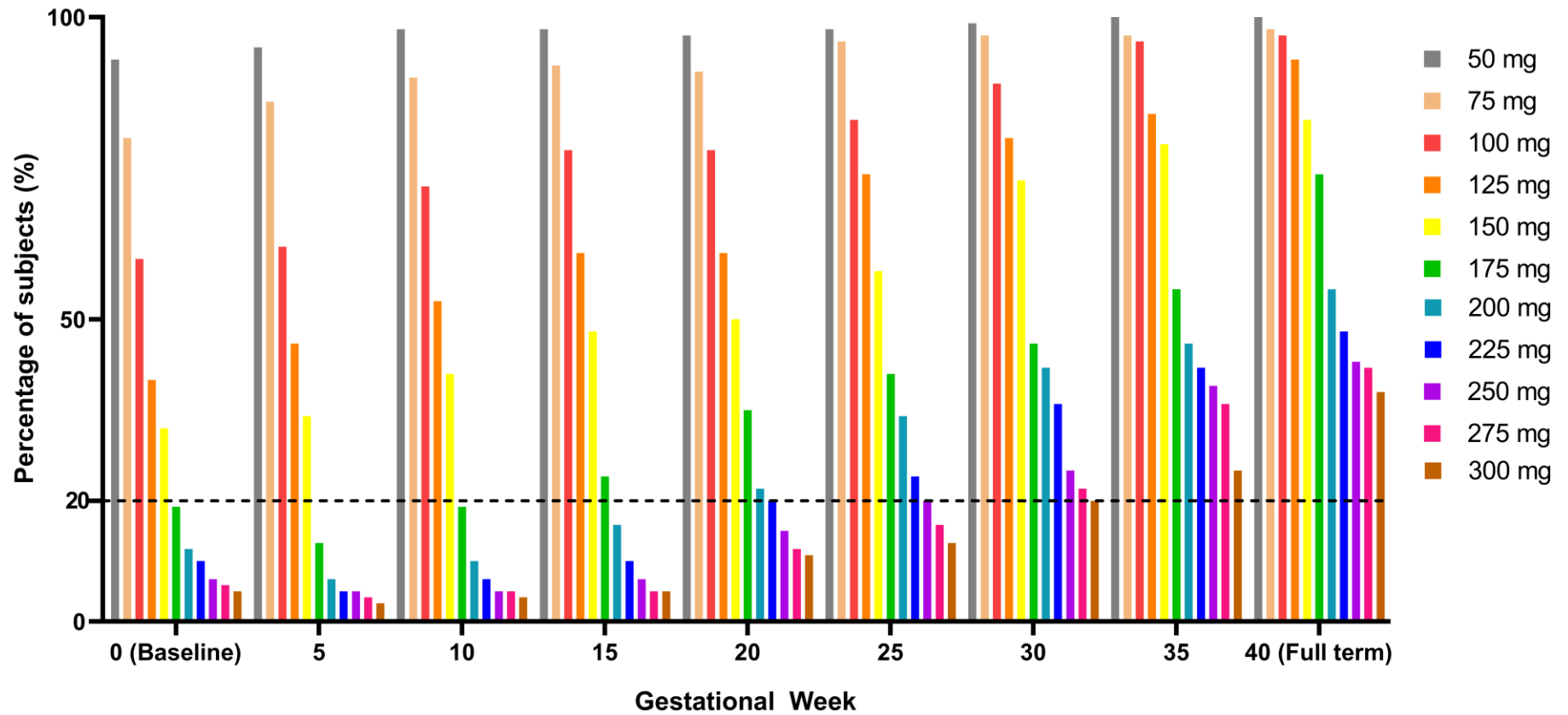


Figure S 2-4 Percentage of Extensive Metaboliser (EM) population with trough concentration below 60 ng/mL
 The dashed horizontal line represents the threshold of 20% of subjects.

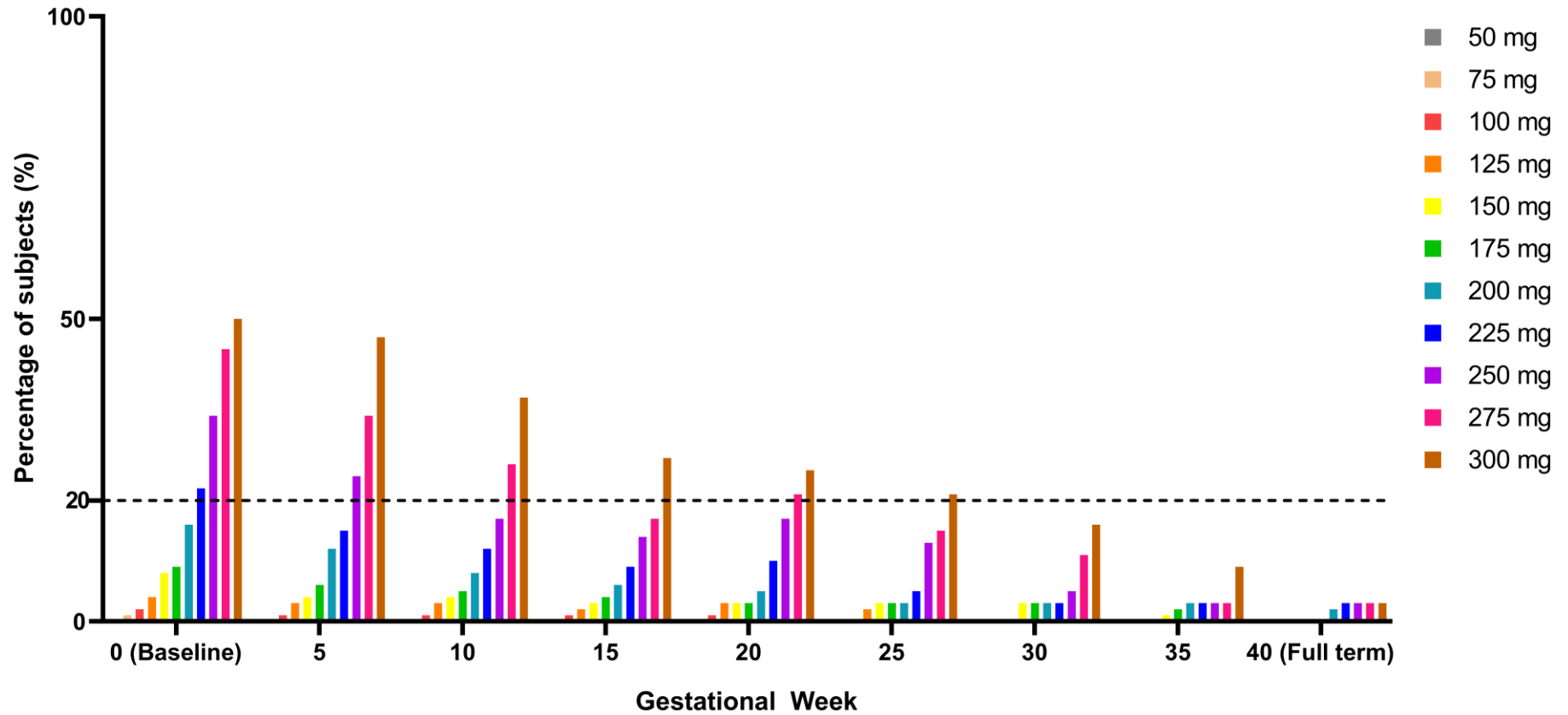


Figure S 2-5 Percentage of EM population with peak concentration above 230 ng/mL

The dashed horizontal line represents the threshold of 20% of subjects.

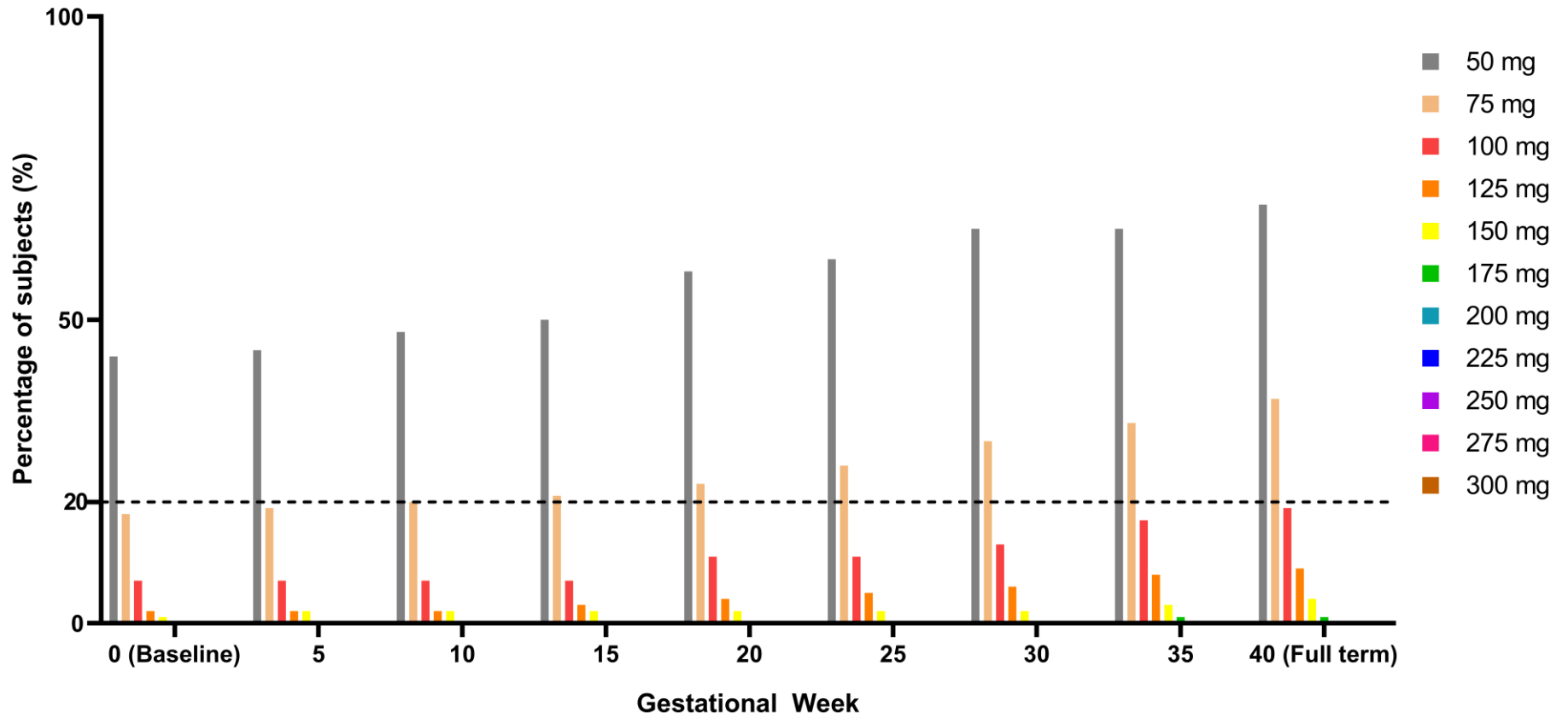


Figure S 2-6 Percentage of Poor Metaboliser (PM) population with trough concentration below 60 ng/mL

The dashed horizontal line represents the threshold of 20% of subjects.

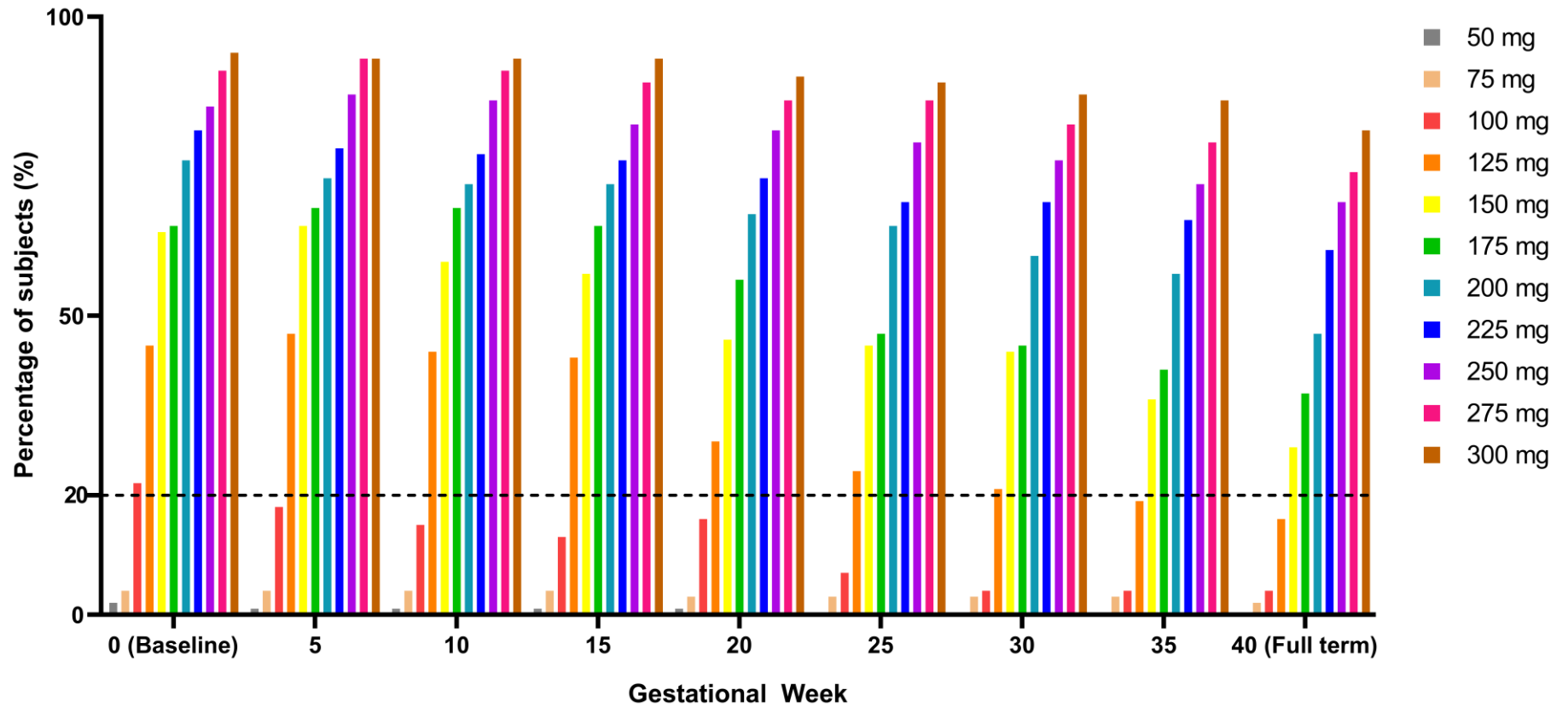


Figure S 2-7 Percentage of PM population with peak concentration above 230 ng/mL

The dashed horizontal line represents the threshold of 20% of subjects.

CHAPTER 3 - The application of physiologically based pharmacokinetic (PBPK) modelling to dose optimising of imatinib pharmacokinetics in obese cancer populations

3.1 Introduction

Obesity is recognised as a global health epidemic, with a prevalence of over 2.6 billion in 2020 and estimated to increase to over 4 billion by 2035 [112]. Furthermore, obesity is linked with an increased risk of cancer and is associated with higher cancer-related mortality [262-264]. Thus, the intertwining of obesity and cancer introduces a complex mesh of physiological changes, such as metabolism enzyme activities, altered tissue composition, change in plasma protein proportions, and renal function that can significantly influence drug absorption, distribution, metabolism and excretion [118, 123-125, 265].

Navigating the dosing approach in obese cancer patients is a conundrum and necessitates careful consideration of how the physiological changes may impact the drug's pharmacokinetics [10]. Research indicates various physiological alterations in obese cancer patients can influence the pharmacokinetic parameters. Among them is the increase of adipose tissue composition in obese cancer patients affecting a drug with high lipophilicity, thus increasing the volume of distribution and reducing plasma concentrations [266]; and the decrease in CYP3A4 metabolism enzyme abundances reported in both obese and cancer patients impact a majority of drugs cleared through the liver [124, 134].

The advent of tyrosine kinase inhibitors (TKIs), notably imatinib, a breakthrough in targeted therapy for chronic myeloid leukaemia (CML) and gastrointestinal stromal tumour (GIST) patients with an oral standard fixed-dose regimen, also poses a challenge in optimising the dose for the obese cancer population [267, 268]. Existing literature reveals a lower rate of major molecular response (MMR) and a longer time to achieve complete cytogenetic response (CCyR) in CML patients with a high body-mass index (BMI) > 25 g/m² treated with imatinib, and a higher dose might be needed in morbidly obese cancer patients [268-270]. Furthermore, a recent study demonstrates a negative correlation between body weight and imatinib trough plasma concentrations [271]. Nonetheless, information on the imatinib pharmacokinetic differences between lean, overweight, and obese cancer populations is still lacking.

Data from multiple studies indicate that the use of imatinib trough concentration is an excellent surrogate marker in predicting the clinical response of CML and GIST patients [272-274]. The robust correlation between the imatinib plasma concentrations and the pharmacological effect combined with significant inter-patient (47% – 75%) and intra-patient variabilities (19% – 30%) suited the criteria as a candidate for therapeutic drug monitoring (TDM) approach with a dynamic and patient-centred dosing optimisation strategy to maximise the therapeutic efficacy and minimise the side effects [275, 276].

A multitude of studies have affirmed the benefit of TDM in guiding dose adjustment for imatinib and an evident cost-effectiveness compared to the standard fixed-dose therapy, specifically

after the accessibility of generic imatinib [277-280]. Moreover, several hospitals in the European region have implemented the TDM approach for imatinib in their clinical practice, and a consensus TDM guideline for imatinib therapy has been established by the International Association of Therapeutic Drug Monitoring and Clinical Toxicology (IATDMCT) [275, 276].

Physiologically based pharmacokinetic (PBPK) modelling capabilities to consider the physiological changes in a population to elucidate and predict a drug disposition and plasma concentrations, even with limited concentration data, serve as a valuable tool to assess the imatinib pharmacokinetics in special populations such as obese cancer patients. The mechanistic modelling concept has been utilised to predict plasma concentrations for various drugs, either obese or cancer populations, individually but not as obese cancer populations [124, 125]. Furthermore, the concept has also been implemented to assess the impact of TDM-guided dose adjustment for imatinib in a Chinese cancer population [281].

Given the paucity of imatinib pharmacokinetics data on obese cancer populations, for the first time, this study has applied the PBPK concept in describing and assessing the physiological and imatinib pharmacokinetic differences between the lean, overweight, and obese cancer populations. Additionally, the effectiveness of the TDM-guided imatinib dose titration approach adapted from Gotta et al. (2014) [277] clinical studies in the obese cancer population was evaluated. The insight gained in this study may contribute to the evolving landscape of precision medicine from the personalised therapeutic intervention perspective.

The objectives of this study are to utilise the principle of PBPK modelling and virtual clinical trials to: (1) delineate the differences in physiological parameters between lean, overweight and obese cancer populations, (2) evaluate the influence of obesity on imatinib pharmacokinetics in adult cancer populations, and (3) assess the ability for TDM-guided dose adjustment for imatinib to regain the sub- and supra-therapeutic trough concentrations into the target concentration level.

3.2 Methodology

The simulations of imatinib plasma profiles on adult cancer populations for validation and TDM were performed using Simcyp® Version 21 (Simcyp Ltd., a Certara company, Sheffield, UK). This study applied the four-step workflow for validation and virtual TDM of imatinib in obese cancer populations (Figure 3.1).

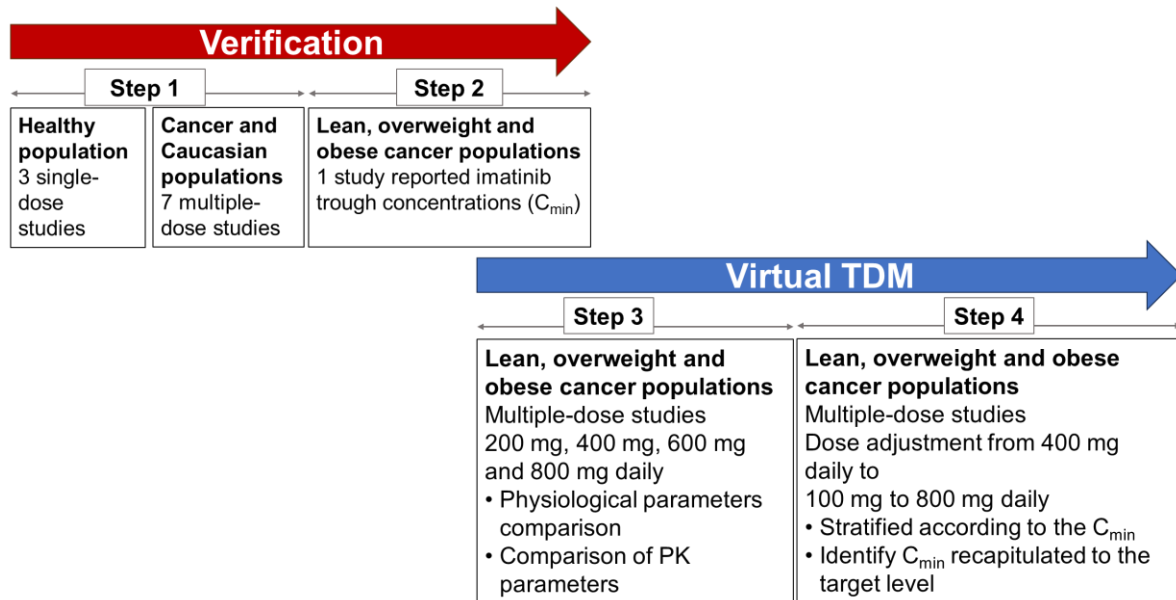


Figure 3.1 Four-step workflow model for Imatinib model verification, TDM and exploration

3.2.1 Step 1: Verification of the imatinib model in healthy, cancer and Caucasian populations

The imatinib compound model that was previously developed, validated and utilised was used without adaptation (Table 3.1) [281-283]. Since an updated version of the Simcyp Simulator software was utilised, verification of the imatinib model was re-performed with published data in three different population groups from 10 studies:

Healthy adults:

- i. Imatinib 400 mg single-dose, 12 adults (40 – 58 years old) [284],
- ii. Imatinib 400 mg single-dose, 33 adults (19 – 60 years old) [285],
- iii. Imatinib 400 mg single-dose, 26 adults (21 – 27 years old) [286],

Adult cancer patients:

- iv. Imatinib 400 mg daily, 34 GIST patients (28 – 84 years old) [287],
- v. Imatinib 400 mg daily, 50 GIST cancer subjects (39 – 82 years old) [288],
- vi. Imatinib 400 mg daily, 103 pulmonary arterial hypertension (PAH) patients (18 – 77 years old) [289],
- vii. Imatinib 400 mg daily, 2,478 CML patients (18.3 – 91.5 years old) [290],
- viii. Imatinib 25 mg to 600 mg daily, 64 CML patients (53.8 ± 12.7 years old) [291],

Caucasian adults:

- ix. Imatinib 400 mg daily, 59 CML and GIST Caucasian patients (20 – 79 years old) [292],
- x. Imatinib 400 mg daily, 49 GIST Caucasian patients (24 – 88 years old) [293].

The healthy population in Simcyp[®] was used for simulation to verify the observed data in (i) to (iii), the cancer population in Simcyp[®] was utilised for verification of published data from (iv) to (viii), while the Simcyp[®] North European Caucasian (NEurCaucasian) population was used to verify clinical data in (ix) and (x) above. The population models selected for validation were based on the patients recruited in the published data and the population model used by the imatinib model developer [283]. Furthermore, simulations were made with 10 trials x 10 patients design with an age range and male percentages matching the published studies.

Three populations used to validate the imatinib compound are default populations available in the Simcyp[®] in-house population library: healthy adult, cancer population, and NEurCaucasian. The difference between the healthy adult and NEurCaucasian populations is that the NEurCaucasian population is considered a general population established from a sizeable European health survey, including a population with medical conditions [283]. As for the cancer population with both healthy and NEurCaucasian, the main difference influencing imatinib pharmacokinetics is the plasma AGP level, which is higher in the cancer population [125, 283].

The re-verification of the imatinib model focused on reproducing pharmacokinetic parameters and plasma concentration profiles, as the model has been validated in multiple studies across diverse ethnic groups and age ranges, particularly in predicting C_{min} with significant inter-subject variability [281-283, 294].

Table 3.1 Imatinib compound parameter values validated and used for simulation

Parameters	Values	Notes
Physical chemistry and blood binding		
Compound type	Diprotic base	
Molecular weight (g/mol)	493.6	Drug Bank [252]
Log P	1.99	Peng et al. (2005) [139]
pKa 1;2	8.07; 3.73	
B/P	0.73	Kretz et al. (2004) [295]
f_u	0.05	Smith et al. (2004) [296]
Plasma binding component	α_1 -acid glycoprotein	
Absorption		
Model	ADAM	
f_{uGut}	1.00	
Q_{Gut} (L/h)	6.04	
P_{eff} in man (10^{-4} cm/s)	0.92	
Distribution		
Model	Full PBPK	
V_{ss} (L/kg)	1.80	Predicted using Method 2 by Rodgers and Rowland approach [60]
K_p scalar		
Elimination		
Model	Enzyme kinetics	
Pathway 1	CYP3A4	N-desmethyl imatinib formation
V_{max} (pmol/min/pmol isoform)	3.00	
K_m (μ mol/L)	10.54	
$f_{u_{mic}}$	0.96	
Pathway 2	CYP2C8	N-desmethyl imatinib formation
V_{max} (pmol/min/pmol - isoform)	56.40	
K_m (μ mol/L)	7.49	
$f_{u_{mic}}$	0.97	
Pathway 3	CYP3A4	Other metabolites
CL_{int} (μ l/min/mg - protein)	33.40	
$f_{u_{mic}}$	1.00	
Pathway 4	CYP2C8	Other metabolites

CL _{int} (µl/min/mg - protein)	24.20	
f _{u_{mic}}	1.00	
HLM CL _{int} (µL/min/mg - protein)	31.00	
CL _R (L/h)	0.50	Bornhauser et al. (2005) [297]

Drug transport – hepatobiliary transporter

Pathway 1	ABCB1
CL _{int,T} (µl/min/million - cells)	1.50
RAF	1.00
Pathway 2	ABCG2
J _{max} (pmol/min/million – cells)	89.40
K _m (µmol/L)	4.37
RAF	0.38
CL _{PD} (ml/min/million – hepatocytes)	0.20

Drug interactions

CYP3A4

Competitive inhibition

K _i (µmol/L)	14.30
f _{u_{mic}}	0.80

Mechanism-based inhibition

k _{inact} (1/h)	4.29
f _{u_{mic}}	0.80

The compound data was adopted from Adiwidjaja et al. (2019) [282]; Log P, partition coefficient; B/P, blood-to-plasma ratio; f_u, unbound fraction; ADAM, Advance dissolution, absorption and metabolism; P_{eff}, human jejunum effective permeability; PSA, polar surface area; HBD, number of hydrogen bond donors; f_{uGut}, unbound fraction of drug in enterocytes; V_{ss}, steady-state volume of distribution; K_p scalar, tissue partition coefficient; HLM CL_{int}, human liver microsomes invitro intrinsic clearance; CL_R, renal clearance; V_{max}, maximum rate of metabolism; K_m, Michaelis-Menten constant; f_{u_{mic}}, fraction of unbound drug in the in vitro microsomal incubation; CL_{int}, in vitro intrinsic clearance; CL_{PD}, passive diffusion clearance; CL_{int,T}, in vitro transporter-mediated intrinsic clearance; J_{max}, in vitro maximum rate of transporter-mediated efflux or uptake; RAF, relativity activity factor; K_i, the concentration of inhibitor that supports half-maximal inhibition; k_{inact}, inactivation rate of the enzyme.

3.2.2 Step 2: Validation of lean, overweight and obese cancer population with imatinib compound model

Before assessing the differences in imatinib pharmacokinetics between lean, overweight and obese oncologic populations, the imatinib compound model was further verified with the Simcyp® cancer population categorised according to the BMI, lean for < 25 kg/m², overweight for 25 kg/m² to < 30 kg/m² and obese for > 30 kg/m² [152].

The cancer population in Simcyp® was developed based on data from patients with advanced solid tumours and generated virtual patients with a range of BMI from 16 kg/m² up to 46 kg/m² [125, 134, 298]. Within the Simcyp® population library, the obese and morbidly obese

populations were also available, but both were not derived based on data from cancer patients, which is one of the primary reasons for selecting the cancer population instead of the obese population [124]. The fundamental physiological differences between cancer and obese populations in Simcyp® are the plasma AGP level, CYP3A4 abundances, human serum albumin, serum creatinine, and haematocrit [124, 125].

Validation was performed with imatinib steady-state trough concentrations (C_{\min}) of lean, overweight, and obese cancer populations reported by Lin et al. (2023) [271] from 201 subjects aged between 24 and 88 years old: 87 patients in the lean category, 83 in the overweight category and 31 in the obese category. For verification with the reported C_{\min} , a virtual clinical trial simulating 1,000 cancer population dosed with 400 mg daily for 28 days matches the demographic population described by Lin et al. (2023) [271], followed by stratification of the virtual subjects according to their BMI categories.

3.2.3 Step 3: Comparison of physiological parameters and imatinib pharmacokinetics parameters between lean, overweight, and obese cancer populations

For the physiological parameters comparison between lean, overweight, and obese cancer populations, 10,000 virtual cancer subjects were simulated with a 1:1 male-to-female ratio and 20 – 88 years of age. Subsequently, the virtual subjects were stratified according to their BMI and made the physiological parameters comparison, which includes height, weight, body surface area (BSA), liver weight, cardiac output, human serum albumin (HSA), haematocrit, α 1-acid glycoprotein (AGP), serum creatinine, glomerular filtration rate (GFR), CYP3A4 liver enzyme abundance, CYP2C8 liver enzyme abundance, ABCB1 (P-gp/MDR1) transporter activity and ABCG2 (BCRP) transporter activity.

The virtual subjects were not stratified according to age, as the PBPK model accounts for physiological variations associated with ageing, such as changes in renal function, enzyme activity, and body composition [125]. In addition, studies have shown no clinically significant impact of age on imatinib pharmacokinetics [272, 290].

In order to identify the differences in imatinib rate and extent of absorption between the BMI categories, four virtual clinical trials were simulated with 1,000 virtual cancer populations. For each trial, the virtual subjects with similar demographic characteristics were dosed with imatinib either at 200 mg, 400 mg, 600 mg or 800 mg daily for 28 days. The simulations were conducted with the age range of 20 to 60 years and 0.5 male-to-female ratio.

The pharmacokinetic parameters that were compared include area-under-the-curve (AUC), maximum concentration (C_{max}), and C_{min} , all at steady-state. Additionally, the percentages of C_{min} fell outside the target range, specifically below 1,100 ng/mL and 750 ng/mL, as well as above 1,500 ng/mL, were reported for each BMI classification. The primary target range of 750-1,500 ng/mL aligns with Gotta et al. (2014) [277], while the sub-criterion of 1,100 ng/mL suggested by Bouchet et al. (2016) [299], was included to highlight specific therapeutic levels adopted by Lin et al. (2023) [271], whose data validated the imatinib model.

3.2.4 Step 4: Imatinib therapeutic drug monitoring (TDM) in lean, overweight and obese cancer populations

Imatinib dose adjustment guided by TDM has been reported to improve its efficacy and implemented in clinical settings in numerous hospitals worldwide [290, 300, 301]. Additionally, the concept of PBPK has been utilised as virtual TDM to assess the pharmacokinetic variabilities of imatinib in the Chinese cancer population [281]. Hence, the TDM-guided imatinib dose adjustment approach executed by Gotta et al. (2014) [277] (Figure 3.2) was adapted in a randomised trial to evaluate the difference in imatinib pharmacokinetics between lean, overweight and obese cancer populations using the virtual clinical trials and PBPK framework.

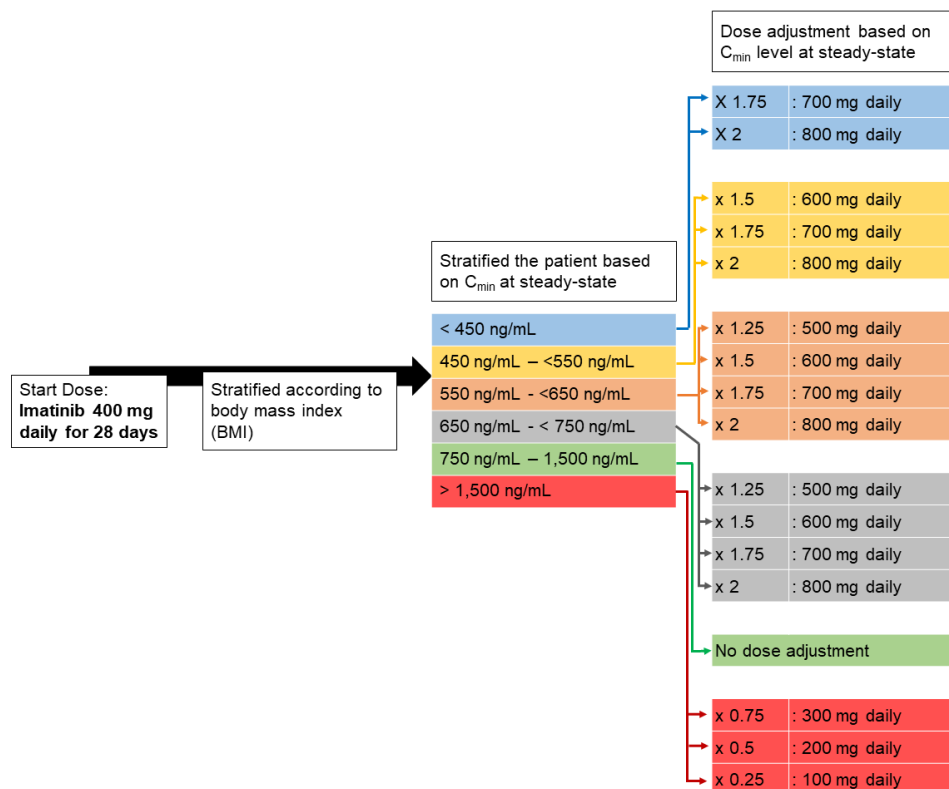


Figure 3.2 Imatinib dose adjustment guided by TDM process

Virtual clinical trials of 1,000 adult cancer subjects (20 to 60 years old, 1:1 male-to-female ratio) were simulated and dosed with imatinib 400 mg daily for 26 days, followed by dose adjustment based on the C_{\min} scheme specified in Figure 3.2 for an additional 30 days. The C_{\min} threshold window of 750 ng/mL to 1,500 ng/mL recommended by Gotta et al. (2014) [277] and Buclin et al. (2020) [276] was fixed in this study. For each virtual trial, subjects were then categorised according to their BMI: lean, overweight, and obese. This was followed by stratification of the virtual subjects for each BMI class according to the C_{\min} after being dosed on Day-26 (before dose adjustment). Subsequently, the ability of dose adjustment to recapitulate the subjects whose C_{\min} were outside the threshold back into the target window was quantified. The demographic of virtual subjects was constant for each dose adjustment cohort.

3.2.5 Prediction performance

Verification of the imatinib compound model with observed clinical data in step 1 was determined by visual predictive check (VPC) and predicted/observed ratio within a two-fold (0.5 – 2-fold) range as the acceptance criteria unless otherwise explained [144, 220, 221, 302]. As for step 2, the VPC method was used as only the imatinib C_{\min} observed data reported by Lin et al. (2023) [271] was used to validate the imatinib model with overweight and obese cancer patients. The acceptance range for VPC is when the overlaid observed plasma concentrations match with the 5th and 95th percentiles of the mean simulated plasma concentration profiles [281, 282, 303].

3.2.6 Data and statistical analysis

All the observed plasma concentration data used for validation, particularly in steps 1 and 2, were extracted from published studies using WebPlotDigitizer version 4.5 (<https://apps.automeris.io/wpd/>). One-way ANOVA with Tukey's multiple comparison tests was performed to compare the physiological and pharmacokinetic parameters between lean, overweight and obese cancer populations in steps 2 and 3. Statistical significance was set at $p < 0.05$. In addition, Spearman's correlation test was implemented to test the correlation between C_{\min} versus body weight in step 2. All the statistical analysis was ran with GraphPad Prism Version 8 for Windows (GraphPad Software, La Jolla, CA, USA).

3.3 Results

3.3.1 Step 1: Imatinib model validation in healthy, cancer and caucasian populations

The imatinib model was validated with three single-dose studies in healthy adults and seven multiple-dose studies in the adult cancer population. The pharmacokinetics parameters prediction-to-observed ratio, including C_{max} , AUC_{0-inf} , AUC_{0-t} , and time to maximum concentration (T_{max}), when compared with observed data from healthy adults, was between 0.72 to 1.04, which was within the acceptance criteria (Table 3.2). Furthermore, all the imatinib observed plasma profiles overlaid within the 5th and 95th percentiles of simulated profiles (Figure 3.3A), thus verifying the imatinib compound model's prediction of imatinib concentration in healthy adults.

Table 3.2 Observed and predicted pharmacokinetic parameters of imatinib for healthy subjects

Reference	Age, no. of subject	Dosing regimen	PK parameter	Observed	Predicted	Predicted/ Observed
Peng et al. (2004) [284]	40 – 58, n: 12	400 mg single-dose	C_{max} (ng/mL)	1,822 ± 1,193	1,669 ± 465	0.92
			AUC_{0-inf} (ng.h/mL)	32,640 ± 16,501	23,645 ± 10,099	0.72
			T_{max} (h)	2.5 (1.0 – 6.0)	2.3 (1.1 – 3.7)	0.92
Nikolova et al. (2004) [285]	19 – 60, n: 33	400 mg single-dose	C_{max} (ng/mL)	1,606 ± 647	1,669 ± 465	1.04
			AUC_{0-24} (ng.h/mL)	18,658 ± 8,016	19,547 ± 6,994	1.04
			AUC_{0-96} (ng.h/mL)	25,150 ± 11,611	23,578 ± 10,002	0.94
			AUC_{0-inf} (ng.h/mL)	25,464 ± 11,846	23,645 ± 10,099	0.93
Pena et al. (2020) [286]	21 – 27, n: 26	400 mg single-dose	C_{max} (ng/mL)	2,029 ± 551	1,669 ± 465	0.82
			AUC_{0-72} (ng.h/mL)	32,378 ± 9,152	23,406 ± 9,805	0.72

n, number of subjects; C_{max} , maximum concentration; AUC_{0-t} , area-under-the-curve to the last time point; AUC_{0-inf} , area-under-the-curve extrapolated to infinity; T_{max} , time to maximum concentration.

As for the adult cancer population, verification was conducted with seven published studies, where a study by Peng et al. (2004) [291] compared with both pharmacokinetic parameters (Table 3.3) and observed plasma profiles (Figure 3.4), while all other six studies compared with the observed plasma profiles only (Figure 3.3).

The study by Peng et al. (2004) [291] was conducted on 14 different doses from 25 mg to 1,000 mg, with published profiles at steady-state on six doses: 25 mg daily, 50 mg daily, 85 mg daily, 350 mg daily, 400 mg daily and 600 mg daily. Pharmacokinetic parameters comparison for the six doses generally adhered to the 0.5 – 2-fold rule except for AUC_{0-24ss} and t_{max} at 25 mg daily dose as well as C_{max} and AUC_{0-24ss} at 350 mg daily dose, where the differences were more than two-fold but less than three-fold (Table 3.3).

Table 3.3 Observed and predicted pharmacokinetic parameters of imatinib for cancer subjects

Reference	Age, no. of subject	Dosing regimen	PK parameter	Observed	Predicted	Predicted/Observed
Peng et al. (2004) [291]	53.8 ± 12.7, n: 3	25 mg at steady-state	C_{max} (ng/mL)	179.9 ± 89.2	237.9 ± 84.6	1.32
			AUC_{0-24ss} (µg.h/mL)	1.9 ± 0.9	4.0 ± 1.8	2.10
			T_{max} (h)	1.0 ± 0.5	2.4 ± 0.4	2.40
	n: 3	50 mg at steady-state	C_{max} (ng/mL)	365.7 ± 75.6	475.8 ± 169.2	1.30
			AUC_{0-24ss} (µg.h/mL)	4.6 ± 0.4	8.0 ± 3.7	1.74
			T_{max} (h)	3.8 ± 3.6	2.4 ± 0.4	0.63
	n: 3	85 mg at steady-state	C_{max} (ng/mL)	799.6 ± 463.1	809.0 ± 287.8	1.01
			AUC_{0-24ss} (µg.h/mL)	9.8 ± 3.3	13.7 ± 6.3	1.40
			T_{max} (h)	2.2 ± 1.4	2.4 ± 0.4	1.09
	n: 5	350 mg at steady-state	C_{max} (ng/mL)	1,407.0 ± 710.7	3,335.1 ± 1,186.5	2.37
			AUC_{0-24ss} (µg.h/mL)	20.0 ± 10.6	56.2 ± 25.8	2.81
			T_{max} (h)	3.1 ± 1.0	2.4 ± 0.4	0.77
	n: 5	400 mg at steady-state	C_{max} (ng/mL)	2,596.0 ± 786.7	3,812.2 ± 1,356.4	1.47
			AUC_{0-24ss} (µg.h/mL)	40.1 ± 15.7	64.2 ± 29.6	1.60
			T_{max} (h)	3.3 ± 1.1	2.4 ± 0.4	0.73
	n: 9	600 mg at steady-state	C_{max} (ng/mL)	3,508.9 ± 1,649.3	5,722.6 ± 2,036.5	1.63
			AUC_{0-24ss} (µg.h/mL)	51.7 ± 26.7	96.5 ± 44.4	1.87
			T_{max} (h)	3.1 ± 1.1	2.4 ± 0.4	0.77

n, number of subjects; C_{max} , maximum concentration; AUC_{0-24ss} , area-under-the-curve for 24 hours at steady-state; T_{max} , time to maximum concentration.

A similar trend was seen in the plasma profile comparison, where only the 350 mg daily dose fell outside the simulated 5th and 95th percentile profile (Figure 3.4D). Notably, the simulated profiles were overpredicted compared to observed profiles, particularly for 25 mg daily dose, 50 mg daily dose, 350 mg daily dose and 600 mg daily dose (Figure 3.4). Nevertheless, the profiles were still within the acceptance profile threshold (Figure 3.4).

The predicted profiles in adult cancer populations were consistent with the sparse imatinib plasma concentration data published by Petain et al. (2008) [287] (Figure 3.3B and Figure 3.3C), Eechoute et al. (2012) [288] (Figure 3.3D and Figure 3.3E), Renard et al. (2015) [289] (Figure 3.3F), and Gotta et al. (2014) [290] (Figure 3.3G). In general, a wider distribution was noticed in observed data from all four publications compared to the 5th and 95th percentile simulated profiles (Figure 3.3). Overprediction was seen when a comparison was made with the steady-state observed data from Petain et al. (2008) [287] (Figure 3.3C); still, the observed data was within the acceptance range of simulated profiles.

As for the observed imatinib concentrations reported by Widmer et al. (2006) [292] (Figure 3.3H) and Haouala et al. (2013) [293] (Figure 3.3I), the comparison was made with the simulated profiles made based on the NEurCaucasian population in Simcyp[®]. The main reason is to match the validation method implemented by the developer of the imatinib compound model [282, 283]. The predicted profiles, including the 5th and 95th percentiles, overlaid within both the publication's broad imatinib observed data (Figure 3.3H and Figure 3.3I). Generally, the inter-individual variability in observed concentrations was broader than predicted, particularly in Figure 3.3B, Figure 3.3D, and Figure 3.3E, reflecting a potential limitation in the model's ability to capture variability fully.

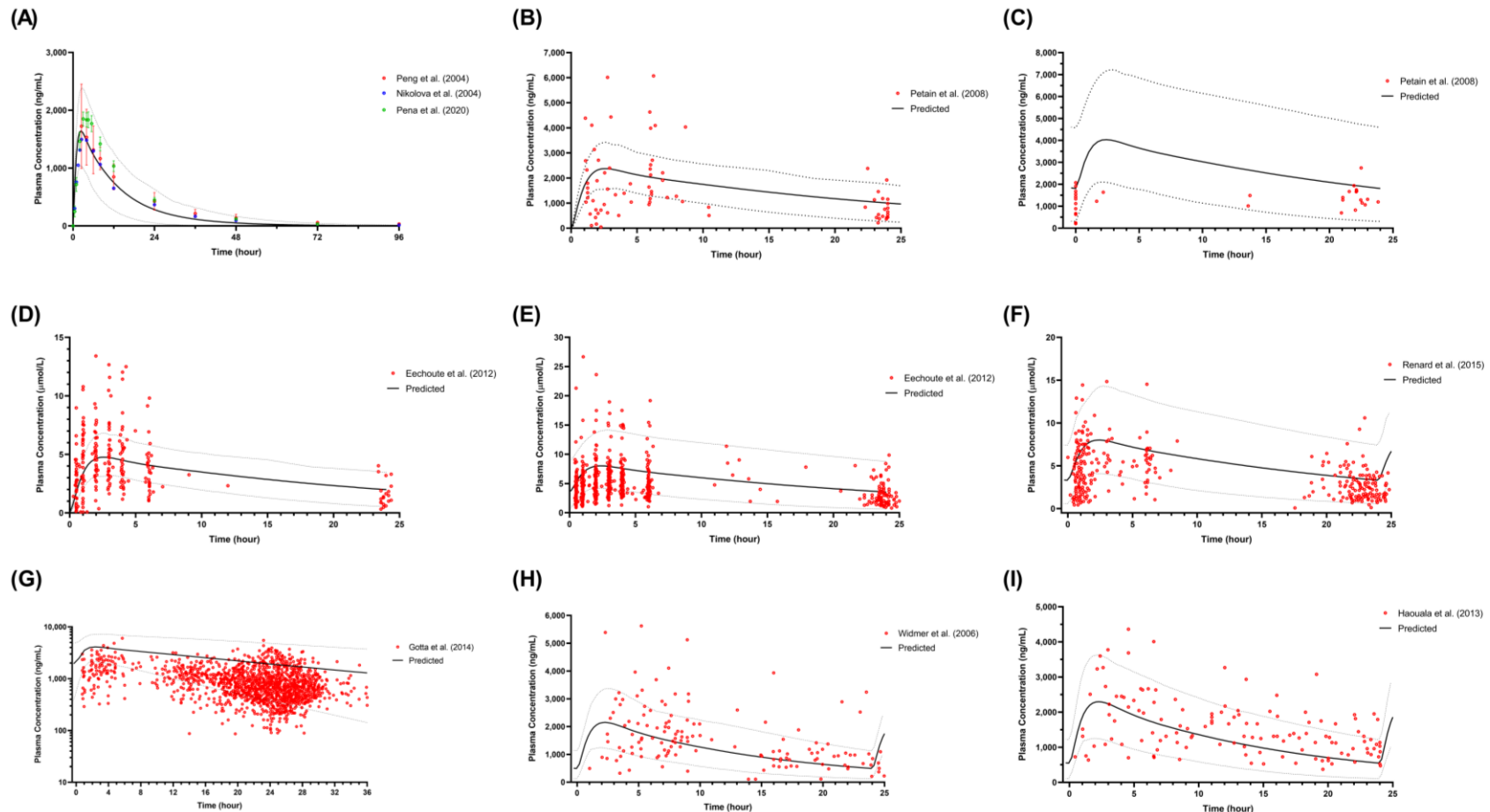


Figure 3.3 Comparison of model-predicted vs. observed concentration data of imatinib in healthy adults (A), adult cancer (B – G) and European adults (H-I).

(A) 400 mg single-dose in healthy adults [284], [285], [286]; (B) 400 mg day-1 and (C) 400 mg at steady-state in cancer populations compared to Petain et al. (2008) [287] observed data; (D) 400 mg day 1 and (E) 400 mg daily at steady-state in cancer populations compared with published data by Eechoute et al. (2012) [288]; (F) 400 mg daily at steady-state in pulmonary arterial hypertension populations compared with Renard et al. (2015) [289] observed data; (G) 400 mg daily at steady-state in cancer populations compared with Gotta et al. (2014) [290] observed data; 400 mg daily at steady-state in European populations compared with observed data by Widmer et al. (2006) [292] (H) and Haouala et al. (2013) [293] (I). Solid lines represent the mean predicted concentration-time profile, with dotted lines representing the 5th and 95th percentile ranges. Solid circles represent observed clinical data from each study.

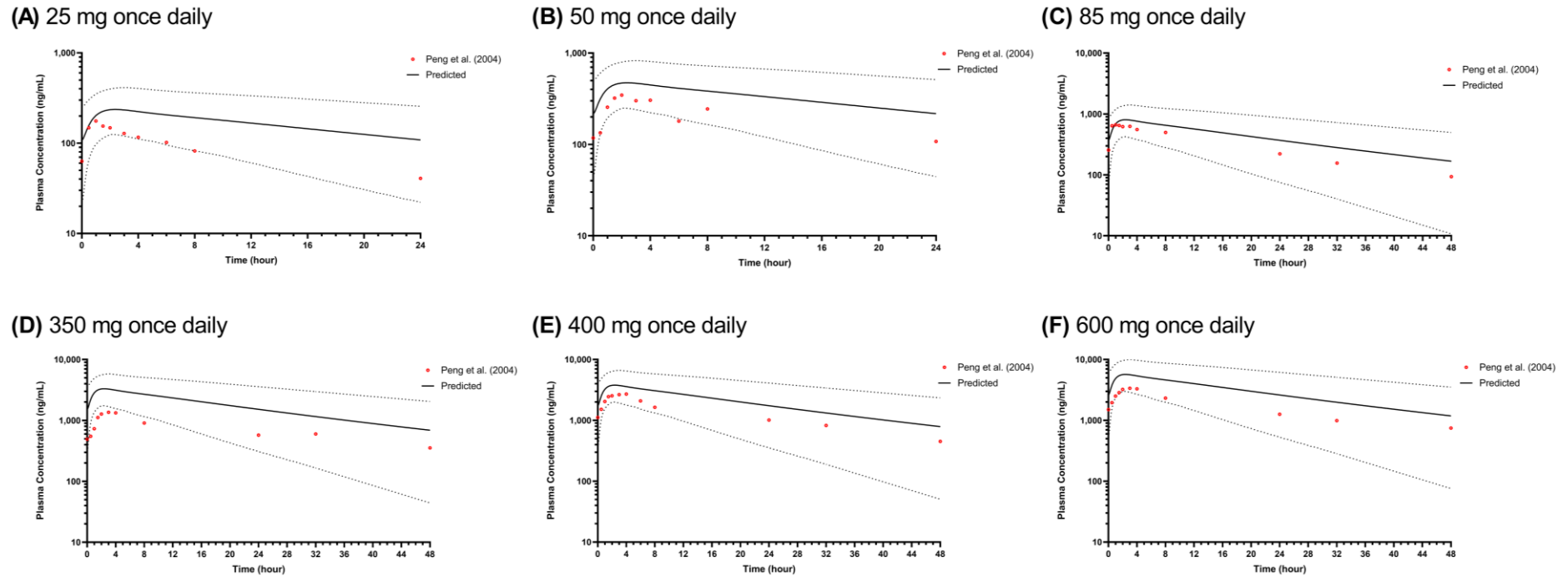


Figure 3.4 Comparison of imatinib simulated profiles with observed plasma profiles at steady-state in cancer populations

Virtual cancer patients were administered 25 mg once daily (A), 50 mg once daily (B), 85 mg once daily (C), 350 mg once daily (D), 400 mg once daily (E), and 600 mg once daily (F). Observed profiles were published by Peng et al. (2004) [291]. Solid lines represent the mean predicted concentration-time profile, with dotted lines representing the 5th and 95th percentile ranges. Solid circles represent observed clinical data from each study.

3.3.2 Step 2: Validation of lean, overweight, and obese cancer population with imatinib compound model

The applicability of the imatinib model in predicting pharmacokinetic parameters of overweight and obese adult cancer populations was validated with observed C_{\min} at steady-state when cancer patients have been dosed with imatinib 400 mg per day, as Lin et al. (2023) [271] reported. The reported C_{\min} superimposed within the distribution of simulated C_{\min} for all three populations: lean (Figure 3.5D), overweight (Figure 3.5E) and obese (Figure 3.5F) adult cancer, as well as the integrated graph of all three populations (Figure 3.5C).

Furthermore, the correlation test results for C_{\min} versus body weight were comparable (r_s :-0.24, $p < 0.001$ vs r_s :-0.13, $p < 0.0001$) between the observed (Figure 3.5A) and simulated data (Figure 3.5B). Besides, the results showed that correlations between body weight and trough levels were significant in both simulated and observed imatinib concentrations. The primary difference between observed and simulated populations was the maximum body weight, with 125 kilograms (kg) for the virtual population and 180 kg for the actual patient.

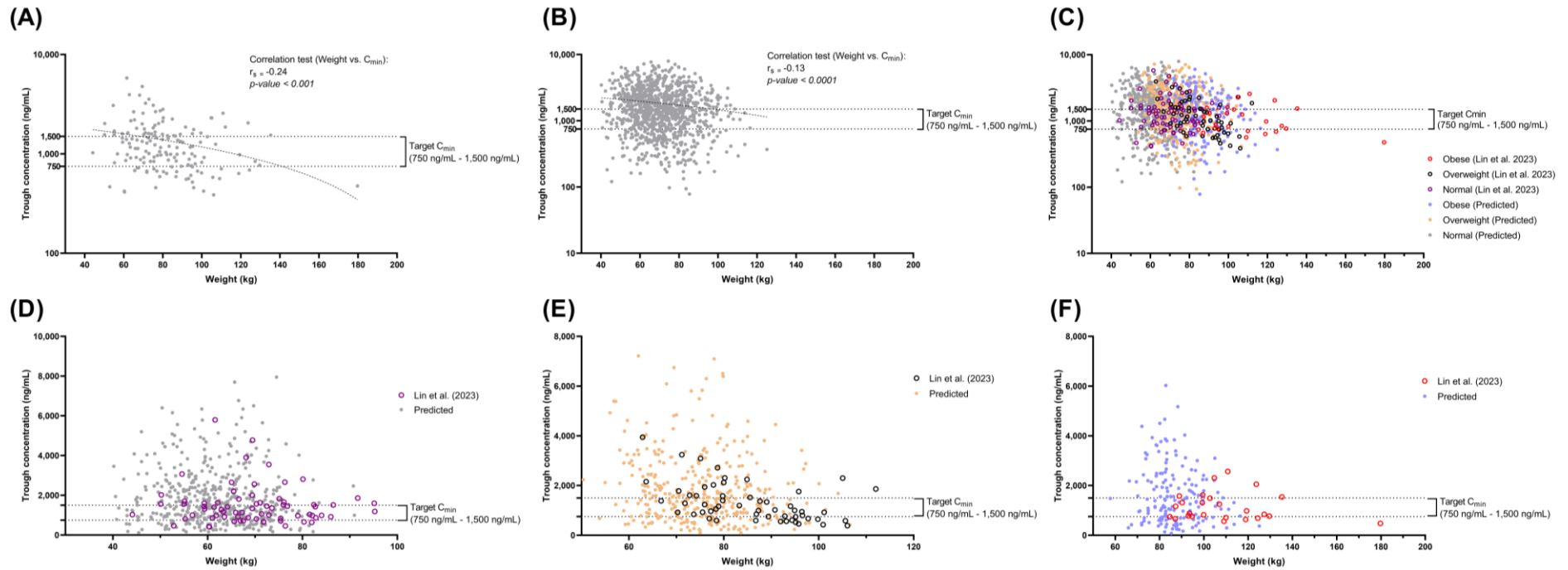


Figure 3.5 Predicted and observed imatinib trough concentrations (C_{min}) in cancer populations were stratified according to the body mass index (BMI) classification.

(A) Correlation and regression line based on the observed imatinib C_{min} by Lin et al. (2023) [271]. (B) Correlation and regression based on the simulated imatinib C_{min} . (C) Predicted versus observed imatinib C_{min} stratified according to BMI classifications. (D) Lean BMI $< 25 \text{ kg/m}^2$. (E) Overweight BMI $25 \text{ kg/m}^2 - < 30 \text{ kg/m}^2$. (F) Obese BMI $> 30 \text{ kg/m}^2$. Close-coloured circles, predicted C_{min} ; open-coloured circles, observed C_{min} .

3.3.3 Step 3: Comparison of physiological parameters and imatinib pharmacokinetics parameters between lean, overweight and obese cancer populations

Since all three BMI categories of cancer populations and imatinib models had been verified in Step 2, and the trend showed a significant correlation between body weight and C_{min} , the differences between all three BMI categories were then investigated from the simulation perspective in terms of the physiological parameters and pharmacokinetic parameters.

3.3.3.1 Comparison of physiological parameters between lean, overweight and obese cancer populations

The comparison focused on 14 physiological parameters generated from 10,000 virtual cancer subjects. A radar chart (Figure 3.6) pictures the approximate differences between lean, overweight, and obese adult cancer populations. A substantial difference was seen in weight, BSA, liver weight, cardiac output, serum creatinine, GFR and CYP3A4 abundance. Excluding the height, haematocrit, AGP, serum albumin, and serum creatinine, the physiological parameters were higher in the obese adult cancer population as opposed to the lean adult cancer population (Figure 3.6).

Furthermore, a statistical comparison test between lean, overweight and obese adult cancer populations was performed for each physiological parameter (Figure 3.7). Significant differences ($p < 0.001$ for HSA and $p < 0.0001$ for other parameters) were noticed between lean and obese populations in all physiological parameters except for haematocrit (Figure 3.7G) and AGP (Figure 3.7H). The differences between lean and overweight were insignificant in five out of 14 parameters, namely, height, HSA, haematocrit, AGP, and serum creatinine. In the comparison between overweight and obese populations, only haematocrit, AGP and CYP2C8 abundance showed no significant difference, whereas the remaining parameters displayed substantial differences.

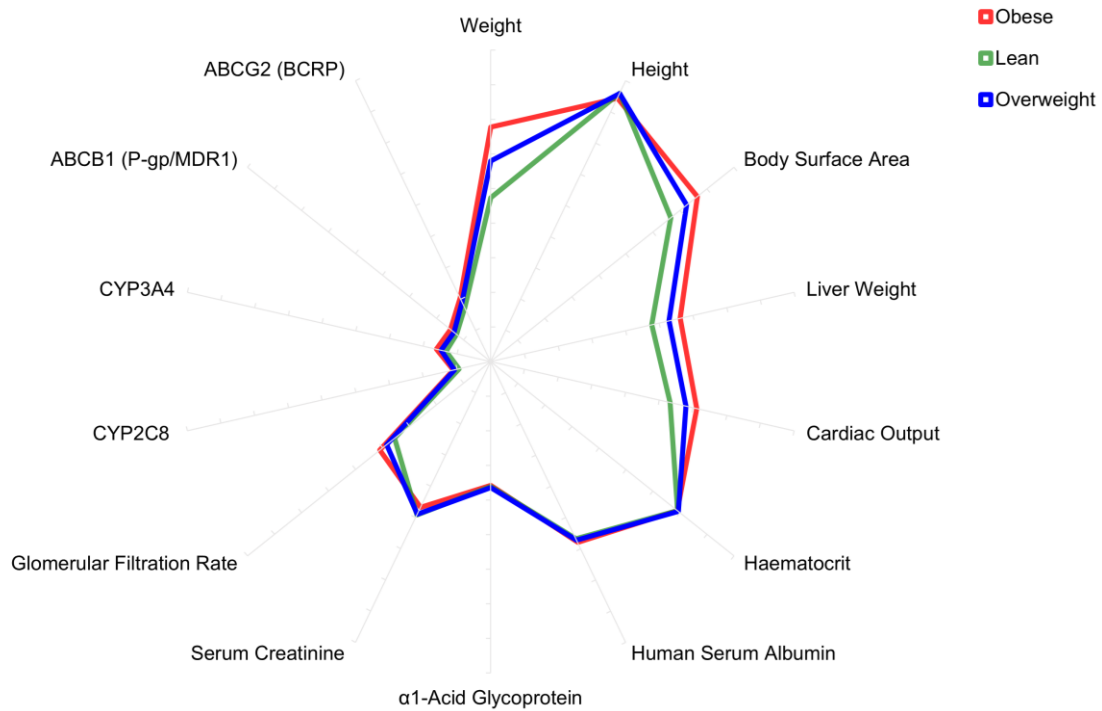


Figure 3.6 Radar graph comparing the mean of lean, overweight and obese adult cancer physiological parameters.

Each colour line represents the mean for each physiological parameter, with the red line as 'obese cancer population', the green line as 'lean cancer population' and the blue line as 'overweight cancer population'. The length of each axis represents the maximum value of the parameters, and the connected point for each line represents the mean of each population.

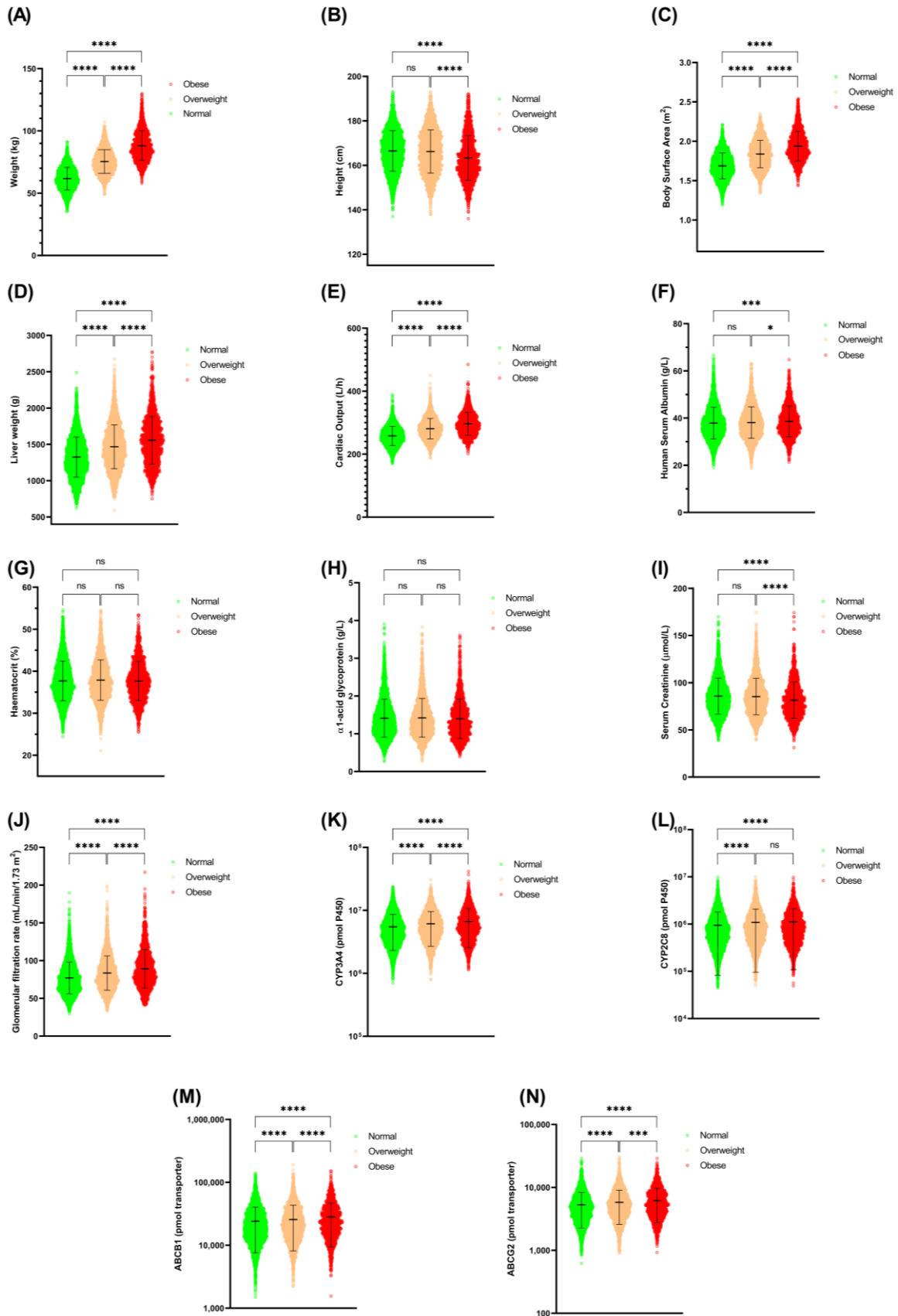


Figure 3.7 Comparison between normal, overweight and obese adult cancer physiological parameters.

Middle horizontal lines represent the mean, with upper and lower horizontal lines representing the standard deviations; *, $p < 0.05$; **, $p < 0.001$; ****, $p < 0.0001$; ns, not significant.

3.3.3.2 Comparison of imatinib pharmacokinetic parameters between lean, overweight and obese adult cancer populations

When compared, lower values for AUC, C_{max} , and C_{min} were observed in obese adult cancer populations compared to lean adult cancer, with statistically significant differences noted for the AUC and C_{max} but not for the C_{min} (Table 3.4). The same trend was seen across all four doses (200-800 mg daily). Multiple comparisons between lean, overweight, and obese adult cancer populations revealed that the differences were significant between each population for the C_{max} parameter, while for AUC, a notable difference was displayed only between lean and obese populations (Figure 3.8). With respect to the C_{min} , the difference between each population was not statistically significant (Figure 3.8).

In relation to the lower value of C_{min} in the obese population, the percentage of subjects with C_{min} below 1,100 ng/mL and 750 ng/mL threshold was higher in the obese population compared to the overweight and lean populations (Table 3.4). On the other hand, the percentage was lower for the number of subjects with C_{min} above the 1,500 ng/mL threshold in the obese adult cancer population (Table 3.4). When the virtual subjects were dosed with a standard starting dose of 400 mg daily, approximately 50% of subjects with C_{min} below 1,100 ng/mL in all three BMI categories with differences between 0.4% and 3.4%. Meanwhile, the percentage difference of subjects with C_{min} below 750 ng/mL across lean, overweight, and obese populations was broader, between 0.66% and 6.67%. Similar to the comparison of the pharmacokinetic parameters above, the pattern was akin across all four doses.

Table 3.4 Comparison of simulated imatinib pharmacokinetic parameters at steady-state between lean, overweight, and obese cancer population

Dose	Body mass index (BMI) status	PK parameters			Percentage of subjects with C _{min}		
		AUC ₀₋₂₄ (ng/mL.h)	C _{max} (ng/mL)	C _{min} (ng/mL)	< 1,100 ng/mL	< 750 ng/mL	> 1,500 ng/mL
200 mg daily	Normal (n=474)	27,050.45 ± 13,070.92	1,726.66 ± 597.63	663.17 ± 472.46	84.81	66.46	6.12
	Overweight (n=359)	25,677.83 ± 12,706.12	1,585.76 ± 579.84	647.58 ± 460.43	85.24	69.36	6.13
	Obese (n=167)	23,266.19 ± 11,103.62	1,441.88 ± 505.74	573.96 ± 393.50	91.02	6.13	3.59
	<i>p-value</i>	<i>0.004</i>	<i><0.0001</i>	<i>0.09</i>			
400 mg daily	Normal (n=474)	54,112.87 ± 26,166.38	3,455.19 ± 1,195.81	1,326.01 ± 945.59	51.69	31.65	33.54
	Overweight (n=359)	51,378.04 ± 25,429.22	3,173.40 ± 1,160.88	1,295.36 ± 921.61	52.09	32.31	30.92
	Obese (n=167)	46,537.47 ± 22,225.62	2,885.32 ± 1,011.40	1,147.28 ± 787.42	55.09	38.32	25.75
	<i>p-value</i>	<i>0.004</i>	<i><0.0001</i>	<i>0.09</i>			
600 mg daily	Normal (n=474)	81,217.85 ± 39,271.51	5,187.34 ± 1,795.56	1,989.59 ± 1,419.27	31.22	15.61	53.16
	Overweight (n=359)	77,100.91 ± 38,162.84	4,763.74 ± 1,741.37	1,943.34 ± 1,382.84	31.75	17.55	53.48
	Obese (n=167)	69,842.12 ± 33,352.38	4,330.59 ± 1,518.87	1,721.86 ± 1,182.03	35.93	21.56	50.30
	<i>p-value</i>	<i>0.004</i>	<i><0.0001</i>	<i>0.09</i>			
800 mg daily	Normal (n=474)	108,336.71 ± 52,396.87	6,921.25 ± 2,395.50	2,653.12 ± 1,893.45	17.72	10.13	68.35
	Overweight (n=359)	102,844.67 ± 50,911.82	6,355.48 ± 2,322.86	2,591.45 ± 1,844.72	21.45	11.14	67.69
	Obese (n=167)	93,158.16 ± 44,494.66	5,777.57 ± 2,026.19	2,295.98 ± 1,576.86	26.35	14.37	61.68
	<i>p-value</i>	<i>0.004</i>	<i><0.0001</i>	<i>0.09</i>			

Mean ± SD; PK, pharmacokinetic; AUC₀₋₂₄, area-under-the-curve from 0 to 24 hours; C_{max}, maximum concentration; C_{min}, trough concentration; *p* < 0.05, statistically significant difference; C_{min} < 1,100 ng/mL is the C_{min} threshold proposed by Bouchet et al. (2016) [299]; C_{min} < 750 ng/mL and > 1,500 ng/mL are the lower and upper threshold for C_{min} suggested by Buclin et al. (2020) [276].

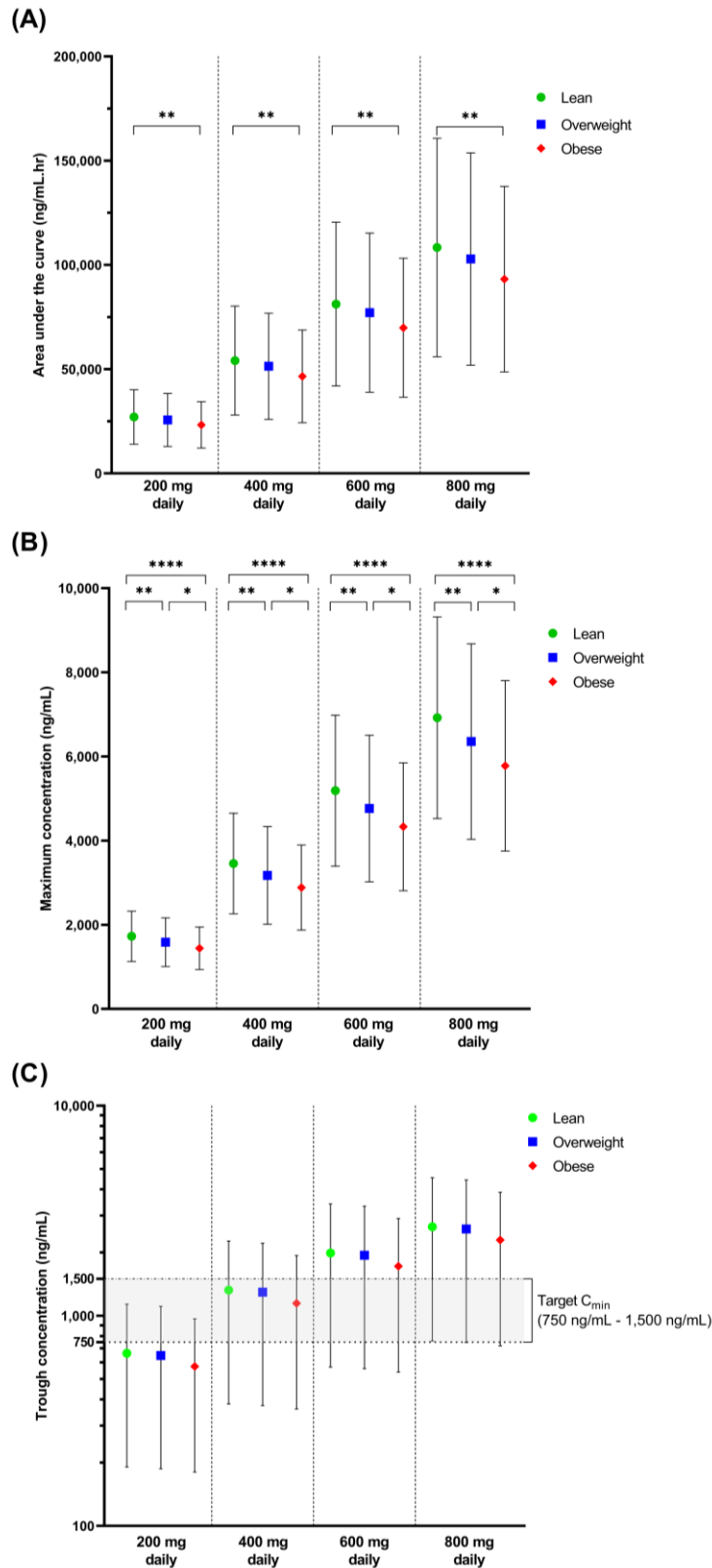


Figure 3.8 Comparison of predicted imatinib pharmacokinetic parameters at steady-state between lean, overweight and obese cancer populations.

(A) Area-under-the-curve (AUC). (B) Maximum concentrations (C_{max}). (C) Trough concentrations (C_{min}). *, $p < 0.05$; **, $p < 0.005$; ****, $p < 0.0001$; The coloured symbol represents the mean, with upper and lower horizontal lines representing the SD. The absence of a comparison bracket (horizontal bracket) on top of each mean and SD graph indicates the differences are not statistically significant.

3.3.4 Virtual therapeutic drug monitoring (TDM) of imatinib in lean, overweight and obese cancer populations

Despite the fact that the difference in the C_{\min} between lean, overweight, and obese adult cancer populations was not statistically significant, the percentage of virtual subjects with C_{\min} below the lower threshold of 750 ng/mL applied by Gotta et al. (2014) [277] was lower across all four doses (Table 3.4). Thus, the TDM-guided dose adjustment was further investigated in all three populations to recapitulate the out-of-range C_{\min} into the target window of 750 ng/mL to 1,500 ng/mL.

After the stratification of subjects according to their C_{\min} level, there was no significant difference between the mean of C_{\min} for the lean, overweight and obese populations ($p > 0.05$) across all six levels (Table 3.5), complementing the results when comparison was made without stratification as reported above.

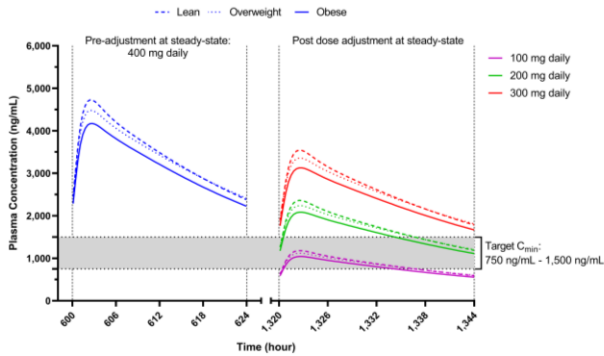
From another perspective, the percentage of subjects with C_{\min} below 550 ng/mL was highest in the obese cancer population, followed by overweight and lean (25.75%, 21.17% and 17.72%). Nevertheless, for virtual subjects with C_{\min} less than 450 ng/mL, despite a two-fold increase in dose, only approximately 20% of subjects achieved the target threshold of 750 ng/mL (Table 3.5), while the mean C_{\min} did not reach the target window (Figure 3.9) for all three populations. On the other hand, for the group with C_{\min} between 450 ng/mL and 549 ng/mL, an increment of 1.75-fold (700 mg daily) or two-fold (800 mg daily), all the trough were raised to the target level for all three populations (Figure 3.9). However, with a 1.5-fold dose increase (600 mg daily), the C_{\min} of approximately 55% of overweight and obese populations ascend to the target window, but only 43.48% for the lean population.

A more comprehensive dose increment option is available to raise the trough to the target concentration for subjects with C_{\min} between 650 ng/mL and 750 ng/mL compared to 550 ng/mL and 649 ng/mL. In general, any increment between 1.25-fold (500 mg daily) to two-fold (800 mg daily) raised all the subjects with a trough between 650 ng/mL and 750 ng/mL up to above 750 ng/mL, while only a 1.5-fold (600 mg daily) to two-fold (800 mg daily) increase in dose was needed to bring up all the troughs between 550 ng/mL and 649 ng/mL, beyond the 750 ng/mL target level (Table 3.5). For the 550 ng/mL to 649 ng/mL stratified group, an increment of 100 mg daily only raised 33.33% to 55% of the trough for all three populations above the target of 750 ng/mL.

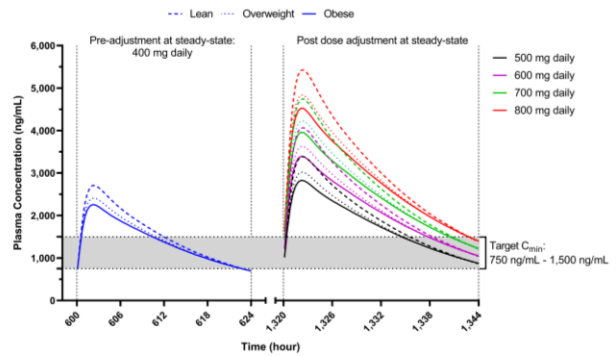
Virtual subjects with a trough concentration above 1,500 ng/mL were simulated with a dose reduction of 0.25-fold (100 mg daily) to 0.75-fold (300 mg daily). A 50% dose reduction across all three populations managed to lower the trough concentration within the aimed level of 750 ng/mL to 1,500 ng/mL (Figure 3.9). In terms of percentages, by reducing the standard dose

by 50%, trough concentrations were reduced to within 750 ng/mL and 1,500 ng/mL for approximately 80% of subjects with C_{min} above 1,500 ng/mL, with the obese population reaching up to 86.05% (Table 3.5). For a dose reduction of 0.75-fold, the trough mean for all three populations was still above 1,500 ng/mL. Contrarily, with a 0.25-fold dose lowering, the mean of C_{min} for all the populations falls below the 750 ng/mL threshold.

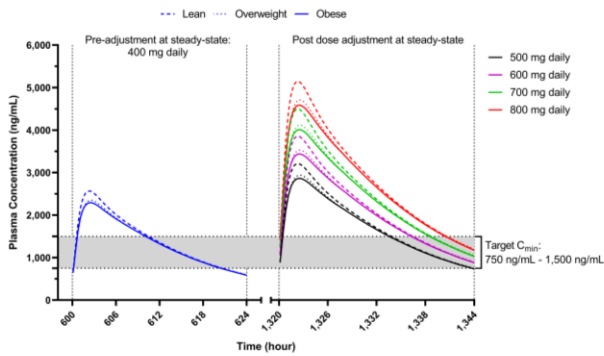
(A) Pre-adjustment C_{min} : > 1,500 ng/mL



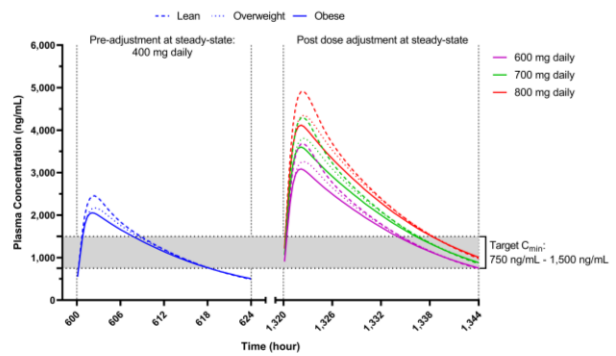
(B) Pre-adjustment C_{min} : 650 ng/mL - 750 ng/mL



(C) Pre-adjustment C_{min} : 550 ng/mL - 649 ng/mL



(D) Pre-adjustment C_{min} : 450 ng/mL - 549 ng/mL



(F) Pre-adjustment C_{min} : < 450 ng/mL

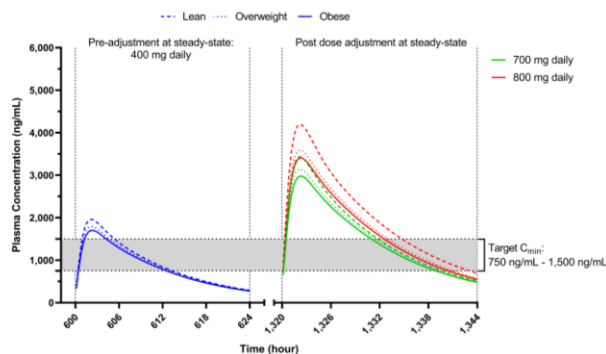


Figure 3.9 Comparison of predicted imatinib pharmacokinetic parameters at steady-state between lean, overweight and obese cancer populations.

(A) Area-under-the-curve (AUC). (B) Maximum concentrations (C_{max}). (C) Trough concentrations (C_{min}). *, $p < 0.05$; **, $p < 0.005$; ****, $p < 0.0001$; The coloured symbol represents the mean, with upper and lower horizontal lines representing the SD. The absence of a comparison bracket (horizontal bracket) on top of each mean and SD graph indicates the differences are not statistically significant.

Table 3.5 Predicted imatinib trough plasma concentrations at different doses in cancer subjects following the application of therapeutic drug monitoring (TDM)

Pre-adjustment				Post-adjustment				
C_{\min} level (ng/mL)	BMI Status	C_{\min} (ng/mL)	Subjects within C_{\min} level (% (proportion))	Dose adjustment	Adjusted Dose (mg)	C_{\min} (ng/mL)	Subjects within target C_{\min} (% (proportion))	
<450	Lean	292.79 ± 94.93	12.87 (61/474)	x 1.75	700	510.65 ± 165.03	4.91 (3/61)	
				x 2	800	583.68 ± 188.84	21.31 (13/61)	
	Overweight	290.63 ± 98.39	14.21 (51/359)	x 1.75	700	506.15 ± 171.81	3.92 (2/51)	
				x 2	800	578.36 ± 196.32	21.57 (11/51)	
	Obese	274.79 ± 108.82	18.56 (31/167)	x 1.75	700	478.63 ± 190.18	9.68 (3/31)	
				x 2	800	546.85 ± 217.31	22.58 (7/31)	
450 -549	Lean	491.47 ± 30.15	4.85 (23/474)	x 1.5	600	736.58 ± 45.64	43.48 (10/23)	
				x 1.75	700	859.05 ± 53.13	100 (23/23)	
				x 2	800	981.51 ± 60.61	100 (23/23)	
	Overweight	502.82 ± 19.69	6.96 (25/359)	x 1.5	600	751.61 ± 29.24	56.00 (14/25)	
				x 1.75	700	876.72 ± 34.18	100 (25/25)	
				x 2	800	1,001.80 ± 39.13	100 (25/25)	
	Obese	506.76 ± 31.42	7.19 (12/167)	x 1.5	600	756.76 ± 47.98	58.33 (7/12)	
				x 1.75	700	882.83 ± 55.95	100 (12/12)	
				x 2	800	1,008.89 ± 63.93	100 (12/12)	
	550 - 649	Lean	592.90 ± 25.11	6.12 (29/474)	x 1.25	500	738.27 ± 30.94	34.48 (10/29)
					x 1.5	600	885.70 ± 37.14	100 (29/29)
					x 1.75	700	1,033.21 ± 43.33	100 (29/29)
x 2					800	1,180.65 ± 49.58	100 (29/29)	
Overweight		602.03 ± 30.39	5.57 (20/359)	x 1.25	500	750.71 ± 37.71	55 (11/20)	
				x 1.5	600	900.76 ± 45.37	100 (20/20)	
				x 1.75	700	1,050.79 ± 53.04	100 (20/20)	
				x 2	800	1,200.78 ± 60.77	100 (20/20)	
Obese		589.15 ± 30.01	5.39 (9/167)	x 1.25	500	734.25 ± 41.31	33.33 (3/9)	

				x 1.5	600	881.00 ± 49.69	100 (9/9)
				x 1.75	700	1,027.73 ± 58.07	100 (9/9)
				x 2	800	1,174.40 ± 66.49	100 (9/9)
650 - 749	Lean	695.11 ± 28.87	7.81 (37/474)	x 1.25	500	867.20 ± 35.70	100 (37/37)
				x 1.5	600	1,040.55 ± 42.73	100 (37/37)
				x 1.75	700	1,213.90 ± 49.93	100 (37/37)
				x 2	800	1,387.05 ± 56.99	100 (37/37)
	Overweight	691.57 ± 25.07	5.29 (19/359)	x 1.25	500	862.38 ± 28.92	100 (19/19)
				x 1.5	600	1,034.65 ± 34.73	100 (19/19)
				x 1.75	700	1,206.87 ± 40.56	100 (19/19)
				x 2	800	1,379.05 ± 46.37	100 (19/19)
	Obese	699.23 ± 31.97	6.59 (11/167)	x 1.25	500	875.70 ± 40.74	100 (11/11)
				x 1.5	600	1,050.03 ± 48.34	100 (11/11)
				x 1.75	700	1,224.37 ± 56.03	100 (11/11)
				x 2	800	1,398.72 ± 63.81	100 (11/11)
750 - 1,500	Lean	1,071.18 ± 205.68	34.39 (163/474)				
	Overweight	1,094.25 ± 209.29	37.05 (133/359)	None	400		
	Obese	1,127.23 ± 225.99	36.53 (61/167)				
> 1,500	Lean	2,382.12 ± 847.35	33.97 (161/474)	x 0.75	300	1,783.48 ± 635.32	44.10 (71/161)
				x 0.5	200	1,188.79 ± 423.38	80.75 (130/161)
				x 0.25	100	594.30 ± 211.61	18.01 (29/161)
	Overweight	2,415.57 ± 798.15	30.92 (111/359)	x 0.75	300	1,808.56 ± 597.80	37.84 (42/111)
				x 0.5	200	1,205.51 ± 398.41	79.28 (88/111)
				x 0.25	100	602.65 ± 199.13	19.82 (22/111)
	Obese	2,227.00 ± 616.96	25.75 (43/167)	x 0.75	300	1,667.83 ± 462.73	53.49 (23/43)
				x 0.5	200	1,111.72 ± 308.34	86.05 (37/43)
				x 0.25	100	555.81 ± 154.09	13.95 (6/43)

TDM, therapeutic drug monitoring; BMI, body mass index; C_{min}, trough concentration; Shaded row represent the target C_{min}; target C_{min}, 750 ng/mL – 1,500 ng/mL.

3.4 Discussion

Several studies have suggested that overweight and obese patients treated with imatinib have lower responses compared with lean patients from the pharmacodynamic perspectives, such as time to achieve the MMR, CCyR, overall objective benefit rate (OOBR), and time to progression (TTP) [269, 270, 273]. Additionally, a case study reported that a higher imatinib dose might be needed in a morbidly obese patient in order to achieve an MMR at the same time as a patient with a lean BMI [268].

When considering the pharmacokinetic perspective, a study by Lin et al. (2023) [271] revealed a negative correlation between body weight and the trough concentration, where higher body weight is associated with lower C_{min} . Nevertheless, the difference was insignificant when comparing the percentage of subjects with C_{min} below 1,100 ng/mL between lean, overweight, and obese patients [271]. Therefore, the PBPK concept was utilised to investigate the pharmacokinetic difference between lean, overweight and obese adult cancer populations and explore the TDM approach in establishing the dose adjustment scheme for effective imatinib treatment outcomes within the pharmacokinetic aspect.

3.4.1 Step 1: Imatinib model validation in healthy, cancer and Caucasian populations

The utilised imatinib compound model was obtained from literature and has been verified in diverse population models, including healthy subjects, cancer patients, Chinese cancer patients, paediatric cancer patients, and subjects of various ethnicities [281-283]. To bolster confidence in utilising the imatinib model in the Simcyp® version 21, the model was validated with healthy, cancer and Caucasian populations, including using the observed data from the latest publications for healthy and cancer populations, which was in 2020 and 2015, respectively.

Verification with healthy subjects showed that the imatinib model predicted comparable plasma profiles and pharmacokinetic parameters within the acceptable margins of the observed data from three single-dose studies. The results were consistent with all the other publications that applied the imatinib models [281-283, 294, 304].

Concerning the cancer patient population, verification was focused on five multiple-dose studies involving GIST and CML patients. Since imatinib exhibits high inter-individual (47% – 75%) and intra-individual variability (19% – 30%) concerning its pharmacokinetic parameters and exposure, the predicted profiles align within the range of imatinib's observed plasma

samples for all the studies, particularly when the comparison was made to those studies that reported sparse samples [288, 290-292, 299, 301, 305, 306].

Overprediction was noticeable when the predicted profiles were superimposed with the observed data from Peng et al. (2004) [291], specifically for the 350 mg daily dose and the elimination section of the 25 mg daily dose. Likewise, the C_{max} and AUC_{0-24ss} of 350 mg daily dose and AUC_{0-24ss} and t_{max} of 25 mg daily dose were not within the 2-fold criteria. The lower number of patients (three for 25 mg daily dose and five for 350 mg daily dose) in the reported data alongside the large inter- and intra-individual of imatinib exposure might be the reason for the overprediction [291, 301]. Nevertheless, the prediction aligned for the other four doses from the same study, and sparse samples from another four studies boosted the verification of the imatinib compound model to predict imatinib pharmacokinetic parameters in the adult cancer population.

For verification with published data by Widmer et al. (2006) [292] and Haouala et al. (2013) [293], the prediction of imatinib profiles in the NEurCaucasian population aligned with the spread of observed data with both publications. The utilisation of the Caucasian population is in line with the validation performed by the imatinib compound model developer [283]. Since imatinib binds extensively to AGP, the AGP level highly influences the imatinib plasma level. Lower plasma AGP was seen in the Caucasian population (0.79 g/L – 0.81 g/L) compared to the cancer population (1.35 g/L – 1.49 g/L), which was the primary justification for the use of the Caucasian population in the verification with data from the two publications [283].

Although the imatinib model demonstrated adequate performance under the predefined validation criteria, certain limitations warrant consideration. For example, broader variability in observed data and overestimation in some outcome simulations suggest potential areas for refinement. Importantly, model parameters were not re-estimated to maintain alignment with previous validations across diverse populations and ethnicities [281-283]. Nevertheless, further refinements may focus on incorporating additional mechanistic insights, such as hepatic enzyme activity and transporter expression, to address the variability while maintaining alignment with the existing model.

3.4.2 Step 2: Validation of lean, overweight and obese cancer population model with imatinib compound model

According to existing literature, data published by Lin et al. (2023) [271] was the only study (to date) that reported the imatinib plasma concentration, specifically trough concentrations in lean, overweight and obese patients with GIST (n=200) and dermatofibrosarcoma (n=1).

Based on the VPC approach, the correlation between body weight and C_{\min} and the spread of C_{\min} for predicted imatinib concentration produced the same pattern as observed data, which verified the capability of the imatinib model to predict the plasma concentration in the lean, overweight, and obese adult cancer population.

A slight deviation in the regression line trends noted between observed and predicted C_{\min} across the body weight in terms of the on-target concentrations was potentially due to the limited number of observed data points for the overweight and obese patients. Moreover, the Simcyp® cancer population model used for simulations was limited to a maximum weight of 125 kg, whereas the observed data included patients weighing up to 180 kg. Extending simulations to higher weights could improve predictive accuracy, particularly on the correlations, though challenges remain due to the lack of validated physiological data for morbidly obese cancer populations.

3.4.3 Step 3: Comparison of physiological parameters and imatinib pharmacokinetics parameters between lean, overweight, and obese cancer populations

3.4.3.1 Analysis of physiological parameters across lean, overweight, and obese cancer populations

The virtual population simulated in this study originated from the default cancer population in Simcyp®, which was established based on patients with advanced solid tumours [125, 134, 298]. Since the Simcyp® simulator simulated the virtual cancer subjects across the whole BMI range, the virtual cancer subjects were arranged conforming to their BMI classes and analysed the differences in their physiological parameters. Significant differences were revealed in all the physiological parameters except for haematocrit and AGP when comparing between lean and obese cancer populations.

Differences observed between obese and lean in most parameters are expected, as larger body weight in obese patients relates to an increase in mass-to-height ratio and is further linked to higher BSA [124, 307]. The differences for most parameters were also seen between lean and overweight, as well as overweight and obese cancer populations. Liver size and cardiac output were predicted based on the BSA, hence the distinctive difference between lean, overweight and obese populations [308]. Besides, higher cardiac output is attributed to elevated heart rate and higher stroke volume in the obese population [155].

The prevalence of impaired renal function is higher in cancer patients, as represented by GFR measurement and estimated from the serum creatinine, which has an inverse relationship between serum creatinine and GFR [132, 309]. From the BMI perspective, higher GFR was seen in higher BMI patients, further explaining the significant differences between all three populations [124, 141]. Since imatinib and its metabolites are mainly excreted via the faeces, with approximately 68% and 13% via the urine, the variation in renal function between the three groups may not influence the imatinib pharmacokinetics [139].

The cytochrome P450 (CYP) enzymes and transporters that play a major contribution in imatinib metabolism and efflux include CYP3A4, CYP2C8, ABCB1 (P-gp/MDR1) and ABCG2 (BCRP) [310, 311]. Due to this fact, the related enzymes and transporter abundances were compared between the three populations.

On the basis of per microgram microsomal proteins, no differences were seen in both CYP3A4 and CYP2C8 enzymes. Thus, significant differences between all three populations for the CYP3A4 enzyme abundance are related to the liver size, as larger liver volumes are seen for virtual subjects with higher BMI values [308]. Additionally, studies have reported a reduction of 30% and 10% to 40% of CYP3A4 activities in both cancer and obese populations, which further suggests the differences between all three populations [124, 134, 312]. There is no specific explanation for the results of no difference between overweight and obese cancer populations for the CYP2C8 enzyme abundance as the lack of information on the CYP2C8 enzyme abundance compared to the CYP3A4 in both cancer and obese populations [124, 134]. The relation between liver weight and transporter abundance for the in vitro-in vivo extrapolation (IVIVE) in the PBPK concept addresses the significant differences noted between all three populations [313].

For the plasma proteins, studies reported lower HSA and higher variability in cancer patients compared to healthy volunteers while unaltered compared to obese subjects [124, 125, 314]. Besides, the positive correlation graph between albumin and BMI in cancer patients published by Cheeti et al. (2013) [125] relates to the notable differences between lean and obese as well as obese and overweight.

The AGP, another plasma protein component, has been reported to be higher in cancer patients by up to 5-fold compared to the healthy population [125, 315]. Likewise, the AGP level is higher in the obese population than in the healthy population by up to 2.5-fold [124, 316, 317]. However, limited information was available for obese cancer patients. Considering AGP is significantly higher in both cancer and obese populations, no difference in the AGP value is anticipated in obese, overweight, and lean cancer patients.

Haematocrit levels in cancer patients are lower than in healthy volunteers but constant throughout the BMI range, clarifying the consistent level between all three populations [124, 125].

3.4.3.2 Assessment of imatinib pharmacokinetic parameters between lean, overweight and obese adult cancer populations

The significant differences illustrated in the imatinib peak concentration between lean, overweight and obese cancer populations are consistent with the considerable differences in the BSA, CYP enzymes and transporters that regulate the imatinib uptake, efflux and metabolism pathway [270]. Additionally, the lipophilic nature of imatinib leads to a higher volume of distribution in the obese cancer population, further contributing to the significantly lower C_{max} compared to overweight and lean groups [138]. Besides, high clearance in the obese population also influences the differences in C_{max} .

On the contrary, although the pattern of trough concentration across all the doses illustrated lower C_{min} in the obese cancer group, the difference is not statistically significant. The subtle differences in the elimination rate resulting from the difference in volume of distribution and clearance potentially explained the C_{min} result. Accordingly, the significant difference in AUC seen only between lean and obese cancer populations is anticipated, because substantial differences across all three populations are only seen in the peak concentration but not the trough concentrations since AUC estimation derived from each measured concentration and time, which includes the C_{max} and C_{min} .

Additionally, a broad intersubject variability in all three pharmacokinetic parameters seen in all three population groups (Figure 3.8) has also been previously documented by other researchers [291, 318, 319]. The high variability is potentially due to the variabilities in the plasma protein binding component, the AGP where imatinib is highly bound, the CYP3A4 metabolism enzymes and transporter expression. Besides, a sensitivity analysis was performed to assess the influence of both AGP and CYP3A4 on imatinib's pharmacokinetic parameters, as described in the subsequent section.

Trough concentration is pivotal in predicting the imatinib therapeutic response and has been used as a target in imatinib TDM practice to attain an optimum treatment response [276, 277, 280]. There are several C_{min} target levels reported either as a range of values, such as 750 ng/mL to 1,500 ng/mL by Buclin et al. (2020) [276] and 1,000 ng/mL to 1,500 ng/mL by Garcia-Ferrer et al. (2019) [300] or cut-off levels like 1,100 ng/mL, 1,000 ng/mL and 760 ng/mL as implemented by various studies [271, 299, 320-322]. In this study, the C_{min} target range of 750

ng/mL to 1,500 ng/mL and the threshold of 1,100 ng/mL was used for comparison between lean, overweight and obese on the percentages of virtual subjects where their C_{min} fall below the lower threshold and above the target level.

The number of subjects with C_{min} below the threshold of both 1,100 ng/mL and 750 ng/mL was higher in the obese, followed by overweight and then lean cancer populations. The hierarchy and percentage difference between each population are similar across all doses and comparable with the results presented by Lin et al. (2023) [271]. Moreover, the percentage differences are more significant with the 750 ng/mL cut-off level, aligning with the median and the lower 25th percentile, which is lower in the obese group compared to overweight and lean populations. On the contrary, the percentage of subjects with C_{min} above the upper threshold is higher in the lean population, followed by overweight and then obese.

3.4.4 Step 4: Virtual therapeutic drug monitoring (TDM) of imatinib in the lean, overweight, and obese cancer population

Achievement of MMR with the percentage of the BCR-ABL gene is less than 0.01%, and CCyR with no Philadelphia chromosome are the goal for imatinib therapy, particularly for the treatment of CML [323]. The correlation between low trough concentrations with the MMR and the CCyR, in addition to the significant between-subject pharmacokinetic variability, meets the requirement for the need to personalise dosing using the TDM approach, and the benefit has been demonstrated in various studies [280, 290, 300, 321, 322].

Considering the differences in imatinib plasma concentration perceived between the lean, overweight and obese cancer populations, added with the ability of the imatinib model to simulate the plasma concentration profiles, the TDM-guided imatinib dose strategy adapted from Gotta et al. (2014) [277] study was implemented by simulating the dose adjustment from a starting dose of 400 mg once daily, spanning to a range of 100 mg to 800 mg daily based on their trough concentration (Figure 3.2).

The difference in mean C_{min} seen in all six stratified levels ($>1,500$ ng/mL, $1,500$ ng/mL – 750 ng/mL, <750 ng/mL – 650 ng/mL, <650 ng/mL – 550 ng/mL, <550 ng/mL – 450 ng/mL and <450 ng/mL) between the lean, overweight, and obese cancer populations were not significant. Aligning with the result in Step 4 and publication by Lin et al. (2023) [271]. However, the percentage of subjects in the two lowest C_{min} (<550 ng/mL) groups is higher in the obese. In contrast, for the <750 ng/mL to 550 ng/mL range, the lean population has the highest percentages. The result is consistent with the comparison made in step 3, where the median and 25th percentile are lower in obese compared to the lean cancer population.

The TDM-guided dose adjustment with the 750 ng/mL - $1,500$ ng/mL target C_{min} managed to recover all the subjects with the trough concentrations between 450 ng/mL – 750 ng/mL for all three groups. Moreover, it is noteworthy that the dose adjustment options are consistent across all three population groups. Although the simulations showed no difference in terms of dose adjustment options between the lean, overweight and obese populations, the result aligns with the approach to monitor the imatinib trough concentration to optimise the imatinib treatment outcome in the obese cancer population, as proposed in several studies [268, 324]. Imatinib dose adjustments assisted by the TDM approach have also been shown to recover and maintain more than 90% of the patient's trough concentrations with subtherapeutic range back to the target level [306].

In addition, simulations showed that when the imatinib trough concentration falls below 450 ng/mL, only 20% of the subjects can be recuperated to the target C_{min} across all three groups, even with the imatinib maximum daily dose (800 mg daily). Based on this data and the

correlation between imatinib trough concentration with MMR and CCR, a suboptimal response, as proposed by European LeukemiaNet (ELN), may be expected in this group of subjects due to the inability to achieve the minimum threshold of C_{\min} even with the maximum dose of imatinib [325, 326]. Imatinib resistance, either due to *BCR-ABL* dependence or independence, can be speculated to be the reason for the treatment failure [327]. Therefore, switching to an alternative therapy, such as other TKIs, at the early stage of treatment can potentially offer therapeutic advantages to the patients [326, 328, 329].

For all three population groups in the simulation, a dose reduction by half recovered approximately 80% of the virtual subjects with trough levels beyond the upper threshold and into the target range. A dose titration of 0.75-fold and 0.25-fold from a standard dose of 400 mg daily resulted in a mean above 1,600 ng/mL and below 650 ng/mL, respectively. Nevertheless, the percentage of subjects with C_{\min} recapitulated into the target window was 35% and above, with a 0.75-fold dose reduction compared to less than 20% with a 0.25-fold dose reduction across all three populations. Aligned with several other studies, a dose reduction due to adverse events from 400 mg daily to 200 mg – 300 mg daily has also demonstrated effective clinical outcomes [322, 330].

For the upper trough concentration threshold of 1,500 ng/mL, no specific stratification based on the C_{\min} range was made, as the primary reason for dose reduction during the imatinib treatment course or treatment discontinuation is the occurrence of intolerable adverse events commonly related to haematological and musculoskeletal systems [277, 306, 322, 330]. Besides, other side effects, such as nausea, vomiting, diarrhoea, oedema, insomnia, depression, and gastrointestinal symptoms, may potentially influence the patient's tolerability, compliance and possibly the treatment efficacy [331].

The trough concentration target window of 750 ng/mL – 1,500 ng/mL proposed by Buclin et al. (2020) [276] was derived based on a specific target C_{\min} of 1,000 ng/mL established by Larson et al. (2008) [272]. Thus, when considering higher C_{\min} threshold levels, particularly the > 1,000 ng/mL as advocated by Larson et al. (2008) [272] for CML patients and >1,100 ng/mL as suggested by Bouchet et al. (2016) [299] for GIST patients, together with the simulated mean of C_{\min} based on the stratified group, the imatinib dose titration guided by trough concentration remain consistent across the lean, overweight, and obese cancer populations (Figure 3.10).

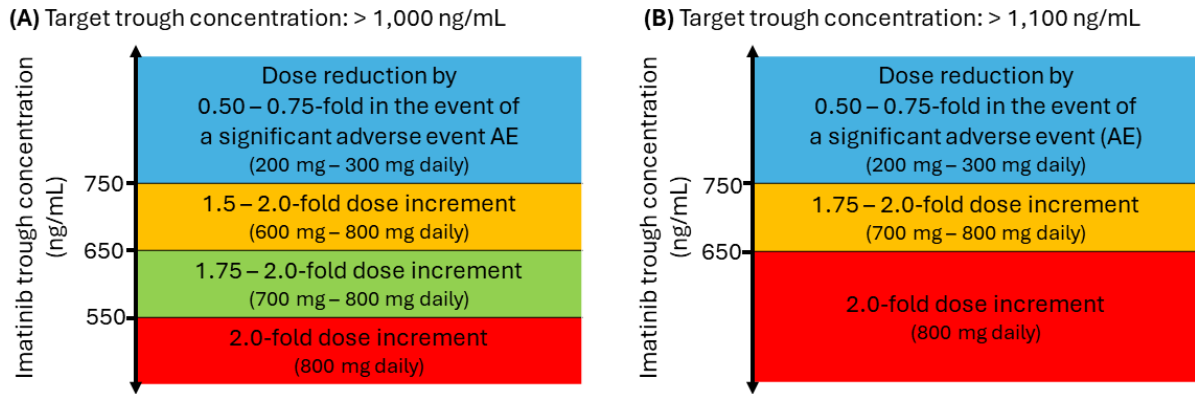


Figure 3.10 TDM-guided dose adjustment according to the target trough concentrations.

Dose adjustments are compiled based on the simulated data following a 400 mg once daily at steady-state and adjustments to be made according to their trough plasma concentration level at steady-state.

The advocacy of using the TDM approach for imatinib for a better clinical outcome has been demonstrated in several studies [275, 276, 300, 301]. Furthermore, cost analysis revealed that TDM-guided doses for imatinib are economically viable and cost-effective in terms of quality-adjusted life-years for the treatment of CML and GIST conditions [278, 279].

Currently, the TDM approach for imatinib is accessible to patients in several hospitals in European regions [276]. Nevertheless, the obstacles to widely implementing the TDM approach for imatinib persist, ranging from constraints associated with precise sampling time points, the hesitancy of prescribers to deviate from existing dosing approaches, lack of experts and supports to interpret and translate the measured concentration to dosing recommendation and limitations on the bioanalytical technique to measure the imatinib plasma concentration [276, 332].

The progress made by researchers worldwide in terms of advancement in bioanalytical methods such as dried blood spot sampling and analysis, development and accessibility of various user-friendly software with artificial intelligence and the trend towards precision medicines is believed to revolutionise the TDM practice and captivate the interest of prescribers [333, 334].

3.4.5 Sensitivity analysis for α 1-acid glycoprotein (AGP) and CYP3A4 hepatic abundances

In light of the significant influence of CYP3A4 enzyme and AGP level on the metabolism, distribution and elimination of imatinib and the scarcity of information on the CYP3A4 abundance as well as AGP level in obese adult cancer, a sensitivity analysis was performed to explore their impact on the key pharmacokinetic parameters, specifically the C_{max} , C_{min} and AUC. Moreover, the results from physiological parameters comparison between the virtual lean, overweight and obese adult cancer populations disclose no difference in both CYP3A4 abundance per microgram microsomal protein and AGP level, reinforcing the necessity for a sensitivity analysis.

The analysis revealed that both the AGP plasma protein binding component and CYP3A4 metabolism enzyme significantly influence all three pharmacokinetic parameters, with the AGP protein exhibiting a more pronounced effect than the CYP3A4 (Figure 3.11). Notably, the results showed a positive correlation between AGP level and imatinib plasma level concentrations, in contrast to the relationship between CYP3A4 and imatinib concentrations, which aligns with findings in other studies [335-337].

The result aligns with the fact that imatinib is primarily bound to AGP with high affinity and has been reported to influence imatinib pharmacokinetics substantially [292, 335]. Furthermore, AGP has been linked to imatinib resistance, where studies have shown that AGP plasma concentrations are higher in resistant CML patients and are categorised as one of the resistant mechanisms that are independent of the BCR-ABL gene [327, 338, 339]. Nonetheless, at the same time, the CYP3A4, as the primary isoenzyme involved in imatinib metabolism, contribute considerably to altering the imatinib pharmacokinetics [291].

A decrease in CYP3A4 activities and an increase in AGP level seen in the obese population is anticipated to increase the imatinib concentrations significantly in the obese cancer population compared to the lean cancer populations [124]. On the contrary, the imatinib concentration was lower in the obese cancer population (Figure 3.8) [271]. The opposite pattern may be attributed to the similar changes in CYP3A4 isoenzyme and AGP levels observed in the cancer patient populations, compounded with the high variabilities of both physiological parameters [125, 134]. Thus, the difference in body weight and BSA is potentially the main contributor to the lower imatinib plasma concentration seen in the obese cancer population [271, 340-342].

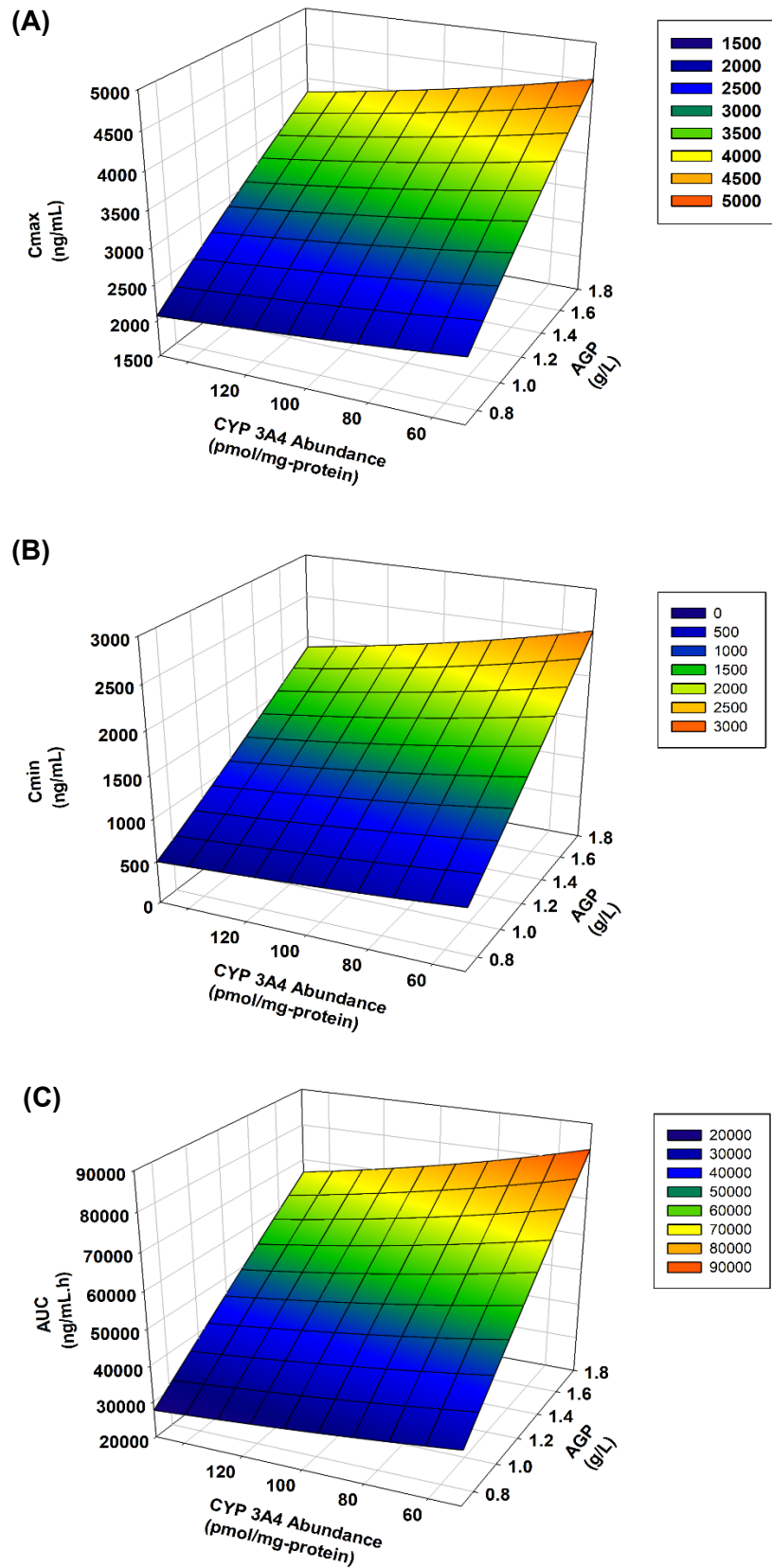


Figure 3.11 Impact of the CYP3A4 hepatic enzyme abundances and α 1-acid glycoprotein (AGP) changes on the maximum concentration (C_{max}) (A), trough concentration (C_{min}) (B), and area-under-the-curve (AUC) (C).

3.5 Conclusion

The application of the PBPK concept in this study addresses the physiological parameters distinctness between lean, overweight, and obese cancer populations and highlights the significant variations in imatinib pharmacokinetics between the populations, particularly for the C_{max} and AUC. Furthermore, this study took a pragmatic approach by implementing the virtual TDM using the PBPK concept to assess the optimal TDM-guided dosing titration for imatinib. Results showed that the TDM-guided dosing strategy for imatinib effectively attained the target trough concentrations in all three population groups, particularly for subjects with trough concentrations above 450 ng/mL. Thus, it reiterates the feasibility of TDM for imatinib in recovering the trough concentrations and further improves the likelihood of treatment efficacy and safety. Nevertheless, future research should focus on validating the TDM-guided dosing strategy using real-world data, particularly from obese cancer patients and correlating the outcomes with clinical endpoints to establish robust dosing recommendations.

In brief, the outcomes highlight the capabilities of PBPK modelling to elucidate the pharmacokinetic differences and refine the TDM dosing strategy in lean, overweight and obese cancer populations. Continuous improvement of the virtual overweight and obese cancer populations with the latest information is imperative, with a specific focus on the physiological data that significantly influence the imatinib absorption, distribution, metabolism and excretion, such as CYP3A4 metabolism enzyme abundances, AGP levels, and transporters.

CHAPTER 4 – The impact of paediatric obesity on drug pharmacokinetics: a virtual clinical trials case study with amlodipine

Disclaimer

This chapter has been published as follows:

Burhanuddin, K., Mohammed, A.R. and Badhan, R. The impact of paediatric obesity on drug pharmacokinetics: a virtual clinical trials case study with amlodipine. *Pharmaceutics*, 2024. 16(4): 489.

DOI: 10.3390/pharmaceutics16040489

4.1 Introduction

The prevalence of paediatric obesity worldwide has risen by approximately 20% over the past few decades, and the latest reports predict that this number would double globally by 2035, affecting 208 million boys and 175 million girls [112]. This trend can be seen in developed countries, such as the United Kingdom, where obesity among children aged 4 to 6 years increased by 4.5% between 2019-2020 and 2020-2021, though it declined by 2.1% to 4.3% between 2020-2021 and 2021-2022, with children living in the most deprived areas still experiencing obesity rates twice as high as those in the least deprived areas [343, 344]. In addition, the pattern has been stagnant in some parts of Europe and high-income English-speaking countries. However, the rise in childhood obesity phenomenon has accelerated in East, South and Southeast Asia [345].

Obesity is known to cause physiological alteration in drug distribution and elimination, among others, increased tissue volume, altered tissue composition, change in blood protein proportions, metabolism enzyme activity, and glomerular filtration rate (GFR) [123, 156, 160, 265, 316, 317, 346]. The complexity becomes even more intricate in paediatric populations due to the interplay of age-related ontogeny and obesity-related factors. The Centre for Disease Control and Prevention (CDC) defined childhood obesity as children with body mass index (BMI) above the 95th percentile, while the World Health Organisation (WHO) set obesity at +3 standard deviation (SD) and +2 SDs from the median line for 0 to 5 years old and 5 to 18 years old, respectively [152, 153].

The primary physiological changes observed in obese children are the physical attributes, namely, weight and height, which are the foundation of BMI classification for obesity. The increase in body weight relates mainly to the rise in total body fat and, to some extent, lean body mass, which impacts the volume of distribution (V_d) of drugs, depending on their lipophilicity and hydrophilicity [154]. Additionally, the composition of plasma components like serum albumin and α 1-acid glycoprotein (AGP), essential for drugs' protein binding, also affects the V_d . Notably, it has been reported that there is no difference in these plasma components between obese and non-obese children [156, 157].

Drug clearance relates mainly to hepatic metabolism and renal functions. Information regarding the difference in metabolism enzyme abundance between paediatric with and without obesity is scarce [156]. Nevertheless, the presence of larger liver size and higher blood flow to the liver in obese children is expected to impact hepatic clearance [156]. As for renal function, the paediatric obesity population tend to have an elevated GFR, which can alter the clearance of drugs, particularly drugs that are predominantly eliminated through renal pathways [160, 347].

Dosing guidelines for obese paediatrics are typically derived from obese adults, and complexities in weight-dosing methodologies can contribute to non-optimal doses. Current dosing approaches in paediatric obesity have highlighted that over 60 % of drugs administered to obese children elicit plasma concentrations outside of the therapeutic range and display clinically significant alterations in pharmacokinetics [162].

An aspect of this non-optimal dosing stems from the appropriate use of body weight and the correct use of body weight in anthropometrics-based dosing approaches. Typically, this involves the use of total body weight (TBW) and other methods, such as an allometric scale and dosing recommendation, which are derived from pharmacokinetic data in non-obese adults or children [348]. Other approaches proposed utilising body surface area (BSA), ideal body weight (IBW), and lean body weight (LBW) methods. However, given that these calculations typically invoke the use of a height component, obesity presents challenges given the normal linear growth of children can be affected [348-350].

Given the various physiological changes occurring longitudinally with ageing across the paediatric spectrum, in addition to the differences in physiologies specific to obese vs non-obese children, dosing approaches based on the holistic consideration of these physiological changes in the drug pharmacokinetics have gained some traction in adults and, more recently children. Physiologically based pharmacokinetic (PBPK) modelling, an advanced quantitative approach, helps to understand drug disposition even with the lack of concentration data and offers a promising avenue for determining optimal dosing regimens in the paediatric obesity population, and the concept has been implemented for compounds such as metformin, midazolam, clindamycin, trimethoprim, sulfamethoxazole, fentanyl and methadone [156, 165, 166].

Childhood obesity contributes to various metabolic and cardiovascular complications and has profoundly changed the frequency of primary hypertension in children, with only 15% in 1988 rising to 90% in 2010 [150]. Calcium channel blockers (CCB), such as amlodipine, felodipine, and nifedipine, are among other antihypertensive agents recommended as first-line therapy [351, 352]. A study by Hanafy et al. (2009) [353] reported that obese children exhibit a significantly lower response to CCBs, including amlodipine, in terms of reducing systolic blood pressure and response rate compared to non-obese children.

Using amlodipine as a case study, this study describes the approach to develop a physiological obesity model to support pharmacokinetic-based dose optimisation, for the first time in paediatric obesity populations. By utilising PBPK advancement, a robust paediatric obesity population model and amlodipine pharmacokinetic model were established, significantly impacting paediatric pharmacotherapy, filling the knowledge gap of drug

disposition in this unique population, and facilitating the design of personalised dosing strategies. Moreover, the insights gained may serve as a model for pharmacokinetic studies in other medications used in paediatric obesity.

The primary objectives of this study are to use the principle of mechanistic pharmacokinetic modelling and virtual clinical trials to (1) develop and validate a paediatric obesity population model, (2) address the impact of obesity on amlodipine pharmacokinetics in paediatrics, and (3) determine the dose adjustment needed for amlodipine in the obese paediatric population.

4.2 Methodology

The PBPK modelling software, Simcyp® (Simcyp Ltd., a Certara company, Sheffield, UK, Version 21) was used to develop a paediatric obesity population group and to assess the optimum dose of amlodipine in the paediatric obesity population using virtual pharmacokinetic studies. A workflow model with four stages was applied for this study (Figure 4.1).

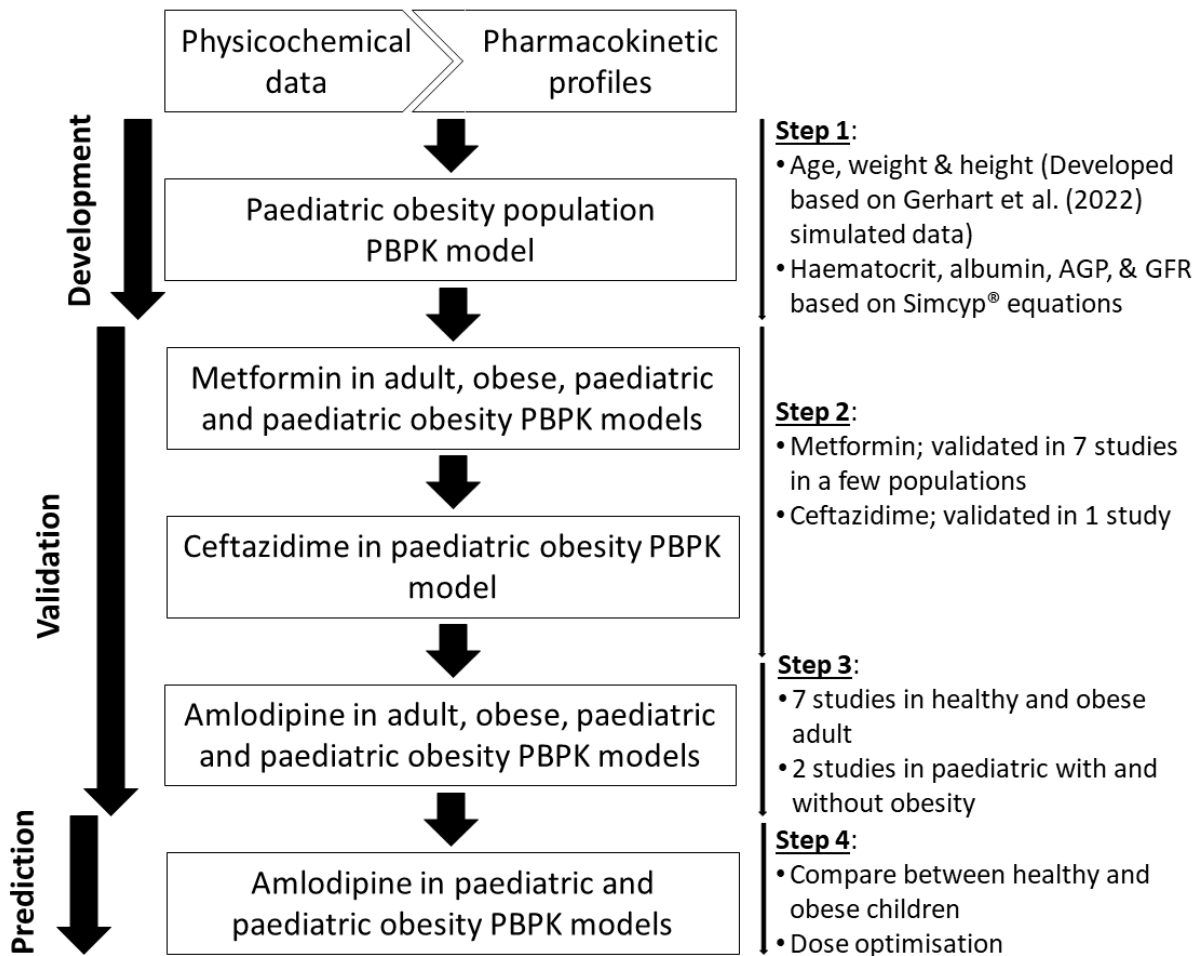


Figure 4.1 A 4-stage workflow was implemented to develop, verify, and explore the amlodipine dose in the paediatric population [156]. AGP, α 1-acid glycoprotein; GFR, glomerular filtration rate.

4.2.1 Step 1: Development of the paediatric obesity population

For the development of the model, this study focused on six physiological parameters that have been reported to change in obese children when compared to non-obese children, namely: (1) weight, (2) height, (3) haematocrit, (4) serum albumin, (5) AGP, and (6) estimated glomerular filtration rate (eGFR). Published data shared by the Gerhart group was used as the primary reference to develop the population group, particularly the simulated age, weight, and height [156].

4.2.1.1 Age, weight and height relationship

The weight, height, and age correlations for paediatric obesity published by the WHO [152] and CDC [153] were the primary guidance in constructing the weight-age, height-age, and weight-height relationship for the paediatric obesity population. The definition by the WHO and CDC was used to develop weight curves. Furthermore, the curve based on the paediatric obesity population developed by Gerhart et al. (2022) [156] was refined.

According to the WHO, the definition of obese for 0 to 5 years old is +3 of SDs from the median line of the BMI-for-age and weight-for-height curves, while for 5 to 18 years old, obese is defined as BMI above +2 of SDs from the median line of the BMI-for-age curve [152, 354, 355]. As for the CDC, child obesity is defined as a BMI range above the 95th percentile or greater based on the BMI-for-age curve [153, 356]. Additionally, the 95th percentile of weight-for-length data published by the CDC for 0 to 5 years old was used to validate the simulated weight-for-height curve [357].

4.2.1.2 Haematocrit-Age relationship

Reported changes in haematocrit are conflicting within the literature. Several publications reported no significant difference between healthy and obese children as well as between genders [156, 358-360], whilst others contradict these findings [361, 362]. Furthermore, a study by Belo et al. (2014) [363] reported significant differences between genders as well as obese and non-obese paediatric for males but not for females. Considering all these reports, no additional change was made to the haematocrit in paediatric obesity.

4.2.1.3 Protein binding-to-age relationship

No significant difference was reported in serum albumin value between paediatrics with and without obesity by several publications [156, 157, 364-366] except for two studies by

Marginean et al. published in 2014 and 2016 [367, 368]. Furthermore, no specific correlation has been reported in terms of the albumin-to-age relationship [156]. Similarly, a significant difference in AGP was reported between obese and non-obese children as well as between genders by Sobieska et al. (2013) [369], Gibson et al. (2014) [370], and Ferrari et al. (2015) [371], but not by Gerhart et al. (2022) [156]. Since conflicting results were reported in both albumin and AGP, the default equations in Simcyp® for both albumin and AGP in paediatric were utilised for simulation and compared to all published data.

4.2.1.4 Glomerular filtration rate (GFR)-to-age relationship

The GFR is an established measure of renal function. The GFR values for paediatric obesity were reported in three publications, namely, Duzova et al. (2013) [372], Goknar et al. (2015) [347], and Correia-Costa et al. (2016) [160], which were used to validate the predicted GFR from the model.

4.2.2 Step 2: Validation of a paediatric obesity population with metformin and ceftazidime compound files

4.2.2.1 Step 2.1: Validation with metformin

A previously developed and fully validated metformin compound file has been reported in the literature and incorporated into the Simcyp® compound library [373]. The compound was utilised in the paediatric obesity model with some adaptations, namely the fraction of dose absorbed (f_a) and V_{ss} parameters (Table 4.1). A revised f_a was fitted based on several publications [374, 375]. The V_{ss} was estimated using the Rodgers and Rowland approach [60, 196]. The estimated V_{ss} value correlates with several published studies [374, 376].

Table 4.1 Metformin compound parameters used for validation studies

Parameters	Values	Notes
Physical chemistry and blood binding		
Compound type	Monoprotic base	
Molecular weight (g/mol)	129.16	
Log P	-1.43	
pKa 1	11.8	
f_u	1	
B/P	1	
Absorption		
Model	1 st order	

fa	0.45	Fitted based on reported values [374, 375].
ka (1/h)	0.27	
Lag time (h)	0.29	

Distribution

Model	Full PBPK	
V_{ss} (L/kg)	1.0172	Predicted using the Rodgers and Rowland method [60, 196].
Kp scalar	1	Fitted based on observed profiles [374, 377].

Elimination (Enzyme kinetics)

Pathway 1	CYP3A4
CL_{int} (μ L/min/pmol – isoform)	0.334
$f_{u_{mic}}$	1
Renal clearance (L/h)	32.3

Drug transport

Pathway 1 (Liver)	SLC22A1 (OCT1)
$CL_{int,T}$ (μ L/min/million – cells)	0.316
$f_{u_{inc}}$	1
RAF/REF	1.84
CL_{PD} (mL/min/million hepatocytes)	0.0000588
Pathway 2 (Kidney)	SLC22A2 (OCT2)
$CL_{int,T}$ (μ L/min/million – cells)	14.21
J_{max}	21084
Km (μ mol)	1483
Pathway 3 (Kidney)	SLC47As (MATEs)
$CL_{int,T}$ (μ L/min/million – cells)	16.64
RAF/REF	0.128
J_{OCT2} (pmol/min/millivolt/million cells)	1.155

Log P, partition coefficient; B/P, blood-to-plasma ratio; f_u , unbound fraction; V_{ss} , steady-state volume of distribution; Kp scalar, tissue partition coefficient; k_a , absorption rate constant; f_a , extent of absorption; CL_{int} , in vitro intrinsic clearance; $f_{u_{mic}}$, fraction of unbound drug in the in vitro microsomal incubation; $CL_{int,T}$, in vitro transporter-mediated intrinsic clearance; $f_{u_{inc}}$, fraction of unbound drug in the in vitro microsomal incubation; RAF/REF, relative activity factor or relative expression factor; CL_{PD} , passive diffusion clearance; J_{max} , in vitro maximum rate of trans-porter-mediated efflux or uptake; Km: Michaelis constant; J_{OCT2} , in vitro OCT2 flux per unit of electrochemical gradient.

Since several changes were made to the metformin compound file, the adapted metformin model was verified in healthy adults, obese adults, and paediatric populations, followed by validation of the paediatric obesity population model with the validated metformin model. All the validations were confirmed with observed data from seven studies (Table 4.2). All virtual clinical trial simulations were run with a 10 x 10 design (10 trials with 10 subjects per trial),

where the dosage regimen, age range, and male-to-female ratio were comparable to the published studies (Table 4.2).

Table 4.2 Datasets of Metformin and Ceftazidime used for validation of the paediatric obesity population.

Reference	Subjects	Age (years)	Dose regimen	PK sampling
Metformin				
Healthy adult subjects				
Tucker et al. (1981) [374]	4 males	30 – 36	Single-dose 500 mg - fed state (Oral)	Up to 24 h post-dose
Gusler et al. (2001) [377]	14 (7 males, 8 females)	37.0 ± 7.7	Single-dose 500 mg - fed state (Oral)	Up to 24 h post-dose
Timmins et al. (2005) [378]	15 (9 males, 7 females)	19 – 40	1000 mg twice daily (Oral)	Up to 24 h post-dose at steady-state
Obese adult				
Padwal et al. (2011) [379]	16 (3 males, 13 females) BMI: 40.5 ± 6.9	43.5 ± 11.7	Single-dose 1000 mg - fast state (Oral)	Up to 24 h post-dose
Paediatric subjects				
Sanchez-Infantes et al. (2011) [380]	4 females	9	850 mg once daily - fed state (Oral)	Up to 24 h post-dose at steady-state
Paediatric obesity subjects				
van Rongen et al. (2018) [381]	22 (6 males, 16 females) (5 overweight, 17 obese)	11.1 – 17.5	1000 mg twice daily (Oral)	Up to 8 h post-dose at steady-state
Sam et al. (2017) [382]	28 obese paediatrics	7.7 – 13.5	1000 mg twice daily (Oral)	Up to 12 h post-dose at steady-state
Ceftazidime				
Maharaj et al. (2021) [383]	29 (17 males, 12 females) (82.80% obese)	2.3 – 20.6	Median: 33.8 mg/kg/dose, Lowest – Highest: 16.5 – 92.9 mg/kg/dose, Maximum dose: 2 g/dose (Intravenous every 8 hours)	Post-dose sparse sampling after at least 8 doses)
(years – years), age range; Mean ± SD; BMI, body mass index; h, hour.				

4.2.2.2 Step 2.2: Validation with ceftazidime

A previously published ceftazidime compound (Table 4.3) was further used to validate the paediatric obesity population model [384]. Several publications have previously validated the ceftazidime compound file in healthy adult and paediatric populations [384-387]. Therefore, the validated ceftazidime compound file was used to validate the paediatric obesity population model using sparse ceftazidime concentration data reported by Maharaj et al. (2021) [383] (Table 4.2).

Table 4.3 Ceftazidime compound parameters used for validation and simulation

Parameters	Values	Notes
Physical chemistry and blood binding		
Compound type	Diprotic acid	
Molecular weight (g/mol)	546.58	
Log P	-3.75	
pKa (1/2)	2.43, 2.89	
fu	0.85	
B/P	0.55	
Distribution (Full PBPK)		
V_{ss} (L/kg)	0.22	Predicted using the Rodgers and Rowland method [60, 196].
Kp scalar	1.03	
Elimination		
Renal clearance (L/h)	6	
Additional systemic clearance (L/h)	0.9	

Log P, partition coefficient; B/P, blood-to-plasma ratio; fu, unbound fraction; V_{ss} , steady-state volume of distribution; Kp scalar, tissue partition coefficient

Although the observed pharmacokinetic data did not differentiate between obese and non-obese subjects, most subjects were classified as obese, which justified using the pharmacokinetic data for paediatric obesity population validation. Simulations were conducted on median, highest, and lowest doses with 10 patients x 10 trials study design. The age and male-to-female ratio corresponded to the published data. Virtual paediatric obese subjects administered with more than 2 g/dose in the simulation were excluded from the predicted mean concentration-time profile.

4.2.3 Step 3: Verification with amlodipine

Physiochemical and pharmacokinetic parameters describing the amlodipine model utilised in this study were obtained and adapted from several publications [388-390] (Table 4.4). For the distribution model, a full-body PBPK model was utilised with the V_{ss} , estimated using the Rodgers and Rowland approach based on the tissue partition coefficients (Kp) [60, 196]. The Kp value was predicted by fitting the simulated with the observed plasma concentrations, with the resulting V_{ss} correlating with that published [391].

Table 4.4 Amlodipine compound parameters used in validation and simulation

Parameters	Values	Notes
Physical chemistry and blood binding		
Compound type	Diprotic base	
Molecular weight (g/mol)	408.88	
Log P	3.43	Zhou et al. (2016) [388]
pKa 1	9.40	Zhou et al. (2016) [388]
pKa 2	1.90	Zhou et al. (2016) [388]
fu	0.07	Zhou et al. (2016) [388]
B/P	0.71	Predicted by Simcyp®.
Absorption		
Model	ADAM	Permeability limited model
f_{uGut}	0.20	Mukherjee et al. (2018) [390]
P_{eff} in man (10^{-4} cm/s)	0.289	Predicted by Simcyp® from PSA/HBD.
PSA (\AA^2)	105.50	Zhou et al. (2016) [388]
HBD	3.00	Zhou et al. (2016) [388]
Distribution		
Model	Full PBPK	
V_{ss} (L/kg)	36.12	Predicted using the Rodgers and Rowland method [60, 196].
Kp scalar	22.70	An estimate based on observed data [392].
Elimination (Enzyme kinetics)		
HLM CL_{int} by CYP3A4 ($\mu\text{L}/\text{min}/\text{mg}$ - microsomal)	42.40	Sun et al. (2012) [393]
Additional HIMEI CL_{int} ($\mu\text{L}/\text{min}/\text{mg}$ - microsomal)	22.00	Kadono et al. (2010) [394]
Renal clearance (L/h)	5.77	Rhee et al. (2018) [389]

Log P, partition coefficient; B/P, blood-to-plasma ratio; fu, unbound fraction; ADAM, advance dissolution, absorption and metabolism; P_{eff} , human jejunum effective permeability; PSA, polar surface area; HBD, number of hydrogen bond donors; f_{uGut} , unbound fraction of drug in enterocytes; V_{ss} , steady-state volume of distribution; Kp scalar, tissue partition coefficient; HLM CL_{int} , human liver microsomes in vitro intrinsic clearance; HIMEI CL_{int} , human intestinal microsomes in vitro intrinsic clearance.

The advance dissolution, absorption and metabolism (ADAM) model was used to describe the absorption kinetics of imatinib, as applied by Rhee et al. (2018) [389]. While the ADAM model accounts for formulation-dependent dissolution and absorption, the simulations did not differentiate between formulation types [27]. A single absorption model was applied across all conditions, assuming that formulation differences had minimal impact on systemic pharmacokinetics.

Renal function was determined firstly by scaling kidney weight in adults (~317 g) based on correlations incorporating body weight [395] with glomerular filtration rate calculated using the Cockcroft and Gault equations [395]. Ghobadi et al. (2011) reported that kidney size showed a similar increase in relation to variations in BMI and BSA [124]. Hence, a separate model was not required to be developed for obesity populations, and therefore, paediatric GFR was simulated using the modification of diet in renal disease (MDRD) equation [124].

The intrinsic clearance by CYP3A4 liver enzymes [393] and human intestinal microsome [394], utilised within the model, and all the adapted parameters were validated with observed data from six studies involving healthy adults, one study with obese adults, one study with paediatrics, and one study involving paediatric both with and without obesity (Table 4.5). The virtual clinical trials were run with a design of 10 patients x 10 trials with the dosing regimen, male-to-female ratio, and age range corresponding to the published studies. For the obese adult population, simulations were performed with 200 subjects taking amlodipine 5 mg and 10 mg daily for 28 days with a 1:1 ratio, given the publication reported the parameters with limited information on the dose taken by the obese subjects.

For comparison with the observed trough concentration (C_{min}) in the paediatric population [396], virtual trials in the paediatric population matching the demographic of observed data were run at three doses daily for 21 days, with the median (0.15 mg/kg/day), 1st interquartile (0.10 mg/kg/day) and 3rd interquartile (0.22 mg/kg/day). Additionally, the virtual paediatric subjects administered with more than 5 mg/day were filtered out following the maximum daily dose allowed, resulting in 99%, 85%, and 58% of the virtual subjects being included for verification for 0.10, 0.15, and 0.22 mg/kg/day doses, respectively.

For verification in the paediatric obesity population, a study by Flynn et al. (2006) [397], who reported concentration profiles for paediatrics with 43.2% of the children categorised as obese, was utilised. The virtual trials were ran with 20 subjects x 10 trials design with a ratio of 50:50 for the male-to-female and obese-to-non-obese paediatric subjects. The simulations were made with once- and twice-daily doses at three dose levels for 28 days, 0.03 mg/kg/day (minimum), 0.17 mg/kg/day (mean), and 0.77 mg/kg/day (maximum), with the absolute doses of 1.3 mg/day and 20 mg/day. With the cap, the percentage of simulated obese children

included for amlodipine model verification in once-daily and twice-daily dosing was 50.73% and 50.86%, respectively.

Table 4.5 Validation datasets used for verification of the amlodipine model

Reference	Subjects	Age (years)	Dose regimen	PK sampling duration
Healthy subjects				
Faulkner et al. (1986) [398]	Single-dose: 12 healthy males Multiple-dose: 56 healthy males	Single-dose: 25.8 ± 3.8 , Multiple-dose: 26.1 ± 3.6	Single-dose fasting: 10 mg intravenous (1 mg/min) in period 1, 34 days washout period, 10 mg oral dose (2 x 5 mg capsule). Multiple-dose: 15 mg once daily (3 x 5 mg capsule) or placebo for 14 days	Single-dose: Up to 144 h post-dose Multiple-dose: Day 1 -up to 24 h post-dose, Day 7: pre-dose and up to 14 h post-dose, Day 14: up to 168 h post-dose
Williams et al. (1998) [392]	12 healthy males	23 – 34	2.5 mg single-dose 5 mg single-dose 10 mg single-dose With 14 days washout period between each dose	Up to 144 h post-dose
Abernethy et al. (1990) [391]	13 patients with hypertension (10 males, 3 females)	28 – 45	1 st dose of 10 mg intravenously, after day 4 of the intravenous dose followed by 2.5 mg oral once daily for 10 days	After 10 days of amlodipine dose, up to 24 h post-dose
Bainbridge et al. (1993) [399]	12 healthy subjects (7 males, 5 females)	46 – 76	5 mg oral once daily for 14 days	Up to 48 h post-dose after the 1 st dose and after the last dose at 14 days
Rausl et al. (2006) [400]	24 healthy subjects	Adult	10 mg oral once	Up to 72 h post-dose
Leenen et al. (2010) [401]	28 patients with hypertension (10 males, 18 females) BMI = 30.6 ± 1.3	22 – 50	5 mg oral once daily for 8 weeks	After the 1 st dose, up to 24 h post-dose After the last dose, up to 240 h
Obese subjects				
Varga et al. (2015) [402]	22 hypertensive patients: - 4 normal - 6 overweight - 12 obese - 27.3% male	16 adults (<65 years old with majority 50 – 60 years old) 6 elderly (≥ 65 years old)	Fixed dose combination of telmisartan and amlodipine once daily: 40/5 mg – 8 subjects 80/5 mg – 6 subjects 80/10 mg – 8 subjects	Up to 72 h post-dose at steady-state

Paediatric subjects				
Van der Vossen et al. (2020) [396]	9 (6 males, 3 females)	0.5 – 12	0.15 (0.10 – 0.22) ^a mg/kg/day (Oral solution)	Sparse trough concentrations
Mixture of paediatric with and without obesity				
Flynn et al. (2006) [397]	73 (49 males, 24 females) - 43.2% obese children	1.0 – 17.7	0.17 ± 0.13 (0.03 – 0.77) mg/kg/day - Absolute dose: 1.3 – 20 mg/day - Administered either once or twice daily (Tablet and suspension)	Sparse samples

^aMedian (range); IV, intravenous; h, hour.

4.2.4 Step 4: Influence of obesity on amlodipine pharmacokinetic parameters and dose adjustment in the paediatric obesity population

Following validation in the paediatric obesity population, the impact of obesity on the pharmacokinetic and plasma concentrations of amlodipine were explored. A design of 10 patients x 10 trials at three different age groups in paediatrics, both with and without obesity populations, was set as follows: i) 2 to 6 years old, ii) 6.01 to 12 years old, and iii) 12.01 to 18 years old.

Each group was dosed with amlodipine at a dose of 2.5 mg, 5 mg, and 10 mg once daily for three weeks, except for group 1 (2 to 6 years old), in which the virtual subjects were simulated to be administered 0.20 mg/kg daily and 2.5 mg once daily for every three weeks. The dose selection for simulation was based on the recommended minimum and maximum dose for children based on age group. In the 2 to 6 years old group, the doses selected were the maximum starting dose for the weight-based dose and for the 6 years old and above group, it was the minimum dose for the fixed dose [403, 404].

In order to assess the need for dose adjustment, the amlodipine therapeutic window of 1 ng/mL to 57.2 ng/mL and the toxic level of 67 ng/mL were used as a general guide to ensure the adjusted doses yield concentrations within the safe window [397, 405-407]. To simulate the amlodipine peak concentrations at a steady-state (C_{maxss}), virtual clinical trials in paediatric obesity were performed with a 10 x 10 design for age groups: i) 2 to 4 years old, ii) 4.01 to 6 years old, iii) 6.01 to 8 years old, iv) 8.01 to 10 years old, v) 10.01 to 12 years old, vi) 12.01 – 14 years old, vii) 14.01 to 16 years old, and viii) 16.01 to 18 years old.

In each virtual clinical trial, amlodipine was administered over two-week periods at varying fixed doses starting from 2.5 to 10 mg daily. In addition, for the age group from 2 to 12 years

old, simulated weight-based dosages ranging from 0.10 mg/kg to 0.40 mg/kg per day were performed. The primary objective was to attain a comparable simulated C_{\max} at steady-state in healthy paediatrics administered with fixed daily doses of 2.5 mg and 5 mg alongside weight-based doses of 0.10 mg/kg and 0.40 mg/kg.

The simulated minimum and maximum dose ranges selected for the simulation were based on the British National Formulary for Children (BNFc) and amlodipine product insert [403, 404].

4.2.5 Prediction performance

For the validation of all the simulated physiological parameters, a visual predictive checking (VPC) strategy was adopted to validate the predicted values. The method was explained at the 2012 United States Food and Drug Administration Paediatric Advisory Committee [221] and was widely used to develop population models [408, 409]. Validation using the VPC approach was carried out by presenting the predicted and observed values with mean and SD graphically in the same graph. Most observed data points should overlap with the simulated values to be considered acceptable. As for the pharmacokinetics profile predictions, the VPC strategy and two-fold (0.5 – two-fold) predicted/observed ratio rules were used to represent the predictive performance as 'optimal' unless otherwise explained [144, 220, 302]. This strategy was used for validation in steps 2 and 3 when comparing the predicted and observed values. As for the VPC, the simulated profiles were considered acceptable when the reported profiles overlapped within the 5th and 95th percentiles of the predicted mean concentration profiles.

4.2.6 Data and statistical analysis

All the population validation and compound data were extracted using WebPlotDigitizer version 4.5 (<https://apps.automeris.io/wpd/>). Statistical analysis was performed using a nonparametric, unpaired Student's *t*-test to compare the simulated amlodipine pharmacokinetic parameters between healthy and obese children in step 4. The significance test was performed with $p < 0.05$. The statistical analysis was run using GraphPad Prism Version 8 for Windows (GraphPad Software, La Jolla, CA, USA).

4.3 Results

4.3.1 Step 1: Development of the paediatric obesity population

The relevant published data for all physiological parameters, including height, weight, haematocrit, serum albumin, AGP, and GFR, were within the range of individual prediction values, which validated the paediatric obesity population. The results are detailed in '4.6 Supplementary materials'.

4.3.2 Step 2: Validation of the paediatric obesity population

4.3.2.1 Step 2.1: Validation with metformin

All predicted pharmacokinetic parameters, namely, maximum concentration (C_{max}), C_{maxss} , area-under-the-curve-to-time (AUC_{0-t}), area-under-the-curve-to-time-at-steady-state (AUC_{0-tss}), time to reach maximum concentration (T_{max}), and oral clearance (CL/F), were within 0.75- to 1.5-fold of the observed parameters reported in publications (Table 4.6). In addition, the BMI (kg/m^2) distribution for the simulated obese adult population was comparable with the observed study population (40.5 ± 6.9 vs 39.5 ± 5.13) [379].

Moreover, the observed profiles from all studies listed in Table 4.2 agree with the simulated profile based on the VPC acceptance criteria, where the published profiles fit within the 5th and 95th percentiles of the predicted plasma-concentration profile, thereby confirming the adaptation of the metformin model (Figure 4.2A-D). As for the paediatric obesity plasma concentration profiles, the individual-reported plasma concentration profiles of metformin for both published multiple-dose studies were centred around the mean simulated metformin plasma concentration (Figure 4.2E-F).

Table 4.6 Observed versus predicted pharmacokinetic parameters for metformin

Study	Dosing	PK parameters	Observed	Predicted	Predicted/ Observed
Healthy adults					
Tucker et al. (1981) [374]	500 mg once	C _{max} (µg/L)	1.02 ± 0.34	0.78 ± 0.28	0.77
		AUC ₀₋₂₄ (hr.µg/mL)	6.71 ± 1.82	6.70 ± 2.16	1.00
		T _{max} (h)	2.20 ± 0.30	2.62 ± 0.70	1.19
Gusler et al. (2001) [377]	500 mg once	C _{max} (ng/mL)	741.00 ± 175.00	782.22 ± 277.48	1.06
		AUC ₀₋₂₄ (h.ng/mL)	5330.00 ± 1400.00	6696.68 ± 2158.24	1.25
		T _{max} (h)	3.50 ± 0.70	2.62 ± 0.70	0.75
Timmins et al. (2005) [378]	1000 mg twice daily	C _{maxss} (ng/mL)	1321.00 ± 234.00	1898.97 ± 630.13	1.44
		AUC _{0-24ss} (h.ng/mL)	20544.00 ± 4445.00	28806.57 ± 9843.03	1.40
		T _{max} (h)	3.00 (1.50 – 6.00)	2.32 (1.35 – 3.45)	0.77
Obese adults					
Padwal et al. (2011) [379]	1000 mg once	C _{max} (µg/mL)	1.80 ± 0.61	1.37 ± 0.49	0.76
		AUC ₀₋₂₄ (h.µg/mL)	11.10 ± 3.60	11.89 ± 4.15	1.07
		T _{max} (h)	3.00 (1.5 – 3.0)	2.75 (1.6 – 4.9)	1.16
Paediatric subjects					
Sanchez-Infantes et al. (2011) [380]	850 mg once daily	C _{maxss} (mg/L)	3.10 ± 0.30	3.40 ± 1.12	1.10
		AUC _{0-12ss} (h.mg/L)	21.20 ± 1.50	24.18 ± 9.40	1.14
		T _{max} (h)	2.40 ± 0.20	2.78 ± 0.56	1.16
Paediatric obesity subjects					
van Rongen et al. (2018) [381]	1000 mg twice daily	C _{maxss} (mg/L)	2.80 ± 0.98	2.44 ± 1.06	0.87
		AUC _{0-12ss} (h.mg/L)	14.30 ± 5.00	18.64 ± 9.87	1.30
		CL/F (mL/min)	1007.00 ± 326.00	1108.83 ± 524.17	1.10
Sam et al. (2017) [382]	1000 mg twice daily	C _{maxss} (mg/L)	1.80 (0.79 – 3.45)	1.64 (0.68 – 4.95)	0.91
		AUC _{0-8ss} (hr.mg/L)	10.06 (4.78 – 18.66)	10.13 (3.59 – 33.83)	1.01
		T _{max} (h)	2.00 (1.00 – 4.00)	2.50 (1.40 – 3.55)	1.25

Mean ± SD; Median (range); C_{max}, maximum concentration; AUC_{0-t}, area-under-the-curve to the last time point; T_{max}, time to maximum concentration; AUC_{0-tss}, area-under-the-curve to time at steady-state; C_{maxss}, maximum concentration at steady-state; CL/F, oral clearance; h, hour.

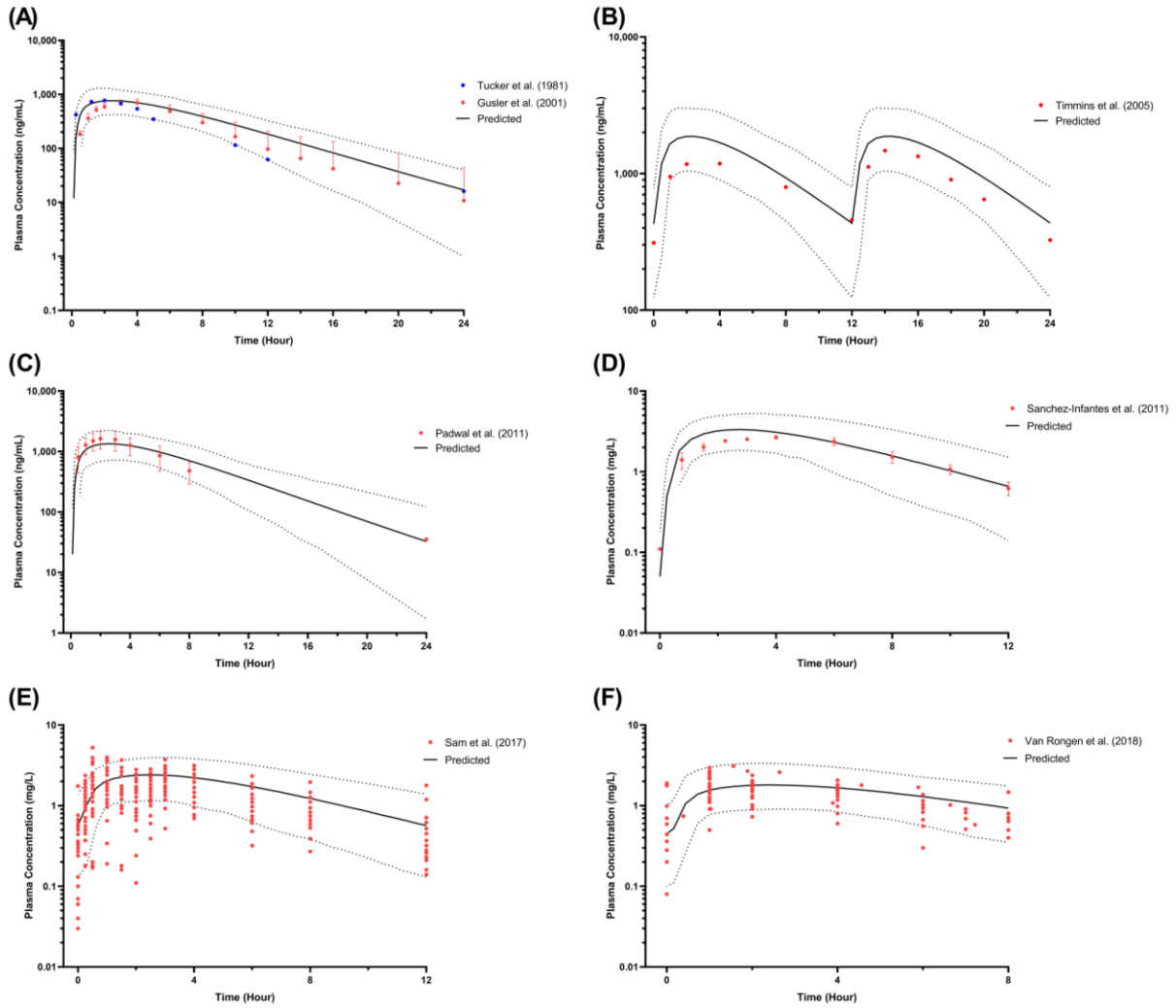


Figure 4.2 Simulated metformin plasma concentration in healthy adults (A-B), obese adults (C), paediatric (D), and paediatric obesity (E-F).

(A) Single-dose 500 mg in healthy adults [374],[377]; (B) Multiple-dose 1000 mg twice daily in healthy adults [378]; (C) Single-dose 1000 mg in obese adults [379]; (D) Multiple-dose 850 mg once daily in paediatric population [380]; (E) Multiple-dose 1000 mg twice daily in paediatric obesity to match Sam et al. (2017) [382] subjects' demographic; (F) Multiple-dose 1000 mg twice daily in paediatric obesity to match Van Rongen et al. (2018) [381] subjects' demographic; Solid lines represent the predicted mean concentration-time profile, with dotted lines representing the 5th and 95th percentile ranges; Solid circles represent individual observed data from each study. Solid circles with error bars represent the mean and SD of the observed data from each study.

4.3.2.2 Step 2.2: Validation with ceftazidime

Furthermore, the paediatric obesity population was validated with the ceftazidime compound model and plasma concentration data published by Maharaj et al. (2021) [383]. Following filtering virtual subjects administered with more than 2 g/dose, the percentages of virtual subjects used for the simulated mean concentration-time profile for 16.5 mg/kg q8h, 33.8 mg/kg q8h, and 92.9mg/kg q8h are 100%, 53% and 4%, respectively.

Considering only the sparse plasma concentration of ceftazidime available for validation of the paediatric obese population, only VPC method was used as acceptance criteria, where a majority (84%) of the observed concentration data fell within the 5th and 95th percentile of the simulated concentration profile (Figure 4.3). Furthermore, the percentage of concentrations within the acceptance limit was comparable with the number of obese subjects recruited in the study (84.00% vs. 82.80%), thus verifying the paediatric obesity population model.

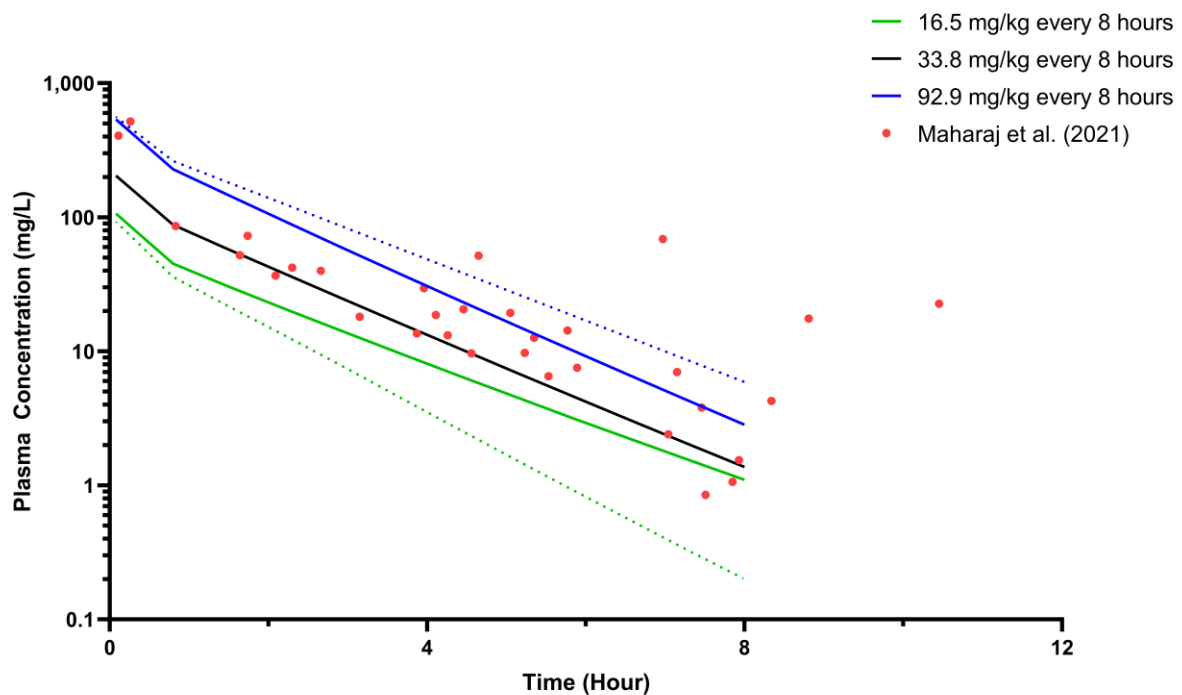


Figure 4.3 Simulated steady-state plasma concentration of ceftazidime for the paediatric population. Solid lines represent the predicted mean concentration-time profile, with dotted lines representing the 5th and 95th percentile ranges. Solid circles represent the mean of the observed clinical data from Maharaj et al. (2021) [383].

4.3.3 Step 3: Verification of the amlodipine model

Predicted pharmacokinetic parameters for adults and obese adults in single and multiple-dose studies, including C_{max} , AUC_{0-t} , AUC_{0-inf} , C_{maxss} , AUC_{0-tss} , area-under-the-curve to infinity at steady-state ($AUC_{0-infss}$), and T_{max} , were within 0.5 – two-fold of the reported data except for $AUC_{0-infss}$ for multiple dose study by Bainbridge et al. (1993) [399] (Table 4.7). Since only pharmacokinetic parameters were revealed for the obese adult population, verification of the amlodipine model in obese adults was based on the comparison between predicted and observed parameters.

Table 4.7 Observed and predicted amlodipine pharmacokinetic parameters in adult

Study	Dosing	PK parameters	Observed	Predicted	Predicted/ Observed	
Adult populations						
Faulkner et al. (1986) [398]	Single-dose 10 mg IV	AUC_{0-inf} (h.ng/mL)	371.00 ± 69.00	668.60 ± 197.38	1.80	
		Single-dose 10 mg oral	C_{max} (ng/mL)	5.90 ± 1.20	6.10 ± 2.45	1.03
			AUC_{0-inf} (h.ng/mL)	238.00 ± 53.00	373.21 ± 132.47	1.57
	T_{max} (h)		7.60 ± 1.80	5.06 ± 0.93	0.67	
	15 mg oral daily for 14 days	Day 1: C_{max} (ng/mL)	6.90 ± 2.60	6.92 ± 1.60	1.00	
		Day 1: C_{min} (ng/mL)	3.30 ± 1.20	3.36 ± 0.90	1.02	
		Day 1: T_{max} (h)	8.90 ± 3.70	5.50 ± 0.79	0.62	
		Day 14: C_{max} (ng/mL)	18.10 ± 7.10	23.55 ± 7.09	1.30	
		Day 14: C_{min} (ng/mL)	11.80 ± 5.30	8.17 ± 3.93	0.69	
		Day 14: T_{max} (h)	8.70 ± 1.90	4.92 ± 0.60	0.57	
Williams et al. (1998) [392]	Single-dose 2.5 mg	C_{max} (ng/mL)	1.20	1.52 ± 0.61	1.27	
		AUC_{0-72} (hr.ng/mL)	41.00	46.51 ± 17.13	1.13	
		T_{max} (h)	5.40	5.06 ± 0.93	0.94	
	Single-dose 5 mg	C_{max} (ng/mL)	2.66	3.05 ± 1.23	1.15	
		AUC_{0-72} (h.ng/mL)	94.00	93.10 ± 34.30	0.99	
		T_{max} (h)	6.30	5.06 ± 0.93	0.80	
	Single-dose 10 mg	C_{max} (ng/mL)	5.49	6.10 ± 2.45	1.11	
		AUC_{0-72} (h.ng/mL)	200.00	186.52 ± 68.78	0.93	
		T_{max} (h)	6.4	5.06 ± 0.93	0.79	
Abernethy et al. (1990) [391]	2.5 mg once daily	C_{maxss} (ng/mL)	4.20 ± 1.10	3.90 ± 1.32	0.93	
		AUC_{0-24ss} (h.ng/mL)	81.00 ± 22.00	77.49 ± 26.36	0.96	
		T_{maxss} (h)	7.00 ± 2.00	4.54 ± 0.72	0.65	

Bainbridge et al. (1993) [399]	Single-dose 5 mg	C_{max} (ng/mL)	3.50 ± 0.80	3.05 ± 1.23	0.87
		AUC_{0-inf} (h.ng/mL)	169.00 ± 53.00	145.60 ± 55.19	0.86
		T_{max} (h)	6.80 ± 1.80	5.06 ± 0.93	0.74
	5 mg once daily for 14 days	C_{maxss} (ng/mL)	10.50 ± 4.40	8.51 ± 2.82	0.81
		$AUC_{0-infss}$ (h.ng/mL)	214.00 ± 78.00	885.10 ± 462.87	4.14
		T_{maxss} (h)	7.00 ± 1.00	4.53 ± 0.71	0.65
Rausl et al. (2006) [400]	Single-dose 10 mg	C_{max} (ng/mL)	4.30 ± 0.90	6.10 ± 2.45	1.42
		AUC_{0-72} (h.ng/mL)	163.00	186.52 ± 68.78	1.14
		T_{max} (h) ^a	7.00 (5.00 – 12.00)	4.98 (2.85 – 7.40)	0.71
Leenen et al. (2010) [401]	Single-dose 5 mg	C_{max} (ng/mL)	2.40 ± 0.20	3.05 ± 1.23	1.27
		AUC_{0-24} (h.ng/mL)	42.00 ± 3.40	49.54 ± 18.60	1.18
		T_{max} (h)	6.90 ± 0.60	5.06 ± 0.93	0.73
	5 mg once daily for 8 weeks	C_{maxss} (ng/mL)	8.10 ± 0.60	9.52 ± 3.25	1.18
		AUC_{0-24ss} (h.ng/mL)	162.90 ± 13.80	194.63 ± 71.84	1.20
		$AUC_{0-240ss}$ (h.ng/mL)	594.50 ± 58.20	949.43 ± 519.01	1.60
	T_{maxss} (h)	6.40 ± 0.60	4.48 ± 0.69	0.70	
Obese adult					
Varga et al. (2015) [402]	5 mg daily 10 mg daily	C_{maxss} (ng/mL)	24.88 ± 13.87	14.75 ± 6.68	0.59
		AUC_{0-72ss} (h.ng/mL)	1176.38 ± 704.86	794.80 ± 383.20	0.68
		$AUC_{0-infss}$ (h.ng/mL)	2387.34 ± 1705.50	2270.93 ± 1474.58	0.95
		T_{max} (h)	5.33 ± 1.97	5.01 ± 0.76	0.94

^aMedian (range); IV, intravenous; C_{max} , maximum concentration; AUC_{0-t} , area-under-the-curve to the last time point; T_{max} , time to maximum concentration; AUC_{0-tss} , area-under-the-curve to time at steady-state; C_{maxss} , maximum concentration at steady-state; T_{maxss} , time to maximum concentration at steady-state.

Observed plasma concentrations for both single-dose and multiple-dose studies in adults concurred with the simulated profiles and fit within the 5th and 95th percentiles (Figure 4.4 and Figure 4.5). Among the 12 observed profiles, only two fell outside the defined acceptance range at the elimination phase, precisely the last three points. These instances were associated with amlodipine administered intravenously at 10 mg single dose (Figure 4.4A) and orally at 15 mg daily for 14 days (Figure 4.5C). In addition, the profiles at steady-state were under-predicted and over-predicted when simulated with once-daily doses of 5 mg and 15 mg for 14 days, respectively (Figure 4.5B and Figure 4.5C).

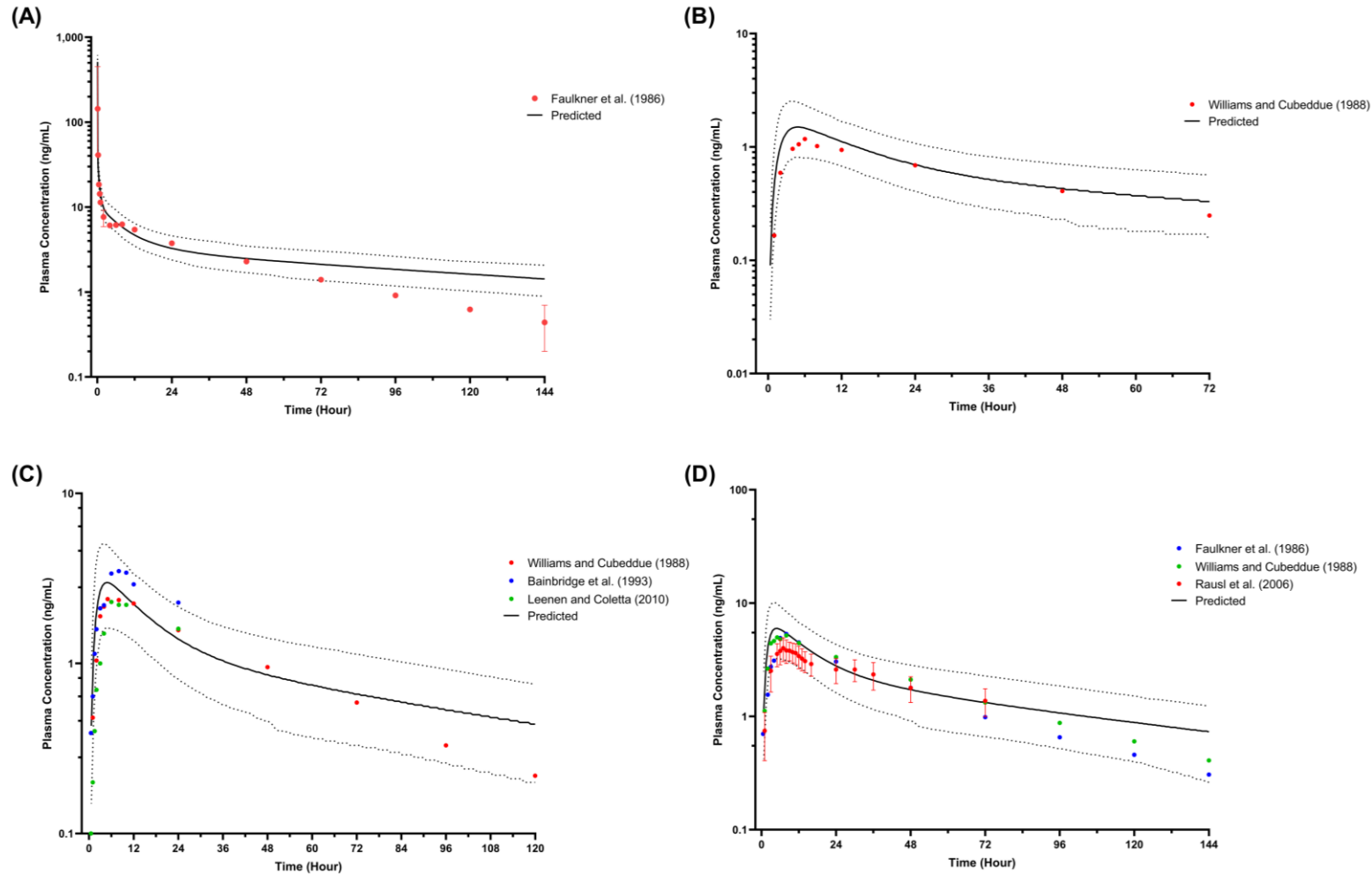


Figure 4.4 Simulated plasma concentration of amlodipine single-dose in healthy adults.

(A) 10 mg intravenous single-dose [398]; (B) 2.5 mg oral single-dose [392]; (C) 5 mg oral single-dose [392], [399], [401]; (D) 10 mg oral single-dose [398], [392], [400]. Solid lines represent the predicted mean concentration-time profile, with dotted lines representing the 5th and 95th percentile ranges. Solid circles represent observed clinical data from each study. Solid circles with error bars represent the mean and range for Faulkner et al. (1986) [398] and the mean and SD of the observed clinical data for Rausl et al. (2006) [400].

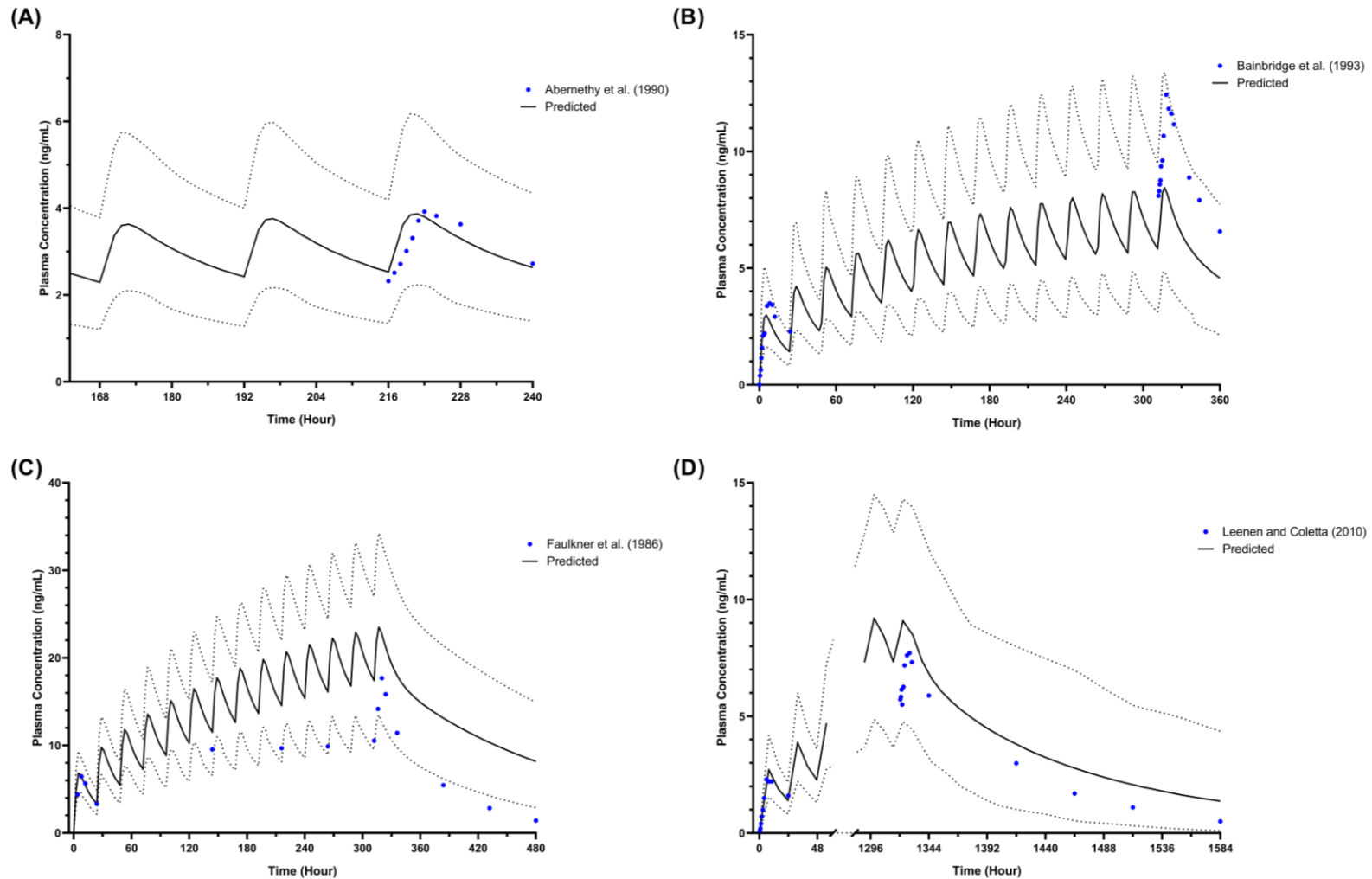


Figure 4.5 Simulated plasma concentration of amlodipine multiple-dose in healthy adults.

(A) 2.5 mg daily for 14 days [391]; (B) 5 mg daily for 14 days [399]; (C) 15 mg daily for 14 days [398]; (D) 5 mg daily for 8 weeks [401]. Solid lines represent the predicted mean concentration-time profile, with dotted lines representing the 5th and 95th percentile ranges. Solid circles represent observed clinical data from each study.

For simulations of paediatric C_{min} , the predicted amlodipine residual concentrations are well within the range of observed amlodipine residual concentrations, with four observed samples above the highest predicted C_{min} (Figure 4.6).

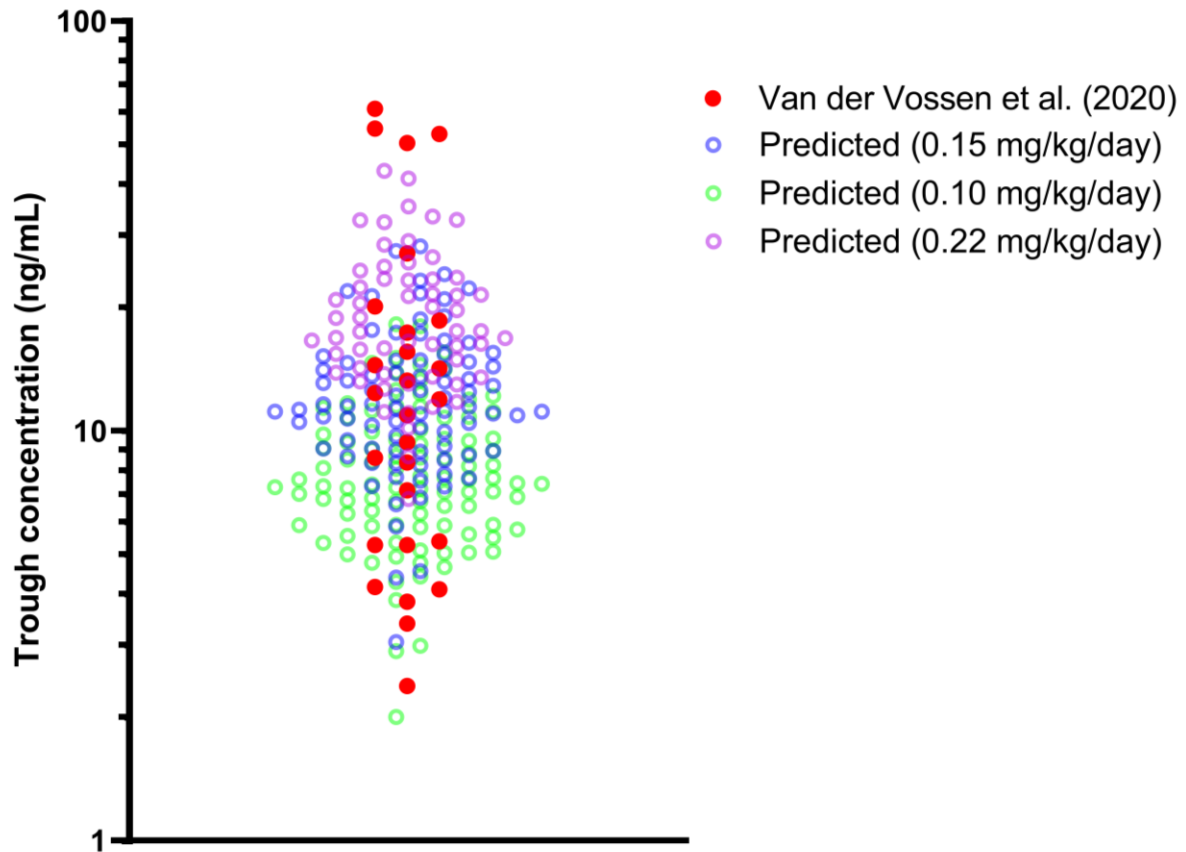


Figure 4.6 Simulated steady-state trough concentration (C_{min}) of amlodipine multiple-dose in the paediatric population.

Solid red circles represent the observed trough concentration of amlodipine published by Van der Vossen et al. (2020) [396]. Coloured open circles represent predicted trough concentration for three doses: 0.15 mg/kg/day, 0.10 mg/kg/day and 0.22 mg/kg/day.

Verification of the amlodipine model in the paediatric obesity populations showed that all the observed plasma concentrations overlapped within the 5th and 95th percentiles of the minimum and maximum daily doses, except for six observed concentrations in the once-daily dose profile (Figure 4.7). Moreover, most observed plasma concentrations spread around the simulated mean dose plasma concentration profiles (Figure 4.7), thus validating the amlodipine model in obese children.

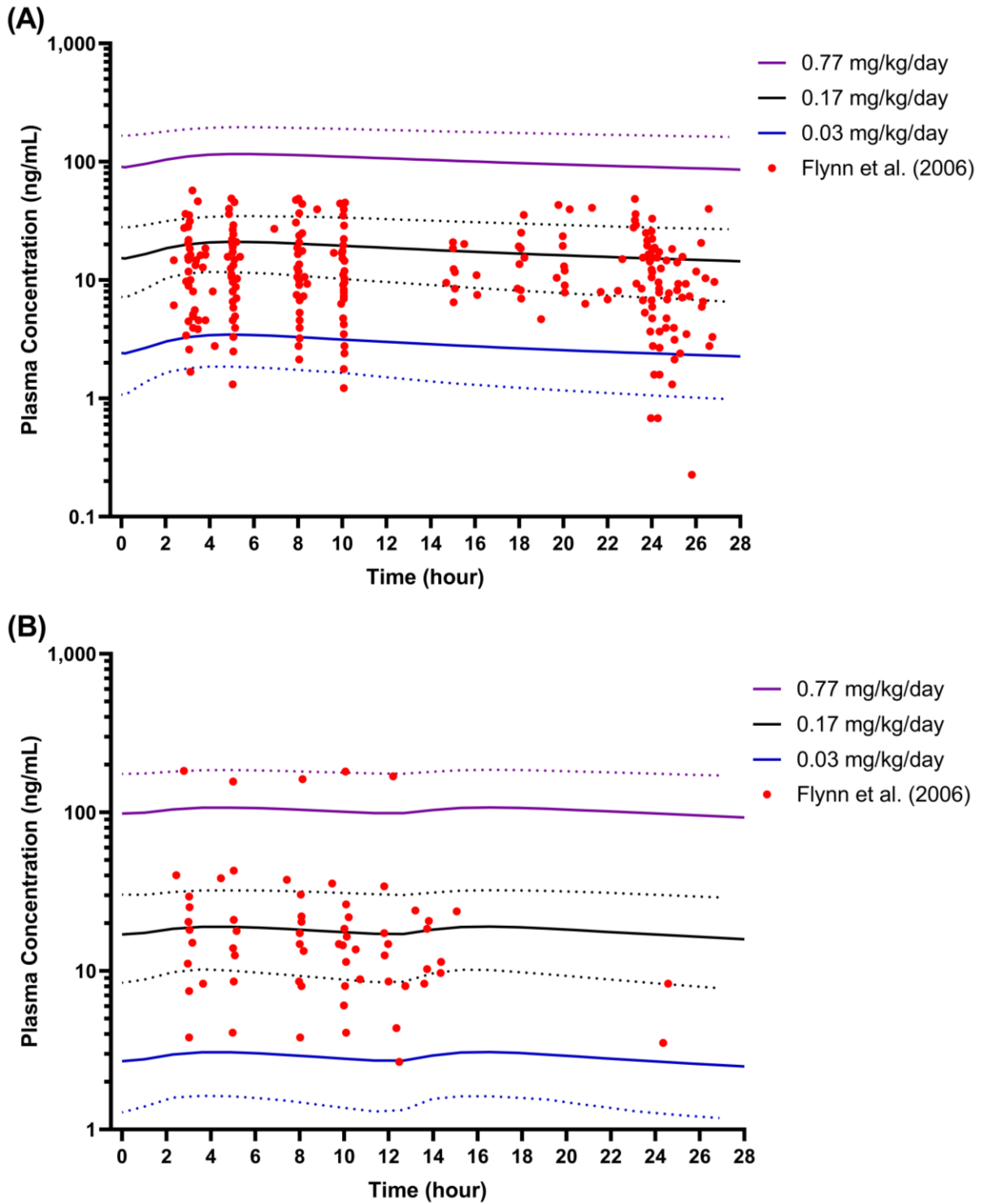


Figure 4.7 Simulated plasma concentration of amlodipine in paediatric with and without obesity.

(A) Once daily dose at steady-state; (B) Twice daily dose at steady-state; Solid lines represent the predicted mean concentration-time profile, with dotted lines representing the 5th and 95th percentile ranges. Solid circles represent observed plasma concentrations from Flynn et al. (2006) [397]

4.3.4 Step 4: Impact of paediatric obesity on amlodipine pharmacokinetics

4.3.4.1 Comparison of non-obese and obese paediatrics

An approximately two-fold decrease was observed in the simulated steady-state plasma concentration profiles (Figure 4.8), AUC and C_{max} (Figure 4.9) as the age group increased. Compared to the non-obese children, the AUC and C_{max} of obese children decreased by 35.30% and 20.49%, respectively (Figure 4.9). Additionally, the comparison of AUC and C_{max} showed a statistically significant difference between obese and non-obese paediatrics for all age groups when administered amlodipine as a fixed dose (Figure 4.9). In contrast, the difference was insignificant when amlodipine was dosed based on TBW in the 2 to 6 years old age group (Figure 4.9). For comparison of clearance and V_{ss} , statistically significant differences were noted for both fixed and weight-based dose regimens as well as all age groups (Figure S 4-9).

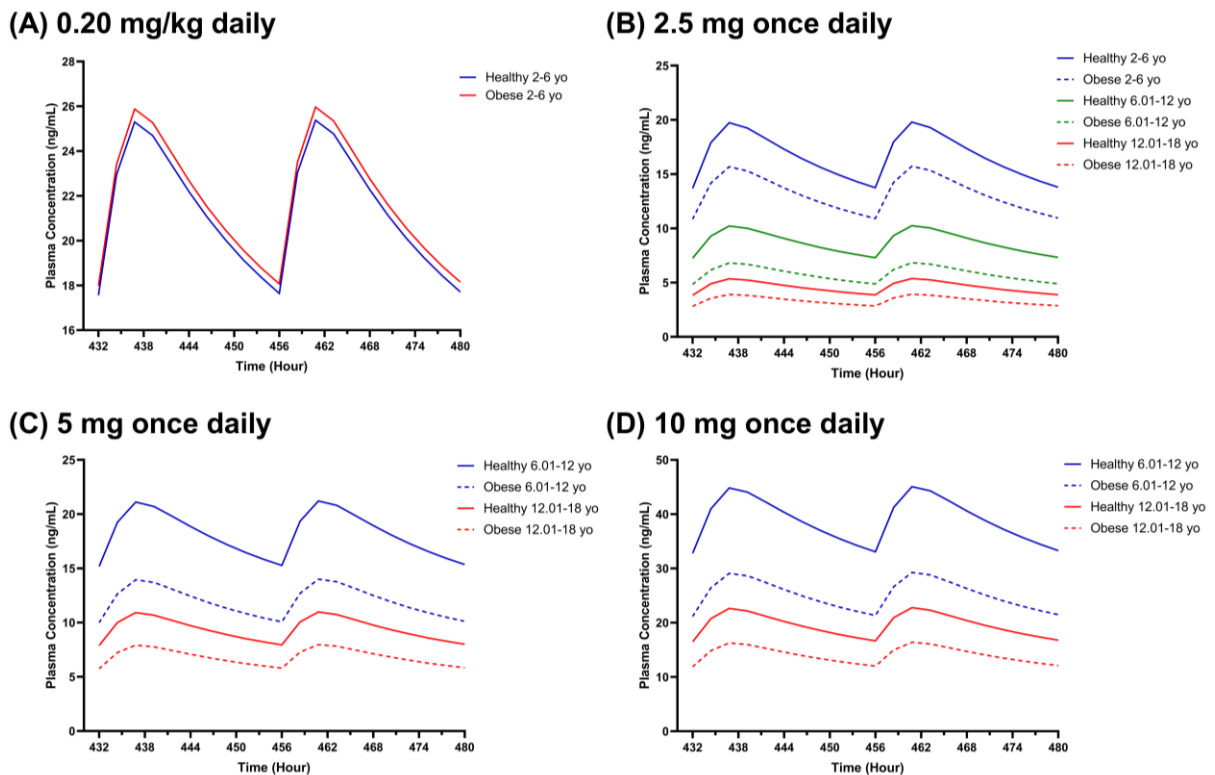


Figure 4.8 Simulated steady-state amlodipine plasma concentration profiles in healthy and obese children for age groups of 2 to 6 years old, 6.01 to 12 years old and 12.01 to 18 years old.

(A) 0.20 mg/kg daily; (B) 2.5 mg once daily; (C) 5 mg once daily; (D) 10 mg once daily. In graph (A), different colours represent paediatric with and without obesity in the 2 to 6 age group. The dotted lines in the (B), (C), and (D) graphs represent obese paediatric populations. Different coloured lines in the (B), (C) and (D) profiles represent different age groups.

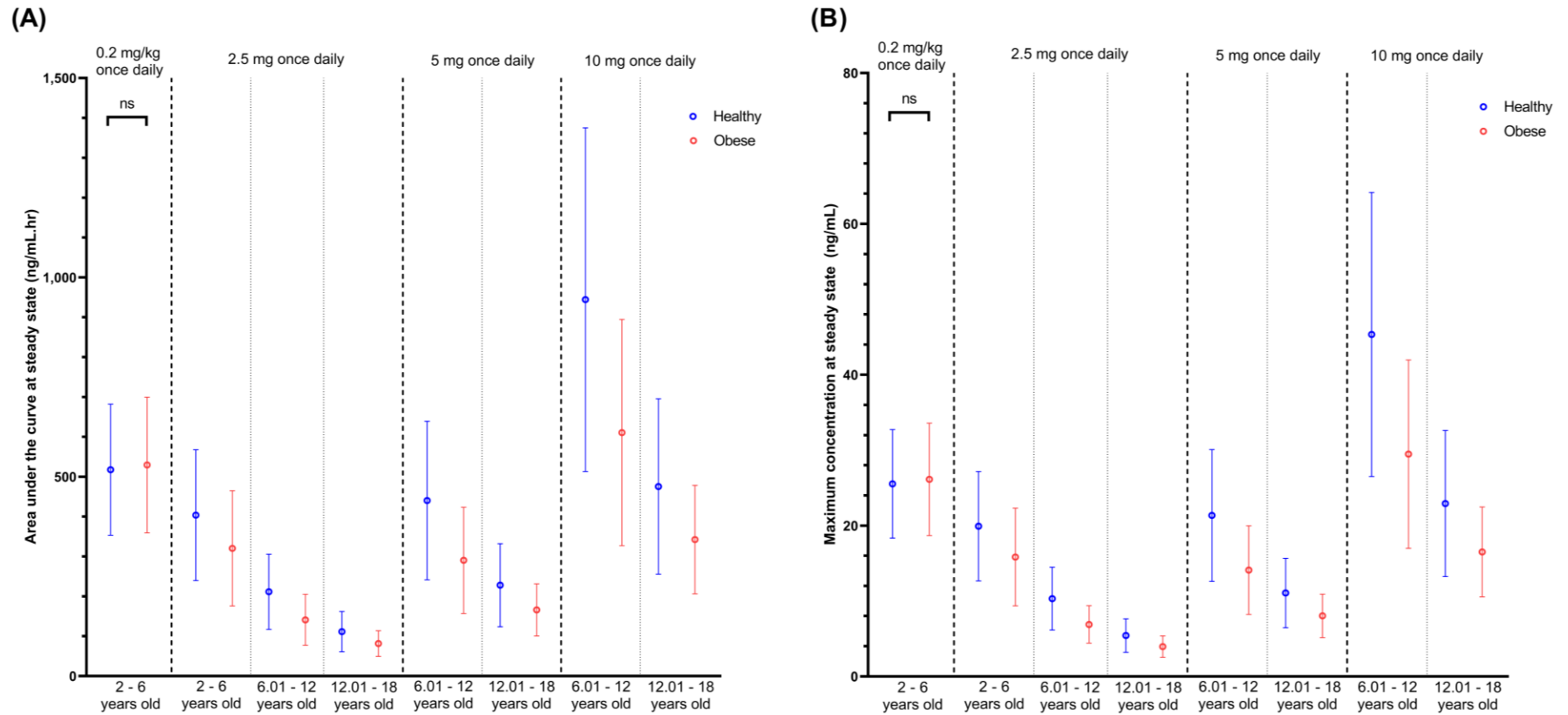


Figure 4.9 Predicted AUC (A) and C_{max} (B) at steady-stated for healthy and obese paediatric for four doses and three different age groups.

The coloured circles represent the mean, and the horizontal lines represent the standard deviations. 'ns', $p > 0.05$.

4.3.4.2 Dose adjustments in paediatric obesity

Simulations showed that weight-based doses resulted in comparable predicted C_{max} in children both with and without obesity populations except for ages 9.01 – 10 years (0.1 mg/kg/day: $p= 0.0453$, 0.4 mg/kg/day: $p= 0.0405$) and 11.01 – 12 years (0.1 mg/kg/day: $p= 0.0380$, 0.4 mg/kg/day: $p= 0.0335$), where the differences were statistically significant (Figure 4.10A). None of the simulated C_{max} values exceeded the maximum therapeutic concentration (57.2 ng/mL) and toxicity level (67 ng/mL) in both populations when dosed with a 0.10 mg/kg amlodipine starting dose (Figure 4.10A). The same was seen for the daily dose, not one simulated subject was administered above the maximum daily dose of 10 mg as recommended by BNFC [403].

In contrast, the maximum dose of 0.40 mg/kg resulted in 7.55% and 1.92% of healthy and obese paediatrics as early as 5.01 – 6 years and 3.01 – 4 years old being dosed above 10 mg daily, respectively. The proportion reached 100% for the age group 7.01 – 8 years old in the paediatric obesity group and more than 90% for the 10.01 – 11 years old group in the non-obese children population (Figure S 4-13 and Figure S 4-14).

For the predicted C_{max} , the percentage that tops the toxicity level (67 ng/mL) was less than 20% for obese children across the age range up to 12 years (Figure S 4-14). On the other hand, for non-obese paediatric, the percentage of C_{max} that exceeded 67 ng/mL was more than 20% in the age group 2 – 4 years (Figure S 4-13). Generally, the number of predicted C_{max} that falls above the maximum therapeutic concentration of 57.2 ng/mL was 28.30% to 38.30% in obese paediatric and 19.15% to 37.50% in non-obese children, depending on the age group (Figure 4.10A).

For fixed-dose simulations, an approximately 1.25 to 1.5 times higher dose is needed in obese children in order to achieve the same C_{max} as non-obese children (Figure 4.10B). A significant difference in C_{max} was seen in the younger age group (2 to 5 years old) even after a 1.5-fold increase in the starting dose in obese children compared to 2.5 mg daily in non-obese paediatric. Another notable difference at the starting dose was seen in the 16 to 17 years old group (Figure 4.10B). As for the maintenance dose of 5 mg daily, the 1.25 to 1.5-fold dose increase in obese paediatrics resulted in comparable C_{max} to the non-obese paediatric populations (Figure 4.10B). A similar trend is seen with higher maintenance doses. The increment was set based on the dose in tablet form available in the market [403]. As for the C_{max} , the lower age group was more at risk of concentrations above the therapeutic and toxicity range than the higher age group in both weight-based and fixed doses (Figure 4.10).

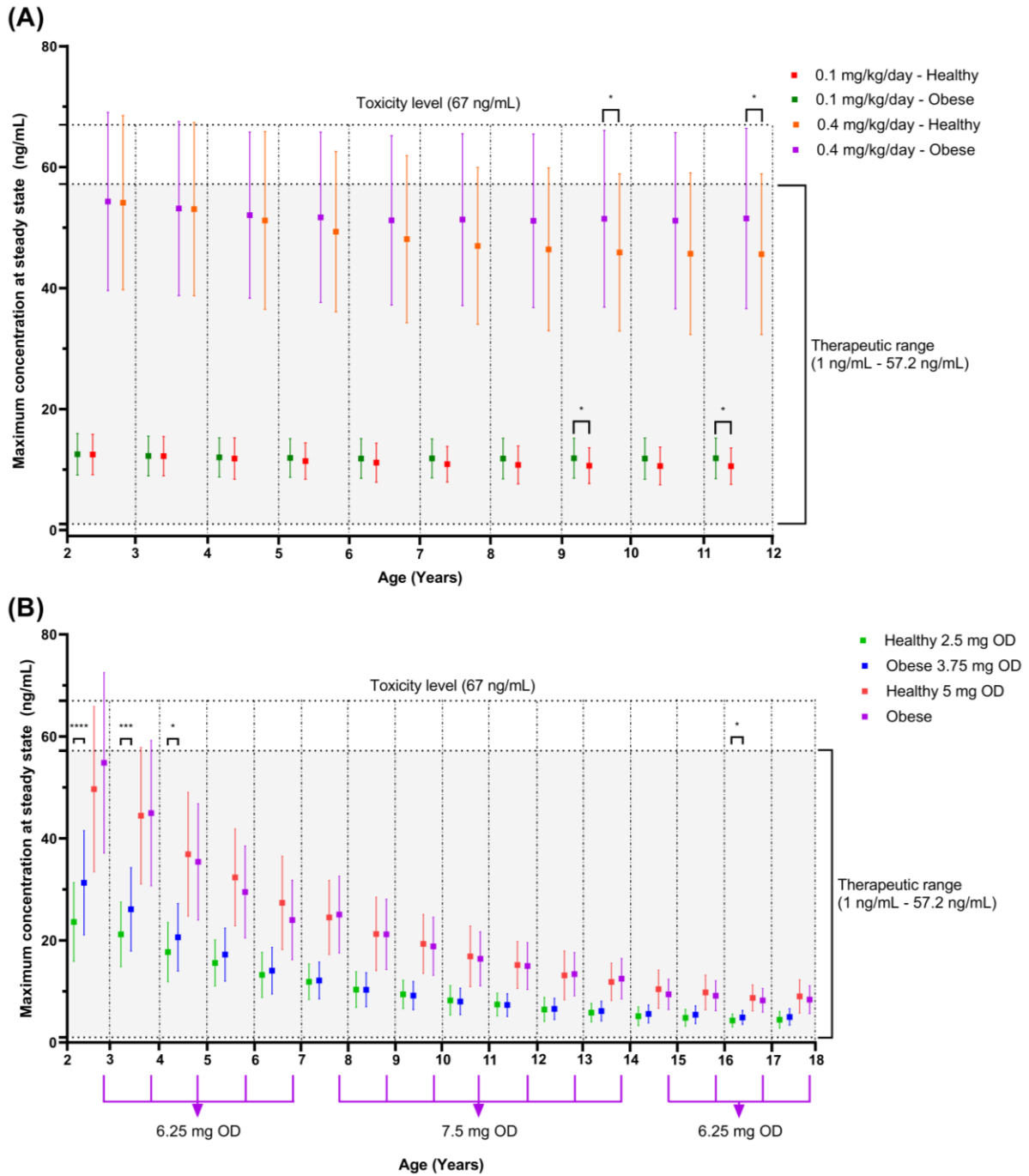


Figure 4.10 Predicted C_{max} in obese and non-obese paediatric with weight-based dose (A) and fixed-dose approaches for dose adjustment.

The horizontal lines represent the mean and standard deviations. For fixed doses, 6.25 mg OD and 7.5 mg OD are suitable in obese children, depending on the age range, to match the healthy children's 5 mg dose, as shown in the purple lines under the x-axis. OD, once daily; ****, $p < 0.0001$; ***, $p < 0.001$; *, $p < 0.05$.

4.4 Discussion

Physiological changes due to obesity, which influence the distribution and elimination process of drugs, might impact the pharmacokinetics and consequently affect the amlodipine response [158]. A study by Hanafy et al. (2009) [353] reported that the effect of CCBs, including amlodipine, in reducing systolic blood pressure and the percentage of response to CCB treatment was significantly lower in obese children when compared to non-obese children. However, the contribution from a pharmacokinetic perspective on the substantially lower efficacy in the paediatric obesity population is lacking due to the paucity of published amlodipine plasma concentration data in the population group.

The application of robust and validated physiologically based pharmacokinetic modelling permits analysis of the influence of obesity on the drug's pharmacokinetics and exploration for a pragmatic recommendation of the optimum dose [165, 410]. Therefore, the PBPK concept was implemented with the development of virtual paediatric obesity population, and utilised it to explore the pharmacokinetic differences and find the optimum dosing strategy for amlodipine in children with obesity.

4.4.1 Step 1: Development of the paediatric obesity population

The development of the paediatric obesity population in Simcyp[®] software Version 21 was adapted from the paediatric population file with the weight and height parameters for obese children were modified and derived based on the defined obese growth charts published by the CDC in 2000 [153], the WHO in 2006 and 2007 [152], as well as Gerhart et al. (2022) [156]. The weight and height changes with age altered all other parameters, which include haematocrit, serum albumin, and AGP, as shown in equations (4.5), (4.6), (4.7), and (4.8) of the 4.6.1 Result section of '4.6 Supplementary materials'. In addition, age is also related to blood flow and tissue-water composition. As for the GFR, the changes are influenced by BSA as per equation (4.9) (4.6 Supplementary materials), which is directly related to weight and height changes. Additionally, weight and height have a direct relationship with organ size. All the equations to address the relationships were defaulted in Simcyp[®] except for age, weight and height (Equations (4.1), (4.2), (4.3), and (4.4) in the '4.6.1 Result' section of '4.6 Supplementary materials').

For the validation of the paediatric obesity population file, verification focused on the relationship between age and BMI, weight, height, protein binding, and GFR because of the availability of published data for obese children. As reported in the results section of '4.6 Supplementary materials', the predicted parameter distributions for all six parameters aligned

with the data reported by various publications involving paediatric obesity. Haematocrit, serum albumin, and AGP showed no specific trend across the age, which concurs with other simulations of paediatric obesity populations and agrees with various publications that report data for paediatrics with and without obesity [156, 358, 371, 411].

For GFR, the BSA-adjusted GFR-to-age plot showed no specific trend, as the weight and height were annulled when plotting the chart (Figure S 4-8). However, an increasing trend can be seen when plotting the absolute GFR-to-age graph, which is in line with the increased kidney volume trend [156]. Additionally, reports showed no statistically significant difference in GFR between obese and normal children, which is in agreement with the equation (4.9) (4.6 Supplementary materials) that used BSA to simulate the absolute GFR trend with age [160, 347, 372].

Information on changes in metabolic enzymes and transporter abundance, which play an essential role in metabolism and elimination, is still limited for the paediatric obesity populations; thus, the default trend for the paediatric population was maintained. Information on the metabolic enzyme changes was only reported in obese adults, for example, the CYP3A4 activity was reduced by 40% in obese adults [265]. A study by van Rongen et al. (2018) [346] reported higher clearance for midazolam, a substrate of CYP3A4, in obese adolescents compared to obese adults, which is the opposite of what was noted in obese adults and may be due to comorbidities and other factors.

4.4.2 Step 2: Validation of paediatric population with metformin and ceftazidime

The paediatric obesity population was further validated with metformin and ceftazidime. For the metformin, the compound file available in Simcyp® was used with minor adjustments to f_a and V_{ss} . As standard practice in verifying modified and newly developed compound files, the adapted metformin file was verified in healthy and obese adults as well as obese and non-obese paediatric populations [165, 199, 302, 412, 413]. All simulated pharmacokinetic parameters and plasma concentration profiles generated with metformin were within the acceptance criteria and hence demonstrated validation.

Subsequently, ceftazidime has been previously developed/validated by Zhou et al. (2019) [384-387], and was used without any adaptation to verify the paediatric obesity population. The reported steady-state plasma concentration data of ceftazidime in obese children used for validation was sparse, with a summary of the median, minimum and maximum dosing information [383]. Acceptance of the result was based on VPC alone, as only the population pharmacokinetic parameter estimates were reported. Nonetheless, the median C_{max} and

clearance estimates in the population pharmacokinetic study are comparable with this study (5.40 L/h vs. 6.25 L/h), which complements the VPC result on validating the paediatric obesity population file [383].

4.4.3 Step 3: Validation of the amlodipine model

The amlodipine compound file that was developed based on compilations of information and parameter optimisation from several publications was verified in four populations, including non-obese adults, obese adults, paediatrics and obese paediatrics [388-390]. The simulated plasma concentrations and pharmacokinetic parameters for adults and obese adults met the acceptance criteria for the VPC and two-fold comparison with observed data except for three out of 54 comparisons.

Firstly, the plasma profile comparison between the simulated single-dose intravenous study in healthy adults and the intravenous plasma profile published by Faulkner et al. (1986) [398], only three out of 16 points at the distal region of the elimination phase were outside the 5th and 95th percentiles. Nevertheless, the simulated AUC_{inf} for intravenous was within the two-fold ratio compared to the reported value.

Secondly, the comparison of plasma concentration profiles between the simulated 15 mg daily for 14 days and the observed profile reported by Faulkner et al. (1986) [398], in which the three last points were not within the 5th and 95th percentile of the simulated profiles. However, all the simulated pharmacokinetic parameters for the same study are within two-fold of the reported parameters. Further, simulated amlodipine plasma concentration profiles at steady-state were stable between the low and high doses due to the simulated plasma profile being overpredicted when administered with 15 mg per day (Figure 4.5C) and underpredicted when dosed with 5 mg daily (Figure 4.5B).

Thirdly, the simulated AUC_{infss} of 5 mg daily for 14 days was not within two-fold compared to the reported AUC_{infss} by Bainbridge et al. (1993) [399]. However, all other parameters were within two-fold, and the published plasma concentration was within the 5th and 95th percentile of the simulated profile. Additionally, the AUC_{infss} is seldom utilised for pharmacokinetic parameter comparisons, especially within the regulatory contexts, due to its reliability, mainly when the percentage difference between AUC_{inf} and AUC_{0-t} is more than 20%, which is exemplified in this case, where the difference undisclosed and exceeded 20% for the reported and simulated, respectively [31]. In addition, the number of samples utilised for AUC_{inf} extrapolation between observed and simulated profiles (6 vs 24) potentially overestimates the parameters of one over the other [230].

Acceptance of the simulation in paediatric populations with and without obesity was based solely on the VPC as only sparse data on amlodipine concentrations were available in paediatric populations to the search [396, 397]. Simulated plasma concentrations that mimicked the study design and dosing range of both studies fell in the middle of the reported plasma concentration data precisely when simulations were performed based on the mean and median doses [396, 397]. Additionally, the proportion of obese children in the simulated population was comparable to one reported by Flynn et al. (2006) [397] (50.73%–50.86% versus 43.2%). The results validated the amlodipine and paediatric obesity population files, which were then used to explore and optimise amlodipine dose in obese children.

4.4.4 Step 4: Impact of obesity on amlodipine pharmacokinetics and dose optimisation in obese children population

4.4.4.1 Influence of obesity on amlodipine pharmacokinetics

The trend of plasma concentration profiles, C_{max} , and AUC decreased as the age group increased when the dose was fixed (Figure 4.8 and Figure 4.9). Nevertheless, when the dose was fixed at 2.5 mg, the dose amount per kilogram body weight was higher in the lower age group compared to the higher age group in obese and non-obese populations, with a 0.07 to 0.26 mg/kg dose in the 2 to 6 years old group, 0.03 to 0.18 mg/kg in the 6.01 to 12 years old group, and 0.02 to 0.10 mg/kg in the 12.01 to 18 years old group. The same pattern can be seen in other studies where younger patients required higher doses per kilogram of body weight than older children [397, 414, 415].

Amlodipine is metabolised in the liver, particularly by the CYP3A4 [416]. Thus, the change in hepatic-to-body size ratio and expression of CYP3A4 enzymes from infancy to adolescence was speculated to be the reason [397, 416, 417]. Additionally, the weight-normalised clearance for the simulation showed an inverse trend with age, which aligns with the theory. Furthermore, the pattern is similar to carbamazepine, where the CYP3A4 enzyme influences the clearance of carbamazepine significantly, in which several studies showed that a higher weight-adjusted dose is required for children to achieve the same effect [418-420].

Significantly lower plasma concentration, C_{max} , and AUC were noted in the obese compared to the non-obese paediatric populations within the same age group when a fixed dose was administered (Figure 4.9). The volume of distribution for obese children is higher than for non-obese children, explaining the requirement for higher doses in the obese population (Figure S 4-9) [138]. Generally, the volume of distribution has an inverse relationship with plasma

concentration, where a high volume of distribution drug is more inclined to be distributed into the tissues [138].

Another factor is clearance, which is higher in obese children than non-obese children (Figure S 4-9). Since amlodipine is cleared through the liver, CYP3A4, liver size, and blood flow to the liver may be the factors that lead to higher clearance in obese children [158]. Simulation data presented that liver weight and blood flow to the liver are higher in the obese than in non-obese paediatric populations. In contrast, the difference in CYP3A4 abundance between obese and non-obese children is subtle. Furthermore, the discovery is consistent with numerous studies involving midazolam, another CYP3A4 substrate, which have observed reduced plasma concentrations in obese compared to non-obese children [346, 421, 422].

In addition, the result agrees with the finding reported by Hanafy et al. (2009) [353] that obese children demonstrate a considerably reduced response to amlodipine in lowering systolic blood pressure and response rate compared to non-obese children. Based on animal studies, plausible explanations speculated by Hanafy et al. (2008) include the downregulation of the L-type calcium channel receptor due to the inflammatory conditions in hypertension, exacerbated further by the obese state [423, 424]. Additionally, the same can be seen in verapamil, another CCB, where the effect of verapamil is reduced in obese adult patients, and another study involving rheumatoid arthritis patients showed that despite the increase in verapamil concentration, the response is diminished, aligning with the theory that increased inflammation mediators possibly reduced the L-calcium channel receptor [425, 426].

4.4.4.2 Dose adjustment in paediatric obesity

From a pharmacokinetic perspective, this study shows that a weight-based dose is suitable for paediatric obesity to achieve the same concentration range as non-obese children, specifically those aged 2 to 12 years old (Figure 4.10). Considering obese paediatrics are heavier, a larger dose was administered based on the weight-based dosing scheme, compensating for the higher clearance and volume of distribution in obese children and leading to the same exposure as in the non-obese population. The finding aligns with the recommendation to use weight-based dosing for the same age group by the BNFC and the European Society for Hypertension in their 2016 clinical practice guideline [352, 403]. Additionally, oral solution and suspension availability in the market made weight-based dosing straightforward for children. Regarding the choice of body weight, the use of TBW in this simulation was appropriate for amlodipine, given its lipophilic nature [427].

On the other hand, with a weight-based dosing regimen, a significant percentage of obese children are expected to reach the maximum daily dose. Therefore, close monitoring of possible side effects related to amlodipine, such as oedema, palpitations, abdominal pain, flushing, dizziness and others, is essential since a higher dose is likely to result in amlodipine concentrations above the suggested therapeutic upper limit (57.2 ng/mL) and toxicity range (67 ng/mL) [404, 414, 428].

Based on the amlodipine product insert and clinical practice guidelines by the American Academy of Pediatrics in 2017, for children 6 years old and older, a fixed-dose regimen starting at 2.5 mg daily with a maximum of 5 mg and 10 mg per day, respectively, is recommended [351, 404]. Simulations demonstrated that a 1.25 to 1.5-fold higher dose in obese children is required to achieve the same amlodipine concentration in non-obese paediatrics (Figure 4.10).

Therefore, a higher initial dose of 3.75 mg daily may be considered in obese children across the 6 to 18 years age group to assist in maintaining blood pressure instantaneously, mainly when physicians opt for fixed-dose regimens. Although the result showed a significant difference in C_{max} between obese and non-obese children for the starting dose in the 16 to 17 years old age group, it may not be clinically significant as the amlodipine concentrations were still within the therapeutic limit.

Following treatment initiation, the systolic and diastolic blood pressure readings and side effects are fundamental factors that drive the dose adjustment, which is practically made after 1 to 2 weeks of the initial dose [351, 403]. Considering therapeutic drug monitoring for any antihypertensive agent is uncommon unless to evaluate medication compliance, the difference in amlodipine plasma concentrations between obese and non-obese children will have minimal influence as the deciding factor in making dose adjustments, specifically after the treatment has started [429].

Amlodipine is available in both solid and liquid dosage forms. Thus, the fixed-dose regimen may be suitable for specific age groups, such as children above 13 years old, as a study showed approximately 30% of children aged 13 to 18 years old favoured tablet rather than liquid formulations (18.3%) [430].

Based on the pharmacokinetic study of amlodipine in children by Flynn et al. (2006) [397], amlodipine concentrations between 1 – 57.2 ng/mL demonstrated no serious adverse events. Thus, this study showed that for children 6 years old and above, a fixed-dose regimen is expected to maintain the amlodipine concentrations within the therapeutic range and reduce the harm that potential adverse events may cause with higher doses. Since significant differences in amlodipine concentration between obese and non-obese were noted at 9 years old with weight-based doses, the fixed-dose can be considered at 9 years old and above.

Nevertheless, any dose below 0.35 mg/kg daily is unlikely to cause side effects as less than 20% of the simulated C_{\max} surpasses the maximum therapeutic range.

4.5 Conclusion

For the first time, mechanistic pharmacokinetic modelling is implemented in this study by establishing a virtual paediatric obesity population as a pragmatic approach to address the impact of obesity on drug pharmacokinetics.

Findings highlight that a suitable dose adjustment is required to achieve the same amlodipine plasma concentration as in non-obese children. The physiological alteration in obese paediatrics led to a significant difference in amlodipine C_{max} and AUC when administered as a fixed-dose regimen compared to non-obese children. Thus, when opting for a fixed-dose regimen, a 1.25 to 1.5-fold higher dose is needed in obese children to achieve a comparable amlodipine plasma concentration to non-obese children. While these recommendations provide valuable insights, further validation with more extensive real-world data is necessary to strengthen the accuracy and applicability of the model. In addition, clinical studies are needed to support these findings, particularly in evaluating dose adjustment guided by the clinical endpoints.

This study highlights the potential of PBPK modelling and its application to addressing personalised dosing in the obese paediatric population. Further improvements can be made with the virtual paediatric obesity population group by refining the physiological information, such as changes in the metabolism enzymes specific to obese children as they evolve with age, and the findings from this study will inform medicines optimisation approaches in future studies.

4.6 Supplementary materials

4.6.1 Results for Step 1: Development of the paediatric obesity population

4.6.1.1 Age, weight and height relationship

Polynomial mathematical correlations for gender-specific height-age and weight-age for the population are described in Equations (4.1), (4.2), (4.3) and (4.4) for ages 2 – 18:

$$\text{Male height (cm)} = 61.463912 + (0.65513619 \times \text{age}^2) - (0.12642816 \times \text{age}^{2.5}) + (17.3579 \times \text{age}^{0.5}) \quad (4.1)$$

$$\text{Female height (cm)} = 64.092976 + (10.720395 \times \text{age}) - (0.29561165 \times \text{age}^2) \quad (4.2)$$

$$\text{Male weight (kg)} = 3.2737 + (0.5346053 \times \text{age}^2) - (0.015322545 \times \text{age}^3) \quad (4.3)$$

$$\text{Female weight (kg)} = 11.809275 + (0.64670616 \times \text{age}^2) - (0.022469269 \times \text{age}^3) \quad (4.4)$$

The WHO and CDC graphs, which are the cut-off lines for children's obesity overlaid at the lower part of the individual simulated BMI-for-age graph (2 – 18 years old) for males and females (Figure S 4-1), indicated that the predictions represent the BMI for the obese children population [152, 357]. For the mean BMI-for-age graph of paediatric obesity, the reference curves by Gerhart et al. (2022) [156] cover the predicted chart, thus validating the simulated BMI-to-age chart.

Additionally, a similar pattern can be seen for the height-for-age curves (2 – 18 years old) for males and females (Figure S 4-2), as well as the weight-for-height curves (2 – 18 Years old) for males and females (Figure S 4-3). The reference graphs of mean height-for-age and mean weight-for-height of the paediatric obesity population published by Gerhart et al. (2022) [156] fit in the middle of the simulated graphs. Thus, it further verified the predicted weight and height of the paediatric obesity population.

Furthermore, for ages 2 to 5, the reference weight-for-age curves published by WHO and CDC were overlaid on the spread of individual simulated weight-for-height graphs for males and females (Figure S 4-4), reinforcing the validation of simulated weight and height distribution of obese children population [152, 357].

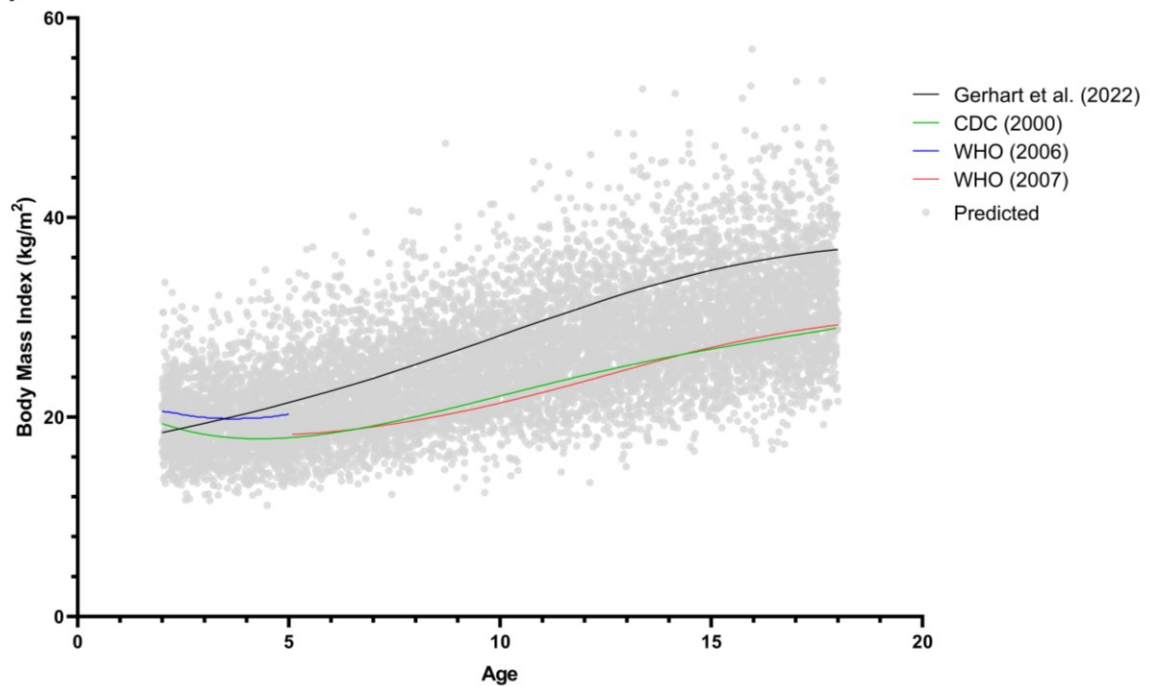
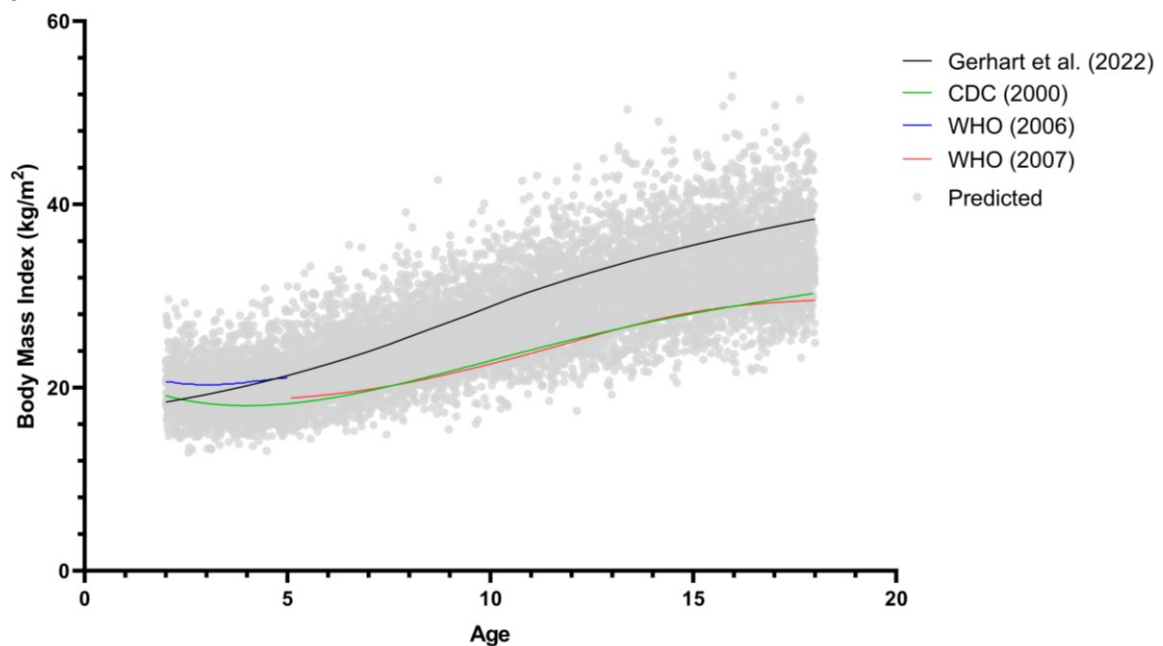
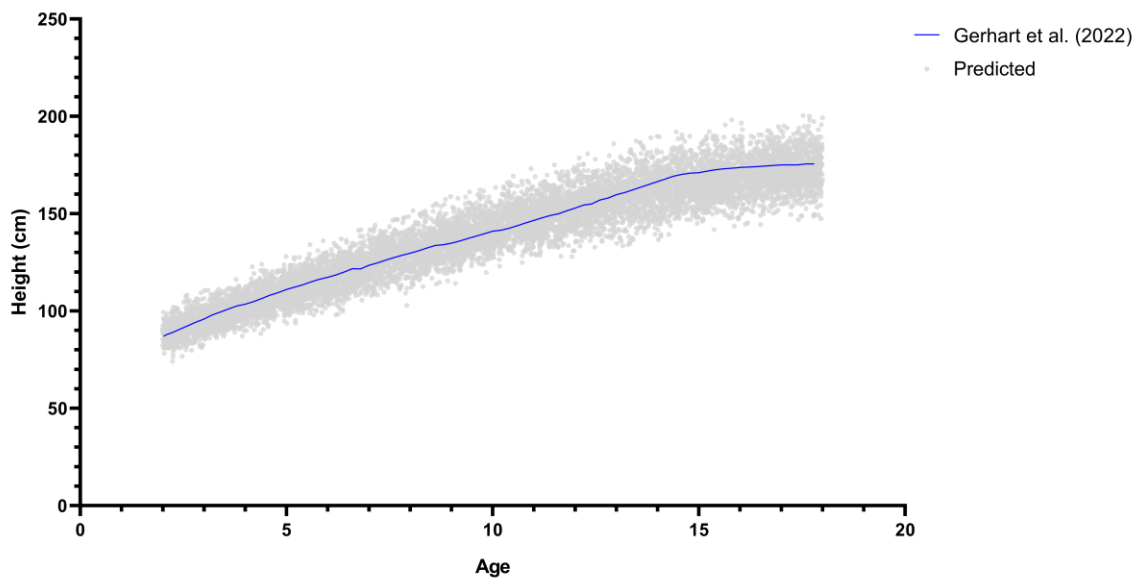
(A) Males**(B) Females**

Figure S 4-1 Simulated BMI-for-age curves for paediatric obesity from 2 to 18 years old for males (A) and females (B).

Gerhart et al. (2022) [156] generated the paediatric obesity BMI-for-age curve at the 95th percentile based on the National Health and Nutrition Examination Survey (NHANES) pooled data from 1999 to 2016. The CDC (2000) BMI-for-age curve is at the 95th percentile, which defines the cut-off curve for obesity in paediatrics [357]. The WHO (2006) BMI-for-age curve is at 3 SD from the median for 2 to 5 years old, while the WHO (2007) [152] is at 2 SD from the median of the BMI-for-age curve for 6 to 18 years old [152].

(A) Males



(B) Females

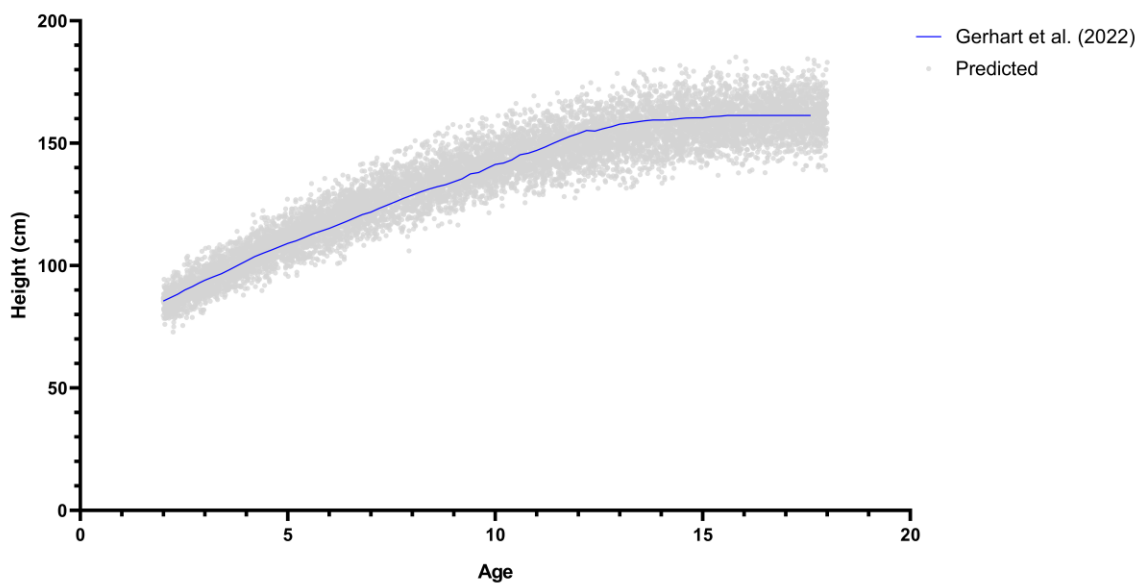
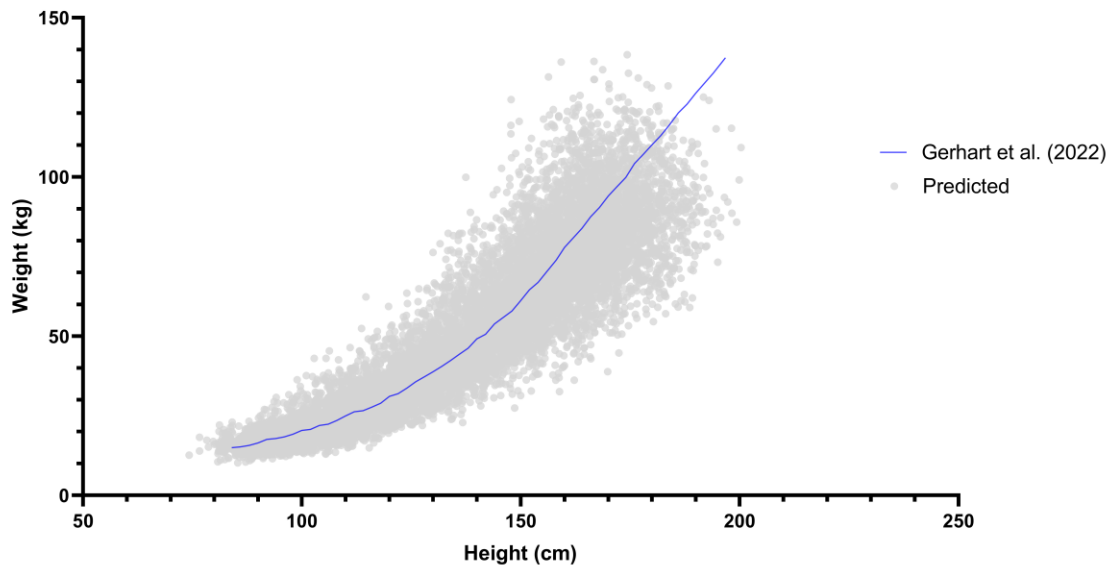


Figure S 4-2 Simulated Height-for-age curve for paediatric obesity from 2 to 18 years old for males (A) and females (B).

Gerhart et al. (2022) [156] generated the central tendency of paediatric obesity's height-for-age curve based on the NHANES pooled data from 1999 to 2016.

(A) Males



(B) Females

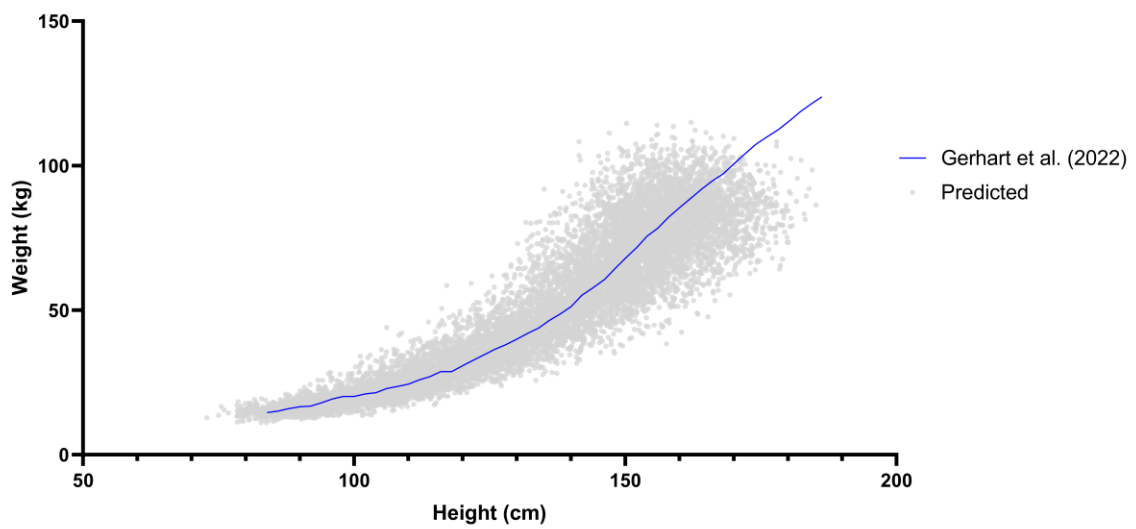
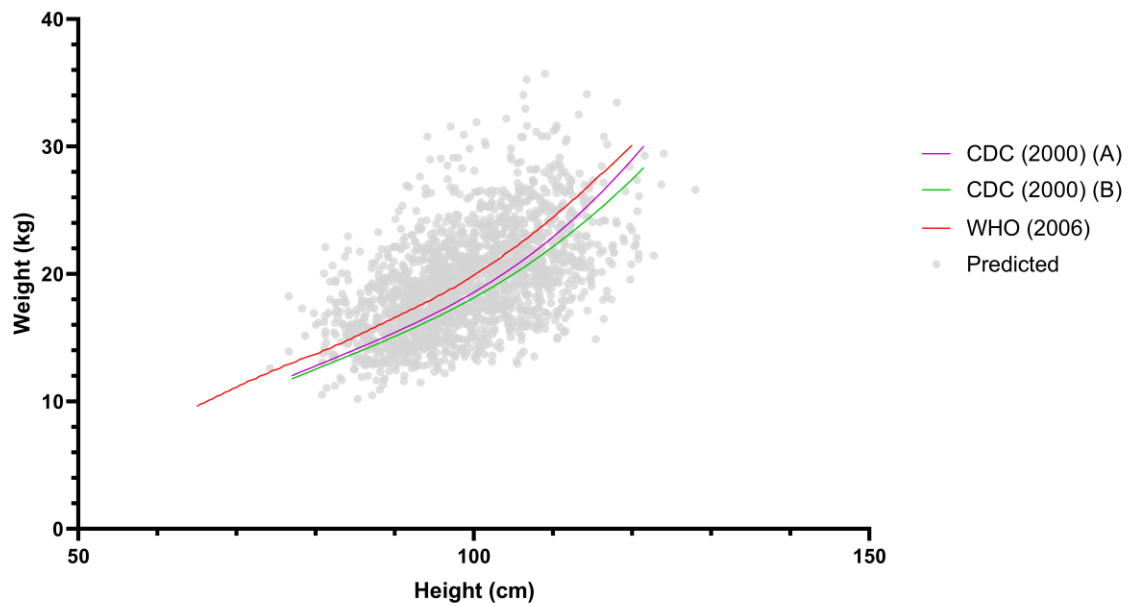


Figure S 4-3 Simulated Weight-for-height curves for paediatric obesity from 2 to 18 years old for males (A) and females (B).

Gerhart et al. (2022) [156] generated the central tendency of paediatric obesity's weight-for-age curve based on the NHANES pooled data from 1999 to 2016.

(A) Males



(B) Females

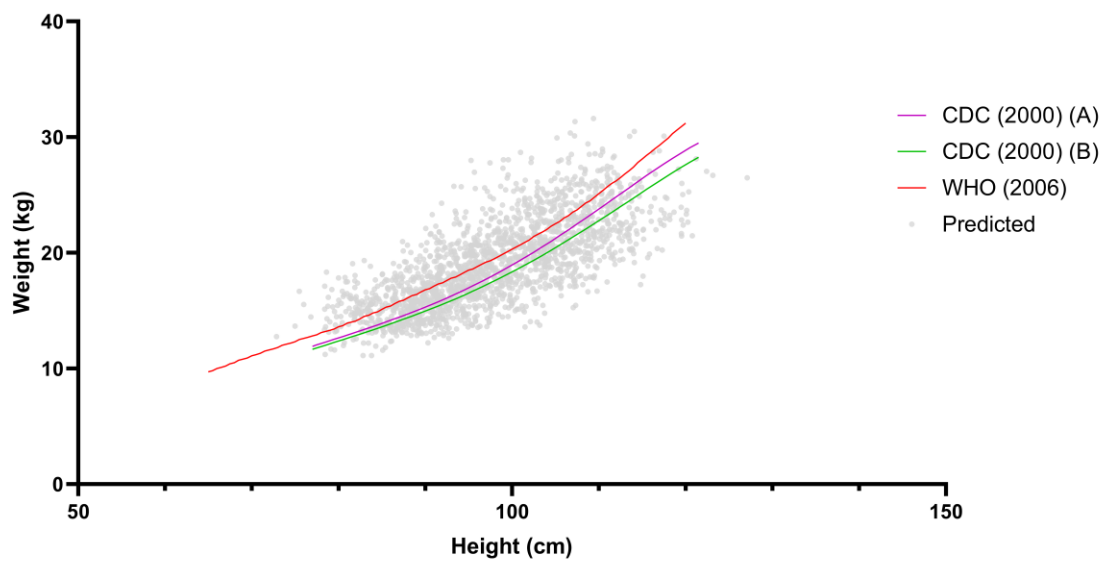


Figure S 4-4 Simulated Weight-for-height curves for paediatric obesity from 2 to 5 years old for males (A) and females (B).

The CDC (2000) (A) Weight-for-height curve is at the 97th percentile [357]. The CDC (2000) (B) Weight-for-height curve is at the 95th percentile, which defines the cut-off curve for obesity in paediatrics [357]. The WHO (2006) Weight-for-age curve is at 3 SD from the median for 2 to 5 years old, which defines the cut-off curve for obesity in paediatrics [152].

4.6.1.2 Haematocrit-to-age relationship

Haematocrit values correlation with age was predicted using gender-specific mathematical statements as described in Equations (4.5) and (4.6);

$$\text{Male (\%)} = 53 - \left(\left(\frac{43 \times \text{age}^{1.12}}{0.05^{1.12} + \text{age}^{1.12}} \right) \times \left(1 + \left(\frac{-0.93 \times \text{age}^{-25}}{0.10^{0.25} + \text{age}^{0.25}} \right) \right) \right) \quad (4.5)$$

$$\text{Female (\%)} = 53 - \left(\left(\frac{37.4 \times \text{age}^{1.12}}{0.05^{1.12} + \text{age}^{1.12}} \right) \times \left(1 + \left(\frac{-0.80 \times \text{age}^{-25}}{0.10^{0.25} + \text{age}^{0.25}} \right) \right) \right) \quad (4.6)$$

The distribution of simulated haematocrit values over age fitted within the range of reported values from 8 different references (Figure S 4-5). Besides, the predicted values for both males and females reflected all the published haematocrit values (Table S 4-1), which validated the paediatric obesity population file.

Table S 4-1 Summarised results from literature search for haematocrit values in paediatric obesity

Reference	Age (years) ^a	Number of subjects (n)	Males (%)	Haematocrit (L/L)
Predicted values	2 - 18	10,000	100	0.40 (0.03) ^e
Predicted values	2 - 18	10,000	0	0.38 (0.03) ^e
Kilic et al. (2016) [358]	6 - 16	37	48.64	0.39 (0.33 – 0.43) ^b
Panichsillaphakit et al. (2021) [359]	5 – 15	63	66.78	0.40 (0.38 – 0.41) ^c
Oni et al. (2021) [361]	6 – 19	2,818	53.40	0.40 (0.396 – 0.399) ^d
Jeong et al. (2021) [362]	10 – 18	297	100	0.44 (0.03) ^e
Jeong et al. (2021) [362]	10 – 18	234	0	0.40 (0.02) ^e
Belo et al. (2014) [363]	4 – 18	168	100	0.42 (0.03) ^e
Belo et al. (2014) [363]	4 – 18	182	0	0.40 (0.02) ^e
Cacciari et al. (1988) [360]	5.17 – 15.58	43	65	0.38 (0.03) ^e
Elhag et al. (2018) [411]	13 – 17	36	100	0.43 (0.03) ^e
Elhag et al. (2018) [411]	13 - 17	43	0	0.39 (0.03) ^e

^a range; ^b median (min-max); ^c median (interquartile range); ^d mean (95% confidence interval); ^e mean (SD)

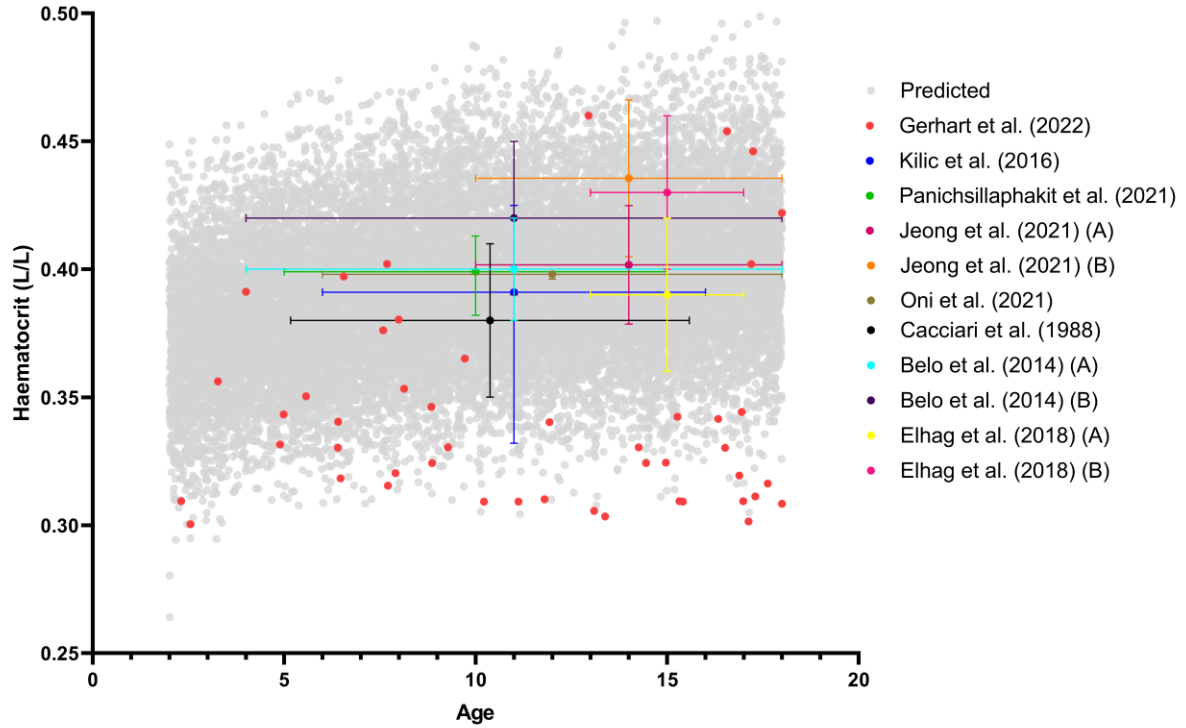


Figure S 4-5 Simulated Haematocrit-to-age relationship for paediatric obesity from 2 to 8 years old (Grey circle).

Gerhart et al. (2022) [156] reported individual haematocrit data for obese children from combined clinical trial data represented in the red circles [156]. Jeong et al. (2021) (A) represented data for girls [362]. Jeong et al. (2021) (B) represented data for boys [362]. Belo et al. (2014) (A) and Belo et al. (2014) (B) represented data for girls and boys, respectively [363]. Elhag et al. (2018) (A) represented data for girls [411]. Elhag et al. (2018) (B) represented data for boys [411]. The horizontal lines showed the age range reported for each published study. The coloured circles with the vertical lines are different for each study; Kilic et al. (2016), median with range; Panichsillaphakit et al. (2021), median with interquartile range; Oni et al. (2021), mean with 95% confidence interval; Jeong et al. (2021) mean with standard deviation (SD); Belo et al. (2014), mean with SD; Cacciari et al. (1988), mean with SD; Elhag et al. (2018), mean with SD.

4.6.1.3 Serum albumin-to-age relationship

As no significant difference was reported in human serum albumin values between genders [156], the relationship for the range of age between 2 to 18 years old was predicted based on the general mathematical equation (4.7);

$$\text{Serum albumin (g/L)} = 33.746 + (1.1287 \times \ln(365 \times \text{age})) \quad (4.7)$$

The spread of simulated serum albumin over age values was within the wide range of published values from seven references (Figure S 4-6). Additionally, the predicted values (27.62 – 58.19 g/L) are echoed with the published reference values (Table S 4-2) and simulated values by Gerhart et al. (2022) [156]. Therefore, it validated the simulated serum albumin values for the paediatric obesity population developed in this study.

Table S 4-2 Summarised results from the literature search for serum albumin values in paediatric obesity

Reference	Age (years) ^a	Number of subjects (n)	Males (%)	Serum Albumin (g/L)
Predicted values	2 - 18	20,000	50	42.80 (4.27) ^b
Yu et al. (2021) [364]	6 – 18	449	62.81	49.40 (2.80) ^b
Elhag et al. (2018) [411]	13 – 17	79	45	41.14 (4.06) ^b
Abitbol et al. (2009) [365]	1 – 21	22	50	40.00 (5.00) ^b
Marginean et al. (2014) [367]	1 – 18	102	57.84	46.60 (4.70) ^b
Marginean et al. (2016) [368]	1 – 18	121	53.72	47.20 (3.70) ^b
Marginean et al. (2019) [366]	5 – 18	77	NR	48.92 (3.26) ^b
Marginean et al. (2020) [157]	5 – 18	91	NR	48.48 (3.46) ^b

NR, not reported; ^a range; ^b mean (SD)

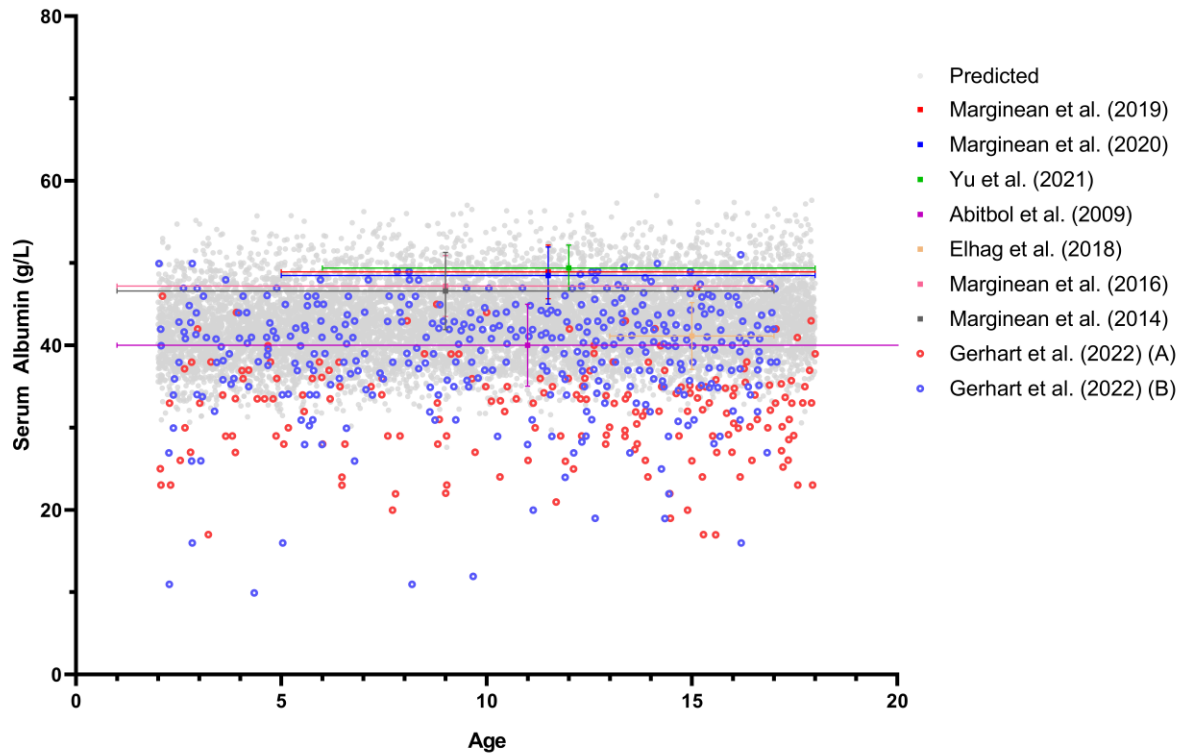


Figure S 4-6 Predicted Serum albumin-to-age relationship for paediatric obesity from 2 to 18 years old (Grey circle).

Gerhart et al. (2022) (A) reported individual serum albumin data for children with obesity from combined clinical trial data in red circles [156]. Gerhart et al. (2022) (B) reported individual data for paediatric obesity from the Paediatric Trial Network (PTN) data repository [156]. The horizontal lines showed the age range reported for each published study. The coloured squares with vertical lines represented the mean with SD.

4.6.1.4 Alpha-1-acid glycoprotein (AGP)-to-age relationship

A similar pattern can be seen in AGP-to-age correlation as another protein-binding component in blood. One polynomial mathematical equation (4.8) to describe the correlation with age from 2 to 18 years old;

$$\text{AGP} \left(\frac{\text{g}}{\text{L}} \right) = \frac{0.887 \times (365 \times \text{age})^{0.38}}{(8.89^{0.38} + (365 \times \text{age})^{0.38}} \quad (4.8)$$

The distribution of predicted AGP values was within the broad range of AGP values observed from four different studies (Figure S 4-7). Furthermore, the predicted values were comparable with the observed values, thus validating the obese children population file (Table S 4-3).

Table S 4-3 Summarised results from the literature search for AGP values in paediatric obesity

Reference	Age (years) ^a	Number of subjects (n)	Males (%)	AGP (g/L)
Predicted values	2 - 18	20,000	50	0.80 (0.10) ^c
Gerhart et al. (2022) [156] ^b	2 – 18	32,001	50	1.07 (0.40) ^c
Sobieska et al. (2013) [369]	12 – 14	28	100	0.94 (0.25) ^c
Sobieska et al. (2013) [369]	12 – 14	23	0	0.91 (0.25) ^c
Sobieska et al. (2013) [369]	15 – 18	33	100	0.90 (0.26) ^c
Sobieska et al. (2013) [369]	15 – 18	40	0	1.33 (0.28) ^c
Gibson et al. (2014) [370]	3 – 6	49	NR	1.05 (0.90 – 1.30) ^d
Ferrari et al. (2015) [371]	12.5 – 17.5	876	46	0.80 (0.60 – 1.10) ^d

NR, not reported; ^a range; ^b Gerhart et al., 2022 AGP values are the simulated values for paediatric obesity; ^c mean (SD); ^d median (range)

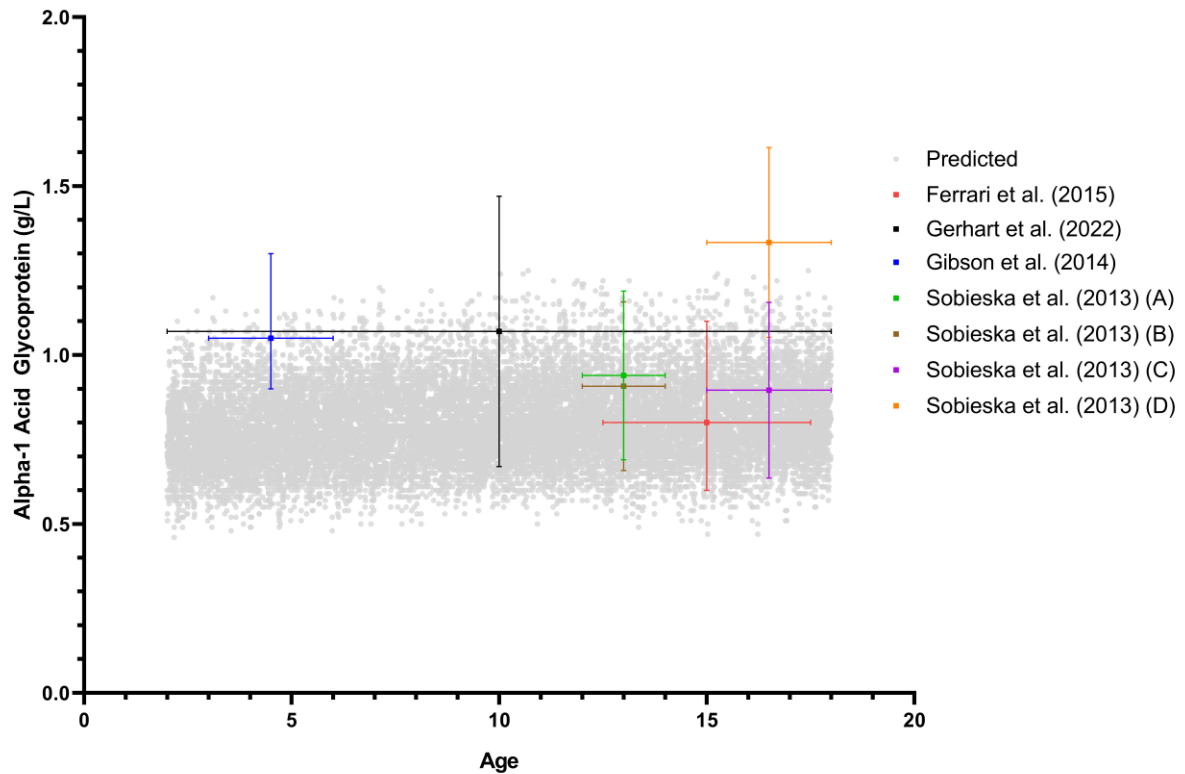


Figure S 4-7 Predicted AGP-to-age relationship for paediatric obesity from 2 to 18 years old (Grey circle).

Sobieska et al. (2013) (A) represented data for boys aged 12 to 14 [369]. Sobieska et al. (2013) (B) represented data for girls aged 12 to 14 [369]. Sobieska et al. (2013) (C) represented data for boys 15 to 18 years old [369]. Sobieska et al. (2013) (D) represented data for girls 15 to 18 years old [369]. The horizontal lines showed the age range reported for each published study. The coloured squares with vertical lines represented the mean with SD for Gerhart et al. (2022) [156] and Sobieska et al. (2013) [369]. The coloured square with vertical lines represented the median with range for Gibson et al. (2014) [370] and Ferrari et al. (2015) [371].

4.6.1.5 Glomerular filtration rate (GFR)-to-age relationship

Since GFR is the function of body surface area (BSA) as described in mathematical equation (4.9), the GFR increases as age increases;

$$\text{GFR} \left(\frac{\text{mL}}{\text{min}} \right) = -17.74 + 99.054(\text{BSA}) - 6.1604(\text{BSA})^2 \quad (4.9)$$

The absolute GFR was comparable with the reported values by Correia-Costa et al. (2016) [160] for paediatric obesity ages 8 to 9 (Figure S 4-8 and Table S 4-4). Additionally, BSA-adjusted GFR for obese children aged 4 – 18 years old was compared with values published by Duzova et al. (2013) [372] and Goknar et al. (2015) [347]. The predicted values in virtual obese children reflected the published values (Table S 4-4) despite a broader range at 16 to 18 years old in the simulated values (Figure S 4-8). Considering that both predicted absolute and BSA-adjusted GFR were in line with observed values, it validated the paediatric obesity population file.

Table S 4-4 Summarised results from the literature search for GFR values in paediatric obesity

Reference	Age (years) ^a	Number of subjects (n)	Males (%)	GFR (mL/min)
Predicted values	8 – 9	1,230	50	103.50 (18.19) ^b
Correia-Costa et al. (2016) [160]	8 – 9	61	66	120.80 (21.50) ^b
Predicted values	5 – 18	16,274	50	137.40 (24.72) ^c
Duzova et al. (2013) [372]	5 – 18	318	NR	122.70 (21.60) ^c
Predicted values	4 – 16	15,104	50	132.70 (20.44) ^c
Goknar et al. (2015) [347]	4 – 16	84	54.76	152.22 (23.94) ^c

NR, not reported; ^a range; ^b mean (SD); ^c unit of mL/min/1.73m², presented as mean (SD).

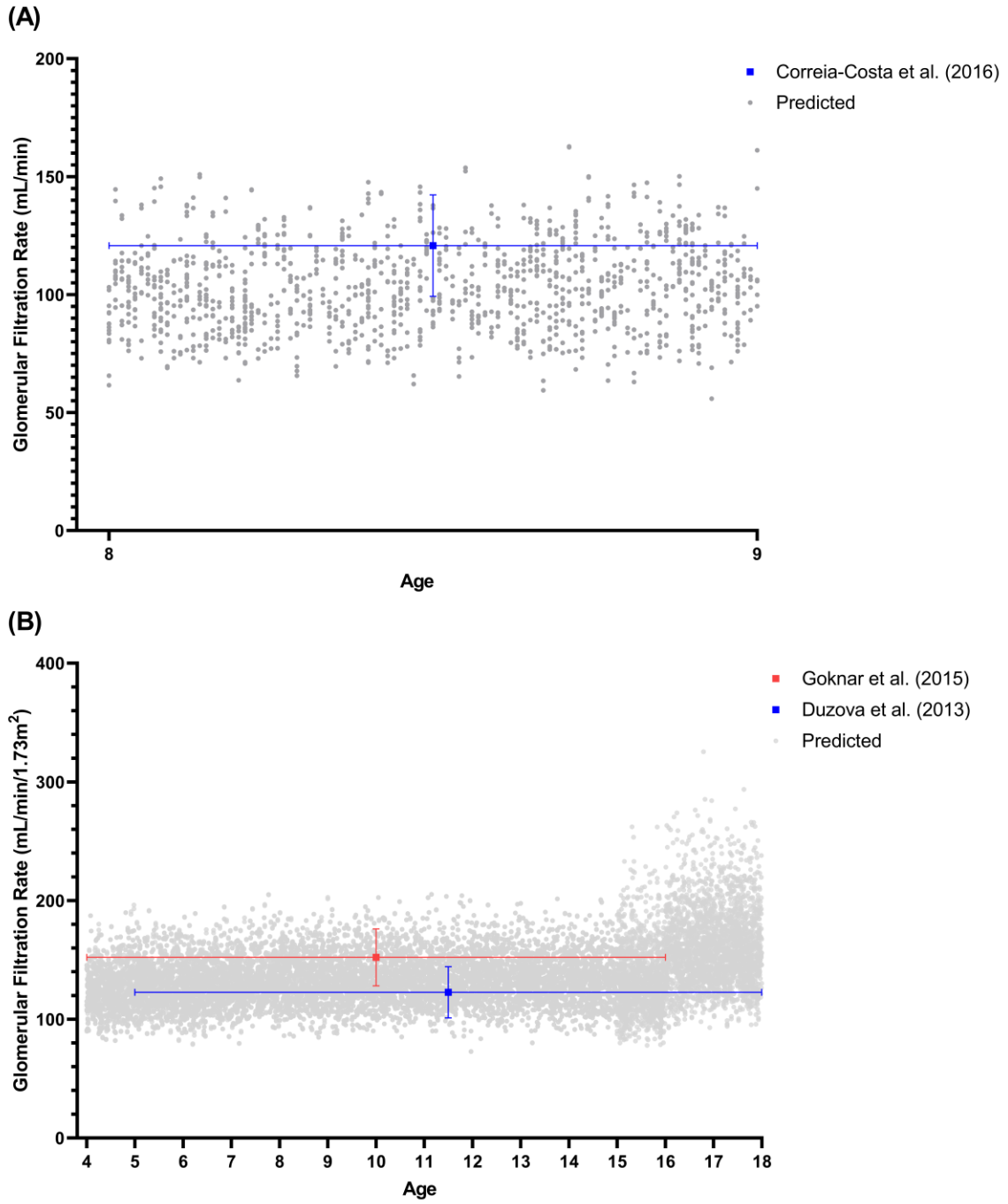


Figure S 4-8 Absolute GFR (mL/min)-to-age relationship for paediatric obesity from 8 to 9 years old (A) and BSA-adjusted GFR (mL/min/1.73m²)-to-age correlation for paediatric obesity from 4 to 18 years old (B).

Grey circles are the predicted value. The horizontal lines showed the age range reported for each published study. The coloured squares with vertical lines represented the mean with SD.

4.6.2 Supplementary figures

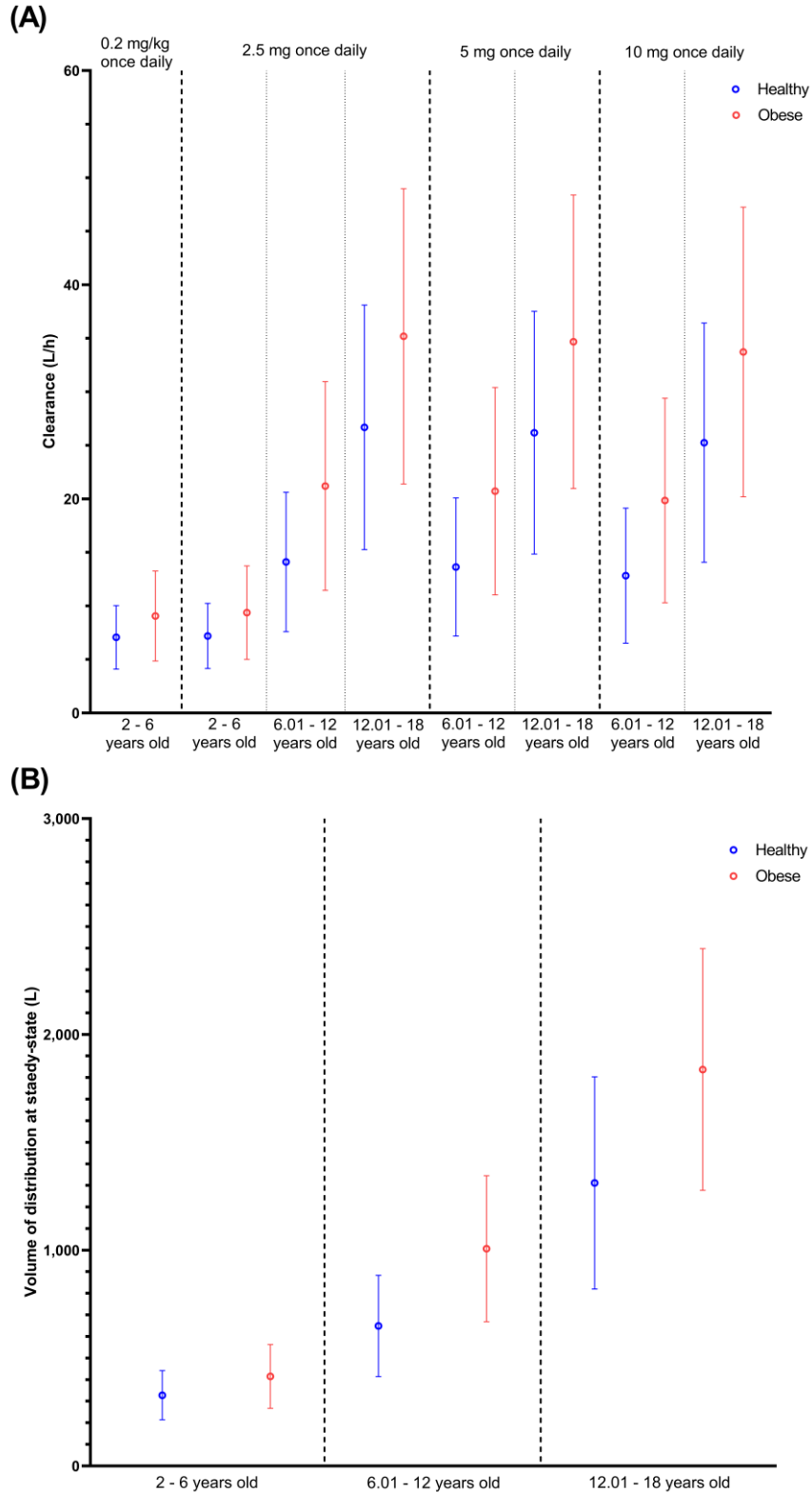
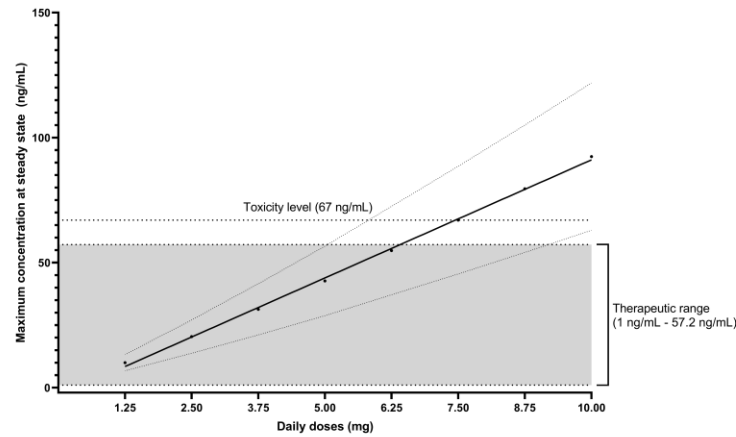


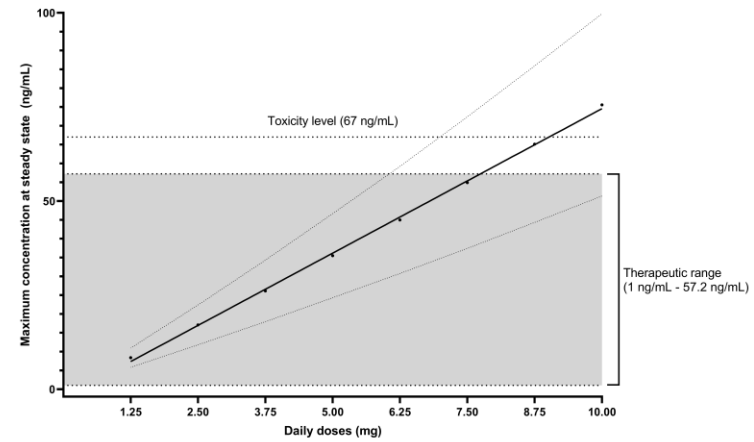
Figure S 4-9 Comparison of predicted clearance (A) and volume of distribution (B) at steady-state for healthy and obese paediatric doses.

The coloured circles represent the mean, and the horizontal lines represent the standard deviations.

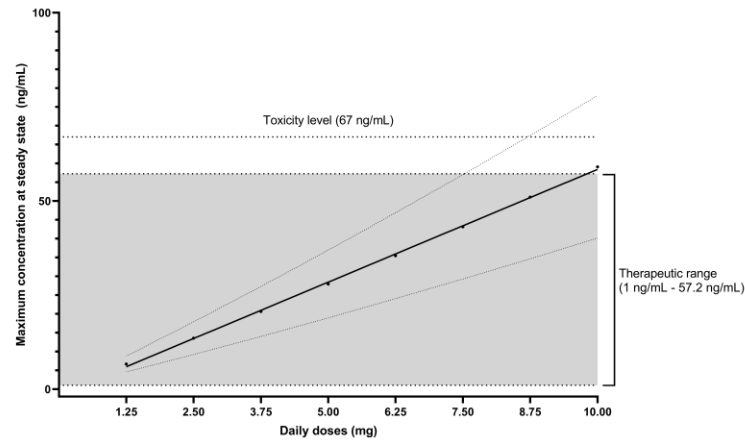
(A) 2 to 3 years old: $y = 9.448x - 3.378$



(B) 3.01 to 4 years old: $y = 7.678x - 2.256$



(C) 4.01 to 5 years old: $y = 5.992x - 1.550$



(D) 5.01 to 6 years old: $y = 4.967x - 1.164$

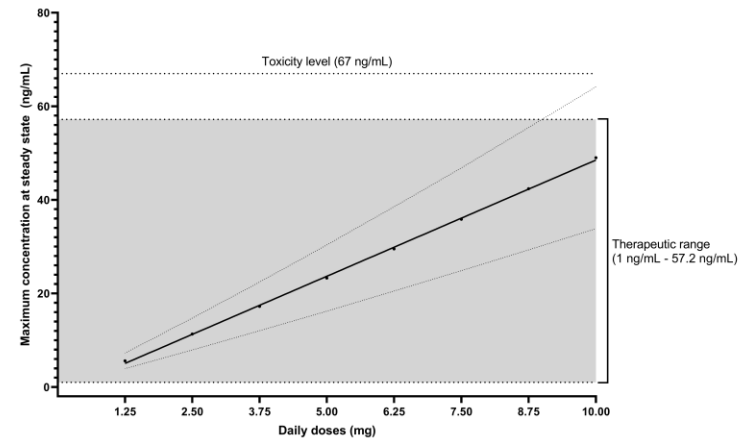
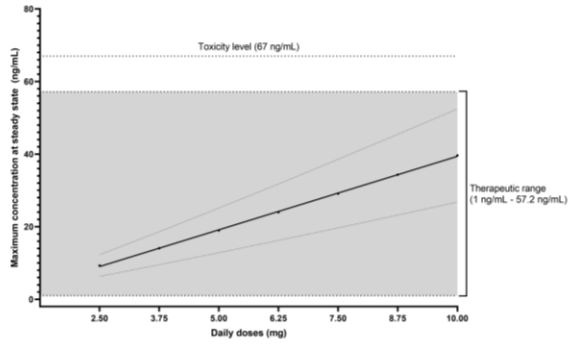


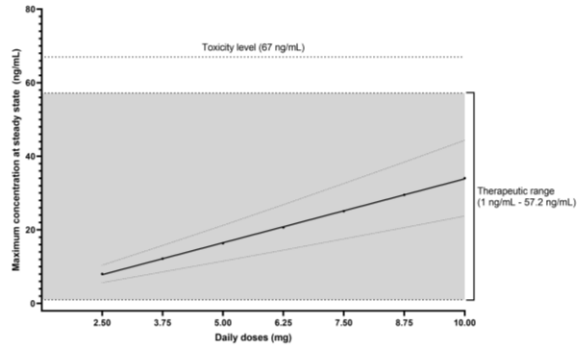
Figure S 4-10 Predicted maximum concentrations (C_{max}) versus daily doses for age group 2 to 6 years old.

Solid lines represent the means, dotted lines represent the SD, and grey area is the therapeutic range for amlodipine (1 ng/mL – 57.2 ng/mL).

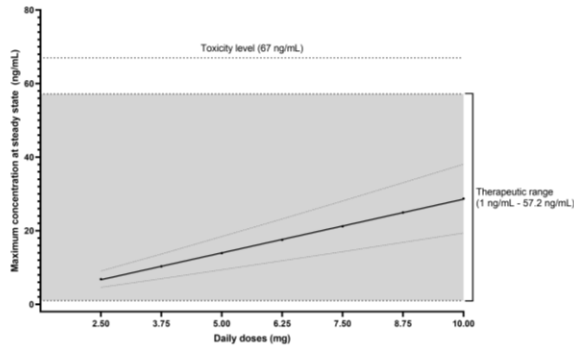
(A) 6.01 to 7 years old: $y = 4.049x - 1.098$



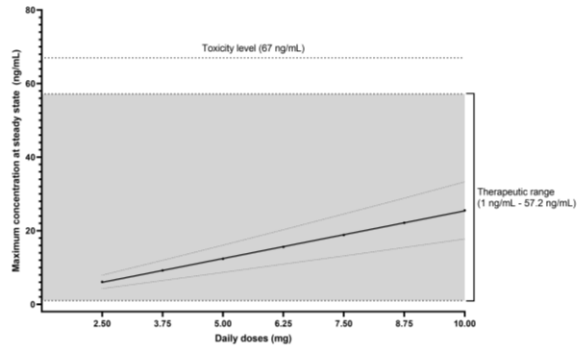
(B) 7.01 to 8 years old: $y = 3.473x - 0.863$



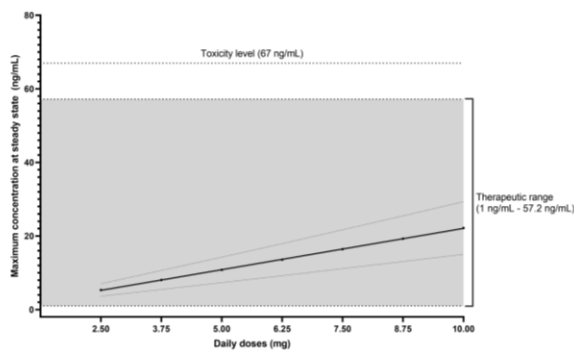
(C) 8.01 to 9 years old: $y = 2.921x - 0.618$



(D) 9.01 to 10 years old: $y = 2.591x - 0.512$



(E) 10.01 to 11 years old: $y = 2.247x - 0.367$



(F) 11.01 to 12 years old: $y = 2.049x - 0.333$

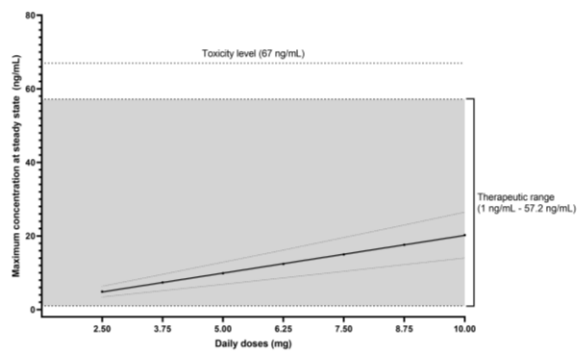
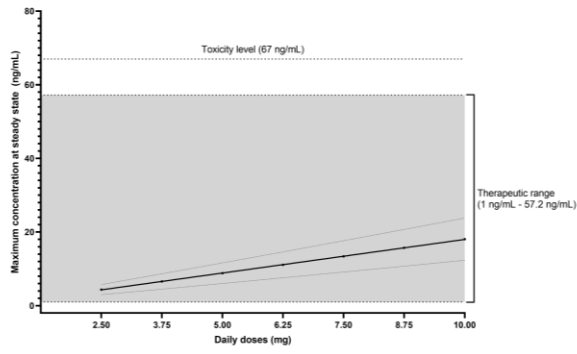


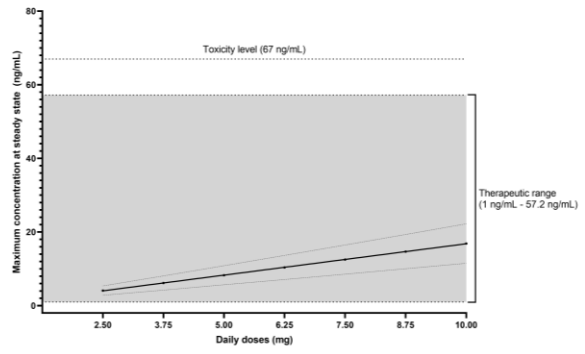
Figure S 4-11 Predicted C_{max} versus daily doses for age group 6.01 to 12 years old.

Solid lines represent the means, dotted lines represent the SD, and grey area is the therapeutic range for amlodipine (1 ng/mL – 57.2 ng/mL).

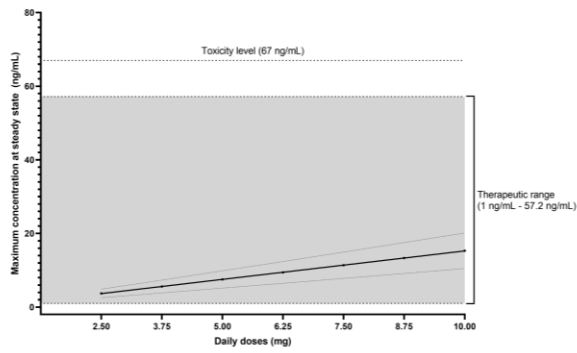
(A) 12.01 to 13 years old: $y = 1.825x - 0.266$



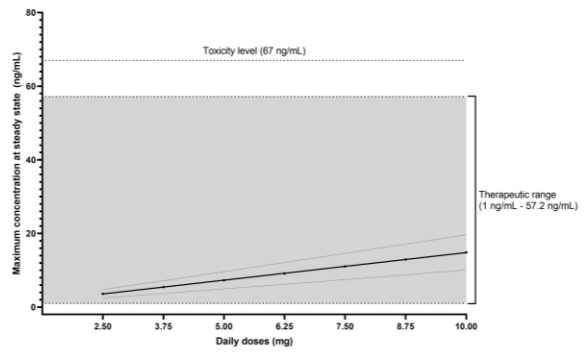
(B) 13.01 to 14 years old: $y = 1.705x - 0.239$



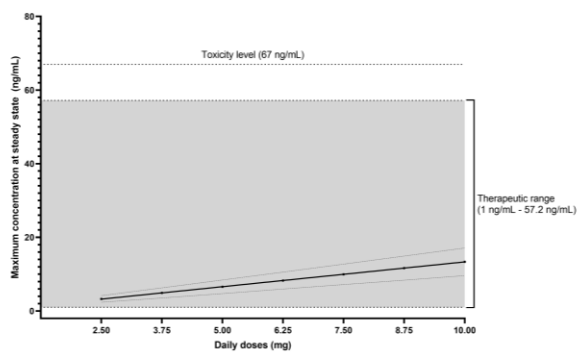
(C) 14.01 to 15 years old: $y = 1.545x - 0.192$



(D) 15.01 to 16 years old: $y = 1.499x - 0.180$



(E) 16.01 to 17 years old: $y = 1.348x - 0.146$



(F) 17.01 to 18 years old: $y = 1.373x - 0.150$

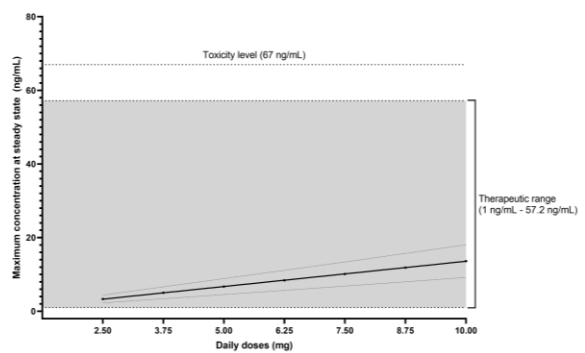


Figure S 4-12 Predicted C_{max} versus daily doses for age group 12.01 to 18 years old.

Solid lines represent the means, dotted lines represent the SD, and grey area is the therapeutic range for amlodipine (1 ng/mL – 57.2 ng/mL).

		Age																	
Dose		2	3	4	5	6	7	8	9	10	11	12	13	14	15	16	17	18	
0.10 mg/kg	C _{max} (ng/mL)	12.48 ± 3.34	12.22 ± 3.26	11.82 ± 3.42	11.4 ± 3.01	11.14 ± 3.23	10.88 ± 2.94	10.76 ± 3.14	10.63 ± 2.95	10.59 ± 3.12	10.56 ± 3.01								
	C _{min} (ng/mL)	8.55 ± 3.1	7.84 ± 2.52	8.21 ± 3.12	7.46 ± 2.34	7.82 ± 2.96	7.21 ± 2.29	7.61 ± 2.88	7.11 ± 2.3	7.53 ± 2.85	7.12 ± 2.34								
	AUC _{0-24ss} (ng/mL.h)	252.8 ± 78.77	240.16 ± 67.56	241.65 ± 79.81	226.58 ± 63.06	229.19 ± 75.7	217.39 ± 62.04	222.11 ± 73.69	213.28 ± 62.38	219.12 ± 73.13	212.5 ± 63.85								
	% dose > 10 mg/day	0	0	0	0	0	0	0	0	0	0								
	% C _{max} > 67 ng/mL	0	0	0	0	0	0	0	0	0	0								
	1 ng/mL < % C _{max} < 57.2 ng/mL	100	100	100	100	100	100	100	100	100	100								
0.40 mg/kg	C _{max} (ng/mL)	54.13 ± 14.41	53.06 ± 14.32	51.19 ± 14.7	49.34 ± 13.27	48.09 ± 13.83	46.98 ± 12.97	46.41 ± 13.46	45.9 ± 13	45.68 ± 13.37	45.6 ± 13.3								
	C _{min} (ng/mL)	38.14 ± 13.38	35.23 ± 11.38	36.48 ± 13.44	33.32 ± 10.56	34.6 ± 12.72	32.06 ± 10.33	33.59 ± 12.38	31.58 ± 10.35	33.21 ± 12.26	31.6 ± 10.56								
	AUC _{0-24ss} (ng/mL.h)	1113.44 ± 339.84	1060.95 ± 302.82	1060.97 ± 344.01	996.25 ± 283.2	1002.63 ± 324.92	953.42 ± 278.05	970.28 ± 316.62	934.52 ± 279.54	956.79 ± 314.49	931.11 ± 286.28								
	% dose > 10 mg/day	0	0	0	7.55	8.51	28.3	65.96	71.7	93.62	96.27								
	% C _{max} > 67 ng/mL	25	21.15	14.89	13.21	10.64	11.32	10.64	9.43	8.51	11.32								
	1 ng/mL < % C _{max} < 57.2 ng/mL	62.5	69.23	68.09	77.36	74.47	77.36	80.85	77.36	80.85	77.36								
2.50 mg OD	C _{max} (ng/mL)	23.63 ± 7.7	21.2 ± 6.34	17.72 ± 5.82	15.59 ± 4.53	13.25 ± 4.42	11.89 ± 3.5	10.37 ± 3.5	9.43 ± 2.79	8.26 ± 2.91	7.44 ± 2.24	6.47 ± 2.35	5.85 ± 1.8	5.15 ± 1.85	4.84 ± 1.67	4.32 ± 1.26	4.46 ± 1.61		
	C _{min} (ng/mL)	16.36 ± 6.82	13.74 ± 4.93	12.38 ± 5.18	10.26 ± 3.56	9.34 ± 3.95	7.91 ± 2.76	7.35 ± 3.13	6.32 ± 2.23	5.88 ± 2.57	5.02 ± 1.8	4.62 ± 2.07	3.96 ± 1.43	3.68 ± 1.62	3.25 ± 1.3	3.02 ± 1.06	3.01 ± 1.23		
	AUC _{0-24ss} (ng/mL.h)	481.54 ± 177.36	418.78 ± 132.96	363.52 ± 134.44	310.64 ± 96.21	273.3 ± 102.44	238.03 ± 74.71	214.28 ± 81.21	189.28 ± 60.14	170.97 ± 67.09	149.71 ± 48.45	134.08 ± 54.14	117.79 ± 38.82	106.75 ± 42.6	97 ± 35.35	88.6 ± 28.07	89.58 ± 33.71		
	% C _{max} > 67 ng/mL	0	0	0	0	0	0	0	0	0	0	0	0	0	0	0	0	0	
	1 ng/mL < % C _{max} < 57.2 ng/mL	100	100	100	100	100	100	100	100	100	100	100	100	100	100	100	100	98.11	
			2	3	4	5	6	7	8	9	10	11	12	13	14	15	16	17	18
5.00 mg OD	C _{max} (ng/mL)	49.66 ± 16.21	44.44 ± 13.39	36.9 ± 12.12	32.36 ± 9.5	27.37 ± 9.13	24.51 ± 7.27	21.28 ± 7.21	19.33 ± 5.78	16.87 ± 5.95	15.19 ± 4.6	13.16 ± 4.8	11.88 ± 3.68	10.45 ± 3.76	9.8 ± 3.41	8.74 ± 2.56	9.04 ± 3.27		
	C _{min} (ng/mL)	34.97 ± 14.39	29.38 ± 10.59	26.13 ± 10.81	21.63 ± 7.55	19.49 ± 8.18	16.48 ± 5.8	15.21 ± 6.44	13.08 ± 4.64	12.1 ± 5.28	10.32 ± 3.72	9.45 ± 4.22	8.1 ± 2.95	7.5 ± 3.3	6.62 ± 2.65	6.14 ± 2.14	6.11 ± 2.51		
	AUC _{0-24ss} (ng/mL.h)	1021.29 ± 374.21	886.59 ± 284.11	762.29 ± 280.81	649.87 ± 203.37	567.53 ± 212.18	493.62 ± 156.35	441.92 ± 167.35	390.04 ± 125.01	350.68 ± 137.65	306.81 ± 100.07	273.65 ± 110.6	240.2 ± 79.64	217.04 ± 86.7	197.06 ± 72.21	179.66 ± 56.95	181.8 ± 68.76		
	% C _{max} > 67 ng/mL	5.77	3.85	2.13	0	0	0	0	0	0	0	0	0	0	0	0	0	0	
	1 ng/mL < % C _{max} < 57.2 ng/mL	88.46	82.69	93.62	95.75	100	100	100	100	100	100	100	100	100	100	100	100	100	
			2	3	4	5	6	7	8	9	10	11	12	13	14	15	16	17	18

Figure S 4-13 Summary of pharmacokinetic parameters at steady-state in healthy paediatric from 2 to 18 years old.

C_{max}, maximum concentration; C_{min}, minimum concentration; AUC_{0-24ss}, area-under-the-curve at steady-state; 67 ng/mL, toxic level; 1 ng/mL to 57.2 ng/mL, therapeutic concentration.

Dose		Age									
		2	3	4	5	6	7	8	9	10	11
0.10 mg/kg	C _{max} (ng/mL)	12.53 ± 3.44	12.25 ± 3.27	12.02 ± 3.22	11.93 ± 3.19	11.83 ± 3.28	11.84 ± 3.21	11.81 ± 3.35	11.86 ± 3.29	11.81 ± 3.4	11.86 ± 3.35
	C _{min} (ng/mL)	8.57 ± 3.18	18.65 ± 5	8.34 ± 3.01	7.83 ± 2.45	8.31 ± 3.03	7.88 ± 2.52	8.36 ± 3.08	7.97 ± 2.58	8.4 ± 3.11	8.03 ± 2.63
	AUC _{0-24ss} (ng/mL.h)	253.57 ± 80.9	25.22 ± 6.78	245.38 ± 76.38	236.85 ± 66.43	243.19 ± 77.23	236.73 ± 67.93	243.87 ± 78.98	238.22 ± 69.85	244.49 ± 80	238.99 ± 71.31
	% dose > 10 mg/day	0	0	0	0	0	0	0	0	0	0
	% C _{max} > 67 ng/mL	0	0	0	0	0	0	0	0	0	0
	1 ng/mL < % C _{max} < 57.2 ng/mL	100	100	100	100	100	100	100	100	100	100
0.20 mg/kg	C _{max} (ng/mL)	25.8 ± 7.07	25.22 ± 6.78	24.74 ± 6.61	24.55 ± 6.62	24.33 ± 6.73	24.36 ± 6.66	24.3 ± 6.89	24.42 ± 6.84	24.3 ± 6.99	24.42 ± 6.97
	C _{min} (ng/mL)	17.82 ± 6.54	16.36 ± 5.19	17.32 ± 6.18	16.29 ± 5.12	17.25 ± 6.23	16.4 ± 5.27	17.36 ± 6.35	16.59 ± 5.41	17.44 ± 6.41	16.71 ± 5.52
	AUC _{0-24ss} (ng/mL.h)	524.99 ± 166.68	497.85 ± 140.33	507.63 ± 156.93	490.39 ± 138.82	502.89 ± 158.82	490.12 ± 142.05	504.31 ± 162.57	493.32 ± 146.13	505.62 ± 164.78	495.01 ± 149.29
	% dose > 10 mg/day	0	0	0	0	0	0	12.77	47.17	74.47	88.68
	% C _{max} > 67 ng/mL	0	0	0	0	0	0	0	0	0	0
	1 ng/mL < % C _{max} < 57.2 ng/mL	100	100	100	100	100	100	100	100	100	100
0.30 mg/kg	C _{max} (ng/mL)	39.75 ± 10.86	38.88 ± 10.49	38.1 ± 10.13	37.83 ± 10.26	37.47 ± 10.31	37.55 ± 10.34	37.43 ± 10.57	37.64 ± 10.62	37.43 ± 10.73	37.65 ± 10.83
	C _{min} (ng/mL)	27.71 ± 10.04	45.94 ± 12.42	26.91 ± 9.48	25.37 ± 8.01	26.78 ± 9.56	25.53 ± 8.24	26.94 ± 9.75	25.82 ± 8.46	27.07 ± 9.85	26 ± 8.63
	AUC _{0-24ss} (ng/mL.h)	812.81 ± 256	53.16 ± 14.38	785.52 ± 240.61	759.68 ± 216.51	777.91 ± 243.67	759.24 ± 221.65	780.12 ± 249.6	764.36 ± 228.11	782.22 ± 253.11	767.14 ± 233.2
	% dose > 10 mg/day	0	0	0	9.43	44.68	67.93	95.75	100	100	100
	% C _{max} > 67 ng/mL	0	0	0	0	0	0	0	0	0	0
	1 ng/mL < % C _{max} < 57.2 ng/mL	93.75	96.15	95.75	94.34	91.49	94.34	91.49	94.34	91.49	92.45
0.40 mg/kg	C _{max} (ng/mL)	54.32 ± 14.74	53.16 ± 14.38	52.06 ± 13.74	51.71 ± 14.08	51.2 ± 13.99	51.33 ± 14.21	51.13 ± 14.35	51.47 ± 14.6	51.15 ± 14.57	51.51 ± 14.9
	C _{min} (ng/mL)	38.19 ± 13.64	35.24 ± 11.24	37.05 ± 12.87	35 ± 11.08	36.85 ± 12.97	35.22 ± 11.4	37.07 ± 13.24	35.62 ± 11.7	37.24 ± 13.39	35.86 ± 11.94
	AUC _{0-24ss} (ng/mL.h)	1115.57 ± 347.7	1060.93 ± 301.79	1077.74 ± 326.48	1043.58 ± 298.7	1067.01 ± 330.73	1042.99 ± 305.89	1070.04 ± 338.98	1050.24 ± 314.9	1073.03 ± 343.88	1054.28 ± 322.11
	% dose > 10 mg/day	0	1.92	23.4	62.26	95.75	100	100	100	100	100
	% C _{max} > 67 ng/mL	18.75	15.38	12.77	15.09	14.89	15.09	14.89	16.98	17.02	16.98
	1 ng/mL < % C _{max} < 57.2 ng/mL	62.5	63.46	61.7	69.81	68.09	71.7	68.09	69.81	68.09	69.81

Figure S 4-14 Summary of pharmacokinetic parameters at steady-state in paediatric obesity from 2 to 18 years old administered with weight-based dose.

C_{max}, maximum concentration; C_{min}, minimum concentration; AUC_{0-24ss}, area-under-the-curve at steady-state; 67 ng/mL, toxic level; 1 ng/mL to 57.2 ng/mL, therapeutic concentration.

Dose	Age																	
	2	3	4	5	6	7	8	9	10	11	12	13	14	15	16	17	18	
2.50 mg OD	Cmax (ng/mL)	20.41 ± 6.65	17.06 ± 5.31	13.52 ± 4.35	11.32 ± 3.4	9.28 ± 3	8.02 ± 2.37	6.83 ± 2.21	6.09 ± 1.82	5.32 ± 1.71	4.87 ± 1.47	4.36 ± 1.38	4.08 ± 1.28	3.72 ± 1.17	3.61 ± 1.16	3.26 ± 0.91	3.32 ± 1.07	
	Cmin (ng/mL)	14.06 ± 5.84	11.02 ± 4.02	9.39 ± 3.85	7.46 ± 2.63	6.51 ± 2.67	5.35 ± 1.89	4.82 ± 1.97	4.09 ± 1.45	3.77 ± 1.53	3.29 ± 1.17	3.1 ± 1.23	2.77 ± 1	2.64 ± 1.04	2.45 ± 0.91	2.29 ± 0.83	2.26 ± 0.83	
	AUC0-24ss (ng/mL.h)	414.67 ± 152.39	335.94 ± 110.08	276.27 ± 100.23	225.22 ± 71.65	190.75 ± 69.33	160.49 ± 50.86	140.8 ± 51.29	122.18 ± 39.05	109.93 ± 39.72	97.98 ± 31.69	90.19 ± 32.09	82.24 ± 27.24	76.91 ± 27.13	72.79 ± 24.58	67.11 ± 20.77	67 ± 22.66	
	% Cmax > 67 ng/mL	0	0	0	0	0	0	0	0	0	0	0	0	0	0	0	0	
	1 ng/mL < % Cmax < 57.2 ng/mL	100	97.92	100	100	100	100	100	100	100	100	100	100	100	100	100	100	
	3.75 mg OD	Cmax (ng/mL)	31.32 ± 10.22	26.11 ± 8.18	20.61 ± 6.64	17.23 ± 5.2	14.08 ± 4.56	12.16 ± 3.61	10.33 ± 3.35	9.2 ± 2.76	8.04 ± 2.59	7.35 ± 2.23	6.58 ± 2.08	6.16 ± 1.93	5.6 ± 1.76	5.44 ± 1.75	4.91 ± 1.38	5 ± 1.62
Cmin (ng/mL)		21.74 ± 8.99	17.01 ± 6.24	14.4 ± 5.88	11.41 ± 4.04	9.92 ± 4.05	8.14 ± 2.88	7.32 ± 2.99	6.2 ± 2.2	5.71 ± 2.31	4.98 ± 1.78	4.68 ± 1.86	4.18 ± 1.51	3.99 ± 1.57	3.7 ± 1.37	3.46 ± 1.2	3.41 ± 1.26	
AUC0-24ss (ng/mL.h)		639.06 ± 234.63	516.44 ± 170.6	422.5 ± 153.11	343.7 ± 110.07	290.11 ± 105.41	243.79 ± 77.63	213.42 ± 77.74	185.06 ± 59.37	166.27 ± 60.09	148.15 ± 48.07	136.22 ± 48.48	124.19 ± 41.24	116.05 ± 40.94	109.81 ± 37.13	101.19 ± 31.32	101.03 ± 34.21	
% Cmax > 67 ng/mL		0	0	0	0	0	0	0	0	0	0	0	0	0	0	0	0	
1 ng/mL < % Cmax < 57.2 ng/mL		100	100	100	100	100	100	100	100	100	100	100	100	100	100	100	100	
5.00 mg OD		Cmax (ng/mL)	42.66 ± 13.93	35.48 ± 11.18	27.91 ± 8.99	23.29 ± 7.07	18.99 ± 6.16	16.38 ± 4.88	13.9 ± 4.52	12.37 ± 3.72	10.79 ± 3.48	9.87 ± 3	8.82 ± 2.8	8.25 ± 2.6	7.51 ± 2.36	7.29 ± 2.34	6.57 ± 1.84	6.69 ± 2.17
	Cmin (ng/mL)	29.83 ± 12.25	23.31 ± 8.6	19.6 ± 7.98	15.51 ± 5.52	13.43 ± 5.47	11 ± 3.91	9.87 ± 4.02	8.36 ± 2.97	7.68 ± 3.1	6.7 ± 2.39	6.29 ± 2.5	5.62 ± 2.03	5.35 ± 2.11	4.97 ± 1.85	4.64 ± 1.61	4.58 ± 1.69	
	AUC0-24ss (ng/mL.h)	873.77 ± 320	704.83 ± 234.49	573.83 ± 207.59	465.96 ± 150.18	392.04 ± 142.34	329.09 ± 105.29	287.49 ± 104.69	249.14 ± 80.22	223.52 ± 80.77	199.09 ± 64.8	182.86 ± 65.08	166.68 ± 55.49	155.65 ± 54.93	147.25 ± 49.86	135.62 ± 41.98	135.42 ± 45.92	
	% Cmax > 67 ng/mL	6.25	0	0	0	0	0	0	0	0	0	0	0	0	0	0	0	
	1 ng/mL < % Cmax < 57.2 ng/mL	83.33	98.08	97.87	100	100	100	100	100	100	100	100	100	100	100	100	100	
	6.25 mg OD	Cmax (ng/mL)	54.39 ± 17.75	45.17 ± 14.3	35.42 ± 11.41	29.51 ± 9.01	24.01 ± 7.79	20.68 ± 6.19	17.52 ± 5.7	15.59 ± 4.7	13.58 ± 4.38	12.41 ± 3.79	11.09 ± 3.52	10.37 ± 3.28	9.43 ± 2.97	9.16 ± 2.95	8.25 ± 2.32	8.4 ± 2.73
Cmin (ng/mL)		38.28 ± 15.62	29.9 ± 11.09	25 ± 10.12	19.75 ± 7.07	17.03 ± 6.92	13.95 ± 4.97	12.47 ± 5.08	10.56 ± 3.77	9.69 ± 3.91	8.45 ± 3.03	7.92 ± 3.14	7.07 ± 2.57	6.74 ± 2.65	6.25 ± 2.32	5.83 ± 2.02	5.76 ± 2.13	
AUC0-24ss (ng/mL.h)		1118 ± 407.84	900.7 ± 301.5	730.04 ± 263.51	591.9 ± 191.89	496.48 ± 180.08	416.35 ± 133.81	362.98 ± 132.12	314.38 ± 101.59	281.64 ± 101.76	250.79 ± 81.88	230.12 ± 81.9	209.73 ± 69.99	195.7 ± 69.07	185.09 ± 62.77	170.4 ± 52.76	170.16 ± 57.78	
% Cmax > 67 ng/mL		16.67	5.77	2.13	0	0	0	0	0	0	0	0	0	0	0	0	0	
1 ng/mL < % Cmax < 57.2 ng/mL		68.75	76.92	95.74	100	100	100	100	100	100	100	100	100	100	100	100	100	
7.50 mg OD		Cmax (ng/mL)	66.48 ± 21.65	55.15 ± 17.54	43.11 ± 13.87	35.87 ± 11	29.12 ± 9.45	25.07 ± 7.53	21.2 ± 6.9	18.85 ± 5.7	16.41 ± 5.29	14.99 ± 4.59	13.39 ± 4.25	12.52 ± 3.96	11.37 ± 3.58	11.04 ± 3.56	9.94 ± 2.8	10.12 ± 3.29
	Cmin (ng/mL)	47.08 ± 19.05	36.76 ± 13.68	30.57 ± 12.32	24.12 ± 8.67	20.73 ± 8.4	16.96 ± 6.15	15.13 ± 4.58	12.81 ± 4.73	11.73 ± 3.67	10.22 ± 3.11	9.57 ± 3.8	8.55 ± 3.11	8.13 ± 3.2	7.54 ± 2.81	7.04 ± 2.44	6.95 ± 2.57	
	AUC0-24ss (ng/mL.h)	1370.97 ± 497.56	1103.59 ± 371.32	890.9 ± 320.68	721.4 ± 235.13	603.34 ± 218.55	505.54 ± 163.17	439.85 ± 160.01	380.78 ± 123.46	340.65 ± 123.05	303.26 ± 99.29	277.98 ± 98.93	253.31 ± 84.73	236.2 ± 83.37	223.35 ± 75.85	205.52 ± 63.65	205.25 ± 69.78	
	% Cmax > 67 ng/mL	35.42	30.77	6.38	0	0	0	0	0	0	0	0	0	0	0	0	0	
	1 ng/mL < % Cmax < 57.2 ng/mL	31.25	48.08	87.23	98.11	97.87	100	100	100	100	100	100	100	100	100	100	100	
	8.75 mg OD	Cmax (ng/mL)	78.91 ± 25.61	65.4 ± 20.88	35.87 ± 11	42.38 ± 13.06	34.33 ± 11.13	29.53 ± 8.91	24.94 ± 8.11	22.16 ± 6.72	19.27 ± 6.22	17.6 ± 5.4	15.7 ± 4.99	14.68 ± 4.66	13.33 ± 4.2	12.94 ± 4.18	11.65 ± 3.28	11.86 ± 3.86
Cmin (ng/mL)		56.2 ± 22.54	43.87 ± 16.38	24.12 ± 8.67	28.63 ± 10.33	24.52 ± 9.9	20.05 ± 7.19	17.84 ± 7.24	15.1 ± 5.41	13.8 ± 5.56	12.03 ± 4.33	11.25 ± 4.46	10.05 ± 3.66	9.55 ± 3.75	8.85 ± 3.3	8.26 ± 2.86	8.15 ± 3.02	
AUC0-24ss (ng/mL.h)		1631.94 ± 588.67	1313.04 ± 443.61	721.4 ± 235.13	854.31 ± 279.81	712.54 ± 257.7	596.61 ± 193.34	518.08 ± 188.33	448.31 ± 145.84	400.51 ± 144.62	356.48 ± 117.04	326.44 ± 116.15	297.44 ± 99.71	277.14 ± 97.83	262 ± 89.1	240.98 ± 74.64	240.68 ± 81.93	
% Cmax > 67 ng/mL		70.83	51.92	14.77	1.89	2.13	0	0	0	0	0	0	0	0	0	0	0	
1 ng/mL < % Cmax < 57.2 ng/mL		22.92	38.46	72.34	84.91	95.75	100	100	100	100	100	100	100	100	100	100	100	
10.00 mg OD		Cmax (ng/mL)	91.64 ± 29.62	75.91 ± 24.3	59.04 ± 18.94	49.02 ± 15.16	39.64 ± 12.85	34.06 ± 10.31	28.73 ± 9.35	25.52 ± 7.77	22.17 ± 7.16	20.24 ± 6.23	18.05 ± 5.73	16.87 ± 5.36	15.31 ± 4.82	14.85 ± 4.8	13.37 ± 3.76	13.62 ± 4.44
	Cmin (ng/mL)	65.6 ± 26.06	51.23 ± 19.16	42.22 ± 16.83	33.27 ± 12.05	28.39 ± 11.43	23.21 ± 8.35	20.6 ± 8.34	17.43 ± 6.26	15.91 ± 6.29	13.86 ± 5	12.95 ± 5.13	11.56 ± 4.22	10.98 ± 4.31	10.18 ± 3.79	9.49 ± 3.28	9.37 ± 3.47	
	AUC0-24ss (ng/mL.h)	1900.24 ± 680.76	1528.62 ± 518.06	1225.57 ± 438.09	990.5 ± 325.84	824.02 ± 297.45	689.51 ± 224.3	597.64 ± 217.05	516.97 ± 168.7	461.22 ± 166.46	410.44 ± 135.12	375.48 ± 133.57	342.09 ± 114.93	318.52 ± 112.43	301.06 ± 102.52	276.79 ± 85.74	276.47 ± 94.22	
	% Cmax > 67 ng/mL	77.08	61.54	25.53	13.21	4.26	0	0	0	0	0	0	0	0	0	0	0	
	1 ng/mL < % Cmax < 57.2 ng/mL	10.42	32.69	53.19	67.93	93.62	100	100	100	100	100	100	100	100	100	100	100	

Figure S 4-15 Summary of pharmacokinetic parameters at steady-state in paediatric obesity from 2 to 18 years old administered with fixed dose.

C_{max}, maximum concentration; C_{min}, minimum concentration; AUC_{0-24ss}, area-under-the-curve at steady-state; 67 ng/mL, toxic level; 1 ng/mL to 57.2 ng/mL, therapeutic concentration.

CHAPTER 5 – Conclusion and future work

5.1 Conclusion

Physiologically based pharmacokinetic (PBPK) modelling has been used as a dynamic modelling technique within this thesis to explore the optimum dosing strategy in special populations such as pregnant women, cancer adults with obesity, and paediatric obesity.

The influence of physiological alterations in pregnant women as a special population with the CYP2D6 phenotypes in fluvoxamine concentration and dosing strategy was the focus of the first part of this thesis. Using the pragmatic approach of mechanistic modelling, the fluvoxamine model was successfully developed and validated to predict fluvoxamine exposure in the healthy adult and pregnant women population. Furthermore, the model was verified with the foetoplacental model for the simulation of fluvoxamine concentration that crosses the placental barrier. Moreover, the fluvoxamine model has been validated in the CYP2D6 extensive metaboliser (EM) and poor metaboliser (PM) adult population and explored the impact of CYP2D6 phenotype on fluvoxamine concentration in pregnant women population and foetus model.

The fluvoxamine pharmacokinetics prediction and plasma concentration profile simulation made based on the model were within the acceptance range when compared with the observed data from 11 studies in healthy subjects, four studies in CYP2D6 EM and PM populations, one study in pregnant women population and three studies in foetal placental subjects. The model was then applied to explore the influence of CYP2D6 phenotype on fluvoxamine concentration in pregnant women and foetus. The results revealed a significant difference between the ultra-rapid metaboliser (UM), EM, and PM pregnant women populations throughout the gestational period, with few exceptions. As for the foetus model, significant differences were seen when compared to the PM population but not between UM and EM. In addition, the decreased trend in pregnant women and elevated pattern in fetuses of fluvoxamine concentrations seen in all three populations was acknowledged for determining optimal fluvoxamine-dosing strategies based on the CYP2D6 phenotype.

The fluvoxamine model indicated the necessity for dose increments in pregnant women, particularly with the UM and EM populations. In addition, the PBPK model demonstrates the advantages of phenotype testing prior to initiation of selective serotonin reuptake inhibitors (SSRI) such as fluvoxamine, potentially assisting the physician in deciding the appropriate dosing regimen throughout the gestational period for better mental health management in pregnant women. While the methodologically robust framework implemented in the development and validation of the models to predict the optimal perinatal dosing strategy for fluvoxamine, it is essential to validate the dosing recommendation in a confirmatory trial, thus

improving the confidence of utilising the mechanistic modelling approach in predicting a precise dose in pregnant women population considering the enzyme phenotype status.

In the second part of this thesis, the focus shifted to the impact of the physiological changes in the adult cancer obese population on imatinib concentration and assessed the TDM-guided dosing adjustment strategy to recover the imatinib through concentration into the target level. Employing the PBPK modelling, the imatinib model was validated to predict the plasma concentration in healthy adults, adult cancer and Caucasian populations with observed data from 10 published studies. Moreover, the model was verified to simulate imatinib concentrations in lean, overweight and obese cancer populations with data from a study.

Assessment in terms of physiological diversity between the three populations based on the simulated demographic cancer population revealed significant differences between obese and lean populations in 12 out of 14 physiological parameters reviewed in this chapter, including body weight, body surface area (BSA), liver weight, cardiac output, serum creatinine, GFR, CYP3A4 and CYP2C8 metabolism enzyme abundances as well as ABCB1 and ABCG2 transporter abundances. The physiological differences led to substantial differences between obese and lean cancer populations, with respect to the pharmacokinetic parameters such as maximum concentration (C_{max}) and area-under-the-curve (AUC) but not the trough concentrations (C_{min}). Nevertheless, the percentage of subjects with C_{min} below the lower threshold of 750 ng/mL was highest in the obese cancer population, followed by overweight, then lean. Therefore, the performance of the TDM-guided dose adjustment was assessed in recovering the subjects with C_{min} outside the recommended C_{min} level back into the target concentration of 750 ng/mL – 1,500 ng/mL.

Simulated virtual clinical trials successfully demonstrated the ability of TDM-guided imatinib dose adjustment to recover the subjects with C_{min} outside the target range back within the aimed concentration level for all three population groups, particularly in the case of virtual subjects exhibiting trough concentrations exceeding 450 ng/mL. Thus, the PBPK model was able to address the physiological and pharmacokinetic differences between the lean, overweight and obese cancer populations and revealed that the same TDM-guided imatinib dosage adjustment scheme was applicable to the lean, overweight, and obese cancer populations in order to attain the target concentration.

The last part of this thesis deals with the paediatric obesity population as a special population and focuses on the impact of obesity on drug pharmacokinetics in paediatric patients, with a case study of optimising the amlodipine dose in the population. With the PBPK framework, the paediatric population model was successfully developed and validated, particularly the six relevant physiological parameters aligned with observed data from several publications.

Furthermore, the ability of the paediatric obesity model to simulate pharmacokinetic profiles was validated with the metformin, ceftazidime, and amlodipine compounds. Comparison of the predicted pharmacokinetic parameters and profiles were made with observed pharmacokinetic data from seven published studies for metformin consisting of healthy subjects, obese adults, paediatric subjects and paediatric obesity subjects, one study for ceftazidime involving both paediatric with and without obesity, and nine studies for amlodipine consisting of healthy adults, obese adults as well as paediatric with and without obesity subjects.

With amlodipine as a case study, the model shows that the physiological changes in paediatric obesity led to significant differences in both C_{max} and AUC between paediatric subjects with and without obesity across the age range of 2 to 18 years old when the subjects were dosed with a fixed dose regimen. However, no difference was observed when administered with the weight-based dosing regimen. Therefore, the obese children required a 1.25 – 1.5-fold higher dose in order to attain a comparable C_{max} as non-obese paediatric when opting for a fixed-dose regimen.

This chapter highlights the capabilities of the paediatric obesity population model to reproduce the observed pharmacokinetic data for metformin, ceftazidime and amlodipine compounds. Moreover, the model was able to discriminate the amlodipine pharmacokinetic concentrations between obese and non-obese paediatrics and identified the optimum dose for the paediatric obesity population to achieve the same exposure as non-obese.

In summary, this thesis effectively showcases the utilisation of PBPK modelling and simulation to address the influence of physiological changes in special populations on the pharmacokinetic parameters. In addition, this thesis further demonstrates the extent of the PBPK approach in exploring the optimal dose for special populations from the pharmacokinetic perspective.

5.2 Future work

The effectiveness of PBPK modelling in comprehensively elucidating the influence of physiological changes in special populations on the drug pharmacokinetics, identifying the difference in terms of pharmacokinetics, and compensating it through dosage modification was demonstrated throughout these three novel projects. Nevertheless, specific dimensions of the population models can be further elaborated and refined. These parts include:

- The influence of CYP metabolism enzyme polymorphism in pregnant women on drug pharmacokinetics was demonstrated in the first part of this thesis, combined with the changes in enzyme activities throughout the gestational period elevated the challenges to provide an informed decision regarding the efficacious dose. Therefore, future work can focus on generating robust and validated CYP metabolism enzyme polymorphism activities in the pregnant women population to be incorporated into the population model.
- Physiological changes that occurred in obese cancer populations have been observed to alter the drug pharmacokinetics in Chapter 3 of this thesis. Nevertheless, information on the changes in CYP metabolism enzymes, transporters, and protein binding demands further in-depth investigation since the data on the changes in both cancer and obese populations was still limited. Thus, it warrants further research for the development of a specific population model for obese cancer.
- The influence of obesity on the paediatric population was observed in Chapter 4, which necessitates a dose adjustment in order to attain the same exposure as non-obese children. Thus, future research can focus on the changes in various CYP metabolism enzymes in obese children as they evolve over the age group, particularly the primary metabolism enzyme involved in drug metabolism and clearance.

References

1. Connor, L., et al., *Evidence-based practice improves patient outcomes and healthcare system return on investment: Findings from a scoping review*. *Worldviews Evid Based Nurs*, 2023. **20**(1): p. 6-15.
2. Powell, J.R., et al., *Drug Dosing Recommendations for All Patients: A Roadmap for Change*. *Clin Pharmacol Ther*, 2021. **109**(1): p. 65-72.
3. Grimsrud, K.N., et al., *Special population considerations and regulatory affairs for clinical research*. *Clin Res Regul Aff*, 2015. **32**(2): p. 47-56.
4. European Medicines Agency. *Scientific guidelines with SmPC recommendations*. 2024 [cited 2024 6 March 2024]; Available from: https://www.ema.europa.eu/en/documents/other/scientific-guidelines-summary-product-characteristics-recommendations_en.pdf.
5. The Medicines and Healthcare products Regulatory Agency. *Guidance, Medicines: packaging, labelling and patient information leaflets*. 2014 22 December 2023 [cited 2024; Available from: <https://www.gov.uk/guidance/medicines-packaging-labelling-and-patient-information-leaflets>.
6. The United States Food and Drug Administration. *Pregnancy and lactation labeling (Drugs) final rule*. 2014 16 November 2021]; Available from: <https://www.fda.gov/drugs/labeling-information-drug-products/pregnancy-and-lactation-labeling-drugs-final-rule>.
7. Guerra-Farfan, E., et al., *Clinical practice guidelines: The good, the bad, and the ugly*. *Injury*, 2023. **54 Suppl 3**: p. S26-S29.
8. Busse, R., et al., *Improving healthcare quality in Europe : characteristics, effectiveness and implementation of different strategies*. Health policy series (European Observatory on Health Systems and Policies) 53. 2019, Paris: OECD Publishing.
9. Molenaar, N.M., et al., *Guidelines on treatment of perinatal depression with antidepressants: An international review*. *Aust N Z J Psychiatry*, 2018. **52**(4): p. 320-327.
10. Griggs, J.J., et al., *Appropriate Systemic Therapy Dosing for Obese Adult Patients With Cancer: ASCO Guideline Update*. *J Clin Oncol*, 2021. **39**(18): p. 2037-2048.
11. Bartelink, I.H., et al., *Guidelines on paediatric dosing on the basis of developmental physiology and pharmacokinetic considerations*. *Clin Pharmacokinet*, 2006. **45**(11): p. 1077-97.
12. Tully, L., et al., *Guidelines for treating child and adolescent obesity: A systematic review*. *Front Nutr*, 2022. **9**: p. 902865.
13. Johnston, B.C., et al., *Updating the Canadian clinical practice guideline for managing pediatric obesity: a protocol*. *CMAJ Open*, 2022. **10**(1): p. E155-E164.
14. Winter, S.S., et al., *Inclusion of special populations in clinical research: important considerations and guidelines*. *J Clin Transl Res*, 2018. **4**(1): p. 56-69.
15. Harnisch, L., et al., *Modeling and simulation as a tool to bridge efficacy and safety data in special populations*. *CPT Pharmacometrics Syst Pharmacol*, 2013. **2**(2): p. e28.
16. Sime, F.B., M.S. Roberts, and J.A. Roberts, *Optimization of dosing regimens and dosing in special populations*. *Clin Microbiol Infect*, 2015. **21**(10): p. 886-93.
17. Krekels, E.H.J., et al., *Evidence-based drug treatment for special patient populations through model-based approaches*. *Eur J Pharm Sci*, 2017. **109S**: p. S22-S26.
18. Hajjar, J., J. Fisher, and M. Gastonguay, *Trends in the application of pharmacometric modeling and simulation in the development of orphan drugs in the 21st century*. *Journal of Pharmacokinetics and Pharmacodynamics*, 2015. **42**: p. S72-S73.
19. Zhang, X., et al., *Application of PBPK modeling and simulation for regulatory decision making and its impact on US Prescribing Information: An update on the 2018-2019 submissions to the US FDA's Office of Clinical Pharmacology*. *J Clin Pharmacol*, 2020. **60 Suppl 1**: p. S160-S178.

20. Grimstein, M., et al., *Physiologically based pharmacokinetic modeling in regulatory science: An update from the U.S. Food and Drug Administration's Office of Clinical Pharmacology*. J Pharm Sci, 2019. **108**(1): p. 21-25.
21. Liu, Q., et al., *Clinical pharmacology regulatory sciences in drug development and precision medicine: Current status and emerging trends*. AAPS J, 2021. **23**(3): p. 54.
22. The United States Food and Drug Administration. *PDUFA reauthorization performance goals and procedures fiscal years 2018 through 2022*. 2017 13 December 2021]; Available from: <https://www.fda.gov/media/99140/download>.
23. Kim, T.H., S. Shin, and B.S. Shin, *Model-based drug development: application of modeling and simulation in drug development*. Journal of Pharmaceutical Investigation, 2018. **48**(4): p. 431-441.
24. Charles, B., *Population pharmacokinetics: an overview*. Australian Prescriber, 2014. **37**(6): p. 210-213.
25. Ette, E.I. and P.J. Williams, *Population pharmacokinetics I: background, concepts, and models*. Ann Pharmacother, 2004. **38**(10): p. 1702-6.
26. Kiang, T.K., et al., *Fundamentals of population pharmacokinetic modelling : modelling and software*. Clin Pharmacokinet, 2012. **51**(8): p. 515-525.
27. Jones, H. and K. Rowland-Yeo, *Basic concepts in physiologically based pharmacokinetic modeling in drug discovery and development*. CPT Pharmacometrics Syst Pharmacol, 2013. **2**: p. e63.
28. The United States Food and Drug Administration. *Population pharmacokinetics: Guidance for industry (Draft guidance)*. 2019 July 2019 [cited 2021 3 December 2021]; Available from: <https://www.fda.gov/media/128793/download>.
29. Ette, E.I. and P.J. Williams, *Population pharmacokinetics II: estimation methods*. Ann Pharmacother, 2004. **38**(11): p. 1907-15.
30. European Medicines Agency. *Guideline on the clinical investigation of the pharmacokinetics of therapeutic proteins*. 2007 22 December 2021]; Available from: https://www.ema.europa.eu/en/documents/scientific-guideline/guideline-clinical-investigation-pharmacokinetics-therapeutic-proteins_en.pdf.
31. European Medicines Agency. *Guideline on the Investigation of Bioequivalence*. 2010 1 August 2010 26 November 2011]; Available from: https://www.ema.europa.eu/en/documents/scientific-guideline/guideline-investigation-bioequivalence-rev1_en.pdf.
32. The United States Food and Drug Administration. *Bioavailability and bioequivalence studies submitted in NDAs or INDs - General consideration: Guidance for industry (Draft guidance)* 2014 22 December 2021]; Available from: <https://www.fda.gov/files/drugs/published/Bioavailability-and-Bioequivalence-Studies-Submitted-in-NDAs-or-INDs-%E2%80%94-General-Considerations.pdf>.
33. Gillespie, W.R., *Noncompartmental versus compartmental modelling in clinical pharmacokinetics*. Clin Pharmacokinet, 1991. **20**(4): p. 253-62.
34. Rosenbaum, S., *Basic pharmacokinetics and pharmacodynamics : an integrated textbook and computer simulations*. 2017, John Wiley & Sons, Inc.,: Hoboken, New Jersey. p. 1 online resource.
35. Rowland, M. and T.N. Tozer, *Clinical pharmacokinetics : concepts and applications*. 3rd ed. 1995, Baltimore: Williams & Wilkins. xiv, 601 p.
36. Shargel, L. and A.B.C. Yu, *Applied biopharmaceutics & pharmacokinetics*. Seventh edition. ed. 2016, New York: McGraw-Hill Education. xvii, 910 pages.
37. Huang, S.M., et al., *Atkinson's principles of clinical pharmacology*. 4. ed. 2021, Waltham: Elsevier. pages cm.
38. Owen, J.S. and J. Fiedler-Kelly, *Introduction to population pharmacokinetic/pharmacodynamic analysis with nonlinear mixed effects models*. 2014, Wiley,: Hoboken, New Jersey. p. 1 online resource.
39. Bischoff, K.B., et al., *Methotrexate pharmacokinetics*. J Pharm Sci, 1971. **60**(8): p. 1128-33.

40. Rowland, M., C. Peck, and G. Tucker, *Physiologically-based pharmacokinetics in drug development and regulatory science*. Annu Rev Pharmacol Toxicol, 2011. **51**: p. 45-73.
41. Peters, S.A., *Physiologically based pharmacokinetic (PBPK) modeling and simulations : principles, methods, and applications in the pharmaceutical industry*. 2021, Wiley,: Hoboken, NJ. p. 1 online resource.
42. Brown, R.P., et al., *Physiological parameter values for physiologically based pharmacokinetic models*. Toxicol Ind Health, 1997. **13**(4): p. 407-84.
43. Abduljalil, K., et al., *Anatomical, physiological and metabolic changes with gestational age during normal pregnancy: a database for parameters required in physiologically based pharmacokinetic modelling*. Clin Pharmacokinet, 2012. **51**(6): p. 365-96.
44. Price, P.S., et al., *Modeling interindividual variation in physiological factors used in PBPK models of humans*. Crit Rev Toxicol, 2003. **33**(5): p. 469-503.
45. Thompson, C.M., et al., *Database for physiologically based pharmacokinetic (PBPK) modeling: physiological data for healthy and health-impaired elderly*. J Toxicol Environ Health B Crit Rev, 2009. **12**(1): p. 1-24.
46. Jones, H.M., et al., *A novel strategy for physiologically based predictions of human pharmacokinetics*. Clin Pharmacokinet, 2006. **45**(5): p. 511-42.
47. Jones, H.M., et al., *Simulation of human intravenous and oral pharmacokinetics of 21 diverse compounds using physiologically based pharmacokinetic modelling*. Clinical Pharmacokinetics, 2011. **50**(5): p. 331-347.
48. Edginton, A.N. and S. Willmann, *Physiology-based simulations of a pathological condition prediction of pharmacokinetics in patients with liver cirrhosis*. Clinical Pharmacokinetics, 2008. **47**(11): p. 743-752.
49. Rowland Yeo, K., et al., *Modeling and predicting drug pharmacokinetics in patients with renal impairment*. Expert Review of Clinical Pharmacology, 2011. **4**(2): p. 261-274.
50. Johnson, T.N., et al., *A best practice framework for applying physiologically-based pharmacokinetic modeling to pediatric drug development*. CPT Pharmacometrics Syst Pharmacol, 2021. **10**(9): p. 967-972.
51. Abduljalil, K. and R.K.S. Badhan, *Drug dosing during pregnancy-opportunities for physiologically based pharmacokinetic models*. J Pharmacokinet Pharmacodyn, 2020. **47**(4): p. 319-340.
52. Jamei, M., G.L. Dickinson, and A. Rostami-Hodjegan, *A Framework for assessing inter-individual variability in pharmacokinetics using virtual human populations and integrating general knowledge of physical chemistry, biology, anatomy, physiology and genetics: A tale of 'Bottom-Up' vs 'Top-Down' recognition of covariates (vol 24, pg 53, 2009)*. Drug Metabolism and Pharmacokinetics, 2009. **24**(5): p. 488-488.
53. Lennernas, H., *Human intestinal permeability*. Journal of Pharmaceutical Sciences, 1998. **87**(4): p. 403-410.
54. Sun, D.X., et al., *Comparison of human duodenum and Caco-2 gene expression profiles for 12,000 gene sequences tags and correlation with permeability of 26 drugs*. Pharmaceutical Research, 2002. **19**(10): p. 1400-1416.
55. Winiwarter, S., et al., *Correlation of human jejunal permeability (in vivo) of drugs with experimentally and theoretically derived parameters. A multivariate data analysis approach*. Journal of Medicinal Chemistry, 1998. **41**(25): p. 4939-4949.
56. Jones, H.M., et al., *Predicting pharmacokinetic food effects using biorelevant solubility media and physiologically based modelling*. Clinical Pharmacokinetics, 2006. **45**(12): p. 1213-1226.
57. Parrott, N., et al., *Predicting pharmacokinetics of drugs using physiologically based modeling-application to food effects*. Aaps Journal, 2009. **11**(1): p. 45-53.
58. Blakey, G.E., et al., *Quantitative structure-pharmacokinetics relationships: I. Development of a whole-body physiologically based model to characterize changes in pharmacokinetics across a homologous series of barbiturates in the rat*. Journal of Pharmacokinetics and Biopharmaceutics, 1997. **25**(3): p. 277-312.

59. Poulin, P. and F.P. Theil, *Prediction of pharmacokinetics prior to in vivo studies. 1. Mechanism-based prediction of volume of distribution*. Journal of Pharmaceutical Sciences, 2002. **91**(1): p. 129-156.
60. Rodgers, T. and M. Rowland, *Physiologically based pharmacokinetic modelling 2: predicting the tissue distribution of acids, very weak bases, neutrals and zwitterions*. J Pharm Sci, 2006. **95**(6): p. 1238-57.
61. Schmitt, W., *General approach for the calculation of tissue to plasma partition coefficients*. Toxicol In Vitro, 2008. **22**(2): p. 457-67.
62. Poulin, P. and F.P. Theil, *Development of a novel method for predicting human volume of distribution at steady-state of basic drugs and comparative assessment with existing methods*. Journal of Pharmaceutical Sciences, 2009. **98**(12): p. 4941-4961.
63. Donato, M.T., et al., *Cell lines: a tool for in vitro drug metabolism studies*. Curr Drug Metab, 2008. **9**(1): p. 1-11.
64. Hallifax, D., J.A. Foster, and J.B. Houston, *Prediction of human metabolic clearance from in vitro systems: retrospective analysis and prospective view*. Pharm Res, 2010. **27**(10): p. 2150-61.
65. Shiran, M.R., et al., *Prediction of metabolic drug clearance in humans: in vitro-in vivo extrapolation vs allometric scaling*. Xenobiotica, 2006. **36**(7): p. 567-80.
66. Mahmood, I., *Interspecies scaling of biliary excreted drugs: prediction of human clearance and volume of distribution*. Drug Metabol Drug Interact, 2012. **27**(3): p. 157-64.
67. Paine, S.W., et al., *Prediction of human renal clearance from preclinical species for a diverse set of drugs that exhibit both active secretion and net reabsorption*. Drug Metab Dispos, 2011. **39**(6): p. 1008-13.
68. Jones, H.M., et al., *Mechanistic pharmacokinetic modeling for the prediction of transporter-mediated disposition in humans from sandwich culture human hepatocyte data*. Drug Metabolism and Disposition, 2012. **40**(5): p. 1007-1017.
69. Khalil, F. and S. Laer, *Physiologically based pharmacokinetic modeling: methodology, applications, and limitations with a focus on its role in pediatric drug development*. J Biomed Biotechnol, 2011. **2011**: p. 907461.
70. Sager, J.E., et al., *Physiologically based pharmacokinetic (PBPK) modeling and simulation approaches: A systematic review of published models, applications, and model verification*. Drug Metab Dispos, 2015. **43**(11): p. 1823-37.
71. Lin, Z., et al., *Performance assessment and translation of physiologically based pharmacokinetic models from acsIX to Berkeley Madonna, MATLAB, and R Language: Oxytetracycline and gold nanoparticles as case examples*. Toxicol Sci, 2017. **158**(1): p. 23-35.
72. Reali, F., et al., *A minimal PBPK model to accelerate preclinical development of drugs against tuberculosis*. Front Pharmacol, 2023. **14**: p. 1272091.
73. Rostami, A.A., et al., *A comprehensive physiologically based pharmacokinetic (PBPK) model for nicotine in humans from using nicotine-containing products with different routes of exposure*. Sci Rep, 2022. **12**(1): p. 1091.
74. El-Khateeb, E., et al., *Physiological-based pharmacokinetic modeling trends in pharmaceutical drug development over the last 20-years; in-depth analysis of applications, organizations, and platforms*. Biopharm Drug Dispos, 2021. **42**(4): p. 107-117.
75. Krstevska, A., et al., *In-Depth Analysis of Physiologically Based Pharmacokinetic (PBPK) Modeling Utilization in Different Application Fields Using Text Mining Tools*. Pharmaceutics, 2022. **15**(1).
76. Johnson, T.N., B.G. Small, and K. Rowland Yeo, *Increasing application of pediatric physiologically based pharmacokinetic models across academic and industry organizations*. CPT Pharmacometrics Syst Pharmacol, 2022. **11**(3): p. 373-383.
77. Sinha, V.K., et al., *From preclinical to human--prediction of oral absorption and drug-drug interaction potential using physiologically based pharmacokinetic (PBPK)*

- modeling approach in an industrial setting: a workflow by using case example.* Biopharm Drug Dispos, 2012. **33**(2): p. 111-21.
78. Chen, Y., et al., *Application of IVIVE and PBPK modeling in prospective prediction of clinical pharmacokinetics: strategy and approach during the drug discovery phase with four case studies.* Biopharm Drug Dispos, 2012. **33**(2): p. 85-98.
 79. Shi, J.G., et al., *Predicting drug-drug interactions involving multiple mechanisms using physiologically based pharmacokinetic modeling: a case study with ruxolitinib.* Clin Pharmacol Ther, 2015. **97**(2): p. 177-85.
 80. Johnson, T.N., et al., *Use of a physiologically based pharmacokinetic-pharmacodynamic model for initial dose prediction and escalation during a paediatric clinical trial.* Br J Clin Pharmacol, 2021. **87**(3): p. 1378-1389.
 81. Zhao, P., et al., *Evaluation of exposure change of nonrenally eliminated drugs in patients with chronic kidney disease using physiologically based pharmacokinetic modeling and simulation.* J Clin Pharmacol, 2012. **52**(1 Suppl): p. 91S-108S.
 82. Wu, F., et al., *Using Mechanistic Modeling Approaches to Support Bioequivalence Assessments for Oral Products.* AAPS J, 2024. **26**(1): p. 19.
 83. Liu, F., et al., *Characterization of preclinical in vitro and in vivo ADME properties and prediction of human PK using a physiologically based pharmacokinetic model for YQA-14, a new dopamine D3 receptor antagonist candidate for treatment of drug addiction.* Biopharm Drug Dispos, 2014. **35**(5): p. 296-307.
 84. Bungay, P.J., et al., *Preclinical and clinical pharmacokinetics of PF-02413873, a nonsteroidal progesterone receptor antagonist.* Drug Metab Dispos, 2011. **39**(8): p. 1396-405.
 85. Suri, A., et al., *Physiologically based and population PK modeling in optimizing drug development: A predict-learn-confirm analysis.* Clin Pharmacol Ther, 2015. **98**(3): p. 336-44.
 86. Samineni, D., et al., *Physiologically based pharmacokinetic model-informed drug development for polatuzumab vedotin: Label for drug-drug interactions without dedicated clinical trials.* J Clin Pharmacol, 2020. **60** Suppl 1: p. S120-S131.
 87. Alenezi, M. and R.K.S. Badhan, *Precision dosing of venlafaxine during pregnancy: a pharmacokinetics modelling approach.* J Pharm Pharmacol, 2024. **76**(2): p. 122-137.
 88. Bonner, J.J., et al., *Development and verification of an endogenous PBPK model to inform hydrocortisone replacement dosing in children and adults with cortisol deficiency.* Eur J Pharm Sci, 2021. **165**: p. 105913.
 89. Luzon, E., et al., *Physiologically based pharmacokinetic modeling in regulatory decision-making at the European Medicines Agency.* Clin Pharmacol Ther, 2017. **102**(1): p. 98-105.
 90. European Medicines Agency. *Guideline on the reporting of physiologically based pharmacokinetic (PBPK) modelling and simulation.* 2018 13 December 2018 29 November 2021]; Available from: https://www.ema.europa.eu/en/documents/scientific-guideline/guideline-reporting-physiologically-based-pharmacokinetic-pbpbk-modelling-simulation_en.pdf.
 91. Zhao, P., *Report from the EMA workshop on qualification and reporting of physiologically based pharmacokinetic (PBPK) modeling and simulation.* CPT Pharmacometrics Syst Pharmacol, 2017. **6**(2): p. 71-72.
 92. Certara. *PBPK's pivotal role in modern drug development: Busting common myths and misconceptions.* 2019 31 December 2021]; Available from: <https://www.certara.com/app/uploads/2020/07/PBPKs-Pivotal-Role-in-Modern-Drug-Development.pdf>.
 93. The United States Food and Drug Administration. *Pre-ANDA program & complex generic products.* 2017 [cited 6 January 2022; Available from: <https://www.fda.gov/industry/generic-drug-user-fee-amendments/pre-anda-program-complex-generic-products>.
 94. Tsakalozou, E., A. Babiskin, and L. Zhao, *Physiologically-based pharmacokinetic modeling to support bioequivalence and approval of generic products: A case for*

- diclofenac sodium topical gel*, 1. CPT Pharmacometrics Syst Pharmacol, 2021. **10**(5): p. 399-411.
95. The Medicines & Healthcare products Regulatory Agency United Kingdom. *MHRA and the Bill & Melinda Gates Foundation to look at the safer, effective use of medicines during pregnancy*. 2019 6 January 2022]; Available from: <https://www.gov.uk/government/news/mhra-and-the-bill-melinda-gates-foundation-to-look-at-the-safer-effective-use-of-medicines-during-pregnancy>.
 96. Cole, S., et al., *Pharmacokinetic characterization to enable medicine use in pregnancy, the potential role of physiologically-based pharmacokinetic modelling: A regulatory perspective*. CPT Pharmacometrics Syst Pharmacol, 2020. **9**(10): p. 547-549.
 97. Coppola, P., E. Kerwash, and S. Cole, *Physiologically based pharmacokinetics model in pregnancy: A regulatory perspective on model evaluation*. Front Pediatr, 2021. **9**: p. 687978.
 98. Sato, M., et al., *Quantitative modeling and simulation in PMDA: A Japanese regulatory perspective*. CPT Pharmacometrics Syst Pharmacol, 2017. **6**(7): p. 413-415.
 99. The Pharmaceuticals and Medical Devices Agency. *Guidelines for analysis reports involving physiologically based pharmacokinetic models*. 2020 [cited 6 January 2022; Available from: <https://www.pmda.go.jp/files/000239317.pdf>.
 100. Kijima, S., *Quantitative modelling and simulation (M&S) and model-informed drug Development (MIDD) in pharmaceuticals and medical devices agency (PMDA): Activity and perspective*. 2021.
 101. The International Council for Harmonisation of Technical Requirements for Pharmaceuticals for Human Use (ICH). *Considerations with respect to future to future MIDD related guidelines*. 2022 [cited 2024 10 Macrh 2024]; Available from: https://database.ich.org/sites/default/files/ICH_MIDD_Roadmap_2022_0503.pdf.
 102. The International Council for Harmonisation of Technical Requirements for Pharmaceuticals for Human Use (ICH). *Final Concept Paper, M15: Model-Informed Drug Development General Principles Guideline*. 2022 [cited 2024 10 March 2024]; Available from: https://database.ich.org/sites/default/files/ICH_M15_ConceptPaper_Final_2022_1102.pdf.
 103. Abduljalil, K., A. Pansari, and M. Jamei, *Prediction of maternal pharmacokinetics using physiologically based pharmacokinetic models: assessing the impact of the longitudinal changes in the activity of CYP1A2, CYP2D6 and CYP3A4 enzymes during pregnancy*. J Pharmacokinet Pharmacodyn, 2020. **47**(4): p. 361-383.
 104. Feghali, M., R. Venkataramanan, and S. Caritis, *Pharmacokinetics of drugs in pregnancy*. Semin Perinatol, 2015. **39**(7): p. 512-9.
 105. Gaohua, L., et al., *A pregnancy physiologically based pharmacokinetic (p-PBPK) model for disposition of drugs metabolized by CYP1A2, CYP2D6 and CYP3A4*. Br J Clin Pharmacol, 2012. **74**(5): p. 873-85.
 106. Tasnif, Y., J. Morado, and M.F. Hebert, *Pregnancy-related pharmacokinetic changes*. Clin Pharmacol Ther, 2016. **100**(1): p. 53-62.
 107. Mattison, D. and L.-A. Halbert, *Clinical pharmacology during pregnancy*. 2. ed. 2021, SanDiego: Elsevier. pages cm.
 108. Dallmann, A., et al., *Applied concepts in PBPK modeling: How to extend an Open Systems Pharmacology model to the special population of pregnant women*. Cpt-Pharmacometrics & Systems Pharmacology, 2018. **7**(7): p. 419-431.
 109. Xia, B., et al., *A simplified PBPK modeling approach for prediction of pharmacokinetics of four primarily renally excreted and CYP3A metabolized compounds during pregnancy*. AAPS J, 2013. **15**(4): p. 1012-24.
 110. Le Merdy, M., et al., *PBPK Modeling Approach to Predict the Behavior of Drugs Cleared by Metabolism in Pregnant Subjects and Fetuses*. Pharmaceutics, 2024. **16**(1).
 111. Chaphekar, N., S. Caritis, and R. Venkataramanan, *Model-informed dose optimization in pregnancy*. J Clin Pharmacol, 2020. **60 Suppl 1**: p. S63-S76.
 112. World Obesity Federation, *World Obesity Atlas 2023*. 2023.

113. Collaborators, G.B.D.O., et al., *Health Effects of Overweight and Obesity in 195 Countries over 25 Years*. N Engl J Med, 2017. **377**(1): p. 13-27.
114. Kivimaki, M., et al., *Body-mass index and risk of obesity-related complex multimorbidity: an observational multicohort study*. Lancet Diabetes Endocrinol, 2022. **10**(4): p. 253-263.
115. Pati, S., et al., *Obesity and Cancer: A Current Overview of Epidemiology, Pathogenesis, Outcomes, and Management*. Cancers (Basel), 2023. **15**(2).
116. Sung, H., et al., *Global Cancer Statistics 2020: GLOBOCAN Estimates of Incidence and Mortality Worldwide for 36 Cancers in 185 Countries*. CA Cancer J Clin, 2021. **71**(3): p. 209-249.
117. Meng, L., et al., *Comprehensive guidance for antibiotic dosing in obese adults: 2022 update*. Pharmacotherapy, 2023. **43**(3): p. 226-246.
118. Barras, M. and A. Legg, *Drug dosing in obese adults*. Aust Prescr, 2017. **40**(5): p. 189-193.
119. Perreault, S., et al., *Evaluating a voriconazole dose modification guideline to optimize dosing in patients with hematologic malignancies*. J Oncol Pharm Pract, 2019. **25**(6): p. 1305-1311.
120. Paice, J.A., et al., *Use of Opioids for Adults With Pain From Cancer or Cancer Treatment: ASCO Guideline*. J Clin Oncol, 2023. **41**(4): p. 914-930.
121. Khorana, A.A., *Cancer and thrombosis: implications of published guidelines for clinical practice*. Ann Oncol, 2009. **20**(10): p. 1619-30.
122. Chau, M.M., et al., *Consensus guidelines for optimising antifungal drug delivery and monitoring to avoid toxicity and improve outcomes in patients with haematological malignancy, 2014*. Intern Med J, 2014. **44**(12b): p. 1364-88.
123. Blouin, R.A., J.H. Kolpek, and H.J. Mann, *Influence of obesity on drug disposition*. Clin Pharm, 1987. **6**(9): p. 706-14.
124. Ghobadi, C., et al., *Application of a systems approach to the bottom-up assessment of pharmacokinetics in obese patients: expected variations in clearance*. Clin Pharmacokinet, 2011. **50**(12): p. 809-22.
125. Cheeti, S., et al., *A physiologically based pharmacokinetic (PBPK) approach to evaluate pharmacokinetics in patients with cancer*. Biopharm Drug Dispos, 2013. **34**(3): p. 141-54.
126. Griggs, J.J., et al., *Appropriate Chemotherapy Dosing for Obese Adult Patients With Cancer: American Society of Clinical Oncology Clinical Practice Guideline*. J Oncol Pract, 2012. **8**(4): p. e59-e61.
127. Silvestris, N., et al., *Antineoplastic dosing in overweight and obese cancer patients: an Associazione Italiana Oncologia Medica (AIOM)/Associazione Medici Diabetologi (AMD)/Societa Italiana Endocrinologia (SIE)/Societa Italiana Farmacologia (SIF) multidisciplinary consensus position paper*. ESMO Open, 2021. **6**(3): p. 100153.
128. Grigg, A., M.H. Harun, and J. Szer, *Variability in determination of body weight used for dosing busulphan and cyclophosphamide in adult patients: results of an international survey*. Leuk Lymphoma, 1997. **25**(5-6): p. 487-91.
129. Field, K.M., et al., *Chemotherapy dosing strategies in the obese, elderly, and thin patient: results of a nationwide survey*. J Oncol Pract, 2008. **4**(3): p. 108-13.
130. Takahashi, T., et al., *Comparison of Dose Adjustment Strategies for Obesity in High-dose Cyclophosphamide Among Adult Hematopoietic Cell Transplantation Recipients: Pharmacokinetic Analysis*. Transplant Cell Ther, 2022. **28**(12): p. 845 e1-845 e8.
131. Shem-Tov, N., et al., *Chemotherapy dose adjustment for obese patients undergoing hematopoietic stem cell transplantation: a survey on behalf of the Acute Leukemia Working Party of the European Society for Blood and Marrow Transplantation*. Oncologist, 2015. **20**(1): p. 50-5.
132. Launay-Vacher, V., et al., *Prevalence of Renal Insufficiency in cancer patients and implications for anticancer drug management: the renal insufficiency and anticancer medications (IRMA) study*. Cancer, 2007. **110**(6): p. 1376-84.

133. Janus, N., et al., *Cancer and renal insufficiency results of the BIRMA study*. Br J Cancer, 2010. **103**(12): p. 1815-21.
134. Schwenger, E., et al., *Harnessing Meta-analysis to Refine an Oncology Patient Population for Physiology-Based Pharmacokinetic Modeling of Drugs*. Clin Pharmacol Ther, 2018. **103**(2): p. 271-280.
135. Frayn, K.N. and F. Karpe, *Regulation of human subcutaneous adipose tissue blood flow*. Int J Obes (Lond), 2014. **38**(8): p. 1019-26.
136. Hanley, M.J., D.R. Abernethy, and D.J. Greenblatt, *Effect of obesity on the pharmacokinetics of drugs in humans*. Clin Pharmacokinet, 2010. **49**(2): p. 71-87.
137. Oie, S., *Drug distribution and binding*. J Clin Pharmacol, 1986. **26**(8): p. 583-6.
138. Mansoor, A. and N. Mahabadi, *Volume of Distribution*, in *StatPearls*. 2023: Treasure Island (FL).
139. Peng, B., P. Lloyd, and H. Schran, *Clinical pharmacokinetics of imatinib*. Clin Pharmacokinet, 2005. **44**(9): p. 879-94.
140. Giraud, E.L., et al., *Dose recommendations for anticancer drugs in patients with renal or hepatic impairment: an update*. Lancet Oncol, 2023. **24**(6): p. e229.
141. Chagnac, A., et al., *Glomerular hemodynamics in severe obesity*. Am J Physiol Renal Physiol, 2000. **278**(5): p. F817-22.
142. Chagnac, A., et al., *Obesity-induced glomerular hyperfiltration: its involvement in the pathogenesis of tubular sodium reabsorption*. Nephrol Dial Transplant, 2008. **23**(12): p. 3946-52.
143. International Council for Harmonisation of Technical Requirements for Pharmaceuticals for Human Use. *Addendum to ICH E11: Clinical investigation of medicinal products in the pediatric population E11 (R1)*. 2017 3 December 2012]; 18 August 2017:[Available from: https://database.ich.org/sites/default/files/E11_R1_Addendum.pdf.
144. Edginton, A.N., W. Schmitt, and S. Willmann, *Development and evaluation of a generic physiologically based pharmacokinetic model for children*. Clin Pharmacokinet, 2006. **45**(10): p. 1013-34.
145. Johnson, T.N. and A. Rostami-Hodjegan, *Resurgence in the use of physiologically based pharmacokinetic models in pediatric clinical pharmacology: parallel shift in incorporating the knowledge of biological elements and increased applicability to drug development and clinical practice*. Paediatr Anaesth, 2011. **21**(3): p. 291-301.
146. Bouzom, F., et al., *Physiologically based pharmacokinetic (PBPK) modelling tools: how to fit with our needs?* Biopharm Drug Dispos, 2012. **33**(2): p. 55-71.
147. Parrott, N., et al., *Development of a physiologically based model for oseltamivir and simulation of pharmacokinetics in neonates and infants*. Clin Pharmacokinet, 2011. **50**(9): p. 613-23.
148. Bi, Y., et al., *Role of model-informed drug development in pediatric drug development, regulatory evaluation, and labeling*. J Clin Pharmacol, 2019. **59** Suppl 1: p. S104-S111.
149. Johnson, T.N., D. Zhou, and K.H. Bui, *Development of physiologically based pharmacokinetic model to evaluate the relative systemic exposure to quetiapine after administration of IR and XR formulations to adults, children and adolescents*. Biopharm Drug Dispos, 2014. **35**(6): p. 341-52.
150. Flynn, J., *The changing face of pediatric hypertension in the era of the childhood obesity epidemic*. Pediatr Nephrol, 2013. **28**(7): p. 1059-66.
151. Di Cesare, M., et al., *The epidemiological burden of obesity in childhood: a worldwide epidemic requiring urgent action*. BMC Med, 2019. **17**(1): p. 212.
152. World Health Organisation (WHO). *Obesity and overweight*. 2021 18 January 2023]; Available from: <https://www.who.int/news-room/fact-sheets/detail/obesity-and-overweight>.
153. Centers for Disease Control and Prevention (CDC). *Defining Childhood Weight Status*. 2022 14 December 2022 [cited 2023 18 January 2023]; Available from: <https://www.cdc.gov/obesity/basics/childhood->

- [defining.html?CDC_AA_refVal=https%3A%2F%2Fwww.cdc.gov%2Fobesity%2Fchildhood%2Fdefining.html](#).
154. Clasey, J.L., et al., *Body mass index percentiles versus body composition assessments: Challenges for disease risk classifications in children*. Front Pediatr, 2023. **11**: p. 1112920.
 155. Vasan, R.S., *Cardiac function and obesity*. Heart, 2003. **89**(10): p. 1127-9.
 156. Gerhart, J.G., et al., *Development and Evaluation of a Virtual Population of Children with Obesity for Physiologically Based Pharmacokinetic Modeling*. Clin Pharmacokinet, 2022. **61**(2): p. 307-320.
 157. Marginean, C.O., et al., *The adipokines and inflammatory status in the era of pediatric obesity*. Cytokine, 2020. **126**: p. 154925.
 158. Gerhart, J.G., et al., *Characterizing Pharmacokinetics in Children With Obesity-Physiological, Drug, Patient, and Methodological Considerations*. Front Pharmacol, 2022. **13**: p. 818726.
 159. Nawaratne, S., et al., *Relationships among liver and kidney volumes, lean body mass and drug clearance*. Br J Clin Pharmacol, 1998. **46**(5): p. 447-52.
 160. Correia-Costa, L., et al., *Normalization of glomerular filtration rate in obese children*. Pediatr Nephrol, 2016. **31**(8): p. 1321-8.
 161. Iyanagi, T., *Molecular mechanism of phase I and phase II drug-metabolizing enzymes: implications for detoxification*. Int Rev Cytol, 2007. **260**: p. 35-112.
 162. Harskamp-van Ginkel, M.W., et al., *Drug Dosing and Pharmacokinetics in Children With Obesity: A Systematic Review*. JAMA Pediatr, 2015. **169**(7): p. 678-85.
 163. Matson, K.L., et al., *Medication Dosage in Overweight and Obese Children*. J Pediatr Pharmacol Ther, 2017. **22**(1): p. 81-83.
 164. Gaeta, F., et al., *Drug dosing in children with obesity: a narrative updated review*. Ital J Pediatr, 2022. **48**(1): p. 168.
 165. Ford, J.L., et al., *Physiologically Based Pharmacokinetic Modeling of Metformin in Children and Adolescents With Obesity*. J Clin Pharmacol, 2022. **62**(8): p. 960-969.
 166. Gerhart, J.G., et al., *Use of physiologically-based pharmacokinetic modeling to inform dosing of the opioid analgesics fentanyl and methadone in children with obesity*. CPT Pharmacometrics Syst Pharmacol, 2022. **11**(6): p. 778-791.
 167. Abduljalil, K., T.N. Johnson, and M. Jamei. *Prediction of Midazolam Concentration Profile in Obese Adolescent Population Using Physiologically Based Pharmacokinetic Model* 2015 [cited 2024 18 March 2024]; Available from: https://www.certara.com/app/uploads/2019/08/Abduljalil_2015_Consortium_Midazolam.pdf.
 168. Gaynes, B.N., et al., *Perinatal depression: prevalence, screening accuracy, and screening outcomes*. Evid Rep Technol Assess (Summ), 2005(119): p. 1-8.
 169. Okagbue, H.I., et al., *Systematic review of prevalence of antepartum depression during the trimesters of pregnancy*. Open Access Maced J Med Sci, 2019. **7**(9): p. 1555-1560.
 170. Bennett, H.A., et al., *Prevalence of depression during pregnancy: systematic review*. Obstet Gynecol, 2004. **103**(4): p. 698-709.
 171. Wichman, C.L. and T.A. Stern, *Diagnosing and treating depression during pregnancy*. Prim Care Companion CNS Disord, 2015. **17**(2).
 172. Hiemke, C., et al., *Consensus guidelines for therapeutic drug monitoring in neuropsychopharmacology: Update 2017*. Pharmacopsychiatry, 2018. **51**(1-02): p. e1.
 173. Andrade, S.E., et al., *Use of antidepressant medications during pregnancy: a multisite study*. American Journal of Obstetrics and Gynecology, 2008. **198**(2).
 174. Molenaar, N.M., et al., *The international prevalence of antidepressant use before, during, and after pregnancy: A systematic review and meta-analysis of timing, type of prescriptions and geographical variability*. J Affect Disord, 2020. **264**: p. 82-89.
 175. Irons, J., *Fluvoxamine in the treatment of anxiety disorders*. Neuropsychiatr Dis Treat, 2005. **1**(4): p. 289-99.

176. Stein, D.J., et al., *Fluvoxamine CR in the long-term treatment of social anxiety disorder: the 12- to 24-week extension phase of a multicentre, randomized, placebo-controlled trial*. International Journal of Neuropsychopharmacology, 2003. **6**(4): p. 317-323.
177. Escalona, R., et al., *Fluvoxamine treatment in veterans with combat-related post-traumatic stress disorder*. Depress Anxiety, 2002. **15**(1): p. 29-33.
178. Milano, W., et al., *Treatment of bulimia nervosa with fluvoxamine: A randomized controlled trial*. Advances in Therapy, 2005. **22**(3): p. 278-283.
179. The United States Food and Drug Administration, *Drug approval package: Luvox (fluvoxamine maleate) 25mg, 50mg, and 100mg tablets*. 2007.
180. The United States Food and Drug Administration, *Fluvoxamine maleate full prescribing information*. 2021.
181. Byatt, N., K.M. Deligiannidis, and M.P. Freeman, *Antidepressant use in pregnancy: a critical review focused on risks and controversies*. Acta Psychiatr Scand, 2013. **127**(2): p. 94-114.
182. Berard, A., J.P. Zhao, and O. Sheehy, *Antidepressant use during pregnancy and the risk of major congenital malformations in a cohort of depressed pregnant women: an updated analysis of the Quebec Pregnancy Cohort*. Bmj Open, 2017. **7**(1).
183. Zakiyah, N., et al., *Antidepressant use during pregnancy and the risk of developing gestational hypertension: a retrospective cohort study*. BMC Pregnancy and Childbirth, 2018. **18**.
184. Westin, A.A., et al., *Selective serotonin reuptake inhibitors and venlafaxine in pregnancy: Changes in drug disposition*. PLoS One, 2017. **12**(7): p. e0181082.
185. Spigset, O., et al., *The major fluvoxamine metabolite in urine is formed by CYP2D6*. Eur J Clin Pharmacol, 2001. **57**(9): p. 653-8.
186. Almurjan, A., H. Macfarlane, and R.K.S. Badhan, *Precision dosing-based optimisation of paroxetine during pregnancy for poor and ultrarapid CYP2D6 metabolisers: a virtual clinical trial pharmacokinetics study*. J Pharm Pharmacol, 2020. **72**(8): p. 1049-1060.
187. Zhuang, X. and C. Lu, *PBPK modeling and simulation in drug research and development*. Acta Pharm Sin B, 2016. **6**(5): p. 430-440.
188. Almurjan, A., H. Macfarlane, and R.K.S. Badhan, *The application of precision dosing in the use of sertraline throughout pregnancy for poor and ultrarapid metabolizer CYP 2C19 subjects: A virtual clinical trial pharmacokinetics study*. Biopharm Drug Dispos, 2021. **42**(6): p. 252-262.
189. Badhan, R.K.S. and R. Gittins, *Precision dosing of methadone during pregnancy: A pharmacokinetics virtual clinical trials study*. J Subst Abuse Treat, 2021. **130**: p. 108521.
190. Olafuyi, O. and R.K.S. Badhan, *Dose optimization of chloroquine by pharmacokinetic modeling during pregnancy for the treatment of zika virus infection*. J Pharm Sci, 2019. **108**(1): p. 661-673.
191. Badhan, R.K.S. and H. Macfarlane, *Quetiapine dose optimisation during gestation: a pharmacokinetic modelling study*. J Pharm Pharmacol, 2020. **72**(5): p. 670-681.
192. Qasqas, S.A., et al., *Cardiovascular pharmacotherapeutic considerations during pregnancy and lactation*. Cardiol Rev, 2004. **12**(5): p. 240-61.
193. Murphy, M.M., et al., *The pregnancy-related decrease in fasting plasma homocysteine is not explained by folic acid supplementation, hemodilution, or a decrease in albumin in a longitudinal study*. Am J Clin Nutr, 2002. **76**(3): p. 614-9.
194. Cheung, C.K., T. Lao, and R. Swaminathan, *Urinary excretion of some proteins and enzymes during normal pregnancy*. Clin Chem, 1989. **35**(9): p. 1978-80.
195. Davison, J.M. and W. Dunlop, *Renal hemodynamics and tubular function normal human pregnancy*. Kidney Int, 1980. **18**(2): p. 152-61.
196. Rodgers, T., D. Leahy, and M. Rowland, *Physiologically based pharmacokinetic modeling 1: predicting the tissue distribution of moderate-to-strong bases*. J Pharm Sci, 2005. **94**(6): p. 1259-76.
197. Mylan. *Faverin 50 mg film-coated tablets, Summary of Product Characteristics (SPC)*. 2019 12 October 2021]; December 2020:[Available from: <https://www.medicines.org.uk/emc/product/1169/smpc#gref>.

198. Vezmar, S., et al., *Pharmacokinetics and efficacy of fluvoxamine and amitriptyline in depression*. J Pharmacol Sci, 2009. **110**(1): p. 98-104.
199. Ezuruike, U., et al., *Guide to development of compound files for PBPK modeling in the Simcyp population-based simulator*. CPT Pharmacometrics Syst Pharmacol, 2022. **11**(7): p. 805-821.
200. Turner, D., et al., *A Mechanistic Model for the Prediction of Equilibrium Blood-to-Plasma Concentration Ratio (B/P) in Human Blood: Basic and Neutral Drugs*, in *AAPS Annual Meeting and Exposition*. 2011: Washington DC, USA.
201. De Vries, M.H., et al., *Pharmacokinetics of fluvoxamine maleate after increasing single oral doses in healthy subjects*. Biopharm Drug Dispos, 1993. **14**(4): p. 291-6.
202. Van Harten, J., et al., *Bioavailability of fluvoxamine given with and without food*. Biopharm Drug Dispos, 1991. **12**(8): p. 571-6.
203. Bahrami, G. and B. Mohammadi, *Rapid and sensitive bioanalytical method for measurement of fluvoxamine in human serum using 4-chloro-7-nitrobenzofurazan as pre-column derivatization agent: application to a human pharmacokinetic study*. J Chromatogr B Analyt Technol Biomed Life Sci, 2007. **857**(2): p. 322-6.
204. de Vries, M.H., et al., *Single and multiple oral dose fluvoxamine kinetics in young and elderly subjects*. Ther Drug Monit, 1992. **14**(6): p. 493-8.
205. Fleishaker, J.C. and L.K. Hulst, *A pharmacokinetic and pharmacodynamic evaluation of the combined administration of alprazolam and fluvoxamine*. Eur J Clin Pharmacol, 1994. **46**(1): p. 35-9.
206. Orlando, R., et al., *Fluvoxamine pharmacokinetics in healthy elderly subjects and elderly patients with chronic heart failure*. Br J Clin Pharmacol, 2010. **69**(3): p. 279-86.
207. Debree, H., J.B. Vanderschoot, and L.C. Post, *Fluvoxamine maleate - Disposition in man*. European Journal of Drug Metabolism and Pharmacokinetics, 1983. **8**(2): p. 175-179.
208. The United States Food and Drug Administration, *Clinical pharmacology and biopharmaceutics review for Luvox extended-release*. 2008.
209. Spigset, O., et al., *Non-linear fluvoxamine disposition*. Br J Clin Pharmacol, 1998. **45**(3): p. 257-63.
210. Carrillo, J.A., et al., *Disposition of fluvoxamine in humans is determined by the polymorphic CYP2D6 and also by the CYP1A2 activity*. Clin Pharmacol Ther, 1996. **60**(2): p. 183-90.
211. Spigset, O., et al., *Relationship between fluvoxamine pharmacokinetics and CYP2D6/CYP2C19 phenotype polymorphisms*. Eur J Clin Pharmacol, 1997. **52**(2): p. 129-33.
212. Hartter, S., et al., *Increased bioavailability of oral melatonin after fluvoxamine coadministration*. Clin Pharmacol Ther, 2000. **67**(1): p. 1-6.
213. Christensen, M., et al., *Low daily 10-mg and 20-mg doses of fluvoxamine inhibit the metabolism of both caffeine (cytochrome P4501A2) and omeprazole (cytochrome P4502C19)*. Clin Pharmacol Ther, 2002. **71**(3): p. 141-52.
214. Abduljalil, K., *Predicting drug pharmacokinetics in pregnancy, fetal, and lactation using PBPK*. 2020.
215. Ryu, R.J., et al., *Pharmacokinetics of metoprolol during pregnancy and lactation*. J Clin Pharmacol, 2016. **56**(5): p. 581-9.
216. Achour, B., et al., *Simultaneous quantification of the abundance of several cytochrome P450 and uridine 5'-diphospho-glucuronosyltransferase enzymes in human liver microsomes using multiplexed targeted proteomics*. Drug Metab Dispos, 2014. **42**(4): p. 500-10.
217. Hostetter, A., J.C. Ritchie, and Z.N. Stowe, *Amniotic fluid and umbilical cord blood concentrations of antidepressants in three women*. Biol Psychiatry, 2000. **48**(10): p. 1032-4.
218. Sit, D., et al., *Mother-infant antidepressant concentrations, maternal depression, and perinatal events*. J Clin Psychiatry, 2011. **72**(7): p. 994-1001.

219. Rampono, J., et al., *Placental transfer of SSRI and SNRI antidepressants and effects on the neonate*. *Pharmacopsychiatry*, 2009. **42**(3): p. 95-100.
220. Ginsberg, G., et al., *Physiologically based pharmacokinetic (PBPK) modeling of caffeine and theophylline in neonates and adults: implications for assessing children's risks from environmental agents*. *J Toxicol Environ Health A*, 2004. **67**(4): p. 297-329.
221. The United States Food and Drug Administration, *Summary minutes of the Advisory Committee for Pharmaceutical Science and Clinical Pharmacology*. 2012.
222. The United States Food and Drug Administration. *Fluvoxamine maleate full prescribing information*. 2021 20 September 2021 16 November 2021]; Available from: https://www.accessdata.fda.gov/drugsatfda_docs/label/2021/021519s018lbl.pdf.
223. The United States Food and Drug Administration. *FDA Drug Safety Communication: Selective serotonin reuptake inhibitor (SSRI) antidepressant use during pregnancy and reports of a rare heart and lung condition in newborn babies*. 2011 [cited 2021 16 November 2021]; Available from: <https://www.fda.gov/drugs/drug-safety-and-availability/fda-drug-safety-communication-selective-serotonin-reuptake-inhibitor-ssri-antidepressant-use-during>.
224. Einarson, A., et al., *Incidence of major malformations in infants following antidepressant exposure in pregnancy: results of a large prospective cohort study*. *Can J Psychiatry*, 2009. **54**(4): p. 242-6.
225. Furu, K., et al., *Selective serotonin reuptake inhibitors and venlafaxine in early pregnancy and risk of birth defects: population based cohort study and sibling design*. *BMJ*, 2015. **350**: p. h1798.
226. McElhatton, P.R., et al., *The outcome of pregnancy in 689 women exposed to therapeutic doses of antidepressants. A collaborative study of the European Network of Teratology Information Services (ENTIS)*. *Reprod Toxicol*, 1996. **10**(4): p. 285-94.
227. Kulin, N.A., et al., *Pregnancy outcome following maternal use of the new selective serotonin reuptake inhibitors - A prospective controlled multicenter study*. *Jama-Journal of the American Medical Association*, 1998. **279**(8): p. 609-610.
228. Sivojelezova, A., *Fluvoxamine (Luvox (TM)) use in pregnancy*. *Clinical Pharmacology & Therapeutics*, 2004. **75**(2): p. P25-P25.
229. Malm, H., et al., *Selective serotonin reuptake inhibitors and risk for major congenital anomalies reply*. *Obstetrics and Gynecology*, 2012. **119**(1): p. 183-183.
230. Noe, D.A., *Criteria for reporting noncompartmental estimates of half-life and area under the curve extrapolated to infinity*. *Pharm Stat*, 2020. **19**(2): p. 101-112.
231. Britz, H., et al., *Physiologically-Based Pharmacokinetic Models for CYP1A2 Drug-Drug Interaction Prediction: A Modeling Network of Fluvoxamine, Theophylline, Caffeine, Rifampicin, and Midazolam*. *CPT Pharmacometrics Syst Pharmacol*, 2019. **8**(5): p. 296-307.
232. Abduljalil, K., et al., *Deciding on success criteria for predictability of pharmacokinetic parameters from in vitro studies: an analysis based on in vivo observations*. *Drug Metab Dispos*, 2014. **42**(9): p. 1478-84.
233. Miura, M. and T. Ohkubo, *Identification of human cytochrome P450 enzymes involved in the major metabolic pathway of fluvoxamine*. *Xenobiotica*, 2007. **37**(2): p. 169-79.
234. Tracy, T.S., et al., *Temporal changes in drug metabolism (CYP1A2, CYP2D6 and CYP3A Activity) during pregnancy*. *Am J Obstet Gynecol*, 2005. **192**(2): p. 633-9.
235. Wadelius, M., et al., *Induction of CYP2D6 in pregnancy*. *Clin Pharmacol Ther*, 1997. **62**(4): p. 400-7.
236. Spigset, O., et al., *Lack of correlation between fluvoxamine clearance and CYP1A2 activity as measured by systemic caffeine clearance*. *Eur J Clin Pharmacol*, 1999. **54**(12): p. 943-6.
237. Yu, T., et al., *Pregnancy-induced changes in the pharmacokinetics of caffeine and its metabolites*. *J Clin Pharmacol*, 2016. **56**(5): p. 590-6.
238. Dawes, M. and P.J. Chowienzyk, *Drugs in pregnancy. Pharmacokinetics in pregnancy*. *Best Pract Res Clin Obstet Gynaecol*, 2001. **15**(6): p. 819-26.

239. van Harten, J., et al., *Pharmacokinetics of fluvoxamine maleate in patients with liver cirrhosis after single-dose oral administration*. Clin Pharmacokinet, 1993. **24**(2): p. 177-82.
240. Orlando, R., et al., *Liver dysfunction markedly decreases the inhibition of cytochrome P450 1A2-mediated theophylline metabolism by fluvoxamine*. Clin Pharmacol Ther, 2006. **79**(5): p. 489-99.
241. van Harten, J., *Overview of the pharmacokinetics of fluvoxamine*. Clin Pharmacokinet, 1995. **29 Suppl 1**: p. 1-9.
242. DeVane, C.L. and H.S. Gill, *Clinical pharmacokinetics of fluvoxamine: applications to dosage regimen design*. J Clin Psychiatry, 1997. **58 Suppl 5**: p. 7-14.
243. Matsuoka, S., et al., *Quantitative prediction of fetal plasma concentration of fluvoxamine during dosage-tapering to the mother*. Placenta, 2017. **58**: p. 74-81.
244. Hicks, J.K., et al., *Clinical Pharmacogenetics Implementation Consortium (CPIC) Guideline for CYP2D6 and CYP2C19 Genotypes and Dosing of Selective Serotonin Reuptake Inhibitors*. Clin Pharmacol Ther, 2015. **98**(2): p. 127-34.
245. Brouwer, J.M.J.L., et al., *Dutch Pharmacogenetics Working Group (DPWG) guideline for the gene-drug interaction between CYP2C19 and CYP2D6 and SSRIs*. European Journal of Human Genetics, 2021.
246. Hodge, L.S. and T.S. Tracy, *Alterations in drug disposition during pregnancy: implications for drug therapy*. Expert Opin Drug Metab Toxicol, 2007. **3**(4): p. 557-71.
247. Anderson, G.D., *Pregnancy-induced changes in pharmacokinetics: a mechanistic-based approach*. Clin Pharmacokinet, 2005. **44**(10): p. 989-1008.
248. Badaoui, S., et al., *Application of Model Informed Precision Dosing to Address the Impact of Pregnancy Stage and CYP2D6 Phenotype on Foetal Morphine Exposure*. AAPS J, 2021. **23**(1): p. 15.
249. Giaginis, C., S. Theocharis, and A. Tsantili-Kakoulidou, *Current toxicological aspects on drug and chemical transport and metabolism across the human placental barrier*. Expert Opin Drug Metab Toxicol, 2012. **8**(10): p. 1263-75.
250. Ewing, G., et al., *Placental transfer of antidepressant medications: implications for postnatal adaptation syndrome*. Clin Pharmacokinet, 2015. **54**(4): p. 359-70.
251. Evseenko, D., J.W. Paxton, and J.A. Keelan, *Active transport across the human placenta: impact on drug efficacy and toxicity*. Expert Opin Drug Metab Toxicol, 2006. **2**(1): p. 51-69.
252. Wishart, D.S., et al., *DrugBank 5.0: a major update to the DrugBank database for 2018*. Nucleic Acids Res, 2018. **46**(D1): p. D1074-D1082.
253. Browne, V.A., et al., *Uterine artery blood flow, fetal hypoxia and fetal growth*. Philos Trans R Soc Lond B Biol Sci, 2015. **370**(1663): p. 20140068.
254. Schoretsanitis, G., et al., *Antidepressant transfer into amniotic fluid, umbilical cord blood & breast milk: A systematic review & combined analysis*. Prog Neuropsychopharmacol Biol Psychiatry, 2021. **107**: p. 110228.
255. Mulder, H., et al., *The association between cytochrome P450 2D6 genotype and prescription patterns of antipsychotic and antidepressant drugs in hospitalized psychiatric patients: a retrospective follow-up study*. J Clin Psychopharmacol, 2005. **25**(2): p. 188-91.
256. Berard, A., et al., *Association between CYP2D6 Genotypes and the Risk of Antidepressant Discontinuation, Dosage Modification and the Occurrence of Maternal Depression during Pregnancy*. Front Pharmacol, 2017. **8**: p. 402.
257. Rau, T., et al., *CYP2D6 genotype: impact on adverse effects and nonresponse during treatment with antidepressants-a pilot study*. Clin Pharmacol Ther, 2004. **75**(5): p. 386-93.
258. Misri, S., et al., *Factors impacting decisions to decline or adhere to antidepressant medication in perinatal women with mood and anxiety disorders*. Depress Anxiety, 2013. **30**(11): p. 1129-36.

259. COVID-19 Treatment Guidelines Panel. *Coronavirus disease 2019 (COVID-19) treatment guidelines*. National Institutes of Health. 2021 [26 October 2021]; Available from: <https://www.covid19treatmentguidelines.nih.gov/>.
260. Womersley, K., K. Ripullone, and M. Agius, *What are the risks associated with different Selective Serotonin Re-uptake Inhibitors (SSRIs) to treat depression and anxiety in pregnancy? An evaluation of current evidence*. *Psychiatr Danub*, 2017. **29**(Suppl 3): p. 629-644.
261. The Medicines & Healthcare products Regulatory Agency United Kingdom. *Guidance: Selective serotonin reuptake inhibitors (SSRIs) and serotonin and noradrenaline reuptake inhibitors (SNRIs): use and safety*. 2014 [17 November 2021]; Available from: <https://www.gov.uk/government/publications/ssris-and-snrri-use-and-safety/selective-serotonin-reuptake-inhibitors-ssris-and-serotonin-and-noradrenaline-reuptake-inhibitors-snrri-use-and-safety#safety-concerns-with-ssrisnrri-use-in-pregnancy>.
262. Ligibel, J.A., et al., *American Society of Clinical Oncology position statement on obesity and cancer*. *J Clin Oncol*, 2014. **32**(31): p. 3568-74.
263. Reeves, G.K., et al., *Cancer incidence and mortality in relation to body mass index in the Million Women Study: cohort study*. *BMJ*, 2007. **335**(7630): p. 1134.
264. Calle, E.E., et al., *Overweight, obesity, and mortality from cancer in a prospectively studied cohort of U.S. adults*. *N Engl J Med*, 2003. **348**(17): p. 1625-38.
265. Krogstad, V., et al., *Correlation of Body Weight and Composition With Hepatic Activities of Cytochrome P450 Enzymes*. *J Pharm Sci*, 2021. **110**(1): p. 432-437.
266. Bruno, C.D., et al., *Effect of lipophilicity on drug distribution and elimination: Influence of obesity*. *Br J Clin Pharmacol*, 2021. **87**(8): p. 3197-3205.
267. Deininger, M., E. Buchdunger, and B.J. Druker, *The development of imatinib as a therapeutic agent for chronic myeloid leukemia*. *Blood*, 2005. **105**(7): p. 2640-53.
268. Yassin, M.A., N. Kassem, and R. Ghassoub, *How I treat obesity and obesity related surgery in patients with chronic myeloid leukemia: An outcome of an ELN project*. *Clin Case Rep*, 2021. **9**(3): p. 1228-1234.
269. Breccia, M., et al., *Delayed cytogenetic and major molecular responses associated to increased BMI at baseline in chronic myeloid leukemia patients treated with imatinib*. *Cancer Lett*, 2013. **333**(1): p. 32-5.
270. Breccia, M., et al., *Association of High Body Mass Index with Response Outcomes in Patients with CML-CP Treated with Dasatinib Versus Imatinib in the First Line: Exploratory Post Hoc Analysis of the Phase 3 DASISION Trial*. *Blood*, 2019. **134**(Supplement_1): p. 4155-4155.
271. Lin, L., et al., *Are novel oral oncolytics underdosed in obese patients?* *Cancer Chemother Pharmacol*, 2023.
272. Larson, R.A., et al., *Imatinib pharmacokinetics and its correlation with response and safety in chronic-phase chronic myeloid leukemia: a subanalysis of the IRIS study*. *Blood*, 2008. **111**(8): p. 4022-8.
273. Demetri, G.D., et al., *Imatinib plasma levels are correlated with clinical benefit in patients with unresectable/metastatic gastrointestinal stromal tumors*. *J Clin Oncol*, 2009. **27**(19): p. 3141-7.
274. Guilhot, F., et al., *Plasma exposure of imatinib and its correlation with clinical response in the Tyrosine Kinase Inhibitor Optimization and Selectivity Trial*. *Haematologica*, 2012. **97**(5): p. 731-8.
275. Clarke, W.A., et al., *Therapeutic drug monitoring in oncology: International Association of Therapeutic Drug Monitoring and Clinical Toxicology consensus guidelines for imatinib therapy*. *Eur J Cancer*, 2021. **157**: p. 428-440.
276. Buclin, T., et al., *The Steps to Therapeutic Drug Monitoring: A Structured Approach Illustrated With Imatinib*. *Front Pharmacol*, 2020. **11**: p. 177.
277. Gotta, V., et al., *Clinical usefulness of therapeutic concentration monitoring for imatinib dosage individualization: results from a randomized controlled trial*. *Cancer Chemother Pharmacol*, 2014. **74**(6): p. 1307-19.

278. Zuidema, S., et al., *Optimizing the dose in patients treated with imatinib as first line treatment for gastrointestinal stromal tumours: A cost-effectiveness study*. Br J Clin Pharmacol, 2019. **85**(9): p. 1994-2001.
279. Conti, R.M., et al., *The cost-effectiveness of therapeutic drug monitoring for the prescription drug-based treatment of chronic myeloid leukemia*. J Manag Care Spec Pharm, 2021. **27**(8): p. 1077-1085.
280. Teng, J.F., V.H. Mabasa, and M.H. Ensom, *The role of therapeutic drug monitoring of imatinib in patients with chronic myeloid leukemia and metastatic or unresectable gastrointestinal stromal tumors*. Ther Drug Monit, 2012. **34**(1): p. 85-97.
281. Yu, H. and R.K.S. Badhan, *The Application of Virtual Therapeutic Drug Monitoring to Assess the Pharmacokinetics of Imatinib in a Chinese Cancer Population Group*. J Pharm Sci, 2023. **112**(2): p. 599-609.
282. Adiwidjaja, J., A.V. Boddy, and A.J. McLachlan, *Implementation of a Physiologically Based Pharmacokinetic Modeling Approach to Guide Optimal Dosing Regimens for Imatinib and Potential Drug Interactions in Paediatrics*. Front Pharmacol, 2019. **10**: p. 1672.
283. Adiwidjaja, J., et al., *Physiologically-based pharmacokinetic model predictions of inter-ethnic differences in imatinib pharmacokinetics and dosing regimens*. Br J Clin Pharmacol, 2022. **88**(4): p. 1735-1750.
284. Peng, B., et al., *Absolute bioavailability of imatinib (Glivec) orally versus intravenous infusion*. J Clin Pharmacol, 2004. **44**(2): p. 158-62.
285. Nikolova, Z., et al., *Bioequivalence, safety, and tolerability of imatinib tablets compared with capsules*. Cancer Chemother Pharmacol, 2004. **53**(5): p. 433-8.
286. Pena, M., et al., *Effect of Cytochrome P450 and ABCB1 Polymorphisms on Imatinib Pharmacokinetics After Single-Dose Administration to Healthy Subjects*. Clin Drug Investig, 2020. **40**(7): p. 617-628.
287. Petain, A., et al., *Population pharmacokinetics and pharmacogenetics of imatinib in children and adults*. Clin Cancer Res, 2008. **14**(21): p. 7102-9.
288. Eechoute, K., et al., *A long-term prospective population pharmacokinetic study on imatinib plasma concentrations in GIST patients*. Clin Cancer Res, 2012. **18**(20): p. 5780-7.
289. Renard, D., et al., *Pharmacokinetic interactions among imatinib, bosentan and sildenafil, and their clinical implications in severe pulmonary arterial hypertension*. Br J Clin Pharmacol, 2015. **80**(1): p. 75-85.
290. Gotta, V., et al., *Large-scale imatinib dose-concentration-effect study in CML patients under routine care conditions*. Leuk Res, 2014. **38**(7): p. 764-72.
291. Peng, B., et al., *Pharmacokinetics and pharmacodynamics of imatinib in a phase I trial with chronic myeloid leukemia patients*. J Clin Oncol, 2004. **22**(5): p. 935-42.
292. Widmer, N., et al., *Population pharmacokinetics of imatinib and the role of alpha-acid glycoprotein*. Br J Clin Pharmacol, 2006. **62**(1): p. 97-112.
293. Haouala, A., et al., *Prediction of free imatinib concentrations based on total plasma concentrations in patients with gastrointestinal stromal tumours*. Br J Clin Pharmacol, 2013. **75**(4): p. 1007-18.
294. Adattini, J.A., et al., *Application of physiologically based pharmacokinetic modeling to understand real-world outcomes in patients receiving imatinib for chronic myeloid leukemia*. Pharmacol Res Perspect, 2023. **11**(4): p. e01082.
295. Kretz, O., et al., *In vitro blood distribution and plasma protein binding of the tyrosine kinase inhibitor imatinib and its active metabolite, CGP74588, in rat, mouse, dog, monkey, healthy humans and patients with acute lymphatic leukaemia*. Br J Clin Pharmacol, 2004. **58**(2): p. 212-6.
296. Smith, P., et al., *The influence of St. John's wort on the pharmacokinetics and protein binding of imatinib mesylate*. Pharmacotherapy, 2004. **24**(11): p. 1508-14.
297. Bornhauser, M., et al., *Elimination of imatinib mesylate and its metabolite N-desmethyl-imatinib*. J Clin Oncol, 2005. **23**(16): p. 3855-6; author reply 3857-8.

298. Thai, H.T., et al., *Optimizing pharmacokinetic bridging studies in paediatric oncology using physiologically-based pharmacokinetic modelling: application to docetaxel*. Br J Clin Pharmacol, 2015. **80**(3): p. 534-47.
299. Bouchet, S., et al., *Relationship between imatinib trough concentration and outcomes in the treatment of advanced gastrointestinal stromal tumours in a real-life setting*. Eur J Cancer, 2016. **57**: p. 31-8.
300. Garcia-Ferrer, M., et al., *Utility of Therapeutic Drug Monitoring of Imatinib, Nilotinib, and Dasatinib in Chronic Myeloid Leukemia: A Systematic Review and Meta-analysis*. Clin Ther, 2019. **41**(12): p. 2558-2570 e7.
301. NS, I.J., et al., *Therapeutic drug monitoring of imatinib in patients with gastrointestinal stromal tumours - Results from daily clinical practice*. Eur J Cancer, 2020. **136**: p. 140-148.
302. Burhanuddin, K. and R. Badhan, *Optimising Fluvoxamine Maternal/Fetal Exposure during Gestation: A Pharmacokinetic Virtual Clinical Trials Study*. Metabolites, 2022. **12**(12).
303. Alenezi, M. and R.K.S. Badhan, *Precision dosing of venlafaxine during pregnancy: a pharmacokinetics modelling approach*. J Pharm Pharmacol, 2023.
304. Gao, D., et al., *Prediction for Plasma Trough Concentration and Optimal Dosing of Imatinib under Multiple Clinical Situations Using Physiologically Based Pharmacokinetic Modeling*. ACS Omega, 2023. **8**(15): p. 13741-13753.
305. Farag, S., et al., *Imatinib Pharmacokinetics in a Large Observational Cohort of Gastrointestinal Stromal Tumour Patients*. Clin Pharmacokinet, 2017. **56**(3): p. 287-292.
306. Lankheet, N.A.G., et al., *Optimizing the dose in cancer patients treated with imatinib, sunitinib and pazopanib*. Br J Clin Pharmacol, 2017. **83**(10): p. 2195-2204.
307. Verbraecken, J., et al., *Body surface area in normal-weight, overweight, and obese adults. A comparison study*. Metabolism, 2006. **55**(4): p. 515-24.
308. Johnson, T.N., et al., *Changes in liver volume from birth to adulthood: a meta-analysis*. Liver Transpl, 2005. **11**(12): p. 1481-93.
309. Levey, A.S., et al., *A more accurate method to estimate glomerular filtration rate from serum creatinine: a new prediction equation. Modification of Diet in Renal Disease Study Group*. Ann Intern Med, 1999. **130**(6): p. 461-70.
310. Nebot, N., et al., *Participation of CYP2C8 and CYP3A4 in the N-demethylation of imatinib in human hepatic microsomes*. Br J Pharmacol, 2010. **161**(5): p. 1059-69.
311. Oostendorp, R.L., et al., *The effect of P-gp (Mdr1a/1b), BCRP (Bcrp1) and P-gp/BCRP inhibitors on the in vivo absorption, distribution, metabolism and excretion of imatinib*. Invest New Drugs, 2009. **27**(1): p. 31-40.
312. Rivory, L.P., K.A. Slaviero, and S.J. Clarke, *Hepatic cytochrome P450 3A drug metabolism is reduced in cancer patients who have an acute-phase response*. Br J Cancer, 2002. **87**(3): p. 277-80.
313. Burt, H.J., et al., *Abundance of Hepatic Transporters in Caucasians: A Meta-Analysis*. Drug Metab Dispos, 2016. **44**(10): p. 1550-61.
314. Woo, J., et al., *Effect of age and disease on two drug binding proteins: albumin and alpha-1-acid glycoprotein*. Clin Biochem, 1994. **27**(4): p. 289-92.
315. Paxton, J.W. and R.H. Briant, *Alpha 1-acid glycoprotein concentrations and propranolol binding in elderly patients with acute illness*. Br J Clin Pharmacol, 1984. **18**(5): p. 806-10.
316. Benedek, I.H., et al., *Serum alpha 1-acid glycoprotein and the binding of drugs in obesity*. Br J Clin Pharmacol, 1983. **16**(6): p. 751-4.
317. Benedek, I.H., R.A. Blouin, and P.J. McNamara, *Serum protein binding and the role of increased alpha 1-acid glycoprotein in moderately obese male subjects*. Br J Clin Pharmacol, 1984. **18**(6): p. 941-6.
318. Singh, N., et al., *Drug monitoring of imatinib levels in patients undergoing therapy for chronic myeloid leukaemia: comparing plasma levels of responders and non-responders*. Eur J Clin Pharmacol, 2009. **65**(6): p. 545-9.

319. Picard, S., et al., *Trough imatinib plasma levels are associated with both cytogenetic and molecular responses to standard-dose imatinib in chronic myeloid leukemia*. Blood, 2007. **109**(8): p. 3496-9.
320. Arora, B., et al., *Therapeutic drug monitoring for imatinib: Current status and Indian experience*. Indian J Med Paediatr Oncol, 2013. **34**(3): p. 224-8.
321. Natarajan, H., et al., *Imatinib trough levels: a potential biomarker to predict cytogenetic and molecular response in newly diagnosed patients with chronic myeloid leukemia*. Leuk Lymphoma, 2019. **60**(2): p. 418-425.
322. Johnson-Ansah, H., et al., *Imatinib Optimized Therapy Improves Major Molecular Response Rates in Patients with Chronic Myeloid Leukemia*. Pharmaceutics, 2022. **14**(8).
323. Iqbal, N. and N. Iqbal, *Imatinib: a breakthrough of targeted therapy in cancer*. Chemother Res Pract, 2014. **2014**: p. 357027.
324. Pavlovsky, C., et al., *Imatinib mesylate pharmacokinetics before and after sleeve gastrectomy in a morbidly obese patient with chronic myeloid leukemia*. Pharmacotherapy, 2009. **29**(9): p. 1152-6.
325. Hochhaus, A., et al., *European LeukemiaNet 2020 recommendations for treating chronic myeloid leukemia*. Leukemia, 2020. **34**(4): p. 966-984.
326. Jabbour, E., J.E. Cortes, and H.M. Kantarjian, *Suboptimal response to or failure of imatinib treatment for chronic myeloid leukemia: what is the optimal strategy?* Mayo Clin Proc, 2009. **84**(2): p. 161-9.
327. Bhamidipati, P.K., et al., *Management of imatinib-resistant patients with chronic myeloid leukemia*. Ther Adv Hematol, 2013. **4**(2): p. 103-17.
328. Marin, D., et al., *European LeukemiaNet criteria for failure or suboptimal response reliably identify patients with CML in early chronic phase treated with imatinib whose eventual outcome is poor*. Blood, 2008. **112**(12): p. 4437-44.
329. Alvarado, Y., et al., *Significance of suboptimal response to imatinib, as defined by the European LeukemiaNet, in the long-term outcome of patients with early chronic myeloid leukemia in chronic phase*. Cancer, 2009. **115**(16): p. 3709-18.
330. Breccia, M., et al., *Cytogenetic and molecular responses in chronic phase chronic myeloid leukaemia patients receiving low dose of imatinib for intolerance to standard dose*. Hematol Oncol, 2010. **28**(2): p. 89-92.
331. Shyam Sunder, S., U.C. Sharma, and S. Pokharel, *Adverse effects of tyrosine kinase inhibitors in cancer therapy: pathophysiology, mechanisms and clinical management*. Signal Transduct Target Ther, 2023. **8**(1): p. 262.
332. Menz, B.D., et al., *Barriers and opportunities for the clinical implementation of therapeutic drug monitoring in oncology*. Br J Clin Pharmacol, 2021. **87**(2): p. 227-236.
333. Johnson, K.B., et al., *Precision Medicine, AI, and the Future of Personalized Health Care*. Clin Transl Sci, 2021. **14**(1): p. 86-93.
334. Francke, M.I., et al., *Best Practices to Implement Dried Blood Spot Sampling for Therapeutic Drug Monitoring in Clinical Practice*. Ther Drug Monit, 2022. **44**(5): p. 696-700.
335. Gambacorti-Passerini, C., et al., *Alpha1 acid glycoprotein binds to imatinib (STI571) and substantially alters its pharmacokinetics in chronic myeloid leukemia patients*. Clin Cancer Res, 2003. **9**(2): p. 625-32.
336. Dutreix, C., et al., *Pharmacokinetic interaction between ketoconazole and imatinib mesylate (Gleevec) in healthy subjects*. Cancer Chemother Pharmacol, 2004. **54**(4): p. 290-4.
337. Bolton, A.E., et al., *Effect of rifampicin on the pharmacokinetics of imatinib mesylate (Gleevec, STI571) in healthy subjects*. Cancer Chemother Pharmacol, 2004. **53**(2): p. 102-6.
338. Larghero, J., et al., *Relationship between elevated levels of the alpha 1 acid glycoprotein in chronic myelogenous leukemia in blast crisis and pharmacological resistance to imatinib (Gleevec) in vitro and in vivo*. Biochem Pharmacol, 2003. **66**(10): p. 1907-13.

339. Gambacorti-Passerini, C., et al., *Role of alpha1 acid glycoprotein in the in vivo resistance of human BCR-ABL(+) leukemic cells to the abl inhibitor STI571*. J Natl Cancer Inst, 2000. **92**(20): p. 1641-50.
340. Horikoshi, A., K. Takei, and S. Sawada, *Relationship between daily dose of imatinib per square meter and its plasma concentration in patients with chronic-phase chronic myeloid leukemia (CML)*. Leuk Res, 2007. **31**(4): p. 574-5.
341. Park, S.J., et al., *Reduced dose of imatinib for patients with chronic myeloid leukemia and low body surface area*. Acta Haematol, 2007. **118**(4): p. 219-21.
342. Breccia, M., et al., *The Importance of Body Surface Area at Baseline and during Treatment in Chronic Myeloid Leukemia Patients Treated with Imatinib*. Acta Haematologica, 2015. **134**(1): p. 57-58.
343. National Health Service Digital, *National Child Measurement Programme, England, 2021/22 school year*. 2022.
344. National Health Service Digital, *National Child Measurement Programme, England 2020/21 School Year*. 2021.
345. NCD Risk Factor Collaboration (NCD-RisC), *Worldwide trends in body-mass index, underweight, overweight, and obesity from 1975 to 2016: a pooled analysis of 2416 population-based measurement studies in 128.9 million children, adolescents, and adults*. Lancet, 2017. **390**(10113): p. 2627-2642.
346. van Rongen, A., et al., *Higher Midazolam Clearance in Obese Adolescents Compared with Morbidly Obese Adults*. Clin Pharmacokinet, 2018. **57**(5): p. 601-611.
347. Goknar, N., et al., *Determination of early urinary renal injury markers in obese children*. Pediatr Nephrol, 2015. **30**(1): p. 139-44.
348. Kyler, K.E., et al., *Drug Dose Selection in Pediatric Obesity: Available Information for the Most Commonly Prescribed Drugs to Children*. Paediatr Drugs, 2019. **21**(5): p. 357-369.
349. Natale, S., et al., *Pediatric Obesity: Pharmacokinetic Alterations and Effects on Antimicrobial Dosing*. Pharmacotherapy, 2017. **37**(3): p. 361-378.
350. Ross, E.L., et al., *Comparison of 3 body size descriptors in critically ill obese children and adolescents: implications for medication dosing*. J Pediatr Pharmacol Ther, 2014. **19**(2): p. 103-10.
351. Flynn, J.T., et al., *Clinical Practice Guideline for Screening and Management of High Blood Pressure in Children and Adolescents*. Pediatrics, 2017. **140**(3).
352. Lurbe, E., et al., *2016 European Society of Hypertension guidelines for the management of high blood pressure in children and adolescents*. J Hypertens, 2016. **34**(10): p. 1887-920.
353. Hanafy, S., M. Pinski, and F. Jamali, *Effect of obesity on response to cardiovascular drugs in pediatric patients with renal disease*. Pediatr Nephrol, 2009. **24**(4): p. 815-21.
354. de Onis, M. and T. Lobstein, *Defining obesity risk status in the general childhood population: which cut-offs should we use?* Int J Pediatr Obes, 2010. **5**(6): p. 458-60.
355. WHO Multicentre Growth Reference Study Group, *WHO Child Growth Standards based on length/height, weight and age*. Acta Paediatr Suppl, 2006. **450**: p. 76-85.
356. Styne, D.M., et al., *Pediatric Obesity-Assessment, Treatment, and Prevention: An Endocrine Society Clinical Practice Guideline*. J Clin Endocrinol Metab, 2017. **102**(3): p. 709-757.
357. Centers for Disease Control and Prevention (CDC). *Clinical Growth Charts*. 2017 16 June 2017 18 January 2023]; Available from: https://www.cdc.gov/growthcharts/clinical_charts.htm.
358. Kilic, E., et al., *Oxidative Stress Status in Childhood Obesity: A Potential Risk Predictor*. Med Sci Monit, 2016. **22**: p. 3673-3679.
359. Panichsillaphakit, E., et al., *The Association between Hepcidin and Iron Status in Children and Adolescents with Obesity*. Journal of Nutrition and Metabolism, 2021. **2021**.
360. Cacciari, E., et al., *Haemorheologic and fibrinolytic evaluation in obese children and adolescents*. Eur J Pediatr, 1988. **147**(4): p. 381-4.

361. Oni, O., O. Orekoya, and M. Bamji, *Prevalence of Disease Conditions and Laboratory Findings in Obese Children: A Decade Analysis of National Health and Nutrition Examination Survey 2005-2014*. Pediatrics, 2021. **147**(3).
362. Jeong, H.R., et al., *Hemoglobin and hematocrit levels are positively associated with blood pressure in children and adolescents 10 to 18 years old*. Sci Rep, 2021. **11**(1): p. 19052.
363. Belo, L., et al., *Body fat percentage is a major determinant of total bilirubin independently of UGT1A1*28 polymorphism in young obese*. PLoS One, 2014. **9**(6): p. e98467.
364. Yu, L., et al., *Association between dietary essential amino acids intake and metabolic biomarkers: influence of obesity among Chinese children and adolescents*. Amino Acids, 2021. **53**(5): p. 635-644.
365. Abitbol, C.L., et al., *Obesity and preterm birth: additive risks in the progression of kidney disease in children*. Pediatr Nephrol, 2009. **24**(7): p. 1363-70.
366. Marginean, C.O., et al., *Early Inflammatory Status Related to Pediatric Obesity*. Front Pediatr, 2019. **7**: p. 241.
367. Marginean, C.O., et al., *The role of IL-6 572 C/G, 190 C/T, and 174 G/C gene polymorphisms in children's obesity*. Eur J Pediatr, 2014. **173**(10): p. 1285-96.
368. Marginean, C.O., et al., *Correlations Between Leptin Gene Polymorphisms 223 A/G, 1019 G/A, 492 G/C, 976 C/A, and Anthropometrical and Biochemical Parameters in Children With Obesity: A Prospective Case-Control Study in a Romanian Population-The Nutrichild Study*. Medicine (Baltimore), 2016. **95**(12): p. e3115.
369. Sobieska, M., et al., *Obesity, physical fitness, and inflammatory markers in Polish children*. Med Sci Monit, 2013. **19**: p. 493-500.
370. Gibson, R.S., et al., *Tissue iron deficiency and adiposity-related inflammation in disadvantaged preschoolers from NE Brazil*. Eur J Clin Nutr, 2014. **68**(8): p. 887-91.
371. Ferrari, M., et al., *Inflammation profile in overweight/obese adolescents in Europe: an analysis in relation to iron status*. Eur J Clin Nutr, 2015. **69**(2): p. 247-55.
372. Duzova, A., et al., *Prevalence of hypertension and decreased glomerular filtration rate in obese children: results of a population-based field study*. Nephrol Dial Transplant, 2013. **28 Suppl 4**: p. iv166-71.
373. Burt, H.J., et al., *Metformin and cimetidine: Physiologically based pharmacokinetic modelling to investigate transporter mediated drug-drug interactions*. Eur J Pharm Sci, 2016. **88**: p. 70-82.
374. Tucker, G.T., et al., *Metformin kinetics in healthy subjects and in patients with diabetes mellitus*. Br J Clin Pharmacol, 1981. **12**(2): p. 235-46.
375. Graham, G.G., et al., *Clinical pharmacokinetics of metformin*. Clin Pharmacokinet, 2011. **50**(2): p. 81-98.
376. Jeong, Y.S. and W.J. Jusko, *Meta-Assessment of Metformin Absorption and Disposition Pharmacokinetics in Nine Species*. Pharmaceuticals (Basel), 2021. **14**(6).
377. Gusler, G., et al., *Pharmacokinetics of metformin gastric-retentive tablets in healthy volunteers*. J Clin Pharmacol, 2001. **41**(6): p. 655-61.
378. Timmins, P., et al., *Steady-state pharmacokinetics of a novel extended-release metformin formulation*. Clin Pharmacokinet, 2005. **44**(7): p. 721-9.
379. Padwal, R.S., et al., *Effect of gastric bypass surgery on the absorption and bioavailability of metformin*. Diabetes Care, 2011. **34**(6): p. 1295-300.
380. Sanchez-Infantes, D., et al., *Pharmacokinetics of metformin in girls aged 9 years*. Clin Pharmacokinet, 2011. **50**(11): p. 735-8.
381. van Rongen, A., et al., *Increased Metformin Clearance in Overweight and Obese Adolescents: A Pharmacokinetic Substudy of a Randomized Controlled Trial*. Paediatr Drugs, 2018. **20**(4): p. 365-374.
382. Sam, W.J., et al., *Effects of SLC22A1 Polymorphisms on Metformin-Induced Reductions in Adiposity and Metformin Pharmacokinetics in Obese Children With Insulin Resistance*. J Clin Pharmacol, 2017. **57**(2): p. 219-229.

383. Maharaj, A.R., et al., *Pharmacokinetics of Ceftazidime in Children and Adolescents with Obesity*. Paediatr Drugs, 2021. **23**(5): p. 499-513.
384. Zhou, L., et al., *Physiologically based pharmacokinetic modelling to predict exposure differences in healthy volunteers and subjects with renal impairment: Ceftazidime case study*. Basic Clin Pharmacol Toxicol, 2019. **125**(2): p. 100-107.
385. Zhou, W., et al., *Predictive Performance of Physiologically Based Pharmacokinetic and Population Pharmacokinetic Modeling of Renally Cleared Drugs in Children*. CPT Pharmacometrics Syst Pharmacol, 2016. **5**(9): p. 475-83.
386. Yao, X., et al., *Development of a Virtual Chinese Pediatric Population Physiological Model Targeting Specific Metabolism and Kidney Elimination Pathways*. Front Pharmacol, 2021. **12**: p. 648697.
387. Coppola, P., E. Kerwash, and S. Cole, *The Use of Pregnancy Physiologically Based Pharmacokinetic Modeling for Renally Cleared Drugs*. J Clin Pharmacol, 2022. **62** **Suppl 1**: p. S129-S139.
388. Zhou, D., et al., *Simulation and Prediction of the Drug-Drug Interaction Potential of Naloxegol by Physiologically Based Pharmacokinetic Modeling*. CPT Pharmacometrics Syst Pharmacol, 2016. **5**(5): p. 250-7.
389. Rhee, S.J., et al., *Physiologically Based Pharmacokinetic Modeling of Fimasartan, Amlodipine, and Hydrochlorothiazide for the Investigation of Drug-Drug Interaction Potentials*. Pharm Res, 2018. **35**(12): p. 236.
390. Mukherjee, D., et al., *Guiding dose adjustment of amlodipine after co-administration with ritonavir containing regimens using a physiologically-based pharmacokinetic/pharmacodynamic model*. J Pharmacokinet Pharmacodyn, 2018. **45**(3): p. 443-456.
391. Abernethy, D.R., J. Gutkowska, and L.M. Winterbottom, *Effects of amlodipine, a long-acting dihydropyridine calcium antagonist in aging hypertension: pharmacodynamics in relation to disposition*. Clin Pharmacol Ther, 1990. **48**(1): p. 76-86.
392. Williams, D.M. and L.X. Cubeddu, *Amlodipine pharmacokinetics in healthy volunteers*. J Clin Pharmacol, 1988. **28**(11): p. 990-4.
393. Sun, H., *Capture hydrolysis signals in the microsomal stability assay: molecular mechanisms of the alkyl ester drug and prodrug metabolism*. Bioorg Med Chem Lett, 2012. **22**(2): p. 989-95.
394. Kadono, K., et al., *Quantitative prediction of intestinal metabolism in humans from a simplified intestinal availability model and empirical scaling factor*. Drug Metab Dispos, 2010. **38**(7): p. 1230-7.
395. Salem, F., B.G. Small, and T.N. Johnson, *Development and application of a pediatric mechanistic kidney model*. CPT Pharmacometrics Syst Pharmacol, 2022. **11**(7): p. 854-866.
396. van der Vossen, A.C., et al., *Use of amlodipine oral solution for the treatment of hypertension in children*. Int J Clin Pharm, 2020. **42**(3): p. 848-852.
397. Flynn, J.T., et al., *Population pharmacokinetics of amlodipine in hypertensive children and adolescents*. J Clin Pharmacol, 2006. **46**(8): p. 905-16.
398. Faulkner, J.K., et al., *The pharmacokinetics of amlodipine in healthy volunteers after single intravenous and oral doses and after 14 repeated oral doses given once daily*. Br J Clin Pharmacol, 1986. **22**(1): p. 21-5.
399. Bainbridge, A.D., et al., *A comparative assessment of amlodipine and felodipine ER: pharmacokinetic and pharmacodynamic indices*. Eur J Clin Pharmacol, 1993. **45**(5): p. 425-30.
400. Rausl, D., et al., *Intestinal permeability and excretion into bile control the arrival of amlodipine into the systemic circulation after oral administration*. J Pharm Pharmacol, 2006. **58**(6): p. 827-36.
401. Leenen, F.H. and E. Coletta, *Pharmacokinetic and antihypertensive profile of amlodipine and felodipine-ER in younger versus older patients with hypertension*. J Cardiovasc Pharmacol, 2010. **56**(6): p. 669-75.

402. Varga, A., et al., *Pharmacokinetics of different formulations of Telmisartan/Amlodipine fixed-dose combination in hypertensive patients*. *Acta Medica Transilvanica*, 2015. **20**(4): p. 45-50.
403. Paediatric Formulary Committee. *BNF for Children (Online)*. 2 August 2023]; Available from: <https://bnfc.nice.org.uk/drugs/amlodipine/>.
404. Drugs.com. *Amlodipine Information from Drugs.com*. 2023 1 June 2023 [cited 2023 2 August 2023]; Available from: <https://www.drugs.com/pro/amlodipine.html>.
405. Linnet, K., L.M. Lang, and S.S. Johansen, *Postmortem femoral blood concentrations of amlodipine*. *J Anal Toxicol*, 2011. **35**(4): p. 227-31.
406. Spiller, H.A., B.A. Milliner, and G.M. Bosse, *Amlodipine fatality in an infant with postmortem blood levels*. *J Med Toxicol*, 2012. **8**(2): p. 179-82.
407. Adams, B.D. and W.T. Browne, *Amlodipine overdose causes prolonged calcium channel blocker toxicity*. *Am J Emerg Med*, 1998. **16**(5): p. 527-8.
408. Zakaria, Z.H., A.Y.Y. Fong, and R.K.S. Badhan, *Clopidogrel Pharmacokinetics in Malaysian Population Groups: The Impact of Inter-Ethnic Variability*. *Pharmaceuticals (Basel)*, 2018. **11**(3).
409. Yu, H. and R.K. Singh Badhan, *The Pharmacokinetics of Gefitinib in a Chinese Cancer Population Group: A Virtual Clinical Trials Population Study*. *J Pharm Sci*, 2021. **110**(10): p. 3507-3519.
410. Machado, T.R., et al., *Physiologically based pharmacokinetic modelling of semaglutide in children and adolescents with healthy and obese body weights*. *Br J Clin Pharmacol*, 2023.
411. Elhag, W., et al., *Evolution of 29 Anthropometric, Nutritional, and Cardiometabolic Parameters Among Morbidly Obese Adolescents 2 Years Post Sleeve Gastrectomy*. *Obes Surg*, 2018. **28**(2): p. 474-482.
412. Zhou, X., et al., *Predicting the correct dose in children: Role of computational Pediatric Physiological-based pharmacokinetics modeling tools*. *CPT Pharmacometrics Syst Pharmacol*, 2023. **12**(1): p. 13-26.
413. van der Heijden, J.E.M., et al., *Physiologically-Based Pharmacokinetic Modeling for Drug Dosing in Pediatric Patients: A Tutorial for a Pragmatic Approach in Clinical Care*. *Clin Pharmacol Ther*, 2023.
414. Flynn, J.T., W.E. Smoyer, and T.E. Bunchman, *Treatment of hypertensive children with amlodipine*. *Am J Hypertens*, 2000. **13**(10): p. 1061-6.
415. von Vigier, R.O., et al., *Antihypertensive efficacy of amlodipine in children with chronic kidney diseases*. *J Hum Hypertens*, 2001. **15**(6): p. 387-91.
416. Stopher, D.A., et al., *The metabolism and pharmacokinetics of amlodipine in humans and animals*. *J Cardiovasc Pharmacol*, 1988. **12 Suppl 7**: p. S55-9.
417. Zhu, Y., et al., *Amlodipine metabolism in human liver microsomes and roles of CYP3A4/5 in the dihydropyridine dehydrogenation*. *Drug Metab Dispos*, 2014. **42**(2): p. 245-9.
418. Pynnonen, S., et al., *Carbamazepine and its 10,11-epoxide in children and adults with epilepsy*. *Eur J Clin Pharmacol*, 1977. **11**(2): p. 129-33.
419. Riva, R., et al., *Free concentration of carbamazepine and carbamazepine-10,11-epoxide in children and adults. Influence of age and phenobarbitone co-medication*. *Clin Pharmacokinet*, 1985. **10**(6): p. 524-31.
420. de Wildt, S.N., et al., *Cytochrome P450 3A: ontogeny and drug disposition*. *Clin Pharmacokinet*, 1999. **37**(6): p. 485-505.
421. van Rongen, A., et al., *Population pharmacokinetics of midazolam and its metabolites in overweight and obese adolescents*. *Br J Clin Pharmacol*, 2015. **80**(5): p. 1185-96.
422. Gade, C., et al., *Midazolam Pharmacokinetics in Obese and Non-obese Children and Adolescents*. *Clin Pharmacokinet*, 2020. **59**(5): p. 643-654.
423. Hanafy, S., et al., *Effects of angiotensin II blockade on inflammation-induced alterations of pharmacokinetics and pharmacodynamics of calcium channel blockers*. *Br J Pharmacol*, 2008. **153**(1): p. 90-9.

424. Sattari, S., et al., *Despite increased plasma concentration, inflammation reduces potency of calcium channel antagonists due to lower binding to the rat heart*. Br J Pharmacol, 2003. **139**(5): p. 945-54.
425. Abernethy, D.R. and J.B. Schwartz, *Verapamil pharmacodynamics and disposition in obese hypertensive patients*. J Cardiovasc Pharmacol, 1988. **11**(2): p. 209-15.
426. Mayo, P.R., et al., *Decreased dromotropic response to verapamil despite pronounced increased drug concentration in rheumatoid arthritis*. Br J Clin Pharmacol, 2000. **50**(6): p. 605-13.
427. Ross, E.L., et al., *Development of recommendations for dosing of commonly prescribed medications in critically ill obese children*. Am J Health Syst Pharm, 2015. **72**(7): p. 542-56.
428. Flynn, J.T., *Efficacy and safety of prolonged amlodipine treatment in hypertensive children*. Pediatr Nephrol, 2005. **20**(5): p. 631-5.
429. Avataneo, V., et al., *Therapeutic drug monitoring-guided definition of adherence profiles in resistant hypertension and identification of predictors of poor adherence*. Br J Clin Pharmacol, 2018. **84**(11): p. 2535-2543.
430. Alessandrini, E., et al., *Children's Preferences for Oral Dosage Forms and Their Involvement in Formulation Research via EPTRI (European Paediatric Translational Research Infrastructure)*. Pharmaceutics, 2021. **13**(5).